AN INVESTIGATION INTO PAEDIATRIC GASTROINTESTINAL PHYSIOLOGY AND ITS APPLICATIONS IN *IN SILICO* PBPK MODELLING FOR AGE-APPROPRIATE FORMULATIONS

by

JAN GOELEN

A thesis submitted to the University of Birmingham for the degree of

DOCTOR OF PHILOSOPHY

Institute of Clinical Sciences

School of Pharmacy

College of Medical and Dental Sciences

December 2022

ABSTRACT

Drug formulations and dosage strengths intended for the adult population may not be appropriate for paediatric patients, due to developmental changes with age. Performing clinical trials in the paediatric population is challenging due to many factors, therefore formulation development for this population relies on predictive tools that simulate in vivo conditions. However, the development of such tools that predict oral drug disposition is hampered by a lack of physiological data describing the gastro-intestinal tract of the paediatric population. Characterising key parameters will progress predictive tools such as physiologically-based pharmacokinetic (PBPK) modelling and improve representability of paediatric subjects. This thesis specifically characterises (i) the abundance and ontogeny of paediatric intestinal drug metabolising enzymes and transporters (DMET) proteins and (ii) the amount of free fluid within the paediatric colon as two currently unknown parameters.

Using pinch biopsies from the paediatric duodenum, the abundance of important DMET proteins were quantified via LC-MS/MS. For this, an established nanoflow method was translated to a microflow, and a new stable-isotope-labelled standard developed. The observed abundancies and ontogeny profiles, such as for intestinal CYP3A4, agreed with adult LC-MS/MS-based data, or historic paediatric data obtained via western blotting.

The amount and distribution of fluid within the paediatric colon were quantified using magnetic resonance imaging. The paediatric colonic fluid was dissimilar from reported adult values (with 50% of the subjects having <1 mL of fluid), but no correlation with covariates (sex, age, weight) were observed.

These newfound paediatric physiological data were then integrated into PBPK models. Adapting the default ontogeny profile of intestinal CYP3A4 to the novel profile did not result

in clinically different disposition of midazolam, confirming the adequacy of the former in current modelling. Integrating the colonic fluid data in a model for an extended-release formulation of quetiapine saw that, when limited amount of fluid in the colon is present (which is the case for half the paediatric population), ineffective absorption and suboptimal antipsychotic treatment might be prevalent.

In conclusion, the abundance of DMET proteins and the amount of fluid were quantified in the paediatric population. These newly generated data can now be used in predictive tools, with the aim to make formulations for the paediatric population more age-appropriate.

ACKNOWLEDGEMENTS

First and foremost, this thesis would not have been possible without the advice and guidance of my supervisors, Prof. Hannah Batchelor and Dr. Richard Horniblow. Besides being brilliant scientists, they were also there for me as great mentors throughout my PhD journey, giving me suggestions on how to improve my skills, my work and myself. I looked forward to every meeting at 11am on Thursdays, as I always felt inspired and motivated by discussing science and life with you. There were many hurdles in this research, but I always felt I could count on both of you. I literally could not have asked for better supervisors.

I also would like to thank Trevor Johnson at Simcyp for his insightful feedback and mentoring. Many thanks to my various collaborators as well; Benoni Alexander – you've been a massive support for the MRI work -, Eleni Papadatou-Soulou and Gopal Pawar for their advice and insight, Haren Wijesinghe and Emily Evans for their aid in mapping out the colon and my sister for letting me annoy her every evening during a pandemic to use her laptop remotely. Also many thanks to the LC-MS group at the University of Strathclyde, especially Nic Rattray and Gillian Farrell. Also Florian Sigloch at Polyquant has been instrumental in developing the LC-MS SOP and constructing PaedCAT.

Lastly, but not least, I'd like to thank my parents, my family and my friends (and especially Frankie) for their support throughout this process, and distraction whenever it was needed.

This work was funded by Certara as part of the Certara Simcyp Division Grant and Partnership Scheme.

TABLE OF CONTENTS

LIST OF ILLUSTRATIONS

LIST OF TABLES

LIST OF ABBREVIATIONS

Abbreviation	Definition
2D	Two-Dimensional
3D	Three-Dimensional
ABC	Adenosine Triphosphate (ATP)-Binding Cassette
ACAT	Advanced Compartmental and Transit
ACE	Angiotensin-Converting Enzyme
ACN	Acetonitrile
ADAM	Advanced Dissolution, Absorption and Metabolism
ADME	Absorption, Distribution, Metabolism and Excretion
AMRT	Accurate Mass and Retention Time
ANOVA	Analysis Of Variance
AQUA	Absolute Quantification
ATP	Adenosine Triphosphate
AUC	Area Under The Curve
BCA	Bicinchoninic Acid
BCH	Birmingham Children's Hospital NHS Trust
BCRP	Breast Cancer Resistance Protein
BCS	Biopharmaceutics Classification System
BDDCS	Biopharmaceutics Drug Disposition Classification System
BMI	Body Mass Index
BSA	Body Surface Area
BW	Body Weight
CDDS	Colon-Specific Drug Delivery Systems
CES2	Carboxylesterase 2
CFV	Colonic Fluid Volume
CL_{PO}	Oral Clearance
CL_R	Renal Clearance
C_{max}	Maximum Plasma Concentration
C_p	Plasma Concentration
CSF	Cerebrospinal Fluid
CT	Computed Tomography
CYP	Cytochrome P450
DDI	Drug-Drug Interaction
DLM	Diffusion Layer Model
DME	Drug Metabolising Enzymes
DMET	Drug Metabolising Enzymes and Transporters
DTT	Dithiothreitol
EDTA	Ethylenediaminetetraacetic acid
EMA	European Medicines Agency

ESI	Electron Spray Ionisation
F	Bioavailability
F_a	Fraction Absorbed
FASP	Filter Aided Sample Preparation
F_g	Gut Bioavailability
F_h	Hepatic Bioavailability
f_m	Fraction Metabolised
GASP	Gel Aided Sample Preparation
GIT	Gastro-Intestinal Tract
HSA	Human Serum Albumin
IAA	Iodoacetamide
IBD	Inflammatory Bowel Disease
ICH	International Conference of Harmonisation
IM	Intramuscular
IR	Immediate Release
IV	Intravenous
LC	Liquid Chromatography
LC-MS/MS	Liquid Chromatography-Tandem Mass Spectrometry
LN_2	Liquid Nitrogen
LOQ	Limit Of Quantification
LSA	Local Sensitivity Assay
LysC	Lysylendopeptidase
M&S	Modelling and Simulation
m/z	Mass-to-charge
MDR	Multidrug Resistance Protein
MIDD	Model Informed Drug Development
MRI	Magnetic Resonance Imaging
MRM	Multiple Reaction Monitoring
mRNA	Messenger RNA
MRP	Multidrug Resistance-Associated Protein
MS/MS	Tandem Mass-Spectrometry
MW	Molecular Weight
Na/K-ATPase	Sodium/Potassium-Transporting ATP-ase Subunit Alpha-1
NDA	New Drug Approval
NSAID	Non-Steroidal Anti-Inflammatory Drug
OCT	Organic Cation Transporter
OD	Once Daily
PBPK	Physiologically-Based Pharmacokinetics
PBS	Phosphate-Buffered Saline
PBSC	Paediatric Biopharmaceutics Classification System
PD	Pharmacodynamic
$P_{eff,man}$	Effective Permeability in man

PEPT1	Peptide Transporter 1
PER/DEF	Personalised-to-Default Ratio
P-gp	P-Glycoprotein
PIC	Protease Inhibitor Cocktails
PK	Pharmacokinetic
popPK	Population Pharmacokinetics
P-PBPK	Paediatric PBPK
PPE	Percentage Prediction Error
PSAQ	Proteins Standards For Absolute Quantification
QconCAT	Quantification Concatemer
QQQ	Triple Quadrupole
RBG	Red Blue Green
RIPA	Radio-Immunoprecipitation Assay
ROI	Regions of Interest
RT	Room Temperature
RT-qPCR	Reverse Transcription – Quantitative Polymerase Chain Reaction
SD	Standard Deviation
SDS	Sodium Dodecyl Sulphate
SIL	Stable Isotope Labelled
SITT	Small Intestinal Transit Time
SLC	Solute Carrier
SOP	Standard Operating Procedure
STL	Stereolithography
TCV	Total Colonic Volume
TDM	Therapeutic Drug Monitoring
TFA	Trifluoroacetic Acid
TQP	Targeted Quantitative Proteomics
t_R	Retention Time
UA	Urea
UBL	Unstirred Boundary Layer
UDP	Uridine 5'-Diphosphate
UGT	Uridine 5'-Diphospho-Glucuronosyltransferases
UHCW	University Hospitals Coventry And Warwickshire NHS Trust
US FDA	Food and Drug Administration of The United States Of America
WHO	World Health Organisation
XR	Extended Release

LIST OF EQUATIONS

1 CHAPTER ONE

INTRODUCTION

CHARACTERISATION OF THE PAEDIATRIC GASTRO-INTESTINAL TRACT TO OPTIMISE PBPK MODELLING OF ORAL DRUG ABSORPTION

1.1 Developing tools to predict oral drug performance for the paediatric cohort

Most paediatric drugs are formulated as an oral product as these are easy to administer, cheap to produce and are well-adhered to[1]. The absorption of an oral drug is dependent on its liberation from the formulation, dissolution into the gut lumen and subsequent transport across the intestinal tissue into the bloodstream (see section 1.1.2)[2]. Dosage form disintegration and subsequent drug release depend on various gastro-intestinal parameters, such as the amount of fluid available, pH or the gastric emptying rate[2]. However, designing appropriate oral formulations where the correct amount of drug is released at the right time and place is challenging due to the inter- and intraindividual variability in the gut[2]. In a paediatric population, prediction of oral drug performance is challenging, as data that describe drug performance in the intestinal tract (both oral paediatric pharmacokinetic data and anatomical-physiological information) are lacking in this understudied population. Characterising the paediatric gut can provide data to address the latter, but access to paediatric patients and gastro-intestinal tissue is difficult, due to many factors (see also section 1.1.4). Differences with the adult population in gut physiology and inherent changes with childhood increase complexity (see section 1.1.2)[3, 4]. For example, expression of gut enzymes involved in drug metabolism[5, 6], intestinal fluid pH and transit times[7] or gut permeability[8], diameter, surface area and length[9] change with age. Furthermore, the pharmaceutical industry neglected paediatric drug development due to a smaller revenue and difficulties conducting studies in this vulnerable cohort[1, 10]. Regulatory efforts to ensure paediatric populations are no longer neglected include mandatory paediatric development plans with new drug submissions[1].

1.1.1 Classification of the paediatric population

Children are commonly classified into different groups based on age. The classification from the International Conference of Harmonisation (ICH) is listed in **Table 1.1**[11]:

Table 1.1. *ICH classification of the paediatric population based on age.*

Name	Age
Preterm Newborns	<0 days (less than 37 weeks gestation[12])
Term Newborns	0 – 27 days
Infants	28 days – 12 months
Toddlers	>12 months – 23 months
Preschool child	2 – 5 years
School age child	6 – 11 years
Adolescent	12 – 17 years

These age bands were determined arbitrarily, rather than based on physiological development data[11, 13]. Some of these age bands still cover a wide range of maturation within one cohort, resulting in a very heterogeneous group. The preterm cohort is recognised as the group for which drug product performance is the most challenging to predict, as the pharmacokinetic (PK) profile is highly variable[14]. The European Medicines Agency (EMA) also suggests classification based on other factors (renal function, genetic polymorphism in drug-metabolising enzymatic status)[14], which should be included in dosing recommendations where these covariates have a significant impact on drug safety or efficacy.

1.1.2 Drug absorption in paediatrics and the Biopharmaceutics Classification System

An orally administered drug needs to liberated from its formulation, dissolve and be absorbed across the mucosal wall lining the gut lumen to be available for systemic circulation[4]. When in the enterocyte, a fraction of the drug could also be excreted back into the lumen via efflux transporters or undergo metabolisation via drug metabolising enzymes

(DME), before reaching the bloodstream and being directed to the liver via the vena porta[15]. In the liver, metabolising enzymes can substantially influence the amount ultimately reaching the general circulation (first-pass effect), after which the distribution phase can commence. Oral bioavailability (F) is then the product of the fraction absorbed (F_a), the fraction passing the enterocyte unchanged (F_g) and the fraction escaping hepatic metabolism (F_h)[4, 16, 17] (**Equation 1.1**)

$$F = F_a * F_g * F_h$$

Equation 1.1. *The oral bioavailability (F) is calculated from the product of the fraction absorbed (F_a), gut bioavailability (F_g) and hepatic bioavailability (F_h).*

Metabolism in the gut wall, limiting F_g, can be a key factor influencing oral drug bioavailability and PK profile as demonstrated by Varma *et al*.[16]. This review found that 30% of more than 300 compounds for oral use underwent intestinal metabolism in adults, with a fraction metabolised higher than 0.2 (thus F_g lower than 0.8), meaning that 20% or more of the dose does exit the enterocytes. Hence, as intestinal metabolism can have a significant impact on the PK profile of a drug, this process and the factors that influence it need to be well-characterised.

Challenges in oral drug absorption include solubility of the drug and permeability across the enterocyte membrane, either via passive permeation or transport (if the drug does not permeate paracellular to the blood veins). The interplay between permeability and solubility led to the development of the Biopharmaceutics Classification System (BCS)-framework in 1995[18]. Here, drugs are classified into 4 categories based on their permeability and solubility:

- Class I having high solubility and permeability,

- Class II low solubility but high permeability,
- Class II having a high solubility but low permeability,
- and Class IV having both a low solubility and permeability.

In 2005, the BCS framework was expended to the Biopharmaceutics Drug Disposition Classification System (BDDCS)– integrating the correlation between intestinal permeability and metabolism[19]. Here, the drugs are classified based on the extent of metabolism rather than permeability (whilst still keeping solubility as a factor). As the BDDCS platform allows to assess the role of DMET proteins and drug-drug interaction (DDI) potential, it has gained wider regulatory acceptance than the BCS[20, 21].

In 2012, a paediatric BCS (PBSC) working group aimed to establish a preliminary similar classification system divided in different age ranges, reflecting the developmental changes in intestinal absorption and permeability[22]. However, key knowledge gaps needed to be addressed to propose a suitable classification system. These included data on the ontogeny of intestinal drug metabolising enzymes and transporter (DMET) proteins, ontogeny of gut physiology and addressing the lack of paediatric PK data required for physiological-based pharmacokinetic (PBPK) modelling.

Other than intrinsic factors (drug properties), many physiological parameters influence gut bioavailability[23]. A few examples are given in **Table 1.2**.

Table 1.2. *Factors involved in gut bioavailability*

Factor	Involved in	Comments/examples
Intestinal fluid volume	Drug product disintegration and dissolution	Fluid volumes in the small intestinal tract[24] and colon[25] of children are much lower than the reported values for adults[26]

Intestinal fluid composition	Solubility of lipophilic drug (by e.g. bile acids)	Bile acids are amphiphilic emulsifiers which facilitate solubilisation and absorption of lipid compounds. Thus, their presence or absence increases or decreases the absorption of lipophilic drugs, like hydrocortisone and progesterone[27].
Intestinal pH	Absorption of ionisable compounds	Itraconazole[28] is a drug with a low pKa and a pH-dependent solubility, where absorption is affected by the pH within the GI tract.
	Degradation of pH-sensitive compounds	Penicillin-G[29] is unstable in acidic environments, thus the drug release from the formulation should not take place in the acidic stomach.
Intestinal transit time	Contact time between the drug and the gut wall	Shorter intestinal transit time means less time for the absorption process to take place. For sustained release formulations, such as theophylline, a prolonged contact time is essential as the drug is released gradually[30].
Gastric emptying time	Dictates how quickly drugs are presented to the duodenum	Conflicting ontogeny reports. Initially found to shorten with maturation, reaching adult values after 6-8 months postpartum[7, 31]. However, recent meta-analysis showed that this finding is rather caused by differences in food type, and age is not a covariate for gastric emptying[32].

Ontogeny of intestinal DMET proteins influence gut bioavailability. Membrane-bound transporter proteins facilitate migration or actively transport compounds across the membrane, and thus are important regulators for drug disposition[13, 33, 34] (see also section 1.3.2 - Transporter proteins). These proteins are most notably found in the liver, kidney, gastro-intestinal tract and at the blood-brain barrier[35]. A change in transporter activity via inhibition or induction[36] or genetic polymorphism may impact a drug's PK and safety profile, but further research is necessary to understand the mechanisms that regulate transporter activity[33, 34]. Depending on their relative location on the plasma membrane of the enterocyte (apical/luminal or basolateral/blood vein) and the direction of transporting (influx/efflux) dictates whether the victim drug has an increased or decreased potential for reaching the bloodstream.

Endogenous and xenobiotic compounds are metabolised so the body can excrete these. Phase I reactions add polar groups to the compound (by oxidation, reduction and hydrolysis), Phase II reactions conjugate the molecule with hydrophilic groups such as glucuronic acid, glutathione or sulphate (among others), resulting in more water-soluble moieties[37, 38]. Cytochrome P450 (CYP)-enzymes is the major family of Phase I catalysts, generally found in the membrane of the endoplasmic reticulum (see also section 1.1.1). Phase II catalysts include uridine 5'-diphospho (UDP)-glucuronosyltransferases (UGTs), which are found also found in the luminal side of the endoplasmic reticulum and transfer the acidic sugar component of UDP-glucuronic acid to compounds[38, 39] (see also section 1.1.1).

Missing data on paediatric physiology (e.g. the unclear ontogeny profile of the efflux transporter P-gp in the intestine, see section 1.3.2) make it hard to predict drug disposition accurately[13]. Lower DME levels in the liver in the paediatric population warrant for a lower dose than the adult strength, but a higher blood flow to the liver and a larger relative size of the liver to the rest of the body argues against this rationale[13, 40]. Thus, there is a clear need to characterise physiological parameters in the paediatric population to explain differences observed in oral absorption between children and adults and predict PK profiles accurately.

1.1.3 Dosing recommendation via allometric scaling

There is a clear need to study drug performance in the paediatric population. A review by Rodriguez *et al*. (2007) found that for 108 drug products where recently a paediatric PK study was conducted (on request of the Food and Drug Administration of the United States of America (US FDA)), more than 20% needed a label or dose change[41], proving the need to

collect pharmacokinetic data in children and caution when extrapolating dosages from adults[13]. Historically, dosing recommendations for unlicensed medicines for children were based on allometric scaling[10, 42, 43]. Here, dose scaling from adults was done via simple algorithms based on scaling factors like body weight (BW), body height or body surface area (BSA), such as Clark's BW (**Equation 1.2**) and BSA rules[44, 45].

$$Dose_{paediatrics} = Dose_{adults} \times \frac{BW_{paediatrics}}{BW_{adults}}$$

Equation 1.2. *Clark's rule to scale an adult to paediatric dose based on body weight (BW).*

However, allometric scaling is problematic as it does not take maturation of drug elimination pathways or organs or changes in blood flow and body composition into account[10, 46, 47].

Modelling approaches are a powerful alternative to allometric scaling to support paediatric drug development and clinical trial design[48]. Computer-based simulations describe drug disposition via mathematically representation of biological systems and pharmacokinetic mechanisms. These simulations support drug development as decision tools, data exploration (e.g. covariates analysis) and to optimise study design[49] (see also section 1.2 - Model Informed Drug Development for paediatrics).

1.1.4 Clinical pharmacokinetic trials in children

Some clinical trials aim to capture the PK profile, i.e. the change in drug concentration in blood/plasma over time. This is convenient to determine drug disposition within the body, but also useful to predict therapy response when the plasma concentration of the drug (C_p) is directly related to the drug response (pharmacodynamic effect, PD)[13]. Paediatric PK

studies are used for formulation development studies, as proof of concept studies or to inform dosing recommendations based on the C_p profile, as the aim is to match drug exposure to adult levels[13].

Multiple factors are involved in the intestinal absorption of a drug compound (as described in section 1.1.2). Hence, there is a need for trials or predictive methods to capture the extent of drug absorption and the inter- and intraindividual variability, and to establishing a dose-concentration-response curve in the target patient population. However, performing clinical trials in children is challenging, owing to various factors:

- Paediatric clinical trials often face ethical constraints, logistical challenges[50] and poor recruitment[51].
- Reluctance by carers or doctors to participate, or special considerations required for paediatric study subjects[52]
- Paediatric trials use study subjects who potentially benefit from the treatment[14], so it is extremely unlikely to have a 'normal or healthy' control group.
- Cross-over studies with a placebo are also very rare, as it is deemed unethical to give a diseased child a placebo when there is an effective treatment available[51, 53].
- The number of paediatric patients available to recruit is often small and inter-individual physiological variability can mask efficacy[40, 54].
- Even with paediatric clinical trials being approved, failures due to lack of efficacy, safety issues or suboptimal design have been reported[54]. Over the period 2007-2014, 10 paediatric clinical trials registered with the FDA failed due to lack of efficacy and suboptimal dosing selection (23% of total failed paediatric trials). Either a single dose or a range of doses were tested, as investigators did not exceed exposure levels

observed in adults, yet these doses did not establish a therapeutic effect in paediatrics[54].

- Additionally, only a limited amount of blood can be sampled from a child[53]. Using a sensitive analytical method can circumvent the requirement of larger blood sampling with alternative sampling routes, such as urine or saliva sampling or microsampling via a prick in the heel or finger[13].

1.2 Model Informed Drug Development for paediatrics

1.2.1 Modelling in the paediatric population

Paediatric new drug approval (NDA) applications frequently rely on modelling and simulation (M&S) approaches. The most common forms of model informed drug development (MIDD) are population pharmacokinetic (popPK) modelling or PBPK modelling[1]. M&S in virtual populations are integral to future of paediatric clinical trials according to the FDA[13]. The EMA endorses the use of MIDD to boost drug development in paediatrics[14]. Paediatric PBPK (P-PBPK) modelling has gained increased interest[40].

1.2.2 Population pharmacokinetic (popPK) modelling

PopPK modelling is a modelling technique that aims to estimate the mean and variability of pharmacokinetic descriptors within a given population[55] by using sparse individual datapoints acquired on a big sample size and using a non-linear mixed effect model (pooling all the data)[14, 56]. Increasing the population size (N) when focussing on a population approach means that a smaller number of samples are required per individual paediatric subject, thus lessens the burden on each child[13, 51]. PopPK allows for sampling from a heterogenous group of subjects, and has less constraints on timing of sample collection[55].

This means that the pool of eligible subjects is larger – and can work across the scope of different clinical trials (such as pooling data from Phase 1/2/3 studies). PopPK modelling is a cornerstone for MIDD. In every new paediatric indication in the period January 2017- June where MIDD was used, popPK modelling was employed[40].

However, popPK is not a suitable method to predict a first time use in a paediatric population[57]. A popPK study for a paediatric dose estimation of abacavir failed to establish a working dose, despite statistical validation and accurate parameter estimation[57].

Demographic covariates still have a large range in this heterogenous group. Additionally, popPK fails in detailing and explaining the underlying mechanistic processes where the differences to the adult population originate from.

1.2.3 Physiological-based pharmacokinetic modelling

PBPK modelling fuses physicochemical properties of the drug (compound and formulation), with physiological and anatomical data of the target population into a mathematical model to describe the pharmacokinetic profile of a drug *in vivo*[46, 58]. It does this via a mechanistic integration of physiological parameters to describe the absorption, distribution, metabolism and excretion (ADME) processes in a mathematical fashion[13, 59]. Hence, by modifying physiological inputs to better represent a different population, PBPK modelling is a rational approach to extrapolated across a range of populations, provided the population is well-characterised[1, 46, 60].

The commercially available PBPK modelling software package Simcyp simulator (Certara) is the most used PBPK simulator in publications over the period of 2005-2020 (55%), followed by PK-Sim (Bayer, 23%) and GastroPlus (Simulations Plus, 6%) amongst others[40].

1.2.3.1 Use, benefits and drawbacks of paediatric PBPK modelling

PBPK modelling has increased interests as it is a cost-effective method to support and replace clinical trials with simulations[61]. In the period of 2008-2018, 15% of drug submissions with a PBPK component reported simulations in paediatrics to the FDA[62], and in 2019 31% of all PBPK publications included a paediatric component[40, 58]. Publications and regulatory reviews on P-PBPK modelling increased 33-fold over the period 2005-2020[40]. P-PBPK models are used for many different reasons (see also section 1.2.4). PBPK modelling is involved in 83% of dose estimation studies in the paediatric population, making it the most used method for this question[1]. Additionally, it has been demonstrated that PBPK modelling is superior to and preferred over allometric scaling strategies based on body height, body surface area or weight[10, 13, 63]. In the age group of 0-2 year olds, the FDA favours PBPK modelling for PK extrapolation from adults[61, 64, 65].

Due to the required population-specific input (see section 1.2.3.3.2), PBPK modelling is perfectly positioned to extrapolate beyond the studied population and explore the influence on drug absorption of physiological changes that arise from e.g. obesity, disease state, ethnicity and age[66, 67]. The model can also account for differences in biological parameters between various target populations (body size, tissue composition and blood flow, transit times, metabolic pathways and maturation). Additionally, it can investigate changes in formulation since drug-specific inputs are required.

The main drawback regarding PBPK modelling is the requirement for reliable and robust rich PK clinical data, which are not always available. A second limitation of P-PBPK models for oral formulations are the sparse paediatric physiological gastro-intestinal tract (GIT) data[57].

It is predicted that further refinement and physiological data mining is pivotal to sustain the increasing use and acceptability of P-PBPK modelling[40].

1.2.3.2 Advanced Dissolution, Absorption and Metabolism (ADAM) component

Since the introduction of the Advanced Dissolution, Absorption and Metabolism (ADAM) component in the Simcyp simulator[10, 68] or the Advanced Compartmental and Transit (ACAT) component in the GastroPlus simulator, drug absorption can be simulated even more mechanistically[69, 70]. The ADAM model divides the gut into eight hypothetical segments: duodenum – jejunum (I/II) – ileum (I/II/III/IV) and the colon, the ACAT model counts nine segments. Each segment is described with various parameters (such as length, diameter, enzyme levels per segment). This model also describes drug absorption per segment and pushes the unabsorbed fraction into the next segment. PBPK modelling and the ADAM model are a powerful tool in paediatric MIDD as they take ontogeny in physiology into account, such as organ maturation and DMET expression[10, 71]. As only the Simcyp simulator has been used for P-PBPK in this thesis, only the Simcyp simulator is discussed from here on. However, GastroPlus (and other PBPK simulators) have a very similar set-up[46, 72]. The major differences between these simulators are the pathway how models are developed and the necessary input parameters, but the predictive performance is similar, as proven by a comparative study for prediction of simvastatin PK in adults using Simcyp and PK-Sim[73].

1.2.3.3 Building a PBPK model

A PBPK model has three components: a drug file, a virtual population and a trial design[74]. The different components are all essential to *in silico* prediction of PK profiles. The PBPK-

simulators commonly have a graphic-friendly interface[75], facilitating the embedding of new data or adapting parameters into the models.

1.2.3.3.1 Drug component

The PBPK model requires physicochemical descriptors of the drug of interest. Parameters such as molecular weight (MW), pKa, tissue partition coefficients and logP-values, *in vitro* information (for example intrinsic enzymatic clearance and induction/inhibition data collected during preclinical analyses) are included within the models[60, 67]. Additionally, formulation characteristics are also described via the drug component. These include drug release via an immediate, delayed (enteric coating) or modified release pattern, particle size and distribution, formulation type (suspension, micro pellets, etc.)[76, 77].

1.2.3.3.2 Virtual population component and scaling factors

This component codes for the population of interest based on descriptive physiological data. Physiological parameters can be included in different levels:

- overall population descriptors such as relationships between height, weight, age, sex.
- general body composition information in terms of organ sizes, blood flow to/from these compartments, body composition, transit times and others with the possibility to virtually represent individual organs[60].
- organ-specific information: the amount of protein in the blood, enzyme levels and activity in the liver and gut, phenotyping (slow – intermediate – extensive metabolisers e.g.), gut surface area, intestinal fluid characteristics and others.

The detail required will depend on how many compartments are included in the model. A full PBPK model is a model with many compartments, each describing a full organ in detail whereas a minimal PBPK model describes the general body with a few non-physiological compartments[66]. To build physiological variability into the model, the physiological parameters are described as a mean value with variation on the mean rather than a fixed value (rarely a median[78])[79]. The input values typically represent the average individual in the (usually adult) population, and specific data for specialised populations (such as paediatrics) are sparse[67].

Crucial to the accurate predictive performance of PBPK modelling are reliable physiological input parameters[46, 57, 79]. Accurate and precise data that captures both the true value of physiological parameters and their variability are required[15, 79, 80], but equally important is to consider the methodology used to characterise the parameters. Especially for drugs with a narrow therapeutic index (such as anti-cancer drugs), it is important to capture interindividual variability[79-81].

Some factors are challenging to determine on organ-scale[79], so values from assays performed on a smaller scale are extrapolated to represent a whole organ, such as intestinal transporter abundance and metabolising activity. This extrapolation however inherently causes a degree of error and uncertainty into the system[67]. Hence, accurate scaling factors and accurate translation of the used procedure to the PBPK input format are needed too[79].

However, even around parameters already investigated, uncertainty remains. Older studies suggested neonates have a longer (slower) small intestinal transit time (SITT) compared to

older infants (towards 1 year old) due to reduced peristalsis[42, 82, 83], causing concern about incomplete absorption of sustained release formulations in the latter age group as motility was increased and SITT shortened[22, 30]. However, recent (2016) meta-analyses found no influence of age on the SITT[7, 23]. Similarly, there are conflicting data on gastric transit times (see also section 1.1.2).

1.2.3.3.3 Trial design

The trial design component enables the user to inform the model how many drug intake events are occurring, how long a virtual trial is running for, in what fed conditions and if there is a selected subpopulation (such as people of a certain age range or sex).

1.2.3.3.4 Building and evaluating a paediatric PBPK model: Learn and confirm approach

There are different ways to build pharmacokinetic models, depending on the amount and quality of available data and the intended use of the model[67]. PopPK models are built on observed clinical data, from which essential information is distilled ("top down"). PBPK models can be built from a mechanistical understanding up to predicting the concentration-time profile for the entire body or organs ("bottom up" approach), but also *via* a "middle out" approach, in which preclinical and observed data are combined in the model and used to estimate unknown or uncertain parameters to better represent observed data[84].

The model can periodically be checked for performance and tweaked, using a "learn and confirm" approach. For this, a first clinical PK dataset can be used to build an initial model (learn). The outcomes of this initial model can be validated against a second, independent clinical PK dataset to evaluate model performance[66]. This approach is useful to develop,

support and verify PBPK models as it combines different datasets from various tools (*in vitro*, clinical, *in vivo*)[10, 66] to maximally use the information available[43, 84].

Model performance is usually assessed by comparing how well the simulated predictions fit the observed second dataset (confirm). However, attention should be paid to check if the estimated parameters are still physiologically plausible[67].

Common ways to compare virtual simulations to observed PK data is looking at the mean ratio, average fold error, root mean squared error, percentage prediction error, determining the proportion of an estimate within a predefined range (similar to a confidence interval), having a visual check of fit or looking at how well the model responds to perturbation of "normal" drug disposition (such as genetic polymorphism or DDI studies)[60, 67]. However, using mathematical parameter estimation could result in parameters being outside their physiological scope[67], even though result comparisons indicate the simulations are acceptable. Therefore, the World Health Organisation (WHO) suggested a more holistic "fit for purpose" assessment framework[85]. Firstly, the biological basis should be verified, like confirming if the reported cardiac output is the sum of all organ perfusion rates and whether this value is physiologically relevant. Secondly, the reliability should be verified by checking parameter estimations and uncertainty. Lastly, the simulations should be compared to observed data, via a visual check or e.g. residual errors to detect systematic errors in the model.

The influence of parameters on the model outcomes can be assessed using a sensitivity analysis[86]. This analysis can also be used to reduce unnecessary complexity in the model. For example, it was possible to reduce a 14-compartment model describing diazepam

distribution in the rat to a 3 compartment model after sensitivity analyses, whilst maintaining accurate prediction of the mean plasma concentration and variability[87].

There is currently no standard approach to build a PBPK model for paediatric use[46, 60]. A best practice framework for P-PBPK model building was recently proposed by Johnson *et al*.[64]. A representative figure is shown in **Figure 1.1** (Yellepeddi *et al*.[46]).

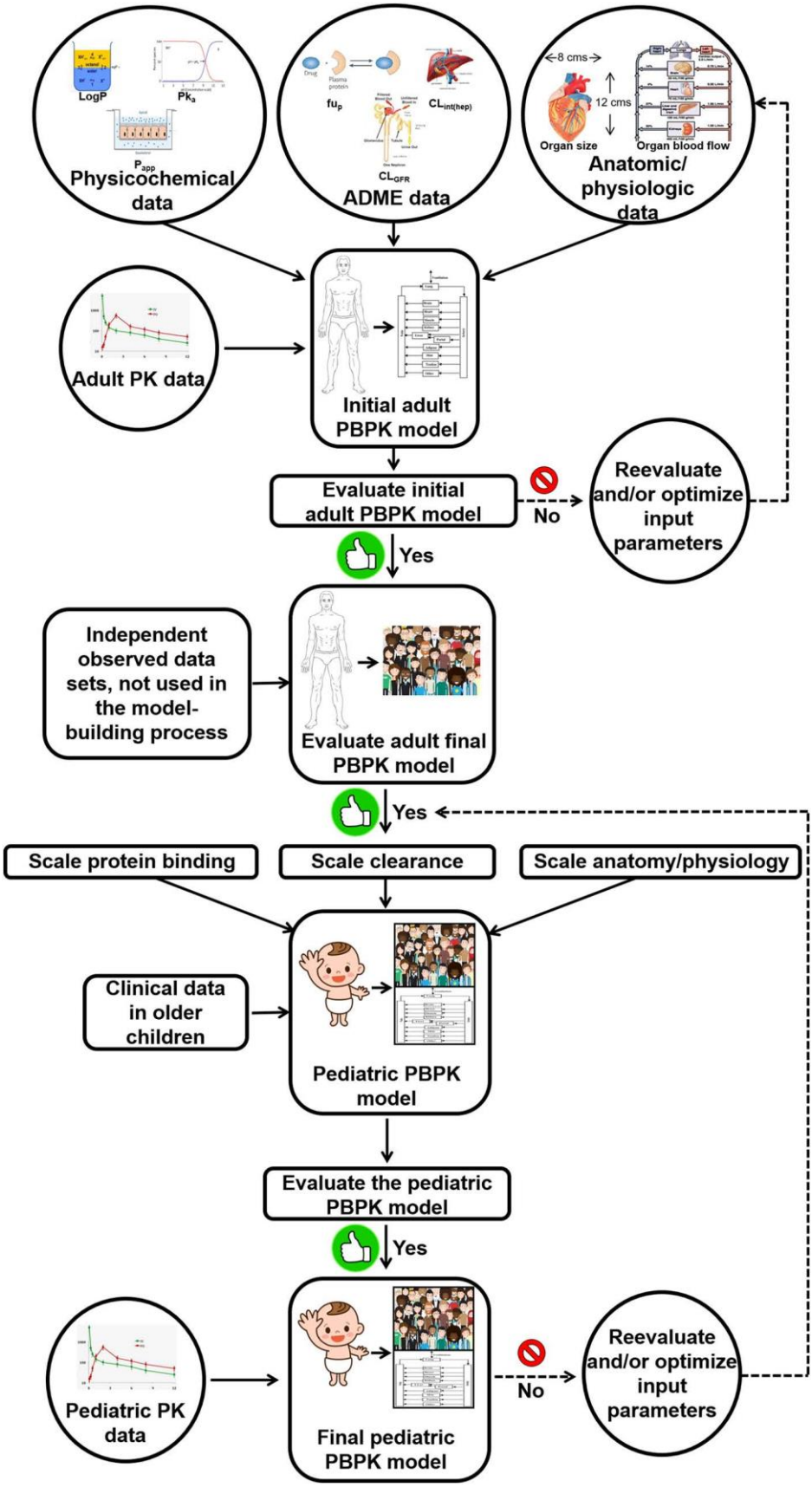

Figure 1.1*. A best practice framework on establishing a paediatric PBPK model starting from adult data (Yellepeddi et al.*[46], with permission*). "Pediatric": paediatric.*

In most paediatric PBPK modelling cases, the model is first built for predicting drug disposition in healthy adults using an intravenous (IV) administration, subsequently incorporating the absorption component. Then, this model should be evaluated, verified and refined using adult data to fine-tune the model. Next, the adult population parameters are switched to paediatric values (starting with older children) whilst maintaining the drug input parameters. The impact of some parameters on the model should be investigated using sensitivity analyses, such as a reduced intestinal fluid volume on the PK profile of drugs with limited solubility (BCS class II or IV drugs[64, 66], see section 1.1.2).

Advantages of this approach are a better understanding of the ADME parameters and improved confidence in the paediatric simulations due to the robust, accurate and verified adult model[46]. The confidence in the paediatric model is a direct result of the confidence in the adult model[60], as models built from clinical PK data will be more reliable than simulations purely based on physicochemical properties of the drug supplemented with preclinical data. This also implies confidence in the adult component is necessary. Errors in the adult model can impact the paediatric model. For example, a lorazepam simulation in adults overpredicted exposure in the first 20 minutes, this fault in model design was carried over to the paediatric PBPK model where exposure was also overpredicted in the first 20 minutes[88].

The learn-and-confirm approach also allows for verification of the drug inputs, meaning any variability or outliers observed in the paediatric simulations arise from the population parameters, hence reliable physiological input representing the paediatric population are essential[60, 88]. Conversely, relaxing some of the model parameters in a way that simulations

lean more towards observed (where available in paediatric populations) clinical data (parameter estimation) can help identify what factors need further investigation within the paediatric population[60].

1.2.3.4 Paediatric PBPK modelling

The standard, adult population in PBPK-simulators is built upon extensive demographic and physiological analysis of Caucasian adults and curated by the software developers[68, 75, 77]. However, various population files are available, recognising the biological differences between people from different ethnicity, sex or health state, such as Chinese, South-African or obese population in Simcyp.

The in-built paediatric population in Simcyp is adapted from the adult population by the software developers, reflecting developmental changes published in literature.

A few examples of changes are:

- Body weight and body surface area code are based on equations by Dubois and Dubois and Haycock[10, 89, 90]
- Liver volume is described using an ontogeny function based on meta-analysis of 5036 paediatric subjects (birth to 18 year old)[91].
- Liver metabolic capacity (CYPs) are based on ontogeny reports[10].
- Cardiac output: adapted from adult values via Guyton and Hall with a development function[92].
- Renal function: based on ontogeny reviews[10, 93].

- First-pass gut metabolism for CYP3A enzymes[94] (see also section 1.1.1): metabolism is calculated based on abundance of the enzyme and the small intestinal gut surface area (which is based on length and diameter):
    - Length and diameter ontogeny functions are based on reference values[95],
    - CYP3A abundance: in adults, the total gut abundance is reported to be 70 000 pmol[96, 97], of which the most is found in the jejunum, but also in the ileum (31%) and duodenum (14%). An ontogeny function is built in using data from Johnson *et al*., 2001[5], with the assumption development in all segments of small intestine happens at same rate. However, nowadays preference is given to ontogeny determination via quantification of the paediatric tract itself rather than scaling via surface area[98].

However, there are a lot of parameters not investigated or only limited data exists in the paediatric population.

1.2.4 Paediatric PBPK models in literature

Most commonly, the course of the plasma level of the drug is observed as a function of time during the virtual trial. This allows PBPK models to have a variety of applications: dose projection for clinical trials, to assess metabolic drug-drug interaction (DDI) or influence of a specific disease state (organ impairment), optimising study design, investigating the influence of different complex formulations (including food effects), substantiating limited paediatric clinical PK data via supplementing with population simulations to even replacing real clinical trials[40, 46, 58, 61, 64-66, 99].

Formulation bridging aims to predict exposure based on a change in formulation; this is often required when introducing an age-appropriate product for children. Drug-drug

interactions studies can also be performed using P-PBPK modelling. Reviews regarding the main disadvantages, considerations and strengths of this approach are available[100, 101].

P-PBPK can also be used for diseases where pathology is different from adults, or disorders that are only observed in the child. This is a promising tool, as it has been observed that most clinical trials fail when the disease progression is dissimilar between adults and children[54]. PBPK modelling can also be used to advise and inform other models, such as for the influence of transporter ontogeny (1 day old – 15 year old) on the renal clearance (CL_R) for a range of hypothetical drugs[102].

Similarly, PBPK modelling can be used to inform trial design and optimal sampling times for maximal data collection during study design.

Literature reports P-PBPK models for a range of the applications given above[61]. **Table 1.3** gives a brief overview of selected P-PBPK models reported in literature, a more detailed discussion is given in **Appendix 1**.

Table 1.3. *Examples of P-PBPK applications in literature.*

Application	Drug (Indication)	Initial model	Set-up of paediatric PBPK	Outcome
Dose finding	Voxelotor[61] (Sickle cell disease)	Adult model was built to represent sickle cell patients (changes in blood binding, haematocrit levels), verified to clinical trials.	Ontogeny of pathophysiological markers were implemented based on adult PBPK model	Dosing recommendations given for 9 months to 12 year olds.
	Everolimus[103] (Adjunctive therapy for tuberous sclerosis complex-associated drug-resistant partial-onset seizures)	A PBPK model was built using clinical data from adults and older children (2-18 year old).	Simulations were made for patients 6-12 months old, using the "redefine over time"* function. A popPD model was linked to predict how effective the drug is in decreasing seizure frequency.	Based on these simulations, oral dosing recommendations were given for <2 year olds.
Formulation bridging	Quetiapine[66] (Schizophrenia)	An adult model was built via the learn and confirm approach for an IR and XR formulation. CYP3A4 induction and inhibition was incorporated in the model.	Using paediatric IR data, the model was extrapolated to compare the exposure between a twice daily IR dose and a once daily XR dose of quetiapine (10-17 years).	As a result of these simulations, a clinical trial of the quetiapine XR formulation in the paediatric population was waived.
	Hydrocortisone[104] (Hormone replacement therapy for adrenal insufficiency)	Initial model predicted exposure of an IR and XR hydrocortisone formulation in adults and paediatrics		PBPK model used to act as a tool to determine dosing regimens in clinical trials
	Lamotrigine[105] (Epilepsy)	Adult model was built to verify DDI potential and was based on clinical data for	Model was adapted to predict lamotrigine exposure following a single or multiple	In close agreement with clinical observed data.

		both an IR and XR formulation.	IR dose in children ages 4-17 years old.	
Paediatric-specific pathology	Deflazacort[61, 65] (Duchenne Muscular Dystrophy)			Accepted as evidence for dosing recommendations and DDI assessment for children >5 years.
	Radiprodil[106] (Infantile Spasm Syndrome)		A P-PBPK model was developed that captured the ADME and ontogeny processes and could predict receptor occupancy (RO). This model was then coupled to a PD-model to predict efficacy.	A low RO and a low dose escalation approach were followed as initial dosing guidance in an ongoing, open trial. The model also provided guidance on dose escalation for three paediatric patients, predictions were in close agreement to observations.
Drug-Drug Interaction	Guanfacine, a CYP3A4 substrate[107, 108] (ADHD)	Model built on existing clinical data in healthy adults using therapy, and was verified against clinical PK data with the presence of inducers and inhibitors.		Dosing recommendations for co-medication with strong CYP3A4 inducers/inhibitors were provided and approved without extra clinical studies in adolescents.
	Risdiplam, a CYP3A4 inhibitor[61, 109] (Spinal Muscular Atrophy)	A PBPK model predicting DDI in healthy adults was built.	Model was extrapolated to paediatric patients (>2 years).	The results show there is a negligible DDI risk in children.
Optimising therapy	Elexacaftor, tezacaftor, and ivacaftor[110-112] (Cystic fibrosis)	Dual therapies are available, but a recent study suggested triple combination of oral elexacaftor, tezacaftor and ivacaftor to be superior	Three P-PBPK models were built, one for every drug and then combined to look at exposure.	Initial models show that immediate transfer of patients >12 years are having a better PD response, clinical trials on children < 12 years are ongoing[61].

*: in the “redefine over time” function , the rapid changes in ontogeny are included as patients are virtually getting older.

1.3 Intestinal DMET protein abundances

1.3.1 DMET proteins

Drug metabolising enzymes and transporter proteins (collectively, DMET proteins) are important regulators of drug disposition of a medicine [13, 113-115]. As these proteins can act on a wide number of xenophobic compounds, they are involved in the ADME-processes of a plethora of compounds. The intestinal bioavailability and subsequent systemic pharmacokinetic profile of oral drugs can be influenced by the relative expression and activity of these DMET proteins along the GIT, where the extent of variation regarding abundance and activity (induction/inhibition) affect the absorption window and safety-efficacy profile of the drug[113, 116, 117].

For example, the interplay of two efflux transporter proteins ABCB1, ABCC2 and the metabolising enzyme UGT1A1 influences the absorption of the cholesterol-lowering ezetimibe[116]. However, co-medication with rifampicin induces intestinal expression of these proteins (more efflux and more metabolism), resulting in a lower plasma concentration of ezetimibe and a reduced cholesterol-lowering effect[116]. Similarly, rifampicin co-administration with the beta1-blocker talinolol, an ABCB1 substrate, resulted in lowered AUC observed for talinolol[118]. Food also influences the activity of intestinal DMET proteins, as evidenced by a reduced uptake of the antihistaminic fexofenadine (competitive inhibition)[117] or reduced gut wall metabolism (CYP3A4 mechanism-based inhibition) of calcium channel blockers felodipine and nifedipine[119] after consumption of grapefruit juice. Metabolites of the immunosuppressant cyclosporin were observed in the plasma after administering the drug into the small intestine of patients undergoing liver transplantation during the anhepatic phase, evidencing the importance of the intestinal metabolism[37, 120].

In a similar approach during liver transplantation, it was observed that 43% of the parent drug midazolam was metabolised by intestinal DMET enzymes[121]. Both cyclosporin and midazolam had a greater bioavailability after co-ingestion with grapefruit juice as intestinal CYP3A4 was inhibited[122, 123]. In adult patients with ulcerative colitis (aged 32-68), the expression of P-gp, ABCC4, CYP3A5 and UGT2B7 was decreased during periods of active inflammation[124]. The observed intestinal interactions warrant investigation of DDI potential in children *via* PBPK modelling. Thus, to model oral absorption and DDI accurately, population-based variation in the expression and activity of DMET proteins needs to be well understood[114, 125]. This is done via integration of specific data on mRNA expression, protein expression or activity data from intestinal tissues[13, 126].

1.3.1.1 DMET protein in adults: intestinal DMET proteins

Current adult intestinal protein abundancy data is based on mRNA[127-133], immunoblotting[116, 118, 134] and LC-MS/MS[80, 125, 135-137] (see also section 1.4: Methods to study DMET protein abundance). However, there is considerably less data on DMET abundance in the intestinal tract compared to the liver. This is likely due to the more complex and heterogeneous tissue in the intestine in contrast to the homogeneous liver[34] (see sections 1.3.4 and 1.4.3.2) and the different function of the organs. As only mature enterocytes express DMET proteins, the presence of other intestinal cells that are also lysed during sample preparation methods dilute the protein pool. As a consequence, historically intestinal DMET assays exhibit low activity in comparison to their hepatic counterparts[79]. In addition, acquiring reproducible intestinal protein fractions is difficult due to the heterogeneity of the tissue and there is a lack of clear scaling approaches for extrapolation of *in vitro* results to *in vivo* implications. A

high interindividual variability is observed in intestinal protein levels, which increases the complexity to predict gut bioavailability[79, 134, 138].

Available data indicate DMET proteins are not expressed at the same level across all GIT segments[80, 125, 136], similar to variation in other physiological parameters like pH, mucosal characteristics and fluid content[139]. This results in absorption windows[140, 141] for certain drugs as the number of efflux transporters decrease or influx transporters increase, such as the proximal and distal windows reported for ezetimibe[116].

Within the adult population, there is no evidence for correlations between intestinal DMET levels and age[80, 137, 142]. Miyauchi *et al.* reported an intermediate correlation between Body Mass Index (BMI) and CYP1A2 expression (R^2=0.58, n=9) but not with other DMET proteins[142]. There is evidence that disease or smoking influences intestinal expression. So did smoking significantly increase expression of UGT1A1 and UGT1A3 (smokers, n=3; non-smokers n=25) [142], or is there a significant decrease for P-gp, ABCC4, CYP3A5 and UGT2B7 proteins during inflammation periods of ulcerative colitis[124], where severity of the inflammation is correlated with the level of decrease. Hence, it is difficult to present a general guideline of DMET expression influencing factors.

1.3.1.2 DMET proteins in paediatrics

In recent years, there has been more investigation into the ontogeny of ADME processes in children as details on intestinal DMET ontogeny are largely unknown[13, 33, 98, 126]. In contrast, the paediatric liver has been more studied, similar to adults, as hepatic DMET activity is usually more significant in both age groups[143, 144].

A recent review (Streekstra *et al*., 2021[145]) on DMET protein quantification via LC-MS/MS (currently the most sensitive technique for measuring protein abundance, see section 1.4, Methods to study DMET protein abundance) in the paediatric liver[145-157] and kidney[158, 159] evidenced these organ-dependent ontogeny patterns (see **Figure 1.2** and **Figure 1.3**) (Figures reprinted with permission, under the Creative Commons Attribution-Non Commercial-No Derivatives License (CC BY NC ND)).

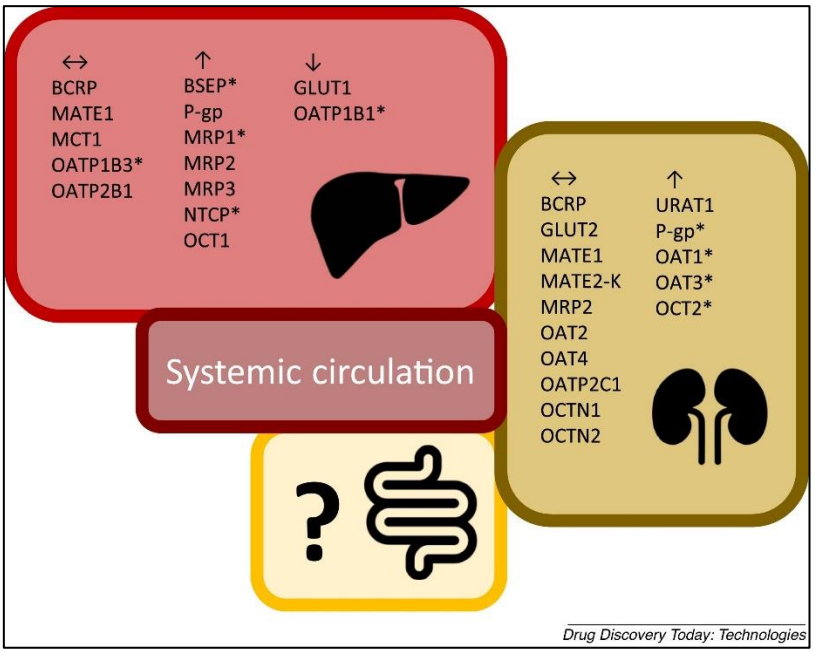

Figure 1.2. *Drug transporters ontogeny in liver (top), kidney (right) and intestine (bottom) (from Streekstra et al., 2021[145], with permission). Arrows indicate a higher (↑), lower (↓) or stable expression with age; *signifies novel reports in the Streekstra review.*

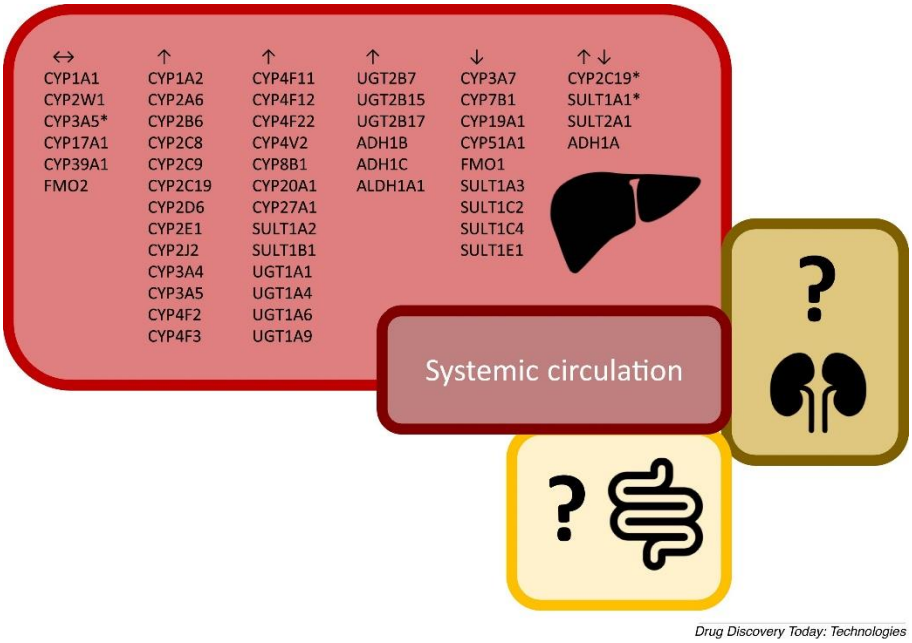

Figure 1.3. *Drug metabolising enzymes ontogeny in liver (top), kidney (right) and intestine (bottom) (from Streekstra et al., 2021[145], with permission). Arrows indicate a higher (↑), lower (↓) or stable expression with age; *signifies novel reports in the Streekstra review.*

In the adult population (studied on 18 -91 year olds), no correlation between age and DMET abundance in liver[39, 160, 161], intestine[142, 162, 163] brain[164, 165] and kidney[163] has been observed, despite a clear difference in expression with paediatric age groups as reported by the review of Streekstra. There was no proteomic quantification of paediatric intestinal DMET proteins available for this Streekstra review, only mRNA expression data, which is not always a good measure for protein abundance. Historic intestinal DMET ontogeny data is based on mRNA expression and immunohistological data from paediatric intestine[5, 6, 146, 166-170].

Johnson *et al*., 2001[5] investigated duodenal CYP3A4 expression in 104 paediatric patients (aged 2 weeks – 17 years, and 11 foetuses) via mRNA expression and western blotting and oxidation of testosterone for CYP3A4 activity measurement. Expression and activity increased significantly with age ($p < 0.05$ in both cases), although this correlation was weak ($R^2 = 0.19$ and 0.17 respectively, **Figure 1.4**).

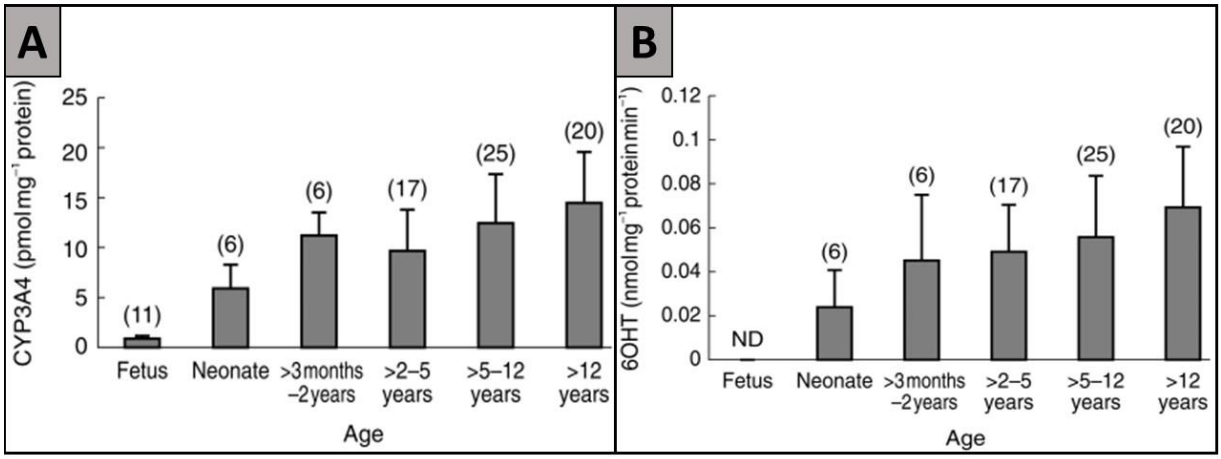

***Figure 1.4**. (A) Expression and (B) activity of duodenal CYP3A4 increases with age. Data presented as mean (bar) and SD (whisker), with number of samples in brackets. Figures reprinted from Johnson et al., 2001[5], with permission.*

Intestinal ABCB1 was not detected using immunochemistry in the first trimester of a foetus, but was found at stable adult levels from around 12 weeks of gestation[33, 171]. There is a large interindividual variability reported, and expression is also influenced by disease as shown for children with coeliac[172] and Crohn's disease[173]. However, most mRNA expression data indicate ABCB1 expression reaches adult level quickly after birth[33, 167, 171, 174-176].

The first (and currently, only) LC-MS/MS-based quantification of intestinal DMET proteins was reported in 2021 (Kiss *et al*., 2021[98]). They reported higher adult levels in the ileum for BCRP, P-gp, PEPT1 and UGT1A1 compared to paediatric ileum samples (0-18 year old). In the jejunum, adult levels of BCRP, MRP2, UGT1A1 and CYP3A4 were higher than the corresponding levels observed in the 0-2 years age group. On a continuous age scale, there was with a clear direct correlation between age and PEPT1 and UGT1A1 abundance and inverse correlation of age with UGT2B7[98].

1.3.1.3 Target proteins of interest

Twenty-one intestinal DMET proteins (**Table 1.4**) are of greatest interest for the pharmaceutical industry due to their clinical relevance (see section 1.1.2) and impact on the

PK profile of a large number of drugs. As these are crucial to drug disposition[145], the most common clinically important proteins from drug transporter and metabolising enzymes are studied. The selection of transporters is based on recommendations from scientific consortia (such as the Paediatric Transporter Working Group[33] or the International Transporter Consortium, which is composed of experts in the PK field from industrial, regulatory and academic institutions[177-179]). The recommendations from the International Transporter Consortium are built on clinical evidence of influence of the drug transporters on drug bioavailability and prevalence/severity of side effects[178].CYP enzymes are involved in the metabolism of nearly 70% of drugs administered to children[13]. Selection of drug transporters was based on clinical relevance and prevalence in involvement in drug-drug interactions based on inhibition/induction mechanisms[180]. Additionally, most of these proteins have previously been studied in adult and paediatric intestinal tissue[80, 98, 124, 125]. **Figure 1.5** gives an overview of the localisation of the intestinal DMET proteins under investigation.

Table 1.4.*An overview of the 21 target DMET proteins of specific interest in this project and two markers.*

Transporter proteins	CYP enzymes	UGT enzymes	Other enzyme	Markers
ABCB1; P-gp; MDR1	CYP2C9	UGT1A1	CES2	Na/K+-ATPase
ABCC2; MRP2; cMOAT	CYP2C19	UGT1A3		VIL1
ABCC3; MRP3	CYP2D6	UGT1A4		
ABCC4; MRP4	CYP2J2	UGT1A8		
ABCG2; BCRP	CYP3A4	UGT1A9		
SLC15A1; PEPT1	CYP3A5	UGT2B7		
SLC22A1; OCT1		UGT2B17		

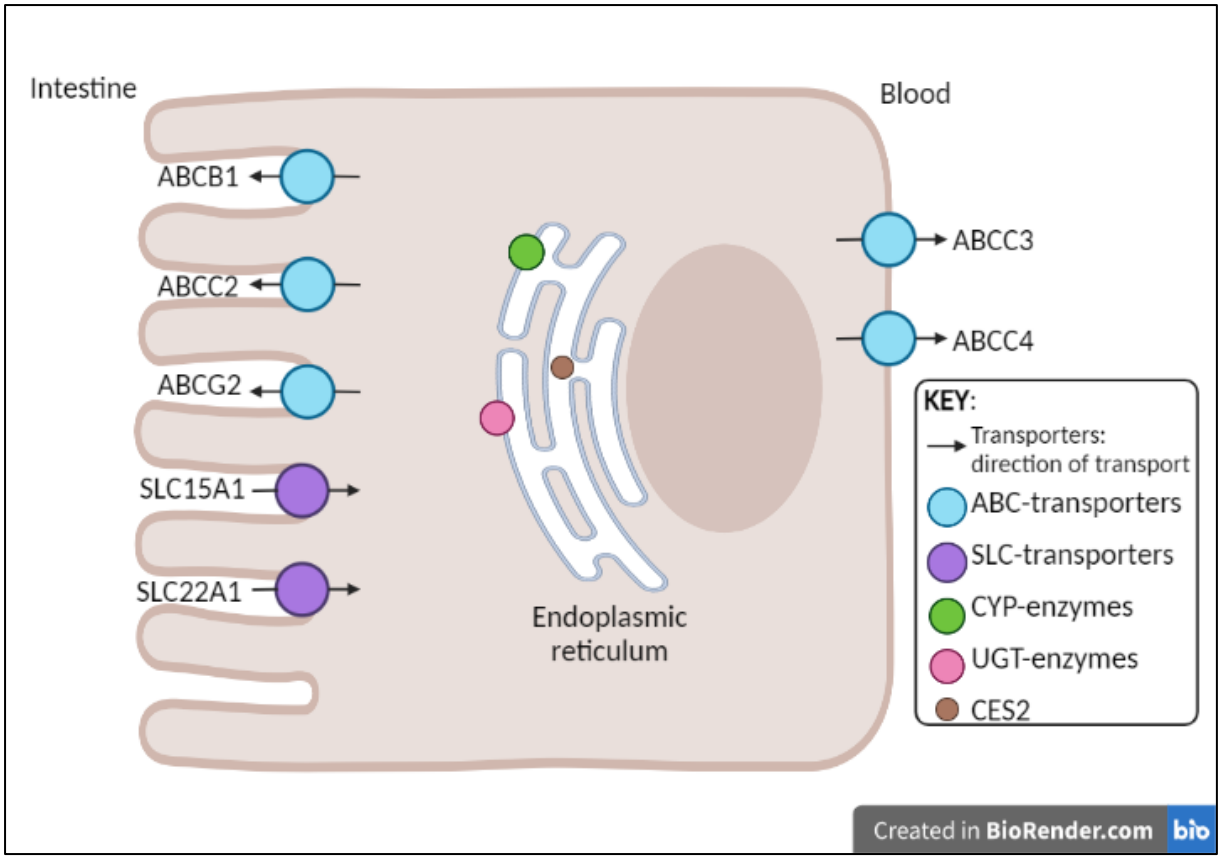

***Figure 1.5.**: Schematic overview of the localisation of the intestinal DMET proteins under investigation within an enterocyte. Created with BioRender.com*

1.3.2 Transporter proteins

More than 400 transporters have been identified in the genome and are classified in one of two superfamilies: the adenosine triphosphate (ATP)-binding cassette (ABC) superfamily and the solute carrier (SLC) superfamily[177]. **Table 1.5** summarises the synonyms, location, direction of transport and adult intestinal expression patterns for the 7 target transporter proteins in this work.

ABCB1 is one of the most studied transporter proteins, due to its broad substrate specificity and clinical relevence[13]. MRP2 transports organic anions across the plasma membrane, such as conjugates with glutathione, sulphate and gluceronides[34, 125, 142, 181].A strong correlation between the expression of UGT1A1 and MRP2 is observed[125, 182, 183], where it is believed MRP2 transports glucuronide metabolites formed by UGT1A1[184]. ABCC3 is involved in

enterohepatic recirculation of bile acids (together with ABCC2 and other transporter proteins)[185]. Similar to ABCC2, glucuronides and anions are substrates for this transporter, where it effluxes drugs and conjugates into the blood[34, 125, 142, 186]. Basolateral MRP3 works synergistically with the apical PEPT1 to increase uptake of e.g. cephalosporins (such as cefadroxil) to transfer these compounds into the blood stream[187]. Similar to ABCC3, ABCC4 enables systemic uptake of compounds. The individual role of MRP4 has not been clarified yet[186], however literature suggests this protein also aids in cefadroxil uptake[187]. PEPT1 imports a wide range of compounds across the plasma membrane, such as antiviral drugs, beta-lactam antibiotics (e.g. amoxicillin[125]), nutritional dipeptides and angiotensin-converting enzyme (ACE)-inhibitors such as fosinopril[188, 189]. It has an expression peak in the proximal ileum, which corroborates with e.g. the absorption window of amoxicillin[125, 190-192]. It also transports di-and tripeptides and prodrugs. PEPT1 is responsible for 90% of the oral absorption of valacyclovir[193, 194], based on comparison to knockout PEPT1 mice[195]. The PK profile of valacyclovir is non-dependent on mRNA expression levels of PEPT1[195], suggesting that mRNA expression and PEPT1 activity are not directly correlated[166, 167]. .

Table 1.5. *Overview of selected drug transporters and observations made in healthy adult intestine.*

Protein name and synonyms	Location	Direction	Adults
ABCB1; P-glycoprotein; P-gp; multidrug resistance protein 1; MDR1[98, 115, 196]	Apical	Efflux	Most[163] or second[80, 137] most expressed ABC transporter in jejunum and ileum. Around 1 pmol of protein per mg total mucosal protein[80, 137, 196] Increases in expression from duodenum to ileum, with three times more expression in distal ileum compared to duodenum[125]. Strongly correlated with CYP3A4 expression[80, 125, 137].
ABCC2; Multidrug resistance-associated protein 2; MRP2; canalicular multispecific organic anion transporter 1; cMOAT	Apical	Efflux	Some papers report this as the most expressed ABC-transporter[136], with peak expression in the jejunum in adults[135, 196], but not all publications are in agreement[80, 115, 137, 142, 197]. Strongly correlated with UGT1A1 expression[125, 182, 183].
ABCC3; Multidrug resistance-associated protein 3; MRP3	Basolateral	Efflux	Expression increased along the GIT[196]. Most abundant transporter protein in the colon[125]
ABCC4; Multidrug resistance-associated protein; MRP4	Basolateral	Efflux	Peak of expression peaks in the colon[135].
ABCG2; Breast Cancer Resistance Protein; BCRP[115]	Apical	Efflux	Most abundant efflux transporter in jejunum and ileum in some[115] but not all reports[125, 196, 198]. Some reports observe a peak of expression in the ileum[125, 135, 196], but not all reports[80, 137].
SLC15A1; influx oligopeptide transporter peptide transporter 1; PEPT1	Apical	Influx	Most expressed transporter along the small intestine, with a peak in proximal ileum, according to most proteomic and mRNA expression based publications [125, 129, 130, 135, 142, 166]
SLC22A1; organic cation transporter 1; OCT1	Apical or basolateral (uncertain localisation[199])	Influx	Adult proteomic assays struggled to quantify this organic cation transporter 1 (OCT1) transporter protein. It was below the limit of quantification (LOQ) in the adult jejunum[142, 196] but was detected in adult ileum[196]. No differences in protein and mRNA expression have been observed between the small and large intestine for this protein.

Table 1.6.*Overview of observed ontogeny of selected transporters based on mRNA, immunohistological or proteomic data.*

Protein name	mRNA/WB ontogeny	Proteomic ontogeny[98]
ABCB1	No difference to adults after 12 weeks of gestation[167, 171, 174-176]	Significantly different in ileal abundance between the 0-2 year old and adults (adult expression was more than threefold higher). Similarly, a positive correlation between age and ileal expression was found in children (0-18 year), although not-significant (n=48). Correlation with PEPT1 was observed
ABCC2	Adults have a significantly higher expression of ABCC2 compared to neonates and infants (along the entire small intestine), based on mRNA expression[167] and proteomic data[98].	
ABCC3		No statistical significant observations were made on paediatric ABCC3 expression[98].
ABCC4	N/A	N/A
ABCG2	No trend with age observed in foetal mRNA expression data[171].	Threefold higher in adult jejunum compared to 0-2 year old cohort. Significantly higher expression in adult ileum compared to in 0-2 year and 12-18 year old cohorts[98]. Significant correlation of jejunal BCRP expression with age in the paediatric (age range not given, n=10)
SLC15A1	Increase with age based on mRNA expression data, [166]. Ileal mRNA levels in neonates were at 80% of adolescent levels	Adult protein levels were at least double than those observed in the ileum of 0-2 year olds. A positive correlation between ileal PEPT1 expression and age observed
SLC22A1		a significant correlation between the protein expression of OCT1 and CYP2C19 in the paediatric ileum[98].

1.3.3 Metabolic enzymes

CYP enzymes, and especially CYP3A enzymes, are the most studied drug metabolic enzymes due to their broad substrate specificity and influence on bioavailability[200]. CYP3A accounts for 70% of all CYP enzymes in the intestine and are involved in the metabolism of 70% of the drugs currently used[13, 121]. Intestinal CYP3A4 is expressed exclusively in the endoplasmic reticulum of mature enterocytes. When enterocytes mature, they migrate to the tip of the villus in the intestine[35, 79, 201].

UGT enzymes catalyse the transfer of a glucuronic acid to amine, carboxyl and hydroxyl groups[38], decreasing the hydrophobicity to facilitate compound elimination[202]. The main route of clearance for 10% of the most prescribed drugs relies on UGT-conjugation[203]. According to proteomic quantification of the adult small intestine, UGT2B17 is the most abundant protein, followed by UGT1A1 and UGT2B7[204, 205]. Large interindividual variability in UGT1A1 levels has been reported (within 35-fold in 15 adults[142]), both in LC-MS/MS based quantification and western blotting[134], which is suggested a link to induction and inhibition of expression via environmental chemicals, diet and drugs such as irinotecan[142, 206]. A significantly higher protein expression level was observed in adult smokers compared to non-smokers[142]. A thirty-fold higher UGT1A8 abundance was found in healthy adult intestinal microsomes[204] compared to obese adult patients[142]. This might be due to inter-individual variability, regional differences (healthy duodenal samples vs obese jejunal samples) or be linked to obesity pathophysiology.

Intestinal carboxylesterase 2 (CES2) , also called cocaine esterase 2, is involved in the hydrolysis of and can be found in the lumen of the endoplasmic reticulum[207]. An overview of the selected metabolising enzymes and intestinal observed data is given in **Table 1.7**.

Table 1.7. *Overview of selected drug metabolising enzymes, substrates and observations made in healthy adult and paediatric intestine.*

Enzyme	Examples of substrates	Adults	Ontogeny
CYP3A4	Ropivacaine[208], midazolam[209-211]	Highest expressed CYP enzyme in the intestinal tract, with significantly higher levels in the jejunum compared to other GIT segments[80, 96, 134, 135, 142, 162]. Correlating with CYP2D6[80, 137], with P-gp[80, 125, 137, 182, 183]	Proteomics ↑[98] Immunohistological data ↑[5, 173, 175, 212], mRNA expression ↓[173, 175, 212].
CYP3A5	Tacrolimus[213, 214]		
CYP2C19	Esomeprazole, pantoprazole[215]	Correlating with CYP2C9[80, 137]	In paediatric ileum, a negative correlation in expression was observed with post-natal age, however not significant[98]. A significant correlation was observed between paediatric CYP2C19 and OCT1 protein levels
CYP2C9		Second most expressed CYP enzyme in the small intestine in most reports[96, 134, 135, 142, 162]. Strong correlations with CYP2C19, and CYP2J2.	
CYP2J2		Strong correlation with CYP2C9 and CYP2D6 expression[80, 137].	
CYP2D6	Codeine[216]	Second most expressed CYP enzyme in jejunum and ileum according to one publication[80]. Significant correlations were found between CYP2D6 and CYP2J2, and CYP3A4 expression[80, 137].	
CES2	Aspirin[217], irinotecan[218]	Stable expression of CES2 along the GIT tract in adults[219]	In neonates- infants (0-332 days), mRNA and protein levels significantly increased with age[212].
UGT1A1		Second most abundant UGT in small intestine[162]. Strong correlations with UGT2B7 levels[80, 137, 142, 204, 205] and MRP2[125, 182, 183].	Tenfold increase for ileal and 24-fold increase of jejunal expression in adults compared to 0-2 year olds[98].

UGT1A3	Bile acids[220], non-steroidal anti-inflammatory drugs (NSAIDs)[221] and statins[38, 222].	Third most abundant UGT enzyme in the small intestine[80], however this enzyme was below the limit of quantification in multiple papers, hence its abundance in adult is not clarified yet.	No proteomic data on paediatric intestinal levels are available[98].
UGT1A4	Midazolam [223, 224]		No paediatric intestinal proteomic data are available[98].
UGT1A8	Raloxifene[225]		
UGT1A9	NSAIDs and steroids[202]	Only three publications attempted to quantify UGT1A9 in adults by LC-MS/MS[204, 205]. One reported an abundance of 6.6 pmol/mg protein (n=3)[204] whereas the other two papers did not detect UGT1A9 in adequate levels for quantification (n=10[205] and n=28[142]).	
UGT2B7	Chloramphenicol[226-230]	Only 0.6% of adult UGT2B7 levels was found in the intestine, with the remaining 99.4% in the adult liver, yet, UGT2B7 is the second most expressed UGT in the small intestine (together with UGT1A1), after UGT2B17[80, 137, 162, 231]. A strong correlation with UGT1A1 expression was detected in intestinal samples[80].	A negative correlation was found between age and ileal expression in children (n=48), indicating UGT2B7 levels decrease with age[98].
UGT2B17		Highest expressed UGT in adult intestine based on proteomic and mRNA data, with an abundance peak in the jejunum[142, 162, 232]. However, despite being the most abundant UGT, proteomic assays failed to detect the enzyme in one adult patient (and just above the limit of detection in a second adult) out of cohort of 28 adults, with a 364-fold inter-individual variability reported[142].	No proteomic data for UGT2B17 in the paediatric intestine has been reported[98].

1.3.4 Heterogeneity in the small intestine: enterocyte markers

Projects aiming to quantify intestinal DMET protein abundance and activity rely on acquiring intestinal tissue. For this, biopsies, waste tissue from surgical procedures and post-mortem organs can be used. However, compared to hepatic tissue, intestinal samples suffer from a large sample heterogeneity as the small intestine is a complex organ consisting of different layers. Only a fraction of a paediatric pinch biopsy will consist of enterocytes[201, 233], as it only accounts for 25% of the wet mucosal weight[79, 234], yet makes up for 90% of the epithelium, with 9% goblet cells and 1% enteroendocrine cells[235]. The small intestinal mucosa is renewed every 4-5 days[236, 237]. Enterocytes line the gut lumen, where microvilli increase the absorptive area of the intestine signficiantly[238, 239]. Upon maturation, enterocytes migrate to the villus tip and become metabolically active and express drug transporters[79]. Thus, to ensure measurement of protein abundance and activity from mature enterocyte only, and to correct for sample heterogeneity (and to allow scaling purposes for PBPK modelling) an enterocyte marker is required[98].

1.3.4.1 Villin-1

Villin-1 is an actin-binding brush border-specific protein, found in enterocytes, the duct cells of pancreas and bile bladder and in the epithelial proximal tubules cells in the nefron[238-242]. In the small intestine, villin-1 levels increase with enterocyte maturation[238-240, 243], so it is a suitable mature enterocyte marker[241]. It is frequently used as marker and correction factor for mature enterocytes when analysing DMET protein abundance (via messenger RNA (mRNA), immunohistological assays or LC-MS/MS). Studies on paediatric intestine do not report significant changes of villin-1 levels across different age groups (from foetus to 16

year old and adults) or influence by sex, and is detected in all intestinal paediatric samples (**Figure 1.6**) [5, 98], hence there is no evidence for ontogeny of this protein.

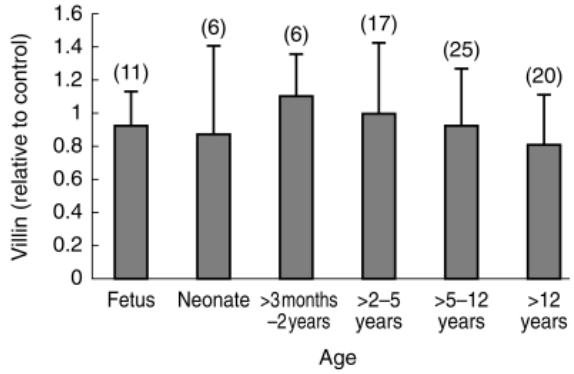

Figure 1.6. *Villin-1 expression across different age groups (relative to the average signal of villin-1 in a sample from a 4 year old and 50 year old). The mean (bar), standard deviation (SD) (error bar) and number of samples (between brackets) are given. Figure reprinted from Johnson et al., 2001[5], with permission.*

Using the epithelial villin-1 protein as a marker of harvested enterocytes, the abundance data results can be corrected for variation in the number of enterocytes in the collected biopsy (deep, shallow etc.)[5, 35, 142, 201]. Reciprocally, a low villin-1 number could indicate a low number of enterocytes have been samples in an intestinal biopsy or premature proteolysis, and would explain if target proteins fall below the limit of quantification in proteomic assays[98].

1.3.4.2 Plasma membrane markers

Historically, proteomic assays aiming to quantify intestinal drug transporters via LC-MS/MS reported difficulties in obtaining a plasma membrane protein fraction (see section 1.4.3.4). In contrast, intestinal microsome fractions (containing the endoplasmic reticulum) can be easily obtained after scraping the mucosa or dissociation of the enterocytes, subsequent homogenisation followed by calcium aggregation and/or centrifugation[244, 245]. However, a wide variation in methodologies exist with different yields, see section 1.4. Differential ultracentrifugation and commercial kits have been used to obtain plasma membrane fractions[115, 125, 196]. To interrogate plasma membrane isolation, two plasma membrane

marker proteins have been used[80, 115, 137]; the sodium/potassium-transporting ATPase subunit alpha-1 (Na/K-ATPase)[115] and the human peptide transporter 1 cadherin-17 (CDH-17)[80, 137].

1.4 Methods to study DMET protein abundance

Reliable quantification of intestinal paediatric DMET proteins are of great interest[33, 142, 177]. However, comparison of results between laboratories is challenging due to a great variation in sample collection, preparation and analytical methods[79]. Pinch biopsies can differ in size and enterocyte count, although this can be accounted for using villin-1 as a marker[5, 142, 201]. Various steps to isolate the enterocytes exist: i) scraping of the mucosal layer[170, 244, 246], ii) dissociation of the tissue layers with enzymes (trypsin, hyaluronidase, collagenase)[114, 244] iii) enterocyte elution with calcium chelation (with ethylenediaminetetraacetic acid, EDTA)[115, 245], iv) sometimes no isolation is carried out[80, 125, 142, 196]. It has been demonstrated that the isolation method has an impact on the subsequent protein quality[79, 144]. Additionally, various methods of cell lysing exist, including mechanical disruption[196, 247] and chemical stress[114, 125] among other methods such as nitrogen cavitation[142]. Multiple ways to isolate the protein fraction from the homogenates have been performed, using specific commercial kits[125, 196] or consecutive (differential) ultracentrifugation steps[142, 247]. A wide range of buffers in both composition and concentration have also been used[79], so it is clear there is no standardised protocol for intestinal DMET isolation and quantification.

Furthermore, different analytical methods to study DMET protein abundance and activity have been used, with some conflicting results[33]. Messenger RNA (mRNA) data has been quantified as a surrogate for protein abundance, as it is assumed the concentration of mRNA is directly related to protein translation[248]. However, it has been demonstrated that this is not necessarily a measure of final protein concentration or activity[125, 142, 167, 196]. Immunohistological quantification and western blotting rely on recognition of an epitopic sequence on the protein via antibodies. However, for accurate quantification of protein

content a significant amount of tissue is required, which is not always directly accessible in paediatric intestine[98].

As a result of recent advances in liquid chromatography-tandem mass spectrometry (LC-MS/MS)-based quantification of peptides, proteins can be quantified[115, 125, 196]. By quantifying a peptide sequence that is unique to a certain protein (proteotypic), the concentration of the peptide is directly equivalent to the concentration of associated proteins in the measured sample[249]. Targeted quantitative proteomics have the advantages of being able to multiplex, i.e. quantifying multiple proteins simultaneously.

1.4.1 mRNA analysis

Isolated mRNA can be quantified using Reverse Transcription – Quantitative Polymerase Chain Reaction (RT-qPCR) quantification[248, 250-253]. The enzyme reverse transcriptase is a DNA polymerase, catalysing synthesis of complementary DNA (cDNA) strands using an RNA strand as template. The cDNA is then amplified in PCR cycles, using DNA sequence-specific oligonucleotide primers and nucleotides and cycles of heating and cooling. The amount of DNA formed can be quantified using fluorescent markers, such as SYBR green[254] and Taqman primers[255, 256]. The cycle in which the measured signal crosses a threshold value (the threshold cycle, C_t) is inversely related to the starting amount of the target DNA. Normalising the Ct value of a specific gene (such as the endogenous eukaryotic 18 sRNA) allows to compare across samples (e.g. between adults and paediatrics) to see fold-changes in expression[252]. However, mRNA is a poor indicator for the intestinal protein abundance, as conflicting trends have been observed and mRNA results are not consistent[127-131]. ABCC2 protein levels were higher in the colon of adults compared to proximal intestine, yet mRNA levels were significantly lower in the colon of the same individuals[135]. As another example,

Mooij *et al*., 2014, saw a decrease in immunohistological staining of transporter PEPT1 with age, whereas mRNA expression was increasing. In addition, mRNA-expression data does not account for post-translational modifications, or enzymatic activity[114, 142, 161].

1.4.2 Western blot

Western blotting is an immunochemical technique where proteins are separated by molecular weight, specifically recognised by antibodies and subsequently visualised and quantified[257-259]. Although having the advantages of being a sensitive method and being able to quantify expression on protein level, immunochemical quantification is a suboptimal technique for quantification of low abundant DMET-proteins in the paediatric intestine[98, 196]. Western blot assays suffer from poor reproducibility and accuracy and sample throughput is low yet the process is labour-intensive[197]. Additionally, antibodies are expensive, can take a while to be produced and in some cases lack specificity, especially in the case of proteins with high homology in amino acid sequence like CYP enzymes, thereby limiting the outcome[118, 197, 260]. Where available, most western blot and proteomic protein data are mostly in agreement. For example, both techniques saw an increase of intestinal CYP3A4 abundance with age[5, 98, 212].

1.4.3 Proteomics

1.4.3.1 Introduction

Proteomics is the gold standard for intestinal DMET protein quantification. Although proven as a valuable tool in quantifying different proteins in a range of tissues, different choices at the various stages of sample preparation makes inter-lab comparison challenging. Indeed, the proteomic community is calling on for a gold standard approach to streamline intestinal

sample processing and to allow comparison of abundance values between laboratories[113, 162]. With normalisation procedures, direct comparison will be facilitated. However, the wide variation in tissue preservation, membrane fractionation, use, timing and concentration of protease inhibitor cocktails (PIC), sonication and digestion procedures and selection of labelling of target peptides do not allow for this comparison to be made currently. Additionally, despite the growing number of publications in the last decade, there still is room for more research, especially concerning quantification in special cohorts[196].

To be able to measure proteotypic (signature) peptides on an LC-MS/MS instrument in a proteomics experiment, a few preparation steps are necessary. A proteomic workflow is described as follows (see also **Figure 1.7**).

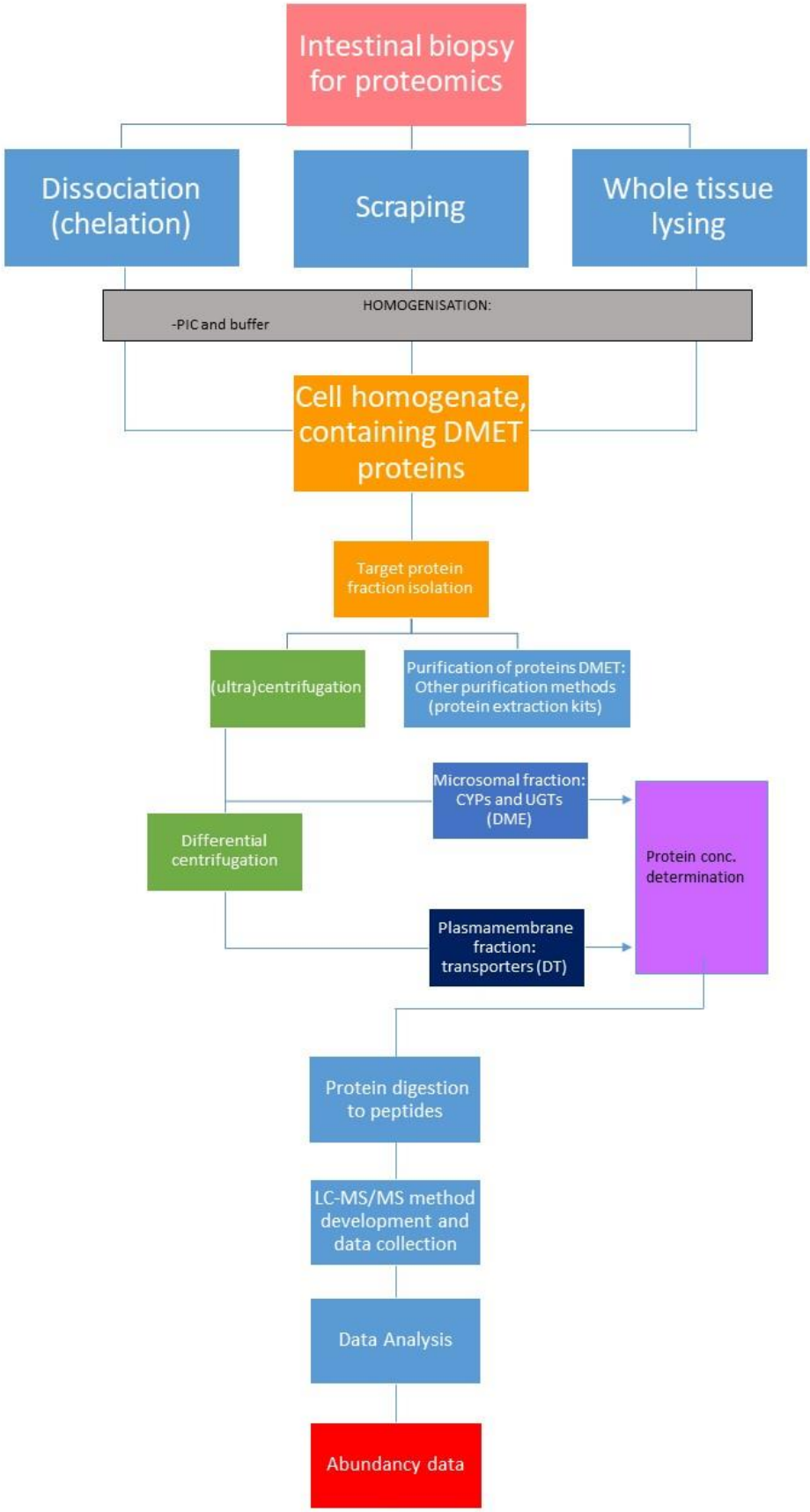

Figure 1.7. *Overview of a proteomics workflow to quantify intestinal DMET proteins*

Firstly, the cells containing the target proteins need to be isolated from the tissue of interest and then lysed to harvest the target proteins. Then the protein fractions are purified, and subsequently digested into peptides by proteases which catalyse the hydrolysis between specific amino acid residues. For example, trypsin hydrolyses the peptide bond at the carboxyl side of arginine (R) or lysine (K) residues, except when the following amino acid is a proline (P)[261-263]. Based on what protease is used, the sequence of the resulting pool of peptides can be predicted. Next, relevant peptides that meet pre-determined criteria (such as amino acid length, certain chemical properties[113, 264, 265]) with amino acid sequences only occurring for the specific protein of interest, are analysed and quantified using mass spectrometry. Peptide identification is based on the sequence-specific mass transitions pattern and quantification on signal intensity (AUC) in relation to the signal of a known concentration. As the tryptic digestion is assumed to be completed (i.e. no missed cleavages), the molarity of the proteotypic peptide in the sample is directly correlated to the initial protein concentration in the sample and the protein abundance in the tissue can be calculated[196].

Over the last decade[196], targeted quantitative proteomics (TQP) has become the standard approach to measure the abundance of proteins, with transporter proteins such as ABCB1, ABCC2, ABCG2 and others already quantified in human tissues (liver, brain, kidney) and cell cultures (hepatocytes and platelets[266])[196]. Kamiie *et al*.[264] reported the first multiplexed analysis of intestinal transporters in mice in 2008, followed by Groer *et al.*[196] in 2013 to publish a validated method on human transporters, with now a bigger number of publications on intestinal DMET proteomics. Recently, proteomics was used for the first time on paediatric intestinal samples, after being used to quantify DMET-proteins in liver

and kidneys. A large interindividual variability has been observed in these paediatric studies, making it challenging to observe changes with age[145].

Targeted proteomics require less material compared to immunoquantification, and allows for simultaneous detection of a range of target in a single run (i.e. multiplexing[267]). As the mass transition (multiple reaction monitoring, MRM) pattern is amino acid sequence-specific, identification of the peptide and quantification are performed at the same time. Cross-specificity with other proteins (which sometimes is the case with antibodies) is not observed with LC-MS/MS, unless a peptide sequence occurs on multiple proteins. However, this could still be useful to quantify multiple proteins simultaneously using a method of difference, as done for UGT1A8 and UGT1A9[98]. Adding an internal standard in the form of a labelled version of the target peptide (stable isotope labelled, SIL[268]) into the sample allows for absolute quantification values rather than a relative fold-change (as done with mRNA expression analysis). Additionally, using a chemical identical version of the target peptide, where only the isotope mass is different but other characteristics are unaltered, allows to account for losses during the sample clean up (e.g. unspecific binding of peptides to lab material) or interference in the mass spectrometer. Method validation in terms of accuracy, precision and stability of the proteomic workflow on intestinal DMET have been demonstrated[125, 196]. Additionally, LC-MS/MS based of proteomics is a good balance of precision (compared to mRNA), required time for method optimisation strategies and cost-effectiveness (compared to expensive antibodies).

For paediatric intestinal DMET protein quantification, three reports are key. Kiss *et al*. (2021)[98] used jejunal and ileal tissue from children (0-18 year, n=58) and adults to quantify a

comparable selection of target proteins. The tissue was cryopulverised (1.4.3.3), homogenised on ice and sonicated for liberation of the proteins. The homogenate was then ultra-centrifuged, and the pellet resuspended in a buffer containing an anionic surfactant. After spiking in stable-isotope-labelled standards (SIL, 1.4.3.12) for every peptide target under investigation, the crude protein fraction was in-solution digested to obtain a peptide pool. This is the only paediatric intestinal DMET proteomic report to date.

Harwood *et al*. (2015)[115] selectively studied transporters from adult intestinal tissue (41 – 70 years old, n=4, jejunum and ileum) using a chelation procedure that liberated the enterocytes from the underlying layers (see also **Table 1.8**). For this, larger pieces of tissue were available, which were placed in tissue adaptors to expose the intestinal mucosa. The isolated enterocytes were then homogenised on ice, and the resulting homogenate was purified using different steps of differential centrifugation to obtain a fraction that only contained the cell membrane fraction. However, using multiple ultra-centrifugation manipulations resulted in a loss of protein[269].Then, TransCAT (a QconCAT standard, see 1.4.3.12.2) was spiked in prior to in-solution digestion. This was the first use of a QconCAT in intestinal proteomics, where the peptide sequences of the different targets are fused together using proteolytic bonds (for a more detailed explanation on QconCAT and its benefits, see 1.4.3.12.2).

Couto *et al*. (2020)[80] used adult jejunal and ileal samples (n=16), where the mucosa was isolated using blunt dissection (**Table 1.8**). The resulting tissue was snap frozen and cryopulverised using a cooled mortar and pestle. The homogenate was then resuspended in radioimmunoprecipitation assay (RIPA) buffer (see also section 1.4.3.5) which contained surfactants to disrupt the cell membranes and solubilise the proteins. As such, a crude membrane fraction was obtained using only minimal manipulation steps. Then, a filter-

assisted sample protocol (FASP, see 1.4.3.7) was used after spiking in two QconCATs, for both transporters (TransCAT) and drug metabolising enzymes (MetCAT). This was the first report to use RIPA for protein extraction, and to investigate metabolising enzymes using a QconCAT technique.

1.4.3.2 Tissue collection and isolation of enterocytes

Proteomic analysis of DMET proteins has been performed on adult intestinal tissue (donors ranged 18 – 80 years old). Sections investigated span the entire intestinal tract, from duodenum to colon[80, 98, 125, 270]. The tissue was frequently obtained during surgical diagnostic biopsies or disease-related resection, where the healthy margin of resected tissue was used (free of macroscopic inflammation or necrosis[80, 98, 115]). Additionally, some tissue was collected post mortem from brain-dead donors, with or without gastrointestinal complications[125, 270]. Different sizes have been investigated, ranging from pinch biopsies[247], to mucosal sections of 50 mg[196] or entire small intestines[270].

Paediatric jejunal and ileal tissue, obtained as leftover tissue from surgery (no diagnosis or procedure mentioned) from 58 patients aged 0.1 week - 17 year old) has also been studied[98], where an average biopsy size of 150 mg was reported. Achour *et al*. reported that an average tissue mass of 100 mg is required for adequate protein collection to ensure an adequate signal in the LC-MS/MS instrument[271].

The quality of tissue may affect protein expression and recovery level[142, 265, 271]. The method and consistency of how the tissue was isolated and preserved before processing, influences final tissue quality[142]. For example, tissue obtained after surgical resection is usually described as being stored cold and (within 30 min) snap-frozen[142], whereas tissue obtained-

post mortem was only frozen after collection of organs for transplantation was collected[125, 270], raising concern on quality. Usually, tissue is kept cold (4°C) and a protease inhibitor is added to prevent premature proteolysis[265, 272].

To improve the signal-to-noise ratio downstream in the MS detector, sample refinement and isolation of the target proteins/cells that contain these are frequently employed[265]. As such, the enterocytes are to be isolated and lysed as DMET proteins are located in the plasma-membrane and endoplasmic reticular-membrane. The extent of enterocyte isolation potential depends on the starting material. On bigger biopsies, mucosal layers or purely enterocytes could be isolated, as contamination of working sample with cells not of interest might dilute sensitivity – however, on smaller biopsies this may not be possible due to limitations in sample working size[79, 265]. Different strategies for enterocyte isolation have been pursued for various uses; yet there is no established best practice method. There is no consensus in literature on the best approach to isolate DMET proteins for investigation[79]. However, most analyses were performed on isolated mucosal tissue, which was separated by muscle and serosal layers by rapid blunt dissection[80], then flash frozen and stored prior to homogenisation[125, 142, 196]. A study on UGT abundance in the rectum[247] used pinch biopsies, which were frozen. Another study on transporters in adult jejunum and ileum[115] used fresh tissue from surgery, where the mucosa was washed and clamped onto custom-made tissue adaptors, after which the enterocytes were eluted via chelation with EDTA-buffers. A third study on CYPs in the entire small intestine[270] slightly thawed 10 cm portions of the entire small intestine and then scraped the mucosal layer off before further processing. An overview of the different methods to selectively isolate enterocytes is given in **Table 1.8**. In conclusion, enterocyte isolation is advised to improve signal, yet not completely necessary for proteomic quantification.

Table 1.8. *Overview of tissue isolation methods used in intestinal proteomic assays (+indicates a positive and – indicates a limitation of each method).*

Method	Explanation	Benefits (+)/disadvantages (-) in general DMET isolation
Blunt dissection[125, 135, 273]	Isolating the mucosa layer from underlying muscle tissue and basal layers by dissection	+ Removal of the outer layers is common in metabolic and permeability assays and proteomic assays[274, 275]; + less contaminating tissue for proteomic assay[79, 265]; + easy; cost-effective - No control of isolation; basal layers may not be removed adequately and contaminating cells could still be present; - cells could lyse prematurely due to cutting
Elution via chelation[115, 276]	Liberating the enterocytes from the basal lamina propria by dissociating cell-to-cell contact[142]. Solutions used include EDTA (a calcium chelating agent), collagenase and dithiotreitol[275, 276].	+ A wide range of elution buffers have been described in literature, yet only one applied for intestinal proteomics[115, 144, 245, 246, 277]. + Gentler than scraping, reduced risk of premature cell lysis[144, 245] + higher enzyme activity recovery than scraping[144, 245] + Can be combined with gentle agitation[115, 246] to vigorous shaking[277] to improve yield. - Yields a lower total membrane protein compared to mucosal scraping[197] (although this might be due to scraping also including the lower layers[115]) - Lack of standard method, with similar methods not giving similar results[275], so requires optimisation[114]. - Elution is not specific for villus-tip enterocyte liberation, also lower villous cells are liberated. Increasing incubation period also releases crypt cells[79, 246]. - Might be a limitation for basolateral membrane-bound transporter proteins[115, 142]

		- Sufficient sample size is needed[142].
Scraping[270]	Scraping of the mucosal layer with a glass slide or spatula, after which the scrape is dipped into a solution[79, 144, 275, 278]	+ Higher proportion of top villous cells (mature enterocytes) isolated[279] + Improved metabolic activity observed compared to whole-tissue lysing[279] (which may be due to dilution of whole tissue lysate by inert proteins). + Yields a higher protein membrane fraction compared to elution, yet this might be due to a fraction of underlaying tissue. - Harsh method, causes premature cell lysis and damages microsomal enzymes (CYP/UGT) as proteases are liberated[245, 280]. - Not selective isolation in comparison with elution[144]
Whole tissue lysing[98, 247]	No separation of cells	+ Easy; no risk of losing enterocytes + Well-developed LC/MS-MS method using internal labelled standards have been shown to be able to deal with whole-lysate targeted proteomics[98, 247] - Overestimation of number of enterocytes, but can be accounted for by villin-1 normalisation[98] - Contamination with muscle and serosal tissue and unwanted cells[79] dilutes protein concentration of target proteins[279].

1.4.3.3 Cell lysis

Different methods have been used to homogenise enterocytes. The most commonly used method homogenise the tissue mechanically manually on ice or with equipment cooled with liquid nitrogen. Historically, glass homogenisers (such as the Dounce[115, 125, 196] and Potter-Elvehjem[98, 142, 276] homogenisers)[142] have been used most frequently, next to bead homogenisers[247], or unspecified crushing methods[270]. However, a trend to cryogrinding can be observed, as the most recent DMET proteomics publications use this method. Cryogrinding (with liquid nitrogen, making the intestinal tissue very brittle) has been used with a mortar and pestle[80, 135, 162] or as an electric cryogrinder (Cryoprep CP02)[98]. Reviews comparing the different mechanical homogenisation techniques based on ease of use and robustness exists, yet not focused on intestinal tissue lysis for proteomic assessment[281]. Cavitation of cells via nitrogen gas bubbling through the cells has also been employed by Miyauchi *et al*.[142], as a second homogenisation step after original disruption with a Potter-Elvehjem homogeniser. By gradually increasing the nitrogen pressure in a cell filled tank, nitrogen dissolves in the cytosol. When the pressure in the tank suddenly drops, the dissolved nitrogen returns to the gas phase (i.e. it bubbles out of the cytosol), lysing the cell as it causes disruption to the cell membrane[282, 283]. Sonication, the use of intense ultrasound waves, is an efficient method to deagglomerate and disperse solid particles in liquids[284-286]. Only one intestinal DMET proteomic paper mention the use of sonication[98], yet it has been employed regularly as adjuvant to prepare intestinal microsomes[272, 279, 287]. Short burst of low intensity has been shown to improve yield of microsomal fractions, but prolonged use is destructive on CYP recovery[288]. Sonication heats up the sample, so a good balance of intensity and duration needs to be considered[79]. Additionally, repeated freeze-thaw cycles also have been used in proteomic quantification of membrane transporters[271].

1.4.3.4 Purification of target proteins

Multiple methods for fractionation exist, to selectively obtain microsomal (endoplasmic reticulum-bound proteins, such as CYPs/UGTs) or plasma membrane proteins (transporters). Commercial kits are available to isolate specific fractions of cellular proteins. The "ProteoExtract Native Membrane Protein" (Calbiochem) kit isolates plasma membrane-bound proteins and has been used for intestinal transporterproteomics[125, 196]. Roche's "cOmplete Lysis-M" isolates cytosolic and nuclear proteins and although shown to work in proteomic assays on HeLa cells, it has not yet been used in intestinal DMET proteomics[289]. However, the most frequently method employed [114, 115, 142] is to isolate and enrich protein fractions for both membrane-bound and microsomal proteins in a series of centrifugation and ultracentrifugation steps at 4°C. Many approaches and speeds have been used, with no standardised method.

Most reports split the homogenate pellet halfway processing to both isolate a membrane and microsomal fraction. Enriched fractions of low abundant proteins allow for highly reproducible quantification of proteotypic peptides as sensitivity is increased[113, 125, 196], however it has been demonstrated that multiple manipulation steps result in inherent loss of proteins[113, 269]. Therefore, recent papers omit this separation step. In the most recent (and only) paper on proteomic quantification of paediatric DMET proteins, the microsomal and membrane fraction were not separated after ultracentrifugation (thus a crude membrane fraction was obtained [98]). Similarly for adults, Couto[80] and Al-Majdoub[162] only used one centrifugation step (at 14,000 *g* for 5 min) as they used RIPA buffer which contains a harsh detergent, Triton X-100[80]. They report a similar recovery as methods that did use an ultracentrifugation step[115], but more importantly, not splitting the homogenate out allows for simultaneously detection of transporters and metabolising enzymes. Additionally,

Transmission Electron Microscopy visualisation has proven that a combination of RIPA-buffer and sonication was able to completely solubilise a protein layer formed by biofilms[290]. A second major limitation for the differential ultracentrifugation step is the necessity of a sufficiently large sample size to ensure adequate quantities at the purified stage. Miyauchi and Akazawa[142, 276] could not isolate plasma membrane fractions after ultracentrifugation from multiple samples due to the very small tissue volumes they had available. A decrease of the epithelial marker villin-1 was also observed (15.0 to 5.21 fmol/µg protein), which indicates protein loss[142].

1.4.3.5 Buffers for protein extraction

To increase homogenisation efficiency, protein extraction and to prevent premature proteolysis, buffer solutions are added as early on as possible. A wide range of buffer solutions are used at different stages in the protocol (protein extraction or as proteolysis buffer), usually containing (in varying concentrations)[80, 142, 162, 276] the following ingredients:

- a protease inhibitor cocktail (since enterocytes contain intrinsic proteases). The "*cOmplete Protease Inhibitor Cocktail (PIC)*" is widely used in 50 µL/mL, but other substances such as phenylmethylsulfonyl fluoride are available too[270].
- a surfactant, such as sodium dodecyl sulphate (SDS), sodium deoxycholate, polymer-based based detergents (Triton X-100 (non-ionic)), commercial surfactants (ProteaseMAX[125, 196, 291] or Rapigest[98]) or none[115, 247]. Poor removal of detergent could influence protease function or LC-MS/MS acquisition[271, 292, 293].
- a pH buffer (TRIS-HCl[115, 270] or phosphate buffer[247]) usually at pH 7.4[98, 115],
- salt components (NaCl[115], KCl[270], $MgCl_2$[115])
- EDTA[98, 247, 270]

- adding components to established buffers such as phosphate-buffer saline (PBS)[98] or radio-immunoprecipitation assay (RIPA)[80].
- and other components such as sucrose[98, 115, 247], histidine[98], leupeptine[270], aprotinin[270]or dithiotreitol[270].

In addition to the protease inhibitor cocktail, the risk of unwanted proteolytic activity is minimised by keeping the sample temperature cold (around 4°C)[125, 196, 247]. Most protocols mention variations in buffers, depending on the requirement sample preparation stage. However, Couto *et al.*[80, 137] used a RIPA buffer to resuspend the cryocrushed intestinal tissue, consisting of:

- 150 mM NaCl,
- 1% (v/v) Triton X-100,
- 0.5% (w/v) sodium deoxycholate,
- 0.1% (w/v) SDS,
- 50 mM Tris base (pH 8.0),
- protease inhibitors: 0.5 mM PMSF and 50 µL/mL PIC.

Incubating the resuspended powder at 4°C in the buffer for 30 minutes under agitation and subsequent centrifugation at 14,000 *g* for 5 minutes at 4°C gave a supernatant containing the target CYP, UGT and transporter DMET proteins. The buffer was not changed throughout the entire process, and no any additional fractionation of the homogenate was required other than the one centrifugation step. RIPA has been used before Couto's publication to extract whole-cell proteins fractions for western blotting[294] and for proteomics[293], including plasma membrane-bound proteins such as Na^+/K^+-ATPase[295] or endoplasmic reticulum-bound calreticulin[294].

1.4.3.6 Protein concentration determination

Before continuing to the next step in the proteomics workflow (protein digestion), the protein concentration needs to be determined. Various colorimetric existing assays are employed, with the most frequent being Pierce Bichinchonic Assay, followed by the Lowry[296-298] (Cu^{2+} to Cu^{+} reduction) and Bradford assay[297-299] (binding of a die to specific amino acid residues). There is no indication one method is superior to the other[300, 301]. The bicinchoninic acid (BCA) assay[302] relies on copper reduction as well. After reduction of the copper, a single Cu^{+} ion chelates with two bicinchoninic acid molecules[303]. This complex has a purplish colour, with A_{max} at 562 nm. The BCA assay is temperature dependent so temperature needs to be controlled[297].

Protein concentration is assessed by interpolation after construction of a standard curve with known concentrations, usually Bovine Serum Albumin (BSA)[80]. It has been proven that BCA assays and RIPA-buffers are compatible[290], whereas dilution of samples with water was required to decrease the interference of RIPA-buffer components on protein concentration determination in a Bradford assay[80, 162].

1.4.3.7 Protein digestion to peptides

In LC-MS/MS, proteotypic peptides are analysed which act as a surrogate for the parent protein. In order for proteases, such as trypsin, to adequately hydrolyse the protein into smaller peptides, every peptide bond of the protein needs to be accessible. To this extent, the proteins in the purified fraction are denatured, reduced, alkylated and ultimately digested. This can happen either in an SDS-PAGE gel (GASP, Gel Aided Sample Preparation)[304, 305], in solution[98, 115, 125, 196] or using filters (Filter Aided Sample Preparation –

FASP)[80]. Irrespective of protein digestion conditions, the methods of denaturation, reduction, alkylation and proteolysis of proteins are quite similar. All intestinal proteomic DMET reports use following chemicals for proteolysis preparation: as a denaturation agent: urea[80, 162, 271, 293] and a raised temperature (56 °C)[125, 196, 247], as reducing agent for disulphide bonds: dithiothreitol (DTT)[125, 196, 247] and to S-carbamidomethylate the free cysteines: the light-sensitive iodoacetamide (IAA)[125, 196].

Various starting amounts of materials have been reported; 50 µg[115] to 500 µg[98] protein for in-solution digestion, 20 µg[80, 162] to 100 µg[135] on FASP. Using in solution digestion, Harwood reported a peptide recovery of 64% after digestion[115]. The FASP method is widely used in proteomic analysis, first published in 2005[306]. In FASP, all steps are performed on a microcentrifugal filter devices[306], so purification of unwanted substances in the final sample is easily done[307]. The proteins are captured on the filter membrane (where cut-off values decide the molecular weight lower limit). After protein digestion, the smaller peptides can be eluted whereas larger compounds will remain on the membrane[293]. Although GASP has been used in DMET proteomics[305], it has not been used for intestinal DMET protein preparation. Two reviews from 2020[271] and 2019[265] recommend FASP as digestion technique when analysing whole lysate cell fractions of ADME proteins[271]. **Table 1.9** gives an overview of the benefits and disadvantages of each method.

Table 1.9. *Overview of the most commonly used digestion methods in proteomics.*

Method	Benefits	Disadvantages
In solution digestion	+ Compatible with commercial membrane extraction kits[265]	- Can cause considerable (36%) sample loss[115] - Removal of detergents and denaturing chemicals is challenging[265] -Dialysis for peptide-clean up can result in loss or contamination of small molecules can still be present. - Solvent-based protein extraction required post-digestion[265], which is not suitable for some samples[142]
FASP[306]	+ Superior method to remove detergents introduced for protein solubilisation[271, 307, 308] + Sample clean-up and digestion are done on the filter[265] + Versatile and compatible with a range of detergents[265] + Selection of filter size (cut-off molecular weight values) allows for flexible clean-up[265]	- Risk of sample loss if protein load is small.[265] - Not compatible with high concentration of detergents, or commercial membrane extraction kits[265] - risk of filter failure[306]
GASP[309]	+ Proteins of selected molecular weight can be isolated for proteolysis + Compatible with commercial membrane extraction kits[265] + Compatible with low loading of protein[265] + Sample clean-up and digestion are done in gel[265] + Versatility; SDS-PAGE gel could be used for Western blotting[265]	- Not compatible with some detergents - Not compatible with urea, a frequent used denaturing chemical (chaotropic) - not compatible with QconCAT technology*, as proteins are separated based on molecular weight

*: see section 1.4.3.12

When the proteins are denatured, disulphide bonds reduced and subsequently alkylated to prevent reoxidation of the bonds, the proteins can be digested by proteases such as lysylendopeptidase [142] (lysC), trypsin or chymotrypsin. Most commonly, trypsin is used as it is seen as the gold standard protease[293], however other proteases are added too to increase proteolysis efficiency[80, 115, 162]. Trypsin cleaves at the carboxylic side of arginine and lysine residues, except when the subsequent amino acid is proline. Lys-C hydrolyses the carboxylic side of lysine. Trypsin is incompatible with high (>2M) urea concentrations[271, 293] , so dilution might be required.

Optimisation of the digestion stage is required, to balance between full protein digestion and nonspecific cleavage of peptides when exposed for prolonged time at 37 °C or autolysis (which is linked to a high trypsin concentration[310]). Groer *et al*.[196] investigated the protein digestion efficiency for intestinal transporter digestion. They found that after a digestion period of 16h, BCRP and MRP2 proteins were fully digested, and a longer exposure degrades the amount of in a drop of proteotypic peptides for P-gp, which did not align with stability measurements at 37°C. Subsequently, they opted to use a 16 h digestion time, a duration which is now the most commonly employed in intestinal DMET proteomics (16 h at 37°C [114, 125, 142, 196]), yet other times have been used too.

If using a QconCAT technique (see section 1.4.3.12), then these heavy isotope proteins need to be spiked in before denaturing. If using standard isotope labelled (SIL) standards (see section 1.4.3.12), then these heavy isotope peptides would be spiked in after proteolysis (either before[80, 162] or after[115, 125, 196] freezing the peptide pool).

Some protocols have included a desalting step over C18 tips after proteolysis[80, 162]. These tips with octadecane carbon chains are used to purify peptides after elution. When bound to the C18 tip via hydrophobic interactions, the peptides can be washed and subsequently eluted in a clean vial, reducing the amount of salts in the sample and thus reducing the chance of adduct formation in LC-MS/MS[311]. Proteomic identification increased significantly after clean-up with C18 tips[311]. Although there is a risk of peptide loss (especially risky for hydrophilic peptides in case the binding capacity of the resin is exceeded), this can be accounted for when adding heavy isotopes before this step. Indeed, due to the identical chemical profile (except for the isotope), a similar loss of both the heavy and light versions of the same peptide is expected, so the ratio light:heavy is presumed to be unaltered.

1.4.3.8 LC-MS/MS analysis

Liquid chromatography (LC) combined with tandem mass spectrometry (MS/MS) is an analytical technique where molecules are physically separated before being ionised by electron spray ionisation (ESI) and subsequently introduced to the MS detector for analysis.

1.4.3.8.1 HPLC

LC separates peptides based on their affinity and partitioning between a mobile phase (solvent) and stationary phase (LC column) with different characteristics[312]. Most commonly used for proteomics is a reversed phase LC (RPLC), with an apolar stationary organic phase (such as *n*-octadecyl (C_{18}) chains on silica beads)[313]. Polar mobile phases commonly used are a mixture of water and organic solvent such as methanol or acetonitrile (ACN) with an increasing gradient of organic solvent during the LC-run. The peptides will elute from the column at a specific time, the retention time (t_R), where a higher t_R indicates a higher affinity

for the stationary phase. Most commonly used method for separation of the peptides in the LC-MS/MS system is a mobile phase gradient of 0% – 60% ACN in water (ranges may vary) – both solvents containing 0.1% formic acid or trifluoroacetic acid (TFA) [115, 125, 142, 196], and a C_{18} column as stationary phase.

Frequently in intestinal DMET proteomics, a nanoflow HPLC system is used[80, 98, 115, 142, 162, 247, 276], but normal flow systems have been employed as well[125, 196]. Theoretically, a nanoflow system allows for a slower flow rate, so peak shape and separation of compounds are improved according to Van Deemter's equation[313]. Introducing smaller droplets into an ESI source allows for improved ionisation, with detection and sensitivity capability[271, 314, 315]. However, upon comparison in proteomic quantification, nano- and normal flow rate HPLC are reported to have similar results, with less interference being observed in normal flow rate HPLC systems[316, 317]. Reproducibility and robustness are a challenge in nanoLC[318]. Additionally, shotgun experiments (see also section 1.4.3.11) were reproducible between a nano- and normal flow rate[314]. With the aim to compare between both standard flow and nano-LC, a similar number of identified proteins of *Escherichia coli* and *Arabidopsis thaliana* via shotgun proteomics has been reported[314].

1.4.3.8.2 MS-MS and ESI

MS-MS or tandem mass spectrometry is an analytical technique to both identify and quantify a peptide based on their mass to charge ratio (*m/z*), with high selectivity and sensitivity.

1.4.3.8.3 Ion source

To enable analysis by a MS detector, the peptides need to be ionised. Frequently, an ESI source is employed. Here, the column eluent is dispersed by electrospray[319] into small droplets over a small capillary, with an counter electrode at the tip with a high applied voltage (±3 – 5 kV)[320]. This causes the droplets to expose opposite charges on their surface, helped by addition of compounds added into the mobile phase[321]. As the solvent within the droplets evaporates, the molecules themselves become charged in the gas state and thus are detectable in the MS detector, based on their *m/z*-ratio[271].

1.4.3.8.4 Quadrupole and MS

After ionisation, the electrically charged ions go through a mass analyser before reaching the detector. Most frequently used is the triple quadrupole (QQQ), where three coupled quadrupoles are placed before the mass spec detector. The quadrupole is a filtering unit which consist of four poles with a current flowing through, with two pair of poles of opposite ACDC[321]. The resulting electric field pushes the ions forward through the quadrupole, with a specific oscillation pattern[321].By changing the current, only one specific ion with a specific *m/z* value will reach the detector. The first and last quadrupole act to filter the ions of interest (first quadrupole, Q1: precursors, last quadrupole, Q3: fragments) based on their target *m/z*-value (tandem mass-spectrometry, MS/MS[322, 323]). The middle quadrupole, Q2, is used as a collision cell, where the precursor ion is bombarded with a collision gas (N_2 or argon) which fragments the precursor[318, 321]. Other mass analysers used for proteomic analysis of intestinal DMET proteins are ion trap (in tandem with a quadrupole, QTRAP)[98] and a hybrid quadrupole-orbitrap[142, 276].

1.4.3.8.5 Mass spectrum and targeted acquisition methods

The intensity of each ion is plotted against the different *m/z*-value, creating a mass spectrum. Stacking all different mass spectra based on the retention time gives a total ion chromatogram. The combination of a precursor with a specific fragment is an MRM transition (multiple reaction monitoring, also known as selected reaction monitoring)[318], the most commonly used methods of detection. This method has already been used in proteomic analysis of brain, liver kidney tissue and blood samples[113]. The advantages of MRM detection are multiplexed (and thus more rapid) analysis, high throughput and good accuracy, sensitivity and reproducibility[113]. Adequate MRM analysis is limited by the prerequisite of a well-developed method.

A lesser used method is quantification based on the accurate mass and retention time (AMRT), without internal standard[113, 308, 324]. Quantification relies on the signal intensity of the precursor ion[113]. Robust and reliable LC peptide separation and high-resolution MS detection are essential to this technique[113]. However, this method lacks the required sensitivity to quantify low-abundant DMET proteins as demonstrated in a recent attempt[161]. Upon comparison with the results of a QconCAT-labelled approach on the same samples, it was observed that most protein abundances were within 2-fold difference, yet the CYP enzymes were seriously underpredicted as their difference was up to 10-fold lower. Additionally, the label free approach failed to detect ABCC2 in all samples, yet the labelled approach quantified this protein in all investigated samples[80, 137]. Clearly, targeted proteomics with internal standards are more powerful to quantify specific proteins compared to label-free proteomics.

1.4.3.8.6 Scheduling, loop and dwell times

In targeted proteomics, it is beneficial to adjust the LC-MS/MS instrument to only target a specific transition around the time point when the analyte is eluting from the column (scheduling)[325]. The number of transitions the system has to cycle through influence the loop time (i.e. the entire time it takes to monitor a given set of transitions after each other) and thus the amount of points across the chromatographic peak. A shorter loop time correlates with more points across the peak, however selecting a good dwell time (i.e. how long the detector records signal for a given transition) will result in a more accurate signal measurement. Ideally, a short loop time with a longer dwell time would give the best signal, only monitoring transitions during the retention time window[326]. A dwell time of 0.15 seconds has been used by Harwood *et al*, yet this was in combination with a nanoflow LC system over a run of 40 min, targeting 7 peptide sequences (14 targets, a light and heavy isotope, with maximum 3 MRM transitions each)[114].

1.4.3.8.7 Detector

When the ion hits the detector dynode (at opposite potential), an electron multiplier cascade create an electric signal[327]. As the detector only records a signal if the *m/z*-criteria (and, in case of scheduled acquisition, a specific t_R criterium) are fulfilled, tandem MS is highly selective and sensitive, capable of analysing particles with low concentrations (such as low abundant DMET proteins in a total mucosal protein fraction)[321].

1.4.3.8.8 Peptide fragmentation

Peptides fragment preferably at their peptide bonds, resulting in a predictable pattern of fragments generated[328]. Using ESI, it has been observed *y*-2 ions of peptides frequently give the greatest signal[196].Thus, peptide fragmentation can be easily predicted.

1.4.3.9 From signal to sample protein concentration

The most used software package for MRM method development and data analysis is Skyline[326, 329-331]. This open source, freely available software package can export (scheduled) MRM-transition lists and import native files from a wide range of LC-MS/MS instruments[332].

The expression data per peptide is then calculated based on the average multiple (usually: 2-4) transition spectra[125, 142, 196]. The expression can be quantified relative or absolute. Relative quantification or inter-sample quantifications is used to compare a fold-change in signal levels inter-samples in e.g. a healthy and disease state sample, however this is not used in intestinal DMET proteomics[165].

Absolute quantification quantifies signal intensity relative to an internal standard. Two methods have been used, either establishing a calibration curve where the concentration is interpolate from signals with known concentration[125, 196] or relatively to a heavy version of the peptide with known concentration (single point-calibration)[80, 115]. The latter is widely used. Kiss spiked in a known concentration of heavy peptide into the sample prior to MS as reference point (after checking signal linearity)[98]. As a double single-point calibration, Harwood spiked in a known concentration of heavy version of a QconCAT (an artificial protein containing heavy versions of the target peptides, see section 1.4.3.12) prior to

digestion[115]. Prior to analysis, a light version of a peptide that does not occur in the human proteome was spiked in. Via single point-calibration, the concentration of QconCAT could be calculated, to which the light peptides were calculated against. As a hybrid approach, Groer and Drozdzik established a calibration curve by using human serum albumin (HSA) as a blank matrix to which they added an increasing amount of light target peptides, whilst maintaining the amount of SIL peptide added constant over the series. Using a representative matrix for calibration purposes is important, as it has been demonstrated the background proteome influences ionisation[333]. Based on both the known concentrations and the peak ratio of the signal of light/heavy peptide, they plotted a calibration curve on which they based their final expression values[125, 196].

In the case where a proteotypic peptide originates from two different proteins, a second, unique proteotypic peptide for at least one protein is necessary to correct and calculate the expression of each protein. Miyauchi calculated the expression of UGT1A8 via calculating the expression of CYP1A8 and 1A9 (based on a common peptide) and correcting via the concentration of a proteotypic peptide only originating from CYP1A9[142].

1.4.3.10 Scaling to organ abundance

Finally, out of the expressed amount of proteotypic peptide in the sample, the abundance of the target protein in the tissue (corrected by villin-1 content) can be derived. This abundance is then scaled up to organ-sized abundance, via biopsy size as percentage of the entire organ weight. Using the appropriate statistical tests, conclusions could be drawn from the data and potentially, a population-wide average for the expression of DMET proteins can be established[125, 142].

1.4.3.11 Peptide probe selection

As the amino acid sequences of DMET proteins are known, *in silico* tools can be used to predict digested to predict the resulting pool of peptides after hydrolysis by a specific protease[264]. From this pool, a peptide sequence that does not occur anywhere else in the human proteome could be a candidate for proteomic quantification[113, 334]. Databases such as UniPRotKB/Swissprot[335] are used to identify proteotypic peptide candidates. For optimal analysis and to minimise the influence of troublesome amino acids, the sequence of these proteotypic peptides (and their SIL counterparts) is restricted to some conditions. Most commonly, these selection criteria are used[113, 125, 196, 264, 265]:

1. *In silico* digestion of the protein with the protease used, with no missed cleavage sites (proteolysis is complete)
2. Length of peptide between 7 - 25 amino acids
3. No post-translational modifications on the sequence
4. No single-nucleotide genetic polymorphism in the peptide (such as proven for UGT2B17 and UGT1A[142])
5. Exclusion of transmembrane sequences (to ensure region is accessible for trypsin)
6. No peptide with a cysteine, methionine (risk of oxidation), tryptophan (chemical stability), asparagine, glutamine or N-terminal glutamic acid (risk of deamidation) residue[113]
7. Good LC-MS/MS features, such as optimal ionizability and hydrophobicity

To aid in probe selection, proteotypic peptide candidates can also be identified in parallel by using shotgun LC-MS/MS experiments[249, 310, 314, 333]. Here, tryptic digests of membrane vesicles containing the target proteins or from over-expressing cell lines are analysed. Based on the MS results and peptide identification (e.g. via the NCBI BLAST software[336]), probes

that give a good signal can be selected. It needs to be noted, peptide ionisation and detection are instrument-specific and not directly transferable[333, 337].

Further optimisation for quantification can be performed, for example only targeting a small selection of the most intense MRM transitions[125, 196], and optimisation of the collision energy per MRM, using built-in tools of software packages such as Skyline[329-331]. Usually, two proteotypic peptides have been used per protein for quantification, with two to three MRMs per peptide .

1.4.3.12 Standards

Most intestinal DMET proteomics papers use targeted proteomics with heavy isotope labelled standards. Use of these standards has various advantages. It can correct for peptide loss during sample clean up post-spiking[98], and normalise the influence of matrix effects on ion suppression or enhancement[196]. To accurately assess the sample proteotypic peptide concentration, and thus the protein expression in the tissue, a stable isotopically labelled (SIL) version (^{13}C and/or ^{15}N) of the proteotypic peptides are added. These heavy versions of the proteotypic peptides have the same retention and detection time[113] as their unlabelled counterparts, but a different *m/z* transition (usually 8 – 10 Da difference, depending on the label)[196]. Using the ratio of peak intensities of unlabelled proteotypic peptides and their SIL counterparts, which were added in a known concentration, the proteotypic peptide concentration can be determined more accurately.[113, 196] Accurate quantitation of proteotypic peptides acting as surrogate for target proteins is the cornerstone of proteomic analysis[113]. Different versions of standard have been used: synthetic peptides, artificial proteins containing the sequence of all proteotypic peptides or labelled target proteins.

1.4.3.12.1 AQUA

The most used widely used peptide versions uses chemically synthesised standard peptides, known as Absolute Quantification (AQUA) peptides[113, 165]. This method requires a heavy version per individual target peptide, and thus each SIL peptide must be synthesised separately. This synthesis can be expensive and time consuming, but this has proven to produce data of a higher quality compared to the label free approach[113, 165]. A known amount of SIL peptides are added to the digested protein. The timing of adding the SIL peptides is important when wanting to account for potential losses of peptide[311]. Most commonly, the AQUA peptides are added after protein digestion, before desalting and fractionating into MS-samples[80]. This ensures a similar potential loss compared to the light version peptides. Stability-issues during long term storage of the SIL peptides leads to precipitation of the SIL peptide, which may corrupt the analysis[113, 338].

1.4.3.12.2 QconCAT

The concatemer technique seeks to reduce the time and costs whilst still retaining the advantages of the AQUA method when analysing multiple (10-50) proteins in a higher number of samples (20-100)[165, 339]. In this technique, a recombinant protein (a quantification concatemer, QconCAT) is expressed using an artificial gene expressed in e.g. *Escherichia coli*[339]. This protein incorporates the sequence of the selected proteotypic peptides, linked together (concatenated) via bonds the upstream protease is selective for. During the incubation, the expression host is grown in medium enriched with heavy isotope amino acids[165], and thus incorporates these heavy isotopes in the protein. The expressed protein is then added prior to digestion, where it gets digested to peptides, identical to the target proteins. The resulting SIL peptides are inherently in an equimolar 1:1 stoichiometry,

making it very beneficial to investigate protein intercorrelations[113]. Although the QconCAT technique can save time and money – taking into account the development and finetuning the concatenated gene and protein[114], it has not shown to be superior nor inferior to the AQUA method[338]. Limitations include the possibility of incomplete digestion and failure of the host to express the recombinant protein. A whole range of QconCATs are available, most notable the TransCAT (transporters)[115] and MetCAT (CYP and UGT enzymes)[80, 162]. However, no QconCAT exists that currently contains peptide sequences for all three families[340].

1.4.3.12.3 PSAQ

A third method is using proteins as standards for absolute quantification (PSAQ)[341]. Similar as the QconCAT technique, recombinant proteins are expressed in a host grown in a heavy isotope enriched medium[165], but here the sequence is identical to the target proteins. PSAQ standards behave in the same manner as the target protein and thus can be used to correct for changes in proteolysis yields and loss during the manipulation steps[165]. However, PSAQ standards have not been used in intestinal DMET proteomics.

In conclusion, isolation of enterocytes specifically decreases contamination of other cells, which might dilute the proteins and effect LC-MS/MS sensitivity. Depending on sample size (i.e. pinch biopsies), elution might not be an option. Cryogrinding of an entire biopsy is preferred over scraping, to decrease the chance of premature proteolysis and loss of enterocytes. Targeting an enterocyte marker (villin-1) in LC/MS-MS detection can correct for changes in enterocyte percentage in the biopsy. Including multiple manipulation methods and different buffers could improve protein recovery, however there is a risk of protein loss

as well. Couto *et al*. demonstrated multiple centrifugation steps for intestinal DMET isolation are not necessary if using a stringent detergent, such as the RIPA buffer. Additionally, this allows for simultaneous quantification of transporters and metabolising enzymes.

1.4.4 Limitations of proteomic quantification of intestinal DMET proteins

Although LC-MS/MS based quantification of abundance of intestinal DMET proteins proves more powerful than mRNA analysis, a few disadvantages should be addressed.

- LC/MS-MS analysis cannot distinguish between the correct proteins and incorrectly folded, spliced, glycosylated or truncated variants, as the method only allows for detection of proteotypic peptides[113, 125]. It is known that UGT1A genes also get translated to an inactive splice variant, so caution should be exercised when selecting the proteotypic peptide candidate[142].
- Abundance assays do not completely estimate protein activity, but abundance is preferred as DMET proteins have a shared broad substrate specificity[113]. Additionally, due to the lack of specific substrates or optimised assays for intestinal DMET activity, measuring abundance is preferred as surrogate for activity[342]. Kumar found a good correlation between *in vitro* transporter activity and expression (R^2>0.9) in cell-lines. In other tissues, like the liver, a good correlation between protein abundance and protein activity has been established[161, 265].
- Other factors at the biological site can majorly influence protein activity. Factors such as pH and proton (H^+) concentration, kinetics, localisation in the enterocyte etc. can influence protein activity[125]. Incorporating ex-vivo techniques, for example

Ussing chambers for transporter assays in addition to these assays might improve our understanding on DMET proteins.

- The lack of representative biological standards (membrane-bound or reticulum-bound proteins) prohibits a validation strategy of the sample preparation.
- There is a risk of losing proteins in the various sample manipulation steps[269], which can be countered using heavy isotope counterpart of the targets, such as QconCAT proteins, and using lab consumables with reduced binging capacity of proteins/peptide such as Protein Lobind Tubes[196, 342].
- In the paediatric population, there is a lack of amount of and access to qualitative tissue, as the tissue normally comes from surgical waste or deceased children[33]. There might be an influence of disease and medication on DMET abundance (although the tissue looks macroscopically healthy)[98]. Additionally, a high inter-individual variability in proteomic analysis of DMET ontogeny other tissues have been reported[145], so efforts should be made to increase the sample size (although this is challenging for paediatric tissue collection).

Acquiring abundancy data in paediatric populations can aid in modelling and dose selection[98].

1.5 Free water in the paediatric colon for XR formulations

Part of a published manuscript was based on this section of the introduction: Goelen, J.; Alexander, B.; Wijesinghe, H.E.; Evans, E.; Pawar, G.; Horniblow, R.D.; Batchelor, H.K. Quantification of Fluid Volume and Distribution in the Paediatric Colon via Magnetic Resonance Imaging. Pharmaceutics 2021, 13, 1729. https://doi.org/10.3390/pharmaceutics13101729

As XR-formulations are associated with high inter-individual variability *in vivo*[343, 344], it is recognised that prediction of performance of these products is challenging. The uncertainty is even more pronounced for paediatric XR-formulations, as the variability is increased due to the lack of physiologically relevant input data for *in vitro* and *in silico* models[13, 60]. Despite the clear advantages of oral formulations, such preparations rely on drug liberation and dissolution to be available for absorption. The free water available at the site of dissolution is a critical parameter for these processes as it also affects local drug concentration and thus permeation[24, 139, 345]. As such, a comprehensive understanding of the amount and distribution of fluid throughout the GIT is required to ensure appropriate and adequate absorption of oral medicines[346].

There is a recognised knowledge gap about the amount and distribution of free fluid in the GIT of the paediatric population[2, 168, 347], resulting in a need to generate physiological data to underpin the development of age appropriate PBPK models. This would improve prediction of drug performance in children. No studies to date have quantified the amount and distribution of fluid in the paediatric colon[2, 168, 347, 348], thus predictions of performance are based on extrapolation of adult data. Direct extrapolation of the adult values to the

paediatric population is less appropriate, due to the reported differences in the paediatric anatomy and physiology of the GIT[4, 349, 350] (see also section 1.1).

1.5.1 XR formulations in the colon

Extended release (XR) formulations are interesting for delivering drugs to the colon for both local action (e.g. inflammatory bowel disease, IBD[351]) and systemic absorption (e.g. insulin therapeutics[352]). The low proteolytic activity and the potential of intact peptide absorption[353] (as demonstrated for insulin[354] or linaclotide[355]) enables the large intestine (with emphasis on the proximal colon) as an appropriate absorption site[139, 356]. As CYP-expression is minimal in colonic enterocytes, some XR formulations specifically target the large intestine (bypassing the small intestine) to minimise intestinal metabolism and thus increase gut bioavailability (F_g)[357]. Additionally, XR formulations can also employ the colon as an extension of the drug absorption window in the GIT[66]. Increasing the absorption window of a drug by targeting the colon offers several advantages over immediate release (IR) formulations. XR formulations can be used to enable once daily (OD) dosing, improving patient convenience[358], resulting in better adherence[359], a more steady therapeutic plasma concentration[360], reduction of side effects[359]and reducing the risk of administration errors[361].

Colon-targeting formulations are designed to exploit local intestinal environment characteristics for drug release, such as pH or the presence of bacterial-derived metabolising enzymes [362, 363], although some XR-formulations are designed to deliver drugs independent of local environmental factors (such as time-dependent release, like mesalazine preparations for ulcerative colitis treatment[364]).

The performance of an XR formulation and bioavailability of its drug depends on both the drug/formulation characteristics and the local environment in the subject[365]. Before the drug of an XR formulations becomes systemically available, it first needs to be released from the formulation, dissolve in the gut lumen, permeate across the GIT membrane and withstand intestinal and liver metabolism[66]. Thus, the performance of these formulations needs to be evaluated in biorelevant conditions that include the colonic macroenvironment in terms of fluid volume and composition[361, 366-368].

1.5.2 Colonic fluid volumes

Data on intestinal fluid (amount, distribution and composition) are necessary for *in vitro* and *in silico* models in drug development[139, 345, 358, 361, 369, 370]. Despite recent efforts, there is no consensus on the volume of water or its distribution throughout the colon of adults[371], which translates in poor estimations for the standardised volume employed for colonic dissolution testing (**Table 1.10**). Currently, *in vitro* and *in silico* models of the colon use a range of volumes for dissolution assays, ranging from 1 mL to 200 mL[66, 372, 373].

Table 1.10. *Reported fluid volumes in the colon of healthy adults when measured using MRI. N/A means that the data was not reported*

Study	Feed status (intake of food/fluid)	Time of Ingestion before MRI acquisition	Number of participants	Median (min-max) (mL)	Mean (± SD) (mL)
Schiller 2005[26]	Fasted	-	12	8 (1-44)	13 ± 12
	Fed (standardised meal)	1 h		18(2-97)	11 ± 26
Pritchard 2017[374]	Fasted	-	11	2 (0-7)	-
	Fed (500 mL Moviprep)	1 h		140 (104 -347)	-
Murray 2017[345]	Fasted	-	12	N/A (0-11)	2 ± 1
	Fed (240 mL water)	30 min		N/A (0-49)	7 ± 4

In addition, the influence of colonic fluid volumes on incomplete dissolution and absorption of poorly soluble drugs in the upper GIT and subsequent accumulation of solid drug particulates in the colon[375, 376] (such as NSAIDs for treatment of colorectal cancer) is not fully understood.

The free fluid in the GIT can be quantified by magnetic resonance imaging (MRI), a non-invasive tool that permits undisturbed visualisation of the GIT[377]. In contrast with scintigraphy or computed tomography (CT), no ionising radiation dose is needed for imaging[371] and its effectiveness in producing qualitative images enabling fluid quantification has been demonstrated[26, 345, 371, 374, 378, 379]. Using MRI scans that show the colon of a paediatric cohort, the amount of free fluid can be determined.

1.5.3 PBPK modelling for XR formulations in paediatrics

PBPK modelling integrates physiological parameters with drug-specific characteristics (see section 1.2.3). Consequently, it has the powerful ability to predict the performance of XR formulations in a target population if reliable input parameters representative of the colon into the model are employed. One such input parameter is the colonic fluid volume (CFV).

The default inputs for colonic volume in Simcyp PBPK modelling are fixed at 13 mL (for both adult and paediatric populations), which is based on adult data obtained from MRI. This volume was maintained in the paediatric population, rather than being extrapolated based on adult values *via* allometric scaling from either weight or body surface area (BSA)[10, 66]. Therefore, it might not be representative for the CFV in the paediatric population, similar to

the disconnection between adults-children that has been observed for small intestinal fluid volume[24].

Only a few P-PBPK models exist for XR formulations in children[66, 105, 380, 381]. Johnson *et al*. published in in 2015[66] a P-PBPK model predicting the PK profile of an XR quetiapine formulation (an atypical antipsychotic). This model was accepted by the US FDA as waiver for clinical trials (so no clinical observed PK data is available). However, this model used the default CFV value of 13 mL, as no data on paediatric colon fluid volumes has been reported.

1.6 Objectives of this thesis

The overarching objective of this thesis is to better characterise the paediatric gastro-intestinal tract to provide reliable data for use with modelling and simulation software to enable robust predictions of pharmacokinetic profiles in this population. Specifically this work will focus on the ontogeny of DMET in intestinal tissue and the volume of free fluid in the paediatric colon as these elements are currently unknown.

Therefore, the aims of this thesis are:

1. To quantify the abundance of 21 clinically relevant DMET-proteins in the duodenum of a paediatric cohort via LC-MS/MS analysis on pinch biopsies
2. To quantify the luminal fluid volume in the colon of a paediatric cohort via MRI data sets
3. To investigate how P-PBPK predictions change when incorporating these novel data in modelling software to predict pharmacokinetic profiles.

2 CHAPTER TWO

QUANTIFICATION OF DRUG METABOLISING ENZYMES AND TRANSPORTER (DMET) PROTEINS IN THE PAEDIATRIC DUODENUM VIA LC-MS/MS PROTEOMICS

2.1 Introduction

Characterising the paediatric GIT physiology is required to enable prediction of oral formulations. The ontogeny of key DMET intestinal proteins involved in drug disposition needs to be further elucidated to accurately predict the PK profile of drugs and to investigate drug-drug interaction potential. Current data are based on mRNA expression analysis or immunochemistry, yet proteomics has become the gold standard to quantify intestinal transporters. Using an LC-MS/MS and QconCAT technique for quantification, the abundance of 21 target proteins (**Table 1.4**) can be quantified in paediatric duodenal pinch biopsies.

2.2 Aim and objectives

The aim of this work is to quantify important DMET-proteins in paediatric intestinal tissue from pinch biopsies.

Specific objectives include:

- To establish and optimise a standard operating procedure (SOP) to process the paediatric intestinal samples, including:
    - Target protein isolation from cell/tissue homogenate
    - Protein tryptic digestion to peptides
    - Targeted peptide analysis via LC-MS/MS (proteomics).
- To use this SOP to quantify the abundance of the selected DMET proteins in paediatric intestinal pinch biopsies, using a QconCAT as heavy standard.

2.3 Methods

2.3.1 Tissue collection

Paediatric pinch biopsies from the duodenum were collected from children younger than 15 years old during endoscopic procedures which were part of their clinical care. Informed consent by a parent, guardian or those with legal responsibility for the child in their care was obtained in every case. The biopsy forceps had a width of 1.8 mm when opened, resulting in biopsies with a theoretical surface area of 2.54 mm^2. Immediately after collection, the biopsies were frozen at -80°C for further processing.

Ethical approval was granted by the South Birmingham NRES Committee (*IRAS 251909; "Characterisation of fluids and mucosal tissues from paediatric stomach and small intestinal tract to enable development of biorelevant models to predict drug absorption; PaedGIFT (Paediatric Gastro-Intestinal Fluid and Tissue)",* **Appendix 2**). Subsequent tissue processing and LC-MS/MS analysis was performed in a blind manner, i.e. uninformed of subject diagnosis and demographics.

2.3.2 Protein extraction from biopsies

A section of methodology development (not essential for the understanding of this work) is given in **Appendix 3**.

All protein extraction steps were performed without interrupting the cold chain, working either in a cold room (4°C) or on ice. A list of chemicals used and manufacturers is given in **Appendix 4**. The frozen biopsies were crushed to a fine powder in a precooled pestle and mortar with liquid nitrogen (LN_2) (cryopulverisation), keeping the tissue frozen by frequently topping up LN_2. The pulverised tissue was resuspended with Radio-Immunoprecipitation Assay (RIPA) lysis/extraction buffer, containing IGEPAL CA-630 (i.e. octylphenoxy

poly(ethyleneoxy)ethanol, branched) 1% (v/v), sodium deoxycholate 0.5% (w/v), sodium dodecyl sulphate 0.1% (w/v) and a protease inhibitor cocktail in 1 tablet per 50 mL solution at a concentration of 100 mg biopsy/mL buffer. This resuspension was snap-frozen in LN_2 and subsequently stored at -70°C. The lysate resuspensions were thawed at 4°C with agitation on a rotating shaker (30 min, 25 rpm) (Rotator SB3, Stuart). Samples were then sonicated using a sonicator pulse on ice for 5 sec (Soniprep 150, Sanyo) before centrifugation (9 000 *g*, 5 min, 4°C) (Biofuge Pico, Heraeus or Centrifuge 5415R, Eppendorf). The supernatant, which contained the target proteins, was isolated. The protein concentration in the supernatant fraction was determined using Pierce's BCA protein assay according to the manufacturer's instructions.

A representative biopsy is shown in **Figure 2.1**.

***Figure 2.1**. Representative image of a paediatric pinch biopsy. The mass of the biopsy shown was 24 mg.*

2.3.3 Protein digestion via FASP

2.3.3.1 PaedCAT design and expression

A stable-isotope-labelled "heavy" standard, in the form of a QconCAT, was used for quantification of the peptides of interest and to correct for potential variation in sample preparation procedures. This protein, PaedCAT, contained the amino acid sequences of peptides that are specific to the selected target proteins (proteotypic peptides).

The selection of peptides was based on literature research (using the most frequently used proteotypic peptide). Additionally, shotgun-experiments performed on a protein digest of a mucosal protein fraction obtained from adult colonic tissue (obtained from the Human Biomaterials Resource Centre and processed in the manner described above/below) aided in identifying potential proteotypic peptide candidates (see also section 1.4.3.11).

Proteotypic peptides were selected based on the criteria set out by Kamiie *et al*.[264] described in section 1.4.3.11.

For every target protein (see **Table 1.4**), 2 to 3 proteotypic peptides were encoded into PaedCAT. One peptide sequence (TYSTSYTLEDLDR) was shared between UGT1A8 and UGT1A9. By also measuring a peptide uniquely coding for UGT1A9 (AFAHAQWK), UGT1A8 levels can be determined using the difference between the abundance of both peptides as done previously by Couto[80]. PaedCAT was expressed in *Escherichia coli*, using stable-isotope-labelled lysine ($^{13}C_6{}^{15}N_2$) and arginine ($^{13}C_6{}^{15}N_4$) (Polyquant, Bad Abbach, Germany). The annotated sequence of PaedCAT showing which peptide was surrogate for which protein is given in **Figure 2.2**.

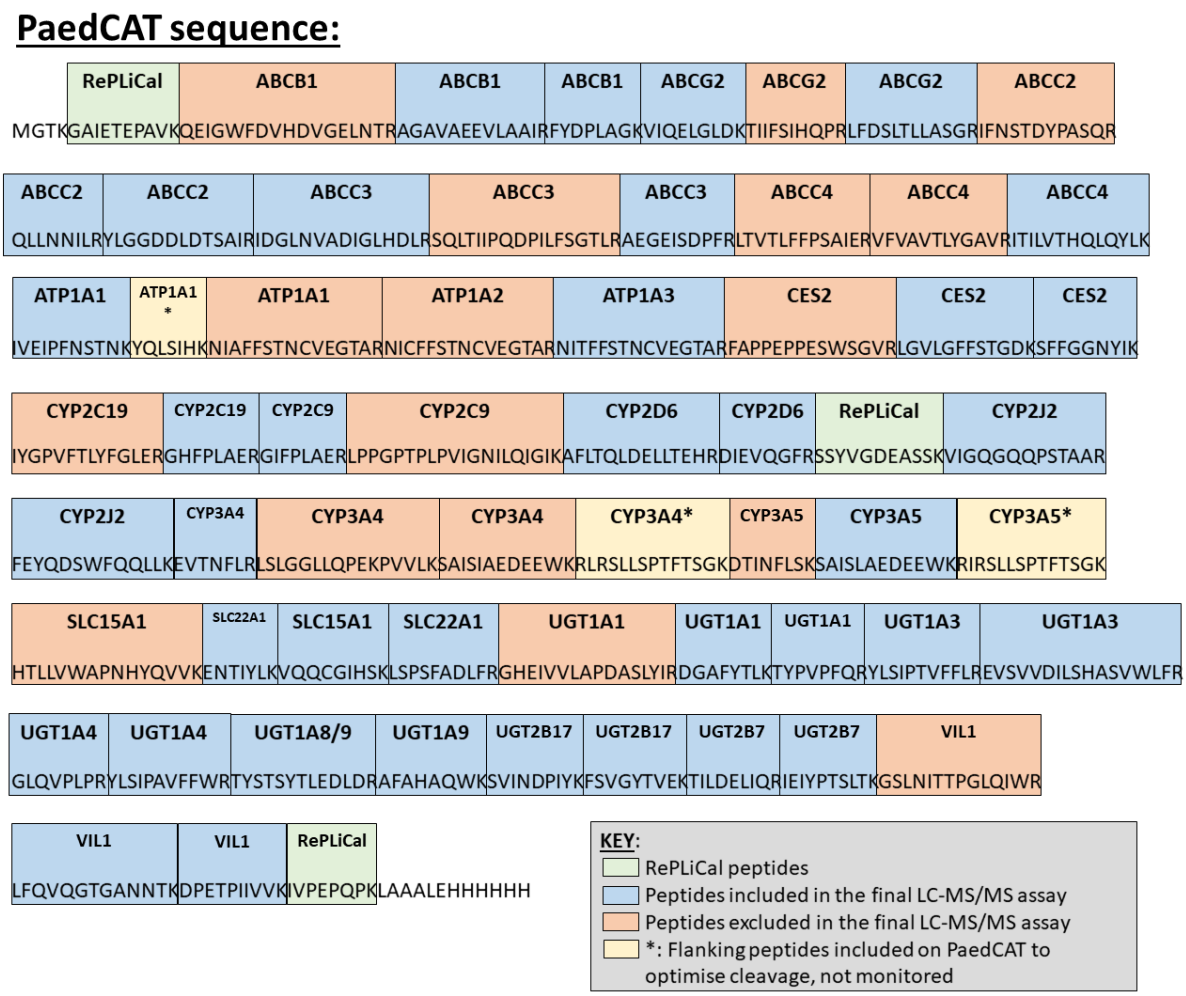

***Figure 2.2**. Annotated PaedCAT sequence, showing which proteotypic peptide acts as surrogate for which protein. The colour coding is based on the results after section 2.4.3.1, 38 peptides were monitored in the final LC-MS/MS assay.*

2.3.3.2 Protein digestion via FASP

Isolated protein fractions were digested by trypsin using a filter-associated sample protocol (FASP). Protein concentrations were diluted using RIPA to obtain a 1 µg protein/µL solution. From this, 20 µg of total mucosal protein (i.e. 20 µL) was mixed with 370 µL urea (UA) buffer (8 M urea in 0.1 M Tris/HCl, pH 8.5) and 10 µL of the QconCAT PaedCat solution was spiked in (concentration spike: 200 fmol/µL). The mixture was vortexed for 30 sec and then rested for 5 mins.

After 5 mins, 40 µl of a 100 mM 1,4-dithiotreitol (DTT) in UA buffer was added to the sample, followed by incubation at 56°C for 40 min. The FASP-filter unit was primed by adding 200 µL of the UA buffer on the filter and spinning for 5 mins at 14,000 *g*, the filtrate was discarded. After the denaturing and reduction step, the cooled mixture was transferred to the filter unit and the sample was centrifuged at 14 000 *g* for 20 min at room temperature (RT) and the filtrate was discarded. Next, 400 µL of the UA buffer was added, together with 20 µl of freshly prepared 300 mM iodoacetamide (IAA) in UA buffer. The alkylation step was performed in the dark for 30 mins. After this, the sample was spun at 14 000 *g* for 20 min at RT and the filtrate discarded. The sample was washed by adding 400 µl UA buffer and spinning at 14 000 *g* for 20 min at RT, discarding the filtrate. Next, three washing steps were included to reduce the urea concentration in the sample, by adding 400 µl of 50 mM ammonium bicarbonate (ABC) in ultrapure water and spinning at 14 000 *g* for 20 min at RT, discarding the filtrate (repeated three times).

Tryptic digestion of the proteins was assisted by Lys-C digestion. A 0.2 mg/mL enzyme concentration (Trypsin/Lys-C Mix, Mass Spec Grade, Promega) was obtained by adding 100 µL trypsin resuspension buffer to a vial containing 20 µg of the enzyme. Together with 10 µL of the enzyme solution, 30 µL of a 25 mM ABC-solution was added to the FASP filter. The samples were incubated at 37°C under agitation (105 rpm) overnight.

Elution of the peptides was performed by adding 50 µL of 100 mM ABC, 5% acetonitrile (ACN) to the sample and spinning at 14 000 *g* for 20 min at RT, collecting the filtrate for every sample in a labelled 0.5 mL LoBind tube. This elution step was performed twice (collecting the filtrates in the identical LoBind tube). Then, the eluates were acidified by

adding 2 µL of 10% trifluoro acetic acid (TFA). Next, the digests were desalted by using C_{18} 100 µL tips on a multistepper pipet. The tips were washed by aspirating 100 µl of a 50% ACN:H_2O solution twice, followed by equilibration by aspirating 100 µl of a 0.1% TFA solution twice. The peptide samples were bound to the C_{18} resin by pipetting the acidified eluate up and down 10 times. After binding, the tips were washed by aspirating 100 µl of a 0.1% TFA/5% ACN solution twice, followed by elution of the peptides with 100 µl of a 0.1% TFA/80% ACN solution into Protein Low Bind Tubes 1.5ml PCR clean. Then, the samples were dried using a Speed-Vacc (45°C) (Concentrator 5301, Eppendorf) and stored at -80°C when possible until shipment to the LC-MS facilities. Upon arrival, peptides were stored at -20°C.

2.3.4 LC-MS/MS based quantification of proteotypic peptides

Concentrations of the endogenous (light) peptides were analysed by LC-MS/MS in relation to the heavy spiked-in peptides. Parameters used in the final LC-MS/MS method are listed in **Table 2.1**.

Table 2.1. *Detailed parameters of the LC-MS/MS method.*

Phase	Item	Details
Sample reconstitution	Dried sample	20 µg mucosal protein
	Resuspension buffer	35 µL of a 98% (v/v) LC-MS-grade water (with 0.1% (v/v) formic acid (FA))/2% ACN (with 0.1% (v/v) FA)
Sample injection	Autosampler	Shimadzu Nexera, SIL-40C X3 at 4°C
	Injection volume	25 µL of the reconstituted sample
Peptide separation	Column	C18, ACQUITY Premier Peptide, 100 x 2.1 mm, 1.8 µm, Waters, UK
	Oven	CTO-40C, Shimadzu at 30°C
	Flow rate	0.5 mL/min
	Mobile phase A	Ultrapure water with 0.1% (v/v) FA
	Mobile phase B	ACN with 0.1% (v/v) FA
	Mobile phase gradient	2 min 97% A, then a ramp to 70% B over 40 min, followed by a column wash (ramp to

		95% B over 5 min), returning to starting conditions (ramp for 5 min, maintaining starting conditions for 2 min) before the next run (Shimadzu Nexera, LC-40D xs solvent delivery module)
Peptide detection and quantification	Triple quadrupole	Shimadzu 8060NX, MRM setting
	Ionisation mode	Electron Spray Ionisation (ESI)
	MRMs per peptide	Usually 4 (range 3-6)
	Acquisition window	96 seconds around the expected retention time
	Dwell time	5 msec
	Pause time	5 msec
	Loop time (max)	1.442 s

Final peptide, precursor and fragment selection and instrument setting optimisation (collision energy, ion focussing voltage, loop time) were performed prior to sample analysis, via an iterative approach of method development, result analysis and method refinement.

2.3.4.1 Peptide selection to infer protein concentration prior to data collection

Before analysing the paediatric samples, specific peptides and transitions were selected to reduce the instrument loop time and increase the number of measurements across the peak. For this, the signal of pure heavy-isotope digested PaedCAT standards were evaluated using following criteria:

- Reproducibility across different standard injections,
- Multiplicity of the signal (i.e., minimal three transitions observed),
- Intensity of the signal.

Appendix 6 gives an overview of the selected peptides, transitions and expected retention time.

Skyline (version 21.2.0.568) was used for method development and optimisation, together with the LC-MS/MS instrument-specific software LabSolutions (version 5.109). Skyline and Microsoft excel (version 1808) were used for data analysis and visualisation.

2.3.4.2 Peptide selection to infer protein concentration after data collection

After collection, the data were analysed and compared to predefined criteria on peak shape, intensity and co-elution of transitions prior to protein abundance determination (**Figure 2.3**).

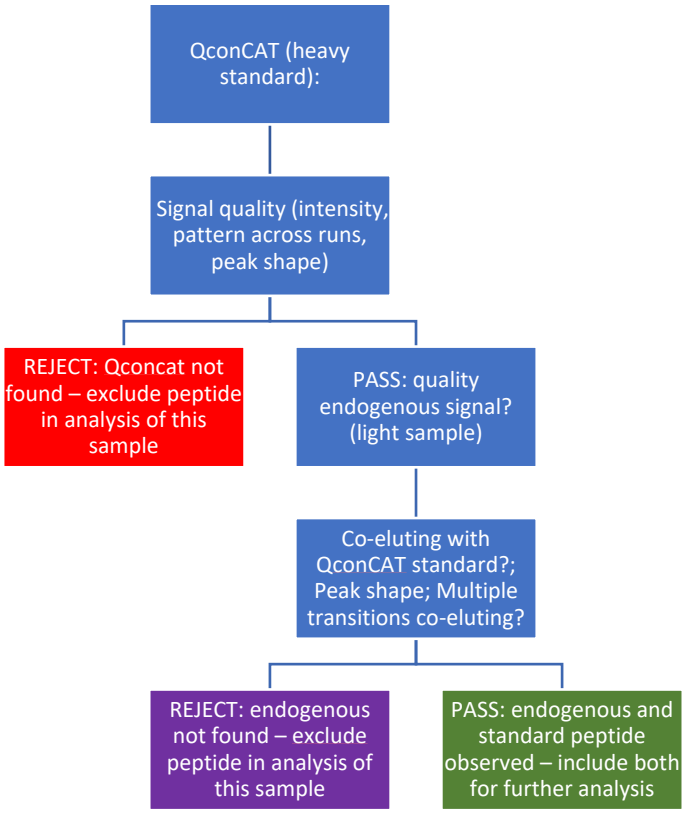

Figure 2.3. *Flowchart depicting peak judging for peptide inclusion/exclusion in final analysis.*

- Initially, the signal for the heavy peptide (deriving from the QconCAT transitions) was analysed, as this is a prerequisite for subsequent protein abundance extrapolation. Signals were assessed on the amount of co-eluting transitions with

good intensity. Peptides with missing heavy standard signal were excluded from the data set.

- After this, the endogenous signal was assessed on peak profile and transitions co-eluting with the heavy standard. Since the target proteins are low in abundance, a minimal limit of three co-eluting light transitions with adequate peak shape (i.e. visibly not noise) was set. If these conditions were not met, the endogenous signal was excluded from further analysis.

Additionally, samples were excluded if the light and/or heavy signal for villin-1 was not observed.

2.3.4.3 Protein abundance calculation

After peak inclusion or exclusion based on the aforementioned criteria, the datapoints were treated as follows:

- The light-to-heavy ratio for every peptide was normalised to the light-to-heavy ratio of the enterocyte marker villin-1. Correction to villin-1 is commonly done to normalise for the heterogeneity of intestinal tissue samples[5, 35, 142, 201], and is not reported to be subject to ontogeny[5, 98]. The villin-1 light-to-heavy ratio is derived from the signal of peptide DPETPIIVV**K**. (Note: the blue letter in bold signifies the stable isotope arginine or lysine).

$$villin\ normalised\ ratio_{ij} = \frac{Ratio\ peptide\ L/H_{ij}}{Ratio\ villin\ L/H_j}$$

Equation 2.1. *Normalisation of the light-to-heavy signal ratio (L/H) of peptide i in sample j is done by division of the original peptide ratio to the light-to-heavy signal ratio of the marker villin-1, given by peptide DPETPIIVV**K**, in sample j. For clarity, the marker villin-1 is written as "villin".*

- The normalised ratios were then multiplied to the initial PaedCAT amount spiked in the sample (2000 fmol in 20 ug protein, or 100 fmol per ug protein).

$$Protein_{\ i}\ abundance\ in\ sample_j = \ villin\ normalised\ ratio_{ij} * 100\frac{fmol}{\mu g} protein$$

Equation 2.2. *Protein abundance for a certain target protein in the sample (given in fmol/µg protein) is obtained by multiplying the villin-1 normalised light-to-heavy peptide ratio with the amount of PaedCAT spiked in, 100 fmol per µg protein. For clarity, the marker villin-1 is written as "villin".*

2.3.4.4 MS signal linearity via calibration curves

As a matrix, homogenates of cultivated HeLa cells were used. The HeLa-homogenates were spiked with PaedCAT and underwent the same FASP-protocol as described above. However, 20 µg of the HeLa homogenate protein (in 1 µg/µL) was spiked with 10 µL of varying concentrations of the PaedCAT solution. From the different concentrations of PaedCAT, 10 µL was spiked into a series of calibrators (spike concentration, fmol/µL): 0.1; 0.5; 0.75; 1; 2.5; 5; 10; 25; 50; 100; 150, 200; 1000; 2000. The calibrator samples were analysed in a similar manner via LC-MS/MS as the samples; the signal of the heavy-channel (PaedCAT) was set out to the injected amount of PaedCAT on the system. The signal of the light-channel was disregarded.

2.3.4.5 Statistical analysis of protein abundancy data

Statistical analysis was performed using the software packages IBM SPSS (version 28.0.1.1) and GraphPad Prism (version 9.4.1). Following statistical tests were employed:

- To investigate correlations of protein abundance with age and between proteins, the nonparametric Spearman correlation was used.
- To investigate differences between more than two groups of samples, a Kruskal-Wallis test was performed.

Statistical tests were deemed significant if the p-value was lower than 0.05 (p<0.05).

Linearity of the MS-signal for every peptide was analysed by plotting the observed MS signal to the amount of PaedCAT injected. Assessment of the goodness-of-fit via a calibration curve (R^2) was performed in Microsoft Excel.

2.4 Results

2.4.1 Tissue collection

Duodenal biopsies were collected from 37 paediatric participants. The participants ranged from 11 months to 15 years old, with a final diagnosis as healthy for 22 children, 12 children with underlying disease and 3 preschool children (aged 2, 4 and 4 years old) without a final diagnosis communicated. A summary in **Table 2.2** and a full overview in **Table 2.3** are given of the demographics, reason for endoscopy and final diagnosis of the paediatric participants included in this study.

***Table 2.2**.: Summary of the demographics of participants whose biopsies were collected for this study*

	Number of biopsies available		
Age range	**Diagnosed as normal**	**Diagnosed with disease**	TOTAL
<2 years (neonate/infant/toddler)	0	1	1
2 – 5 years (pre-school children)	4	2	9*
6 – 11 years (school-age children)	9	4	13
12 – 16 years (adolescents)	9	5	14
TOTAL	**22**	**12**	37*

*. * For three preschool children, no final diagnosis (healthy or diseased) was available.*

On average, the paediatric pinch biopsies had a mass of 17.85 mg (standard deviation (SD) 6.41 mg, median 16.7 mg), with a range of 8.4 mg to 32.1 mg, which is in line with literature for pinch biopsy sizes[382].

Table 2.3. *Demographics, reason for endoscopy and final diagnosis of the participants included in this study.*

Participant ID code	Ethnicity	Age (years)	Height (cm)	Weight (Kg)	Reason for the endoscopy	Final diagnosis
UK001	White British	13	158.6	48.5	Bleeding per rectum	Colonic polyp
UK002	Any other ethnic group, not specified	10	142	33.2	Abdominal pain	Normal
UK003	White- not specified	13	173	56.2	Diarrhoea + Anaemia	Coeliac Disease
UK004	Not known	2	84.1	11.9	Vomiting	Eosinophilic oesophagitis
UK005	Asian/Asian Brit- Indian	11	151	38	Abdominal pain	Normal
UK006	White British	8	134.9	44.3	Vomiting	Normal
UK007	White British	6	112.8	21	Vomiting	Normal
UK008	White - not specified	2	94.2	14.9	Diarrhoea	Normal
UK011	Black/Black British - any other black background	14	166.6	57.4	Abdominal pain	Normal
UK012	White British	15	154	40.7	Abdominal pain	Crohn's Disease
UK013	Asian/Asian Brit- Pakistani	11	147.5	66.6	History of choking episodes	Normal
UK014	Mixed White and Black Caribbean	14	169.9	79.9	Abdominal pain	Normal
UK017	White British	14	152.6	52.5	Dyspepsia	Normal
UK018	White British	12	169	60.9	Abdominal pain	Normal
UK020	Not stated	3	91.8	15.1	Asymptomatic type 1 diabetic patient, screening for Coeliac Disease	Coeliac Disease
UK024	White British	11	158	38.2	Abdominal pain	Normal
UK026	Not known	13	150.2	42.1	Abdominal pain	Normal
UK028	White British	12	153.7	47.1	Surveillance endoscopy	Eosinophilic oesophagitis
UK029	White British	15	179.2	61.8	Abdominal pain	Normal
UK031	White English	9	136.6	25.9	Abdominal pain	Normal
UK033	Asian/ Asian Brit - Indian	15	155.6	39.8	IBD surveillance	Normal

UK034	White British	15	167.8	47.4	Slow weight gain	Normal
UK036	White British	5	117.4	22.6	Suspected Coeliac Disease	Normal
UK041	White British	12	141.3	29.9	Surveillance of Crohn's Disease	Crohn's Disease
UK042	White British	3	99.7	14.4	History of blood in vomit	Normal
UK044	White English	8	119.8	21.9	Suspected Coeliac Disease	Coeliac Disease
UK046	White British	3	97.1	15.4	Complaints of Diarrhoea	Normal
UK047	White British	7	112.6	17.6	Surveillance of Crohn's Disease	Crohn's Disease
UK048	White English	6	115.2	19.9	History of diarrhoea	Normal
UK049	White British	11 months	65	7.4	Suspected Coeliac Disease	Coeliac Disease
UK050	White English	10	129.1	25.5	Suspected Coeliac Disease	Coeliac Disease
UK051	White English	10	133.6	28.9	Suspected Coeliac Disease	Normal
UK052	Asian/ Asian British	6	129	24.1	Surveillance of Ulcerative Colitis	Ulcerative Colitis
UK053	White Irish Traveller	4	99.7	16.5		
UK054	White English	2	88.3	14.1		
UK055	Asian/ Asian British - Indian	4	109.1	18.2		

2.4.2 Protein digestion via FASP

2.4.2.1 PaedCAT design and expression

A QconCAT named PaedCAT containing proteotypic peptides for the 21 target proteins and markers was developed by Polyquant GmbH. The 55 proteotypic peptide sequences of PaedCAT, together with the protein to which they belong, are given in **Table 2.4**. The full amino acid sequence of PaedCAT, together with details such as labelling efficiency, storage buffer and purification method, is given in **Appendix 5**.

Table 2.4. *Proteotypic peptide sequences included on the QconCAT PaedCAT. The terminal lysine (K) or arginine (R) were labelled with a stable isotope.*

Gene	Protein	Peptide
ABCB1	P08183	QEIGWFDVHDVGELNTR
ABCB1	P08183	AGAVAEEVLAAIR
ABCB1	P08183	FYDPLAGK
ABCG2	Q9UNQ0	VIQELGLDK
ABCG2	Q9UNQ0	TIIFSIHQPR
ABCG2	Q9UNQ0	LFDSLTLLASGR
ABCC2	Q92887	IFNSTDYPASQR
ABCC2	Q92887	QLLNNILR
ABCC2	Q92887	YLGGDDLDTSAIR
ABCC3	O15438	IDGLNVADIGLHDLR
ABCC3	O15438	SQLTIIPQDPILFSGTLR
ABCC3	O15438	AEGEISDPFR
ABCC4	O15439	LTVTLFFPSAIER
ABCC4	O15439	VFVAVTLYGAVR
ABCC4	O15439	ITILVTHQLQYLK
ATP1A1	P05023	IVEIPFNSTNK
ATP1A1	P05023	NIAFFSTNCVEGTAR
ATP1A2	P50993	NICFFSTNCVEGTAR
ATP1A3	P13637	NITFFSTNCVEGTAR
CES2	O00748	FAPPEPPESWSGVR
CES2	O00748	LGVLGFFSTGDK
CES2	O00748	SFFGGNYIK
CYP2C19	P33261	IYGPVFTLYFGLER
CYP2C19	P33261	GHFPLAER
CYP2C9	P11712	GIFPLAER
CYP2C9	P11712	LPPGPTPLPVIGNILQIGIK
CYP2D6	P10635	AFLTQLDELLTEHR
CYP2D6	P10635	DIEVQGFR
CYP2J2	P51589	VIGQGQQPSTAAR

CYP2J2	P51589	FEYQDSWFQQLLK
CYP3A4	P08684	EVTNFLR
CYP3A4	P08684	LSLGGLLQPEKPVVLK
CYP3A4	P08684	SAISIAEDEEWK
CYP3A5	P20815	DTINFLSK
CYP3A5	P20815	SAISLAEDEEWK
SLC15A1	P46059	HTLLVWAPNHYQVVK
SLC22A1	O15245	ENTIYLK
SLC15A1	P46059	VQQCGIHSK
SLC22A1	O15245	LSPSFADLFR
UGT1A1	P22309	GHEIVVLAPDASLYIR
UGT1A1	P22309	DGAFYTLK
UGT1A1	P22309	TYPVPFQR
UGT1A3	P35503	YLSIPTVFFLR
UGT1A3	P35503	EVSVVDILSHASVWLFR
UGT1A4	P22310	GLQVPLPR
UGT1A4	P22310	YLSIPAVFFWR
UGT1A9; UGT1A8	O60656	TYSTSYTLEDLDR
UGT1A9	O60656	AFAHAQWK
UGT2B17	O75795	SVINDPIYK
UGT2B17	O75795	FSVGYTVEK
UGT2B7	P16662	TILDELIQR
UGT2B7	P16662	IEIYPTSLTK
VIL1	P09327	GSLNITTPGLQIWR
VIL1	P09327	LFQVQGTGANNTK
VIL1	P09327	DPETPIIVVK

2.4.2.2 Protein digestion via FASP

Proteins were digested into peptides using trypsin and Lys-C in a FASP protocol. The BCA assay used most of the sample and the remaining fraction was too limited for FASP digestion for sample UK053.

2.4.3 LC-MS/MS based quantification of proteotypic peptides

2.4.3.1 Peptide selection to infer protein concentration prior to data collection

The first step in refining the LC-MS/MS method was to identify which peptides met the inclusion criteria set out in section 2.3.4.1 (i.e. reproducible signal of co-eluting transitions

with good intensity), to reduce the overall MS loop time and thus increase signal collection for all other targets. This was done based on the signal of the heavy standard PaedCAT. Out of the 55 target peptides, 38 peptides met the inclusion criteria (**Appendix 6**).

For example, a small signal belonging to the peptide QEIGWFDVHDVGELNT**R** (belonging to transporter ABCC1) was not reproducible. It was observed only once in two heavy standard injections (containing pure FASP-digested PaedCAT) (**Figure 2.4**). This peptide was subsequently excluded from monitoring in the final method, as the other two peptides for ABCC1 gave a more reproducible and more intense signal (**Figure 2.5**) in the same assays.

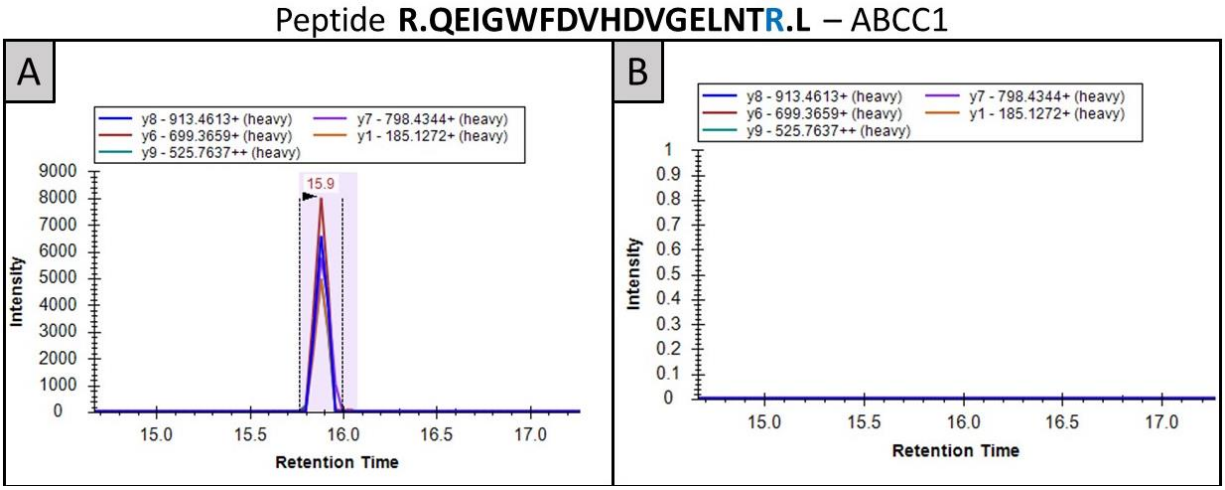

Figure 2.4. *Peptide QEIGWFDVHDVGELNT**R** (ABCC1) was observed in the results of a pure PaedCAT injection (A), but not in a second, identical injection (B).*

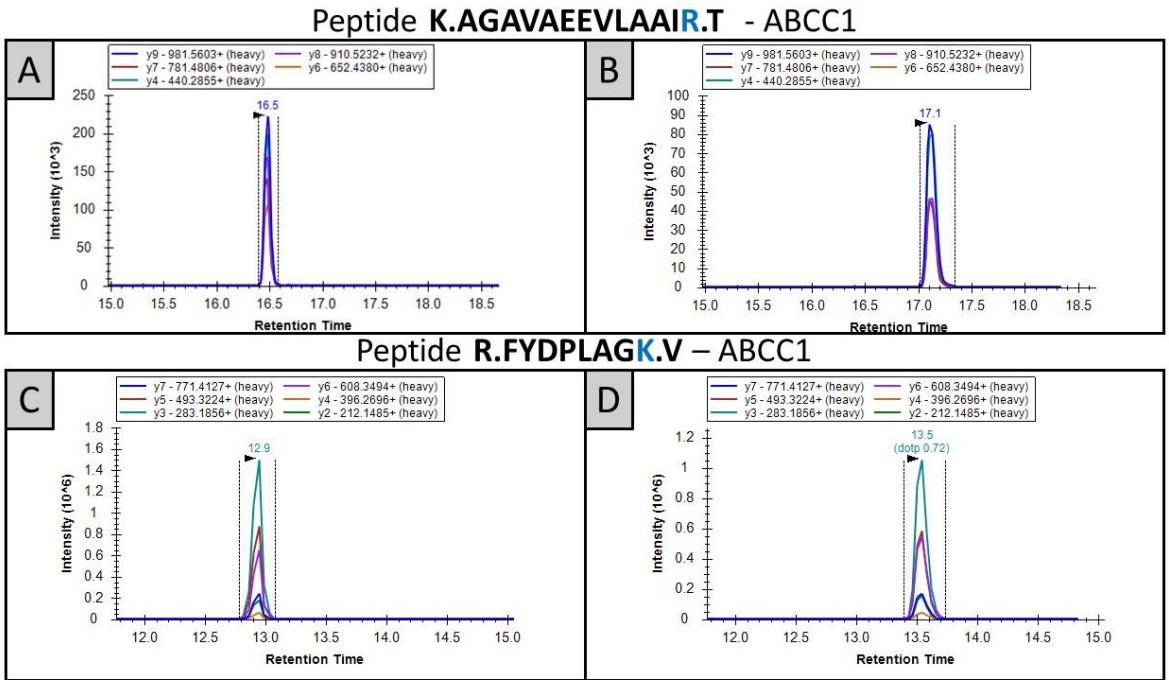

Figure 2.5. *Peptides AGAVAEEVLAAIR and FYDPLAGK (both belonging to ABCC1) were observed in the result of two pure PaedCAT injections, with coeluting transitions in intense signals.*

Additionally, peptides SAISIAEDEEWK (CYP3A4) and SAISLAEDEEWK (CYP3A5) eluted at the same time, and as the optimised transitions could not differentiate between both peptides (isoleucine and leucine have an identical molar mass), both peptides were excluded for further analysis.

2.4.3.2 Peptide selection to infer protein concentration after data collection

Using the final method monitoring 38 peptides, all paediatric were analysed via LC-MS/MS. Then, the collected data were assessed using predefined criteria set out in section 2.3.4.2, **Figure 2.3**. After qualitative review of the heavy peptide signals, for every peptide and all samples, the following were excluded:

- four peptides (being: ITILVTHQLQYLK (ABCC4), NITFFSTNCVEGTAR (ATP1A3), YLSIPAVFFWR (UGT1A4) and LFQVQGTGANNTK (VIL-1)) as no intense signal or co-

eluting transitions for the heavy peptide were observed, and thus no light-to-heavy ratio could be determined.

- One sample (UK020) as the heavy signal of VIL-1 was not observed, so no correction to villin-1 would be possible.

Then, the endogenous (light) signal was evaluated for the remaining 34 peptide for every sample against the pre-determined criteria as set out in section 2.3.4.2, **Figure 2.3**. In more than 90% of the samples, no qualitative endogenous (light) signal was found for the peptides listed in **Table 2.5**. An example for CYP2J2 is given in **Figure 2.6**. Peptides for which a qualitative signal was recorded are listed in **Table 2.6**. There were some occasions where an endogenous signal was not observed in some samples, when it was observed in others. The peptides for which an endogenous signal was observed in more than 50% of the samples were not excluded.

Table 2.5. *Peptides for which no qualitative endogenous signal was observed.*

Protein Gene	Peptide Sequence
ABCC2	YLGGDDLDTSAIR
ABCC3	AEGEISDPFR
ABCC3	IDGLNVADIGLHDLR
CES2	LGVLGFFSTGDK
CYP2D6	AFLTQLDELLTEHR
CYP2J2	FEYQDSWFQQLLK
CYP2J2	VIGQGQQPSTAAR
SLC15A1	VQQCGIHSK
SLC22A1	LSPSFADLFR
UGT1A3	EVSVVDILSHASVWLFR
UGT1A3	YLSIPTVFFLR
UGT1A4	GLQVPLPR
UGT1A8/9	TYSTSYTLEDLDR
UGT1A9	AFAHAQWK

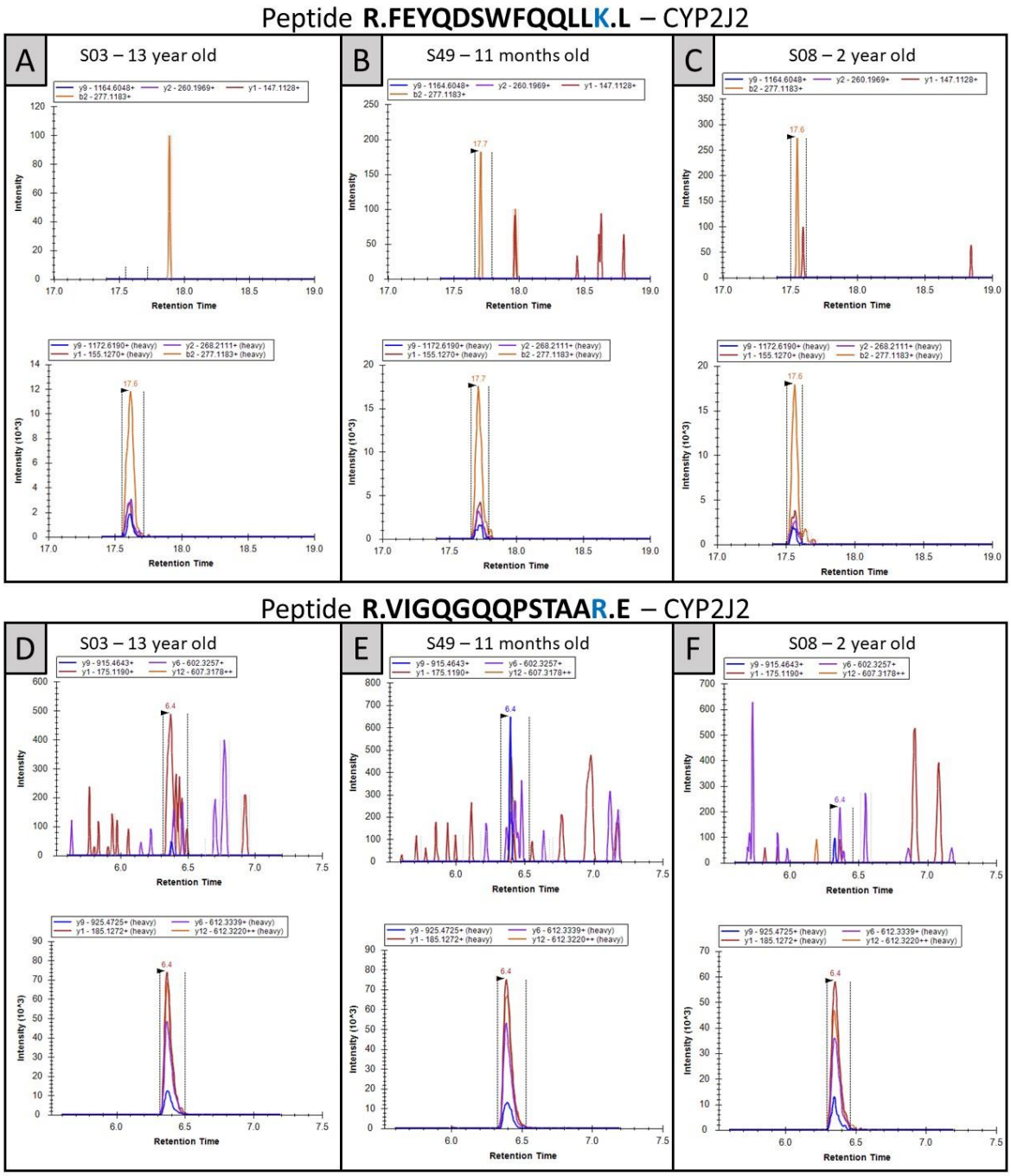

Figure 2.6. *Example of missing endogenous signal for the two target peptides of CYP2J2, for biopsies taken from a child aged (A, D) 13 years, (B, E) 11 months and (C, F) 2 years. The top graphs show the light (endogenous) channel, the bottom graphs show the heavy (PaedCAT standard) channel.*

Table 2.6. *Peptides for which a qualitative endogenous signal was observed in most samples.*

Protein Gene	Peptide Sequence
ABCB1	AGAVAEEVLAAIR
ABCB1	FYDPLAGK
ABCC2	QLLNNILR
ABCG2	LFDSLTLLASGR
ABCG2	VIQELGLDK
ATP1A1	IVEIPFNSTNK

CES2	SFFGGNYIK
CYP2C19	GHFPLAER
CYP2C9	GIFPLAER
CYP2D6	DIEVQGFR
CYP3A4	EVTNFLR
CYP3A5	DTINFLSK
SLC22A1	ENTIYLK
UGT1A1	DGAFYTLK
UGT1A1	TYPVPFQR
UGT2B17	FSVGYTVEK
UGT2B17	SVINDPIYK
UGT2B7	IEIYPTSLTK
UGT2B7	TILDELIQR
VIL1	DPETPIIVVK

For five proteins (ABCB1, ABCG2, UGT1A1, UGT2B17 and UGT2B7), two peptides were suitable for quantification (i.e. a qualitative heavy and light peptide signal recorded). The light-to-heavy ratios of the two peptides of UGT2B7 are in close correlation, which is also the case for two peptides of UGT1A1 (p<0.05 for both) (see **Figure 2.7**). However, this was not the case for the peptides for ABCB1 and ABCG2 (p>0.05 for both, **Figure 2.8**). Thus, no average of the data for two peptides of one protein was taken, and the protein data reported below (**Table 2.7**) is based on the signals for every individual peptide. It should be emphasised that for the proteins with discordant abundancy values, the order of magnitude of the signal strength is considerably lower than for the concordant peptides.

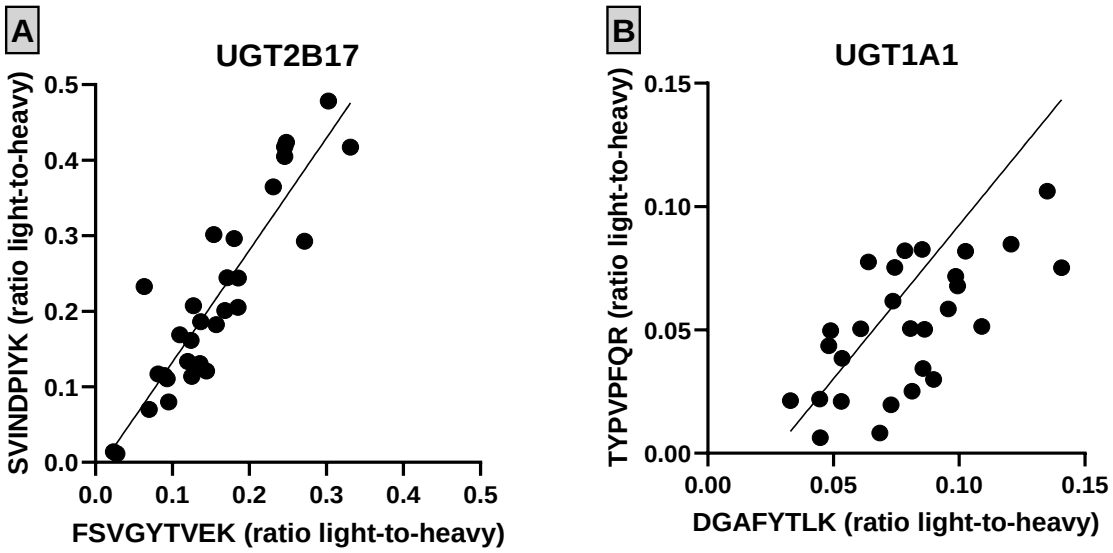

Figure 2.7. *Correlation of the light-to-heavy ratios for two peptides of (A) UGT2B17 and (B) UGT1A1. The black line depicts the trendline for a linear regression. For UGT2B17: Spearman r 0.86,* p*<0.0001; Y = 1.483*X - 0.01572- linear regression R^2 0.81. For UGT1A1: Spearman r 0.66, p<0.0001; Y = 0.6395*X + 0.0007977 - linear regression R^2 0.43.*

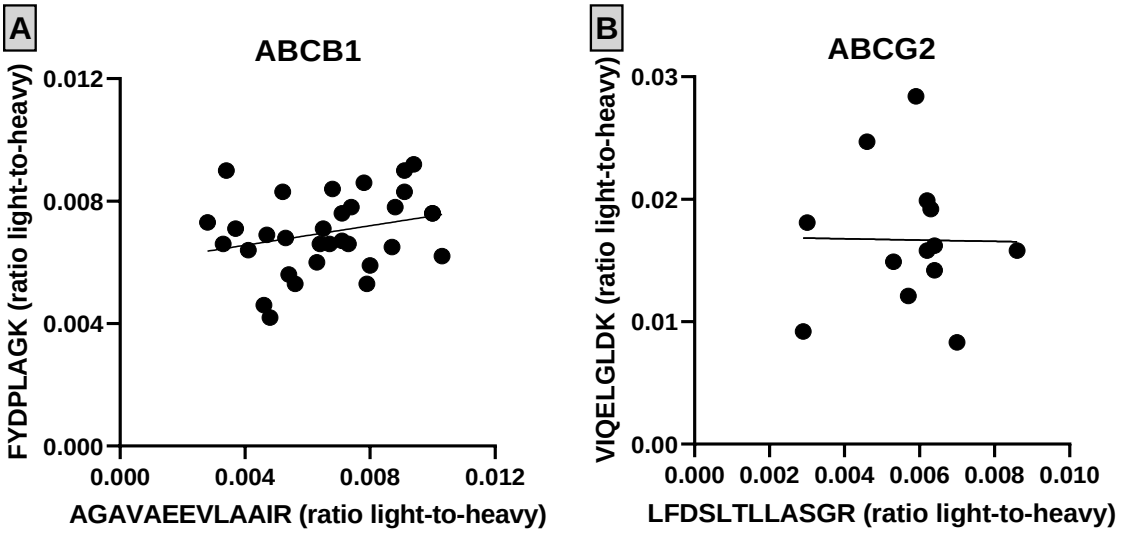

Figure 2.8. *Correlation of the light-to-heavy ratios for two peptides of (A) ABCB1 and (B) ABCG2. The black line depicts the trendline for a linear regression. For ABCB1: Spearman r 0.25, p=0.16; Y = 0.1597*X + 0.005918 – linear regression R^2 0.07. For ABCG2: Spearman r -0.13, p=0.65; Y = -0.05237*X + 0.01698– linear regression R^2 0.00.*

Representative co-elution profiles are given in **Figure 2.9**.

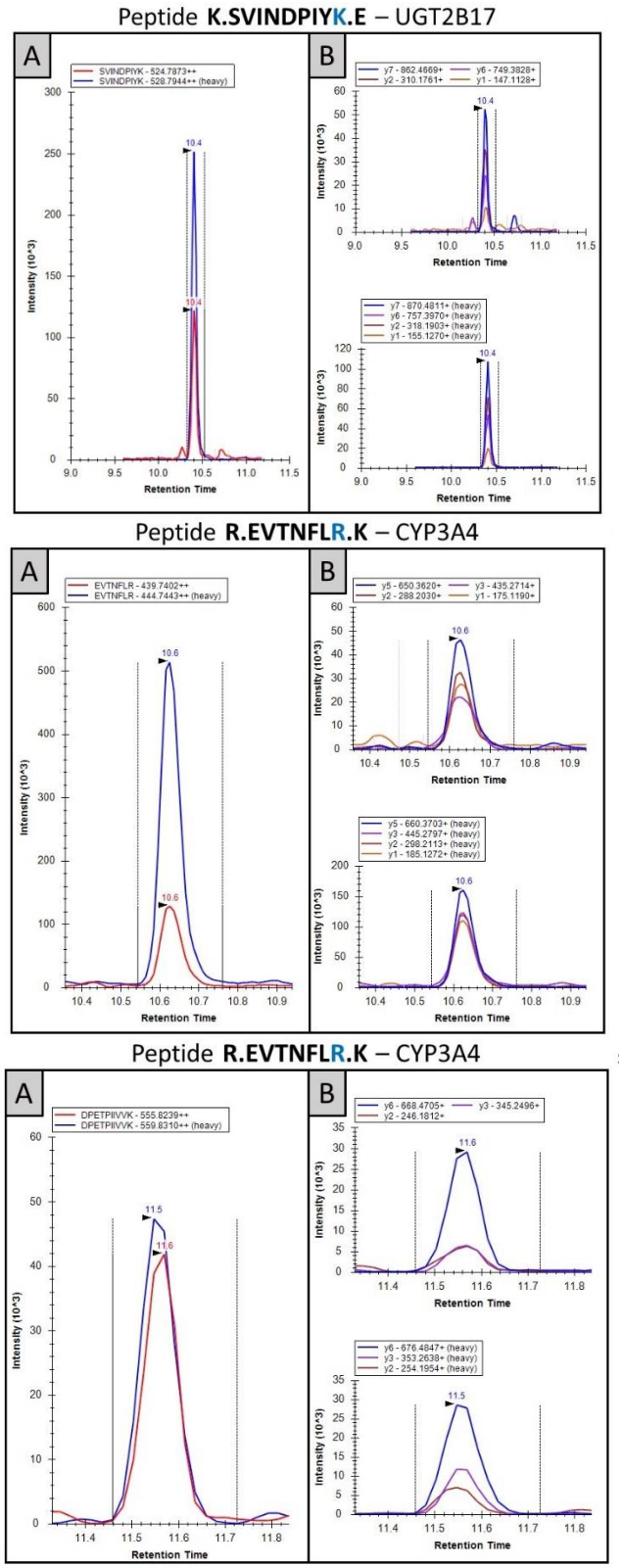

Figure 2.9. *Representative co-elution profiles examples for three different peptides, captured by Skyline. Panel A shows the cumulative elution profile of the different transitions for (red) the endogenous light signal and (blue) the standard heavy signal. Panel B shows the peak profiles for the selected transitions, with on the top the transitions for the endogenous light signal and bottom for the standard heavy signal.*

As result, 20 proteotypic peptides could be used to infer protein concentration from an initial method of 38 peptides.

2.4.3.3 MS signal linearity via calibration curves

The linearity of the MS signal over the range of the expected protein amount was assessed using calibrators. The calibrators ranged from 0.1 to 2000 fmol/µL, where the expected range of DMET-protein abundance was 1-200 fmol/µL.

Linear regression of signal versus amount PaedCAT injected onto the MS gave a close correlation of >0.97 for all peptide targets, except for peptides ITILVTHQLQYLK (ABCC4) (R^2 = 0.05), NITFFSTNCVEGTAR (ATP1A3) (R^2 = 0.67), VQQCGIHSK (SLC15A1) (R^2 = 0.32) and EVSVVDILSHASVWLFR (UGT1A3) (R^2 = 0.00).

The first two peptides were excluded before data collection, and no endogenous signal was observed for the latter two peptides, hence no data needed to be excluded post-analysis.

2.4.4 Protein abundancy data

Based on the light-to-heavy ratio for the probe peptides, protein abundances were calculated after correction to villin-1. The ratio light-to-heavy for villin-1 (given by peptide DPETPIIVVK) span a 12-fold difference in range (mean: 0.57 ± 0.29, range 0.13-1.5).

Table 2.7 summarises the protein abundancy of the quantified proteins in 34 paediatric intestinal biopsies (total, diagnosed normal and diagnosed diseased), the data for individual samples is given in **Appendix 7** and age-stratified subgroups in **Appendix 8**. Out of the 21 target proteins, 13 could be quantified (with addition of two markers).

Table 2.7. *DMET-protein abundance in paediatric duodenum. Values are expressed in pmol/mg protein. N shows the number of samples in which the protein was quantified, SD standard deviation.*

	TOTAL					Diagnosed normal*					Diagnosed diseased*				
Protein	N	Min.	Max.	Mean	SD	N	Min.	Max.	Mean	SD	N	Min.	Max.	Mean	SD
CES2	34	33.36	132.34	77.70	23.91	21	41.02	126.63	77.55	23.51	11	33.36	132.34	79.15	27.71
CYP2C19	33	0.58	5.41	2.18	1.12	20	0.58	5.41	2.17	1.20	11	1.00	4.53	2.30	1.08
CYP2C9	34	1.33	6.60	2.36	0.97	21	1.33	6.60	2.40	1.14	11	1.48	3.47	2.23	0.68
CYP2D6	31	0.51	7.79	2.18	1.54	20	0.51	7.79	2.07	1.67	9	0.85	5.25	2.21	1.44
CYP3A4	32	4.80	31.89	17.57	7.03	21	6.76	29.35	19.04	5.71	9	6.60	31.89	16.74	8.33
CYP3A5	31	1.36	10.43	4.32	2.23	19	1.36	10.43	4.00	2.54	11	1.75	6.71	4.86	1.67
UGT1A1[a]	30	6.60	30.79	15.52	5.46	20	6.60	30.79	14.65	6.15	8	13.85	21.97	17.06	3.21
UGT1A1[b]	32	1.85	98.83	11.84	16.57	20	4.27	13.04	9.22	2.52	10	1.85	98.83	18.67	29.16
UGT2B17[c]	28	4.19	61.32	28.14	12.39	19	4.19	41.97	25.85	10.59	8	20.10	61.32	34.49	15.35
UGT2B17[d]	34	1.43	106.30	36.93	25.10	21	1.43	62.64	33.13	17.80	11	4.18	106.30	47.93	34.55
UGT2B7[e]	28	1.99	11.56	4.96	2.35	18	1.99	8.51	4.18	1.56	8	2.38	11.56	6.13	3.12
UGT2B7[f]	33	1.14	6.28	2.59	1.03	21	1.24	6.28	2.86	0.97	10	1.14	4.56	2.18	1.05
ABCB1[g]	32	0.46	6.28	1.50	1.08	20	0.46	6.28	1.50	1.23	10	0.63	3.00	1.34	0.77
ABCB1[h]	32	0.57	4.22	1.57	0.82	20	0.57	4.22	1.47	0.85	10	0.65	3.40	1.67	0.81
ABCC2	31	0.56	5.73	1.75	1.13	19	0.56	5.73	1.62	1.14	10	0.80	4.52	1.81	1.20
ABCG2[i]	19	0.49	1.89	1.11	0.45	12	0.49	1.89	1.01	0.45	7	0.85	1.88	1,27	0.42
ABCG2[j]	24	1.32	10.12	4.11	2.05	14	1.32	7.80	4.26	1.89	9	1.55	10.12	3.87	2.49
SLC22A1	23	1.59	17.50	5.20	3.55	15	1.59	17.50	4.67	3.89	7	3.05	10.25	6.14	2.97

Using [a]: DGAFYTLK, [b]: TYPVPFQR, [c]: FSVGYTVEK, [d]: SVINDPIYK, [e]: IEIYPTSLTK, [f]: TILDELIQR, [g]: AGAVAEEVLAAIR, [h]: FYDPLAGK, [i]: LFDSLTLLASGR, [j]: VIQELGLDK as probe to infer protein abundance for these five proteins with two proteotypic peptides.
Min: minimum. Max: maximum. *: abundancy values of participants for which no diagnosis were available are only included in the "total"

column

2.4.4.1 Abundance of DMET proteins and ontogeny

2.4.4.1.1 CYP enzymes and CES2

It was possible to quantify 5 out of 6 Cytochrome P450 isoform targets in the paediatric duodenum. A qualitative endogenous signal for CYP2J2 was not observed in any sample for either target peptide (**Table 2.5**, **Figure 2.6**). The measured proteins were in following rank order for the entire paediatric cohort: CYP3A4>CYP3A5>CYP2C9, CYP2D6, CYP2C19 in comparable levels (**Figure 2.10**).

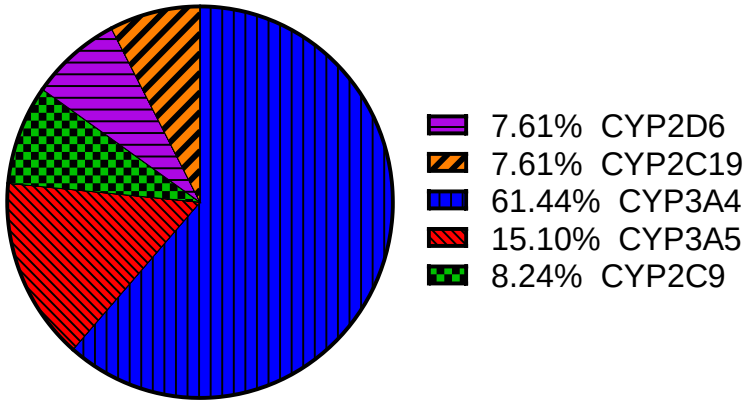

Figure 2.10. *Mean relative abundance of the quantified CYP enzymes in paediatric duodenum of 34 participants.*

The mean (and SD) of the different CYP and CES2 protein abundances for the entire paediatric cohort and per age group are given in **Figure 2.11** and **Figure 2.12**.

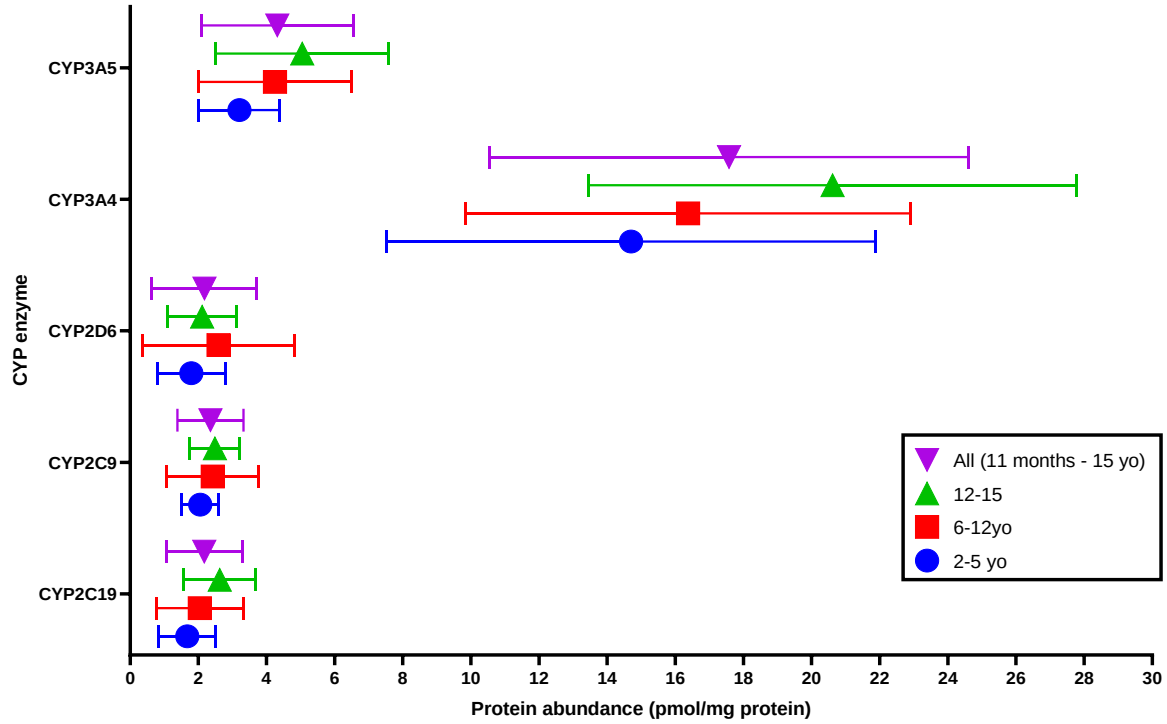

Figure 2.11. *CYP enzyme protein abundance in paediatric duodenum for the entire cohort and different age groups. Symbols depict the mean, error bars denote the SD.*

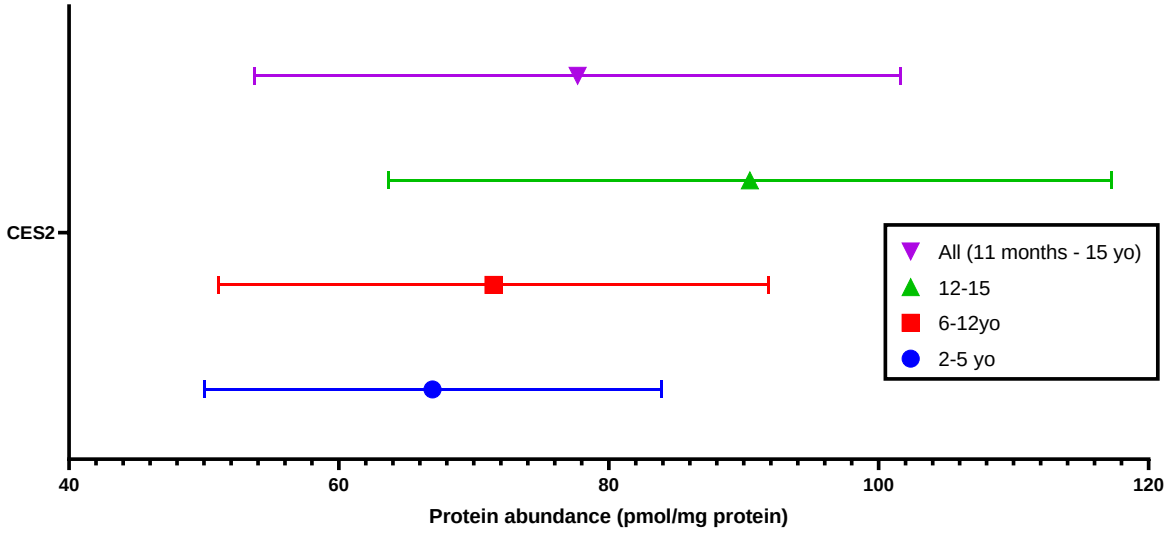

Figure 2.12. *CES2 enzyme protein abundance in paediatric duodenum for the entire cohort and different age groups. Symbols depict the mean, error bars denote the SD.*

The protein abundance between the different age groups (2-5 year old, 6-11 and older than 12) were compared via Kruskal-Wallis tests. Infants were excluded as there was only one participant (11 months old) in this cohort. The Kruskal-Wallis test was not significant for any protein.

Significant correlations were observed for age and the protein abundance of CES2 and CYP3A4 (Spearman's correlation 0.440, *p*=0.009 for CES2 and Spearman's correlation 0.381, p=0.032 for CYP3A4) (**Figure 2.13**). No statistically significant correlations between the abundance of other proteins and age on continuous scale were found.

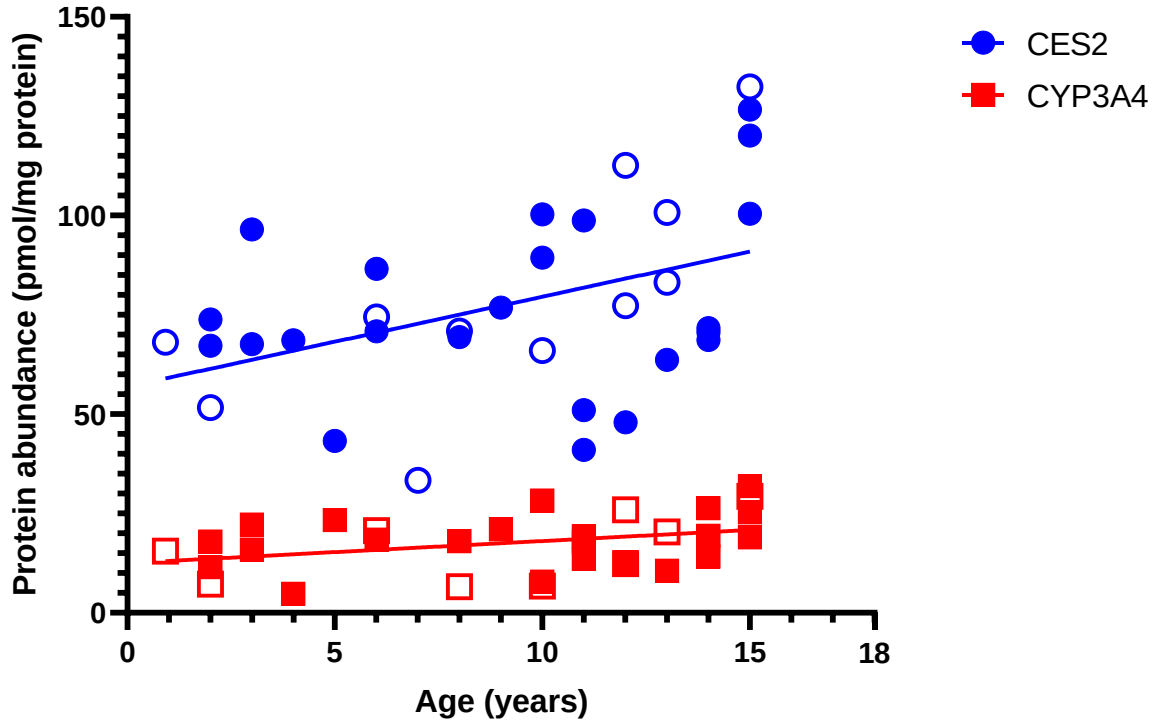

Figure 2.13. *Correlation between age and the protein abundance of CES2 and CYP3A4. (Spearman's correlation 0.44 and 0.381 for CES2 and CYP3A4 respectively, p<0.05 in both cases). Open symbols indicate participants who were diagnosed as diseased, closed symbols diagnosed as normal.*

2.4.4.1.2 Transporters

Out of the 7 transporter proteins included in the assay, 4 could be quantified. No endogenous signal was observed for basolateral efflux transporters ABCC3 and ABCC4, or for the peptide transporter PEPT1 (SLC15A1). SLC22A1 was the most expressed transporter, ABCC2 and ABCB1 were expressed in similar levels (**Table 2.7**, **Figure 2.14**). However, the rank order of ABC-transporters could not be determined, as ABCG2 is either the most or the least abundant ABC-transporter depending on which proteotypic peptide for protein quantification is used. Similarly, two peptides were suitable for quantification for ABCB1

(**Figure 2.8**, **Figure 2.5**), so the results for both proteins are reported using two proteotypic peptides.

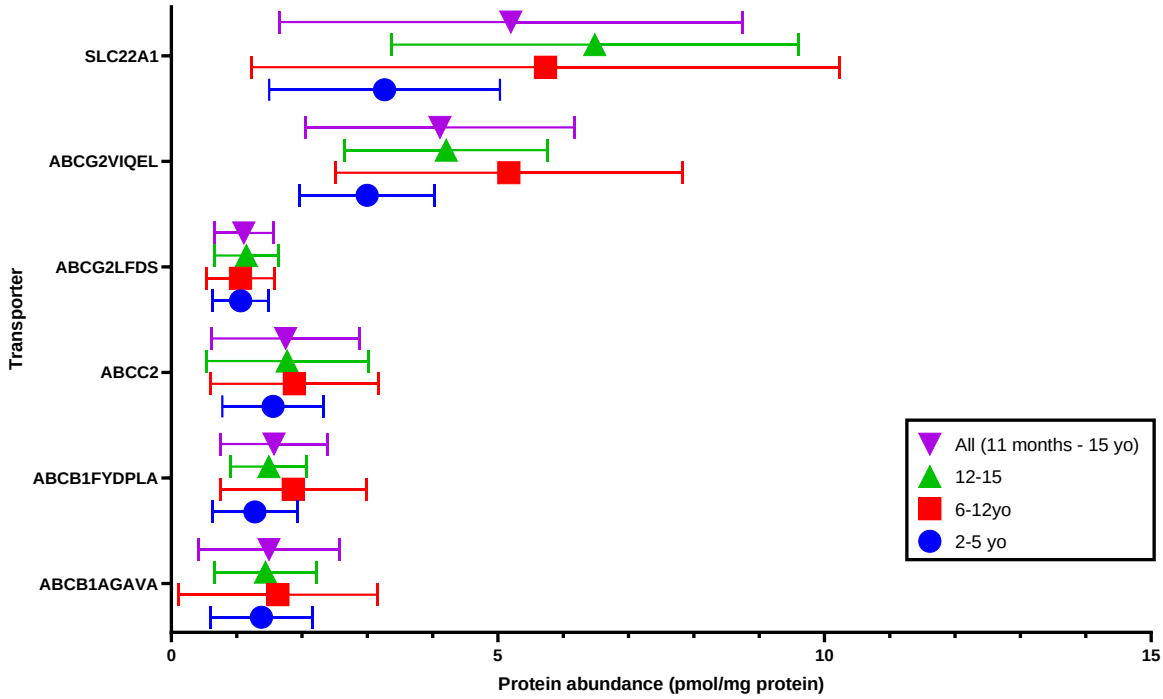

Figure 2.14. *Transporter protein abundance in paediatric duodenum for the entire cohort and different age groups. Symbols depict the mean, error bars denote the SD.*

2.4.4.1.3 UGT enzymes

Three from the seven targeted UGT enzymes were quantified in paediatric duodenum. For UGT1A3, UGT1A4, UGT1A8 and UGT1A9 no endogenous signal was observed. UGT2B17 was the most expressed enzyme, followed by UGT1A1 and UGT2B7. For all three quantified proteins, two proteotypic peptides were used (examples given in **Figure 2.7**). Quantifying the protein abundance with either proteotypic peptide does not influence the overall rank order of the UGT enzymes as observed in **Figure 2.15**.

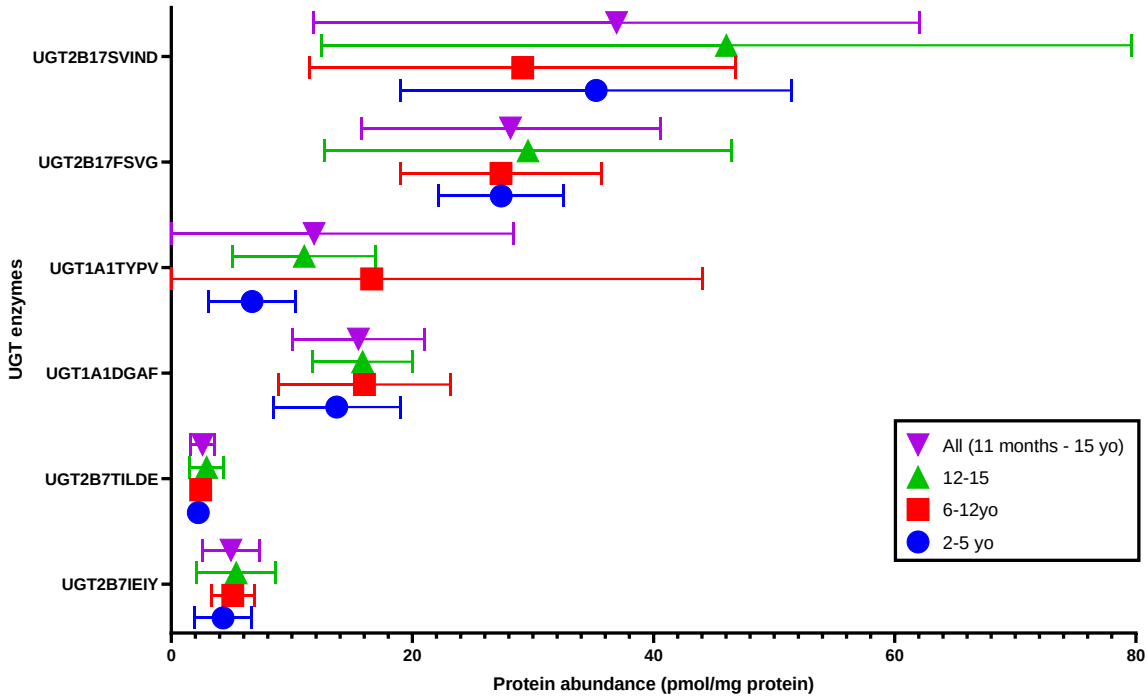

Figure 2.15. *UGT enzyme protein abundance in paediatric duodenum for the entire cohort and different age groups. Symbols depict the mean, error bars denote the SD.*

2.4.4.2 Interprotein correlations

Pairwise protein abundance correlations were tested using the nonparametric Spearman test. Strong significant Spearman correlations ($r>0.5$, $p<0.05$) are listed in **Table 2.8**. The abundance of all transporter proteins are correlated with each other.

Table 2.8. *Spearman r for significant interprotein correlations observed in paediatric duodenum (p<0.05 for all).*

	ABCB1[b]	ABCC2	ABCG2[c]	ABCG2[d]	ATP1A1	CYP2C19	CYP2C9	CYP2D6	CYP3A5	SLC22A1	UGT1A1[e]	UGT2B17[f]	UGT2B17[g]	UGT2B7[h]
ABCB1[a]	0.68	0.64	0.62	0.57	0.62		0.66	0.39	0.56	0.51				
ABCB1[b]		0.78	0.79	0.69	0.68	0.53	0.66	0.74	0.73	0.68	0.52			0.76
ABCC2			0.60	0.69	0.71		0.65	0.75	0.65	0.66	0.61			0.76
ABCG2[c]							0.68		0.65					0.58
ABCG2[d]							0.69	0.68	0.58	0.55				
ATP1A1						0.62	0.74		0.67	0.66	0.69			0.64
CES2						0.53	0.59							
CYP2C19							0.63		0.67		0.56	0.60	0.54	
CYP2C9									0.60	0.62	0.58			0.70
CYP2D6									0.52	0.63	0.58			0.60
CYP3A4												0.54		
CYP3A5										0.51	0.55			0.52
SLC22A1											0.64			0.73
UGT1A1[e]														0.71
UGT2B17[f]													0.85	

Protein concentration assessed by proteotypic peptide: [a]: AGAVAEEVLAAIR, [b]: FYDPLAGK, [c]: LFDSLTLLASGR, [d]: VIQELGLDK, [e]: DGAFYTLK, [f]: FSVGYTVEK, [g]: SVINDPIYK, [h]: IEIYPTSLTK

2.5 Discussion

2.5.1 Quantification of selected DMET protein abundances in paediatric intestinal pinch biopsies

Gut bioavailability can play a significant role for drugs orally administrated[16, 168]. As DMET-proteins can either metabolise the drug, or transport it out to the gut lumen (thus lowering exposure) or to the blood stream (hereby increasing exposure), their influence and physiological properties need to be well-characterised. Existing tools for drug development should be readily adapted to enable representative simulations of vulnerable populations to be made, such as the paediatric population, where data are lacking[13, 168]. Using pinch biopsies from the paediatric duodenum of 36 participants, important DMET-proteins have been quantified.

2.5.1.1 CYP enzymes and CES2 abundance

CYP3A4 was the most abundant CYP enzyme within the paediatric duodenum, followed by 3A5, and similar levels for 2C9, 2D6 and 2C19. An identical rank order is reported on adult intestinal tissue[80], with CYP3A4 as most expressed CYP enzyme[142, 231, 270, 276] followed by CYP2C9 and comparable levels of CYP2D6, CYP2C19 and CYP2J2[80, 134]. CYP levels for the eldest age group (12-15 year old) in the paediatric duodenum are comparable to reported values in adult duodenum, jejunum and ileum (**Figure 2.16** for CYP3A4, **Table 2.9** for all target CYP enzymes). Visual inspection of the graphical data presented in Kiss *et al*.[98] confirms CYP3A4 as the most abundant CYP-enzyme in paediatric jejunum and ileum, however detailed data are not available from this publication.

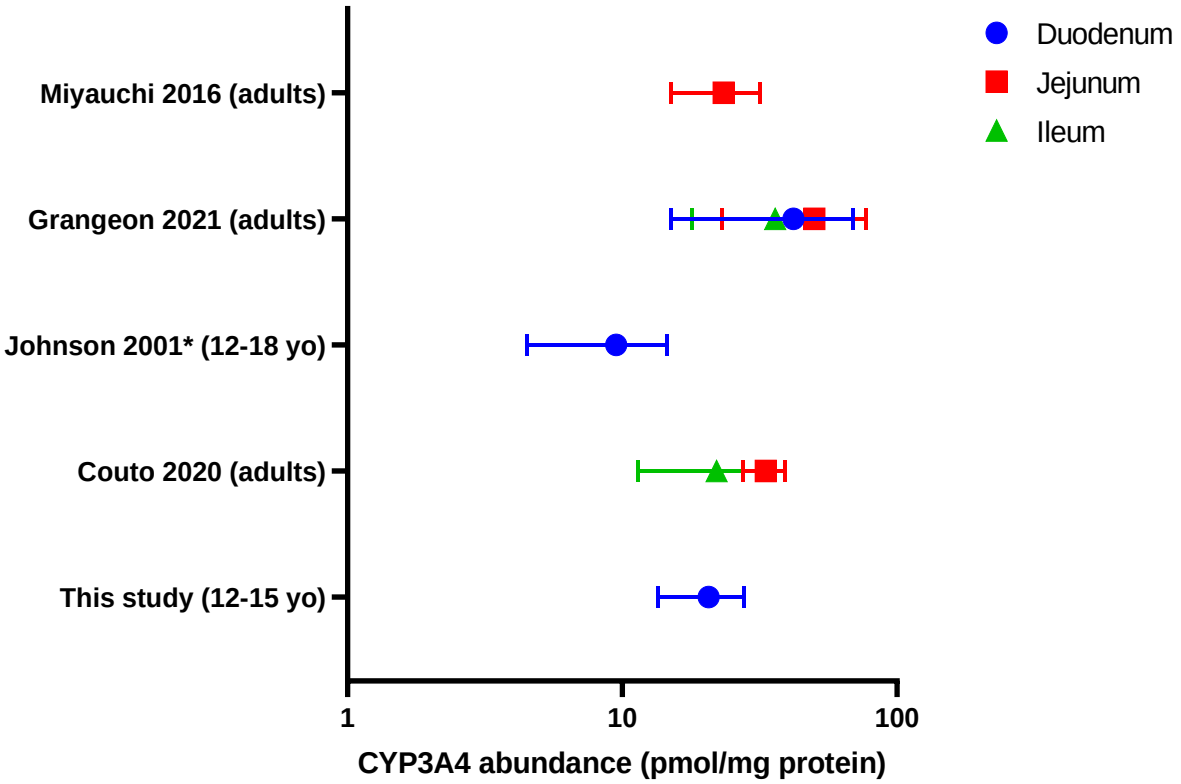

Figure 2.16. *Intestinal CYP3A4 abundance values for the eldest age group in this study (12-15 years old (yo)) and key publications on adult intestinal proteomics. *: the results by Johnson et al.[5] are based on western blotting. Symbols indicate mean, error bars denote the SD.*

Table 2.9. *Intestinal CYP enzyme expression values for the eldest age group in this study (12-15 years old) and adult studies. Values are expressed in pmol/mg protein, mean ± SD are given.*

Protein	This study (12-15 yo), duodenum	Grangeon 2021[270], adults, duodenum	Couto 2020[80], adults, jejunum	Couto 2020, adults, ileum	Miyauchi 2016[142], adults, jejunum	Gröer 2014[273], adults, jejunum[273]	Drozdzik 2017[135], adults, jejunum	Drozdzik 2017, adults, ileum	Akazawa, 2018[276], adults, jejunum	Akazawa, 2018, adults, ileum
CYP2C9	2.48 ± 0.73	5.1 ± 2.6	1.52 ± 0.61	1.42 ± 0.60	3.15 ± 1.25	4.27 ± 0.97[a] 0.32 ± 0.18[b]	0.034 ± 0.023	0.009 ± 0.004	0.51 ± 0.09[c] 3.74 ± 0.25[d]	0.72 ± 0.08[c] 3.23 ± 0.08[d]
CYP2C19	2.63 ± 1.06	1.4 ± 0.83	1.08 ± 0.11	1.25 ± 0.60	0.43 ± 0.17	2.79 ± 1.32[a] 1.43 ± 0.25[b]	0.003 ± 0.003	BLQ	N/A	N/A
CYP2D6	2.11 ± 1.01	0.38 ± 0.41	1.91 ± 0.46	1.64 ± 0.55	1.87 ± 1.11	<BLQ[a,b]	0.004 ± 0.003	0.003 ± 0.004	BLQ[c] 1.18 ± 0.1[d]	BLQ[c] 1.16 ± 0.05[d]
CYP3A4	20.61 ± 7.16	42 ± 27	33.33 ±5.70	22.04± 10.60	23.4 ± 8.4	18.7 ± 6.26[a] 1.85 ± 0.36[b]	0.135 ± 0.134	0.092 ± 0.126	6.2 ± 0.36[c] 9.84 ± 0.43[d]	8.03 ± 0.4[c] 12.9 ± 0.5[d]
CYP3A5	5.05 ± 2.53	0.52 ± 0.21	N/A	N/A	1.29 ± 1.37	<BLQ[a,b]	N/A	N/A	N/A	N/A

yo: years old. [a]: commercially bought intestinal microsomes (n=8), [b]: in-house prepared intestinal microsomes, [c]: individual A (measured in triplicate), [d]: individual B (measured in triplicate). BLQ: below limit of quantification. N/A: no data available.

For younger age groups, the abundancy of CYP3A4 in paediatric duodenum is similar to the values reported by Johnson *et al*[5], obtained via western blots on 104 paediatric samples (**Figure 2.17**). A significant increase of CYP3A4 with age was observed on continuous scale (**Figure 2.13**), but no statistical difference was found between different age groups. An increase of CYP3A4 with age was also reported by proteomic analysis on paediatric jejunum and ileum[98]. No statistically significant effect of age on expression of other CYP enzymes has been found in the present study, nor for UGT-enzymes and transporter proteins. A significant trend with age for CES2 duodenal expression was observed in this study, which corroborates previous results via mRNA and protein level in the paediatric duodenum[212]. This also correlates with ontogeny of hepatic CES2, and an increase in dietary esters and amides[383, 384].

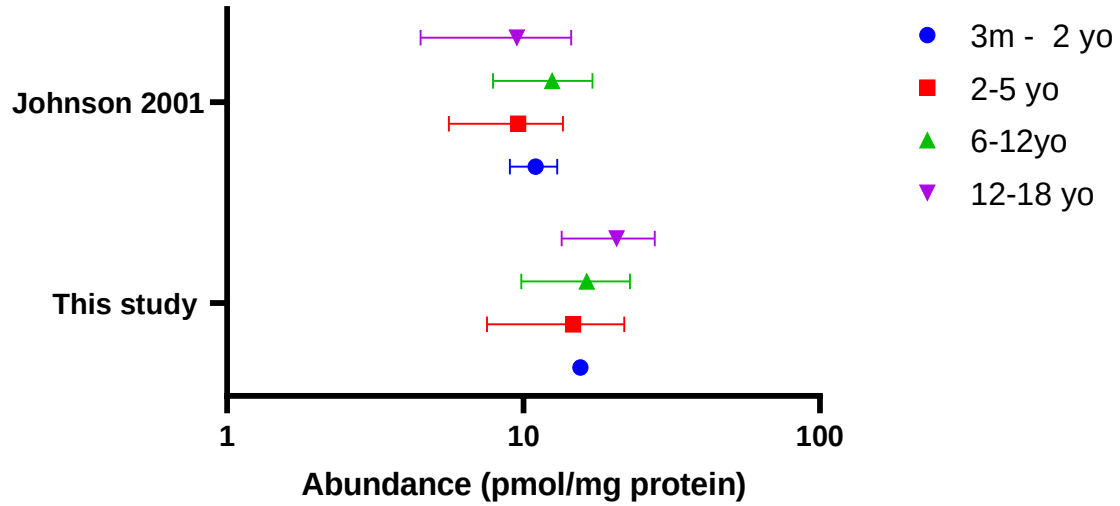

Figure 2.17. *Reported CYP3A4 abundance in this study and Johnson et al across different age groups. Symbols indicate the mean, error bars denote the SD.*

This ontogeny of CYP3A4 can be linked to higher bioavailability (i.e. lower intestinal metabolism) of oral midazolam in young children. Midazolam is a benzodiazepine frequently used in neonatal and paediatric medicine for sedation[385, 386]. Midazolam is metabolised by intestinal and hepatic CYP3A4, and its PK-PD profile is extensively studied in children[387-393].

Adult bioavailability is reported to be around 30%[394], whereas high bioavailability (92.1%, range 67-95%) was observed in preterm neonates[94]. In CHAPTER THREE, the influence of CYP3A4 ontogeny on midazolam bioavailability and PK will be explored using PBPK modelling.

It needs to be noted, although a similar trend with age is observed for CYP3A4, the reported abundance values for CYP3A4 by Kiss *et al*. are very dissimilar from the values reported in Johnson *et al*. or this study. Additionally, the adult abundancy values reported in their paper do not resonate with other studies for adult intestine. For example, Kiss reported adult jejunum CYP3A4 abundance as 536 ± 588.1 pmol/mg protein (mean ± S.D.), which was 33.33 ± 570 pmol/mg protein in Couto's publication. These discrepancies could be due to differences in sample preparation and analysis protocol[265, 395, 396], as addressed by Kiss.
An example on how sample preparation procedures influence the abundancy data is demonstrated in Groer *et al*[273] . Here, pooled human intestinal microsomes were quantified on CYP- and UGT-content. One set of intestinal microsomes was prepared in-house, a second set were commercially bought. Although both sets of microsomes were derived from macroscopically healthy jejunal tissue, were prepared for LC-MS in the same laboratory and analysed on the same instrument, a large difference in e.g. CYP3A4-content can be measured. Gröer hypothesised the differences in abundance to be due to dissimilar microsomal isolation procedures. It is recognised in literature that interlaboratory differences between intestinal DMET abundance are associated with the different methodological approaches in the proteomic workflow to quantify intestinal DMET-abundance[80]. An example on how LC-MS-set-up influences the abundancy data is demonstrated by reported differences in abundancy values by Couto[80] and Al-Majdoub[162].

Here, the same samples were analysed, with one protocol using a targeted MS approach using QconCATs as heavy standard. The other protocol used a semi-targeted approach where identification was based on accurate mass and retention times (AMRT), quantification relied on the ion peak intensity of heavy and light version across samples, with the relative abundance interpolated from the intensity ratios[162, 397]. The difference in reported abundance for CYP3A4 are ten-fold, with 33.33 (±5.7) pmol/mg for the target approach, in contrast to 2.47 (±2.68) pmol/mg for the AMRT method. However, this does not fully explain the observed differences with Kiss *et al*. as a target approach was also used. Differences in the use of a QconCAT compared to SIL-peptides, and at which point these are spiked into the samples, potentially impact the data. Another potential factor is extensive contamination with other cells in the latter skewing their results, as there was no procedure to isolate enterocytes. Although this was also not employed in the present study, the pinch biopsies included here were on average 15 mg, whereas Kiss used intestinal tissue samples with an average weight of 150 mg. No procedure to dissect the mucosa from the underlaying tissue has been reported in their work, which has been performed in other proteomic papers[80, 270]. Using other methods, such as tissue dissociation with collagenase and selective enterocyte harvesting with anti-EpCAM antibodies can further select enterocytes selectively and diminish the influence of other cell types[398]. Additionally, the intestinal tissue from Kiss were obtained as surgical leftover material, whereas the pinch biopsies in this study were collected from children, some of which who were ultimately diagnosed as healthy. An effect of disease state can further influence the results presented by Kiss[2, 37, 399, 400]. The use of medication, potentially influencing DMET-expression, was not recorded in the current work. Similarly, the method of normalisation to villin-1 also differs between the presented work here and Kiss. Here, the protein abundances are normalised to

villin-1 for every individual target, on every individual sample (**Equation 2.1** and **Equation 2.2**). However, Kiss adjusted the observed protein abundances in two different methods. The first method used the cohort-average villin-1 abundance, to which individual samples were normalised. This was deemed unsuitable, as the paediatric population is very heterogeneous and using a cohort-average might skew the results. The second method used relative abundances compared to the villin-1 signal (as performed in this study), but then these were log_2-transformed which resulted in negative normalised values. Finally, additional factors suggested by Kiss include a difference in membrane fractionation among other factors.

Some proteins, such as CYP2J2, could not be quantified in any paediatric duodenal biopsy. Despite a well-observed signal for the heavy standard, no endogenous signal was detected (**Figure 2.6**). Additionally, it was observed the amount of peptide was in the linear range of the MS-detector, as the goodness-of-fit of the calibration curve (R^2) for both peptides were >0.9. CYP2J2 has been quantified before via LC-MS/MS in adult intestine[270], where intestinal tissue samples were taken from recently diseased adults due to head trauma, with or without GIT comorbidities. The expression of CYP2J2 significant increased along the small intestine, with lowest expression in the duodenum. Expression of CYP2J2 is closely correlated with CYP2C9 and CYP2D6 in adult intestine[80, 137], the latter two were quantified in paediatric duodenum. Thus, potentially a mixed effect of ontogeny and disease effect on the expression of CYP2J2 in the lowest expression region explains the lack of endogenous signal, although no ontogeny for CYP2J2 has been reported. Potentially, the used sample protocol was not ideal for CYP2J2 stability, or the LC-MS/MS acquisition settings not fully optimised for detection of the endogenous signal in low amounts. To assess the suitability of the

employed LC-MS/MS method, transfected overexpressing cell-lines could be used for all proteins where no endogenous signal was observed[125]. Additionally, it is recognised that identical proteotypic probes not necessarily give rise to a qualitative signal using different mass spectrometers[115, 142] So did a peptide for transporter SLC51A1 give a detectable signal for all samples in one study on adult jejunum[142], but detection of the same peptide failed for 2 out of 3 samples in a different study[115]. The authors hypothesised this is due to differences in sample prep. Similarly, Gröer *et al*. were not able to detect some CYP-proteotypic peptides that were described before[273]. Performing shot-gun experiments on the intended equipment for quantification can help identify more suitable peptide targets, however this was not available for our study.

2.5.1.2 Transporter protein abundance

In this study, similar levels of ABCC2 (MRP2) and ABCB1 (P-gp) were observed. ABCG2 (BCRP) was either the most or least abundant ABC-transporter, depending on the used proteotypic peptide for quantification. A similar trend (ABCG2>ABCB1>ABCC2) was also observed using proteomics in adult jejunum and ileum[115, 142] and via immunoquantification in the adult duodenum[197]. However, conflicting trends in adult jejunum/ileum have also been reported, such as ABCC2>ABCB1>ABCG2[80, 125, 196], or ABCB1>ABCC2>ABCG2[196] (**Table 2.10**).

Table 2.10. *Intestinal ABC-transporter expression values for the paediatric cohort in this study and adult studies. Values are expressed in pmol/mg protein, mean ± SD are given.*

Protein	ABCB1		ABCC2	ABCG2	
This study (11 mo – 15 yo), duodenum	1.50 ± 1.08[a]	1.57 ± 0.82[b]	1.75 ± 1.14	1.11 ± 0.45[c]	4.11 ± 2.05[d]
Harwood[115] 2015, adults, jejunum	1.9 ± 1.1[f]	0.8 ± 0.3[g]	0.6 ± 0.2	2.6 ± 0.8[f]	2.1 ± 1.1[g]
Harwood 2015, adults, ileum[e]	0.2[f]	BLQ[g]	BLQ	1.6[f]	0.44[g]
Couto[80] 2020, adults, jejunum	0.74 ± 0.22		3.33 ± 0.76	0.59 ± 0.27	
Couto 2020, adults, ileum	0.96 ± 0.56		2.66 ± 0.65	0.45 ± 0.13	
Groer 2013[196], adults, jejunum	0.61 ± 0.04		1.06 ± 0.16	0.57 ± 0.04	
Groer 2013, adults, ileum	0.64 ± 0.1		0.35 ± 0.07	0.69 ± 0.07	
Drozdzik 2014[125], adults, duodenum	0.3 ± 1.2		0.77 ± 0.4	0.20 ± 0.27	
Miyauchi 2016[142], adults, jejunum	1.22 ± 0.37		0.116 ± 0.044	1.25 ± 0.54	
Kiss[98] 2021, adults, ileum	154.3 ± 53.78		N/A	102.3 ± 37.19	
Kiss 2021, adults, jejunum	N/A		71.45 ± 24.11	92.33 ± 16.55	
Kiss 2021, paediatrics, ileum	43.57 ± 21.76[h]		N/A	31.75 ± 33.84[h] 28.72 +- 17.18[g]	
Kiss 2021, paediatrics, jejunum	N/A		15.39 ± 10.48[h]	31.98 ± 11.11[h]	

Using [a]: AGAVAEEVLAAI**R**, [b]: FYDPLAG**K**, [c]: LFDSLTLLASG**R** or [d]: VIQELGLD**K** as probe to infer protein abundance. [e]: n=1. [f]: assay by Harwood lab, [g]: assay by Bertin Pharma lab, [h]: 0-2 years old, [i]: 12-18 years old. mo: months old, yo: years old. BLQ: below limit of quantification. N/A: no data available

No ontogeny of ABCB1 has been observed in this study, in agreement of existing literature on mRNA expression or immunoquantification of proteins[167, 171, 174-176] or paediatric proteomics[98]. Kiss *et al*. [98] reported a significant trend with age for ABCG2 abundance, but this is not supported by the findings in this study or mRNA analysis[171]. No effect of age has been observed in this study for the duodenal abundance of ABCC2, where this has been observed in a proteomic study on paediatrics[98]. However, Kiss *et al*. had samples from 29 participants aged 0-2 years, in our study only one such sample was collected. Obtaining more paediatric duodenal samples for DMET-quantification, with additional efforts for the youngest cohort, could further elucidate ontogeny profiles that were not observed at this stage, as the major intestinal changes happen within the first two years of life[13].

Potentially, intestinal ABC-transporters are challenging to quantify. In Harwood *et al*.[115], using a selective procedure to isolate the enterocytes from the underlaying tissue layers, ABCB1 and ABCC2 were below the limit of quantification. In Kiss *et al*.[98], the mean ileal ABCG2 abundance is lowest in the 12-18 year old group, with higher expression levels for the 0-2 age group and highest for adults. No other evidence for such an ontogeny function has been reported. Similarly, it was challenging to find a final abundance value for ABCB1 and ABCG2, as the endogenous signals of the two probes for either protein were not in correlated. This could be due to dissimilar chemical stability characteristics of the peptides. In this study, the chemical stability of the proteotypic peptides in human matrices was investigated, although similar work report adequate stability of peptide samples upon reconstitution[115, 196, 273]. Additionally, uncharacterised protein isoform or detected posttranslational modifications can also explain this discrepancy[273]. However, it is still useful to report the protein abundance assessed by both probes, as this can give tools used for

drug prediction a wider range to model with, so extreme values would be covered. As such, there is no clear consensus on the abundance and rank of ABC-transporters; further efforts to elucidate are required.

In adult duodenum, the reported abundance for SLC22A1 (OCT1) is 0.7 ± 0.35 pmol/mg[125], in a previously study on paediatric duodenum around 5-10 pmol/mg. Values similar to the latter are found in this study for SLC22A1, using the identical proteotypic probe. However, no endogenous signal for SLC15A1 (PEPT1) was observed for any sample despite MS-optimisation based on the internal standard. As endogenous signal for SLC15A1 has been observed in paediatric and adult intestinal tissue[98, 125, 196] with different probes, the chosen proteotypic peptide here was potentially not optimal. SLC15A1 shares substrate specificity with basolateral efflux transporters ABCC3 and ABCC4[187], neither were detected in this study. The expression of these ABC-transporters increased along the GIT with highest levels observed in the adult colon[125, 135, 196].

2.5.1.3 UGT enzyme abundance

The observed rank order for the UGT-enzymes that were quantified in paediatric duodenum was UGT2B17>UGT1A1> UGT2B7. This correlates to the observed rank orders in adult intestine[80, 142, 196]. Previously, a significant difference has been reported for the UGT1A1 abundance in the ileum and jejunum of 0-2 year olds compared to adults; however no difference with age was observed here. This could be due to limited number of neonatal biopsies as previously described.

Table 2.11. *Intestinal UGT-enzyme expression values for the paediatric cohort in this study and adult studies. Values are expressed in pmol/mg protein, mean ± SD are given.*

Protein	UGT1A1	UGT2B17	UGT2B7
This study, 11 mo – 15 yo, duodenum	15.52 +- 5.46[a] 11.84 +- 16.57[b]	28.14 +- 12.39[c] 36.93 +- 25.10[d]	4.69 +_ 2.35[e] 4.96 +- 2.35[f]
Couto 2020[80], adults, jejunum	2.93 ± 2.17	N/A	1.84 ± 0.97
Couto 2020, adults, ileum	1.52 ± 0.55	N/A	1.17 ± 0.23
Groer 2014[273], adults, jejunum	7.83 ± 0.97[g] 1.0 ± 0.28[h]	N/A	2.83 ± 0.24[g] BLQ[h]
Akazawa 2018 [276], adults, ileum	BLQ[i] 5.05 ± 0.38[j]	7.63 ± 0.32[i] 33.7 ± 1.3 [j]	BLQ[i] 5.59 ± 0.63[j]
Akazawa 2018, adults, jejunum	BLQ[i] 4.57 ± 0.22[j]	4.91 ± 0.12[i] 7.63 ± 2.3[j]	BLQ[i] 5.29 ± 0.98[j]
Miyauchi 2016[142], adults, jejunum	11 ± 3.3	38 ± 20	4.22 ± 1.35
Drozdzik 2018[231], adults, jejunum	0.101 ± 0.068	N/A	0.023 ± 0.012
Drozdzik 2018, adults, ileum	0.036 ± 0.021	N/A	0.006 ± 0.004
Kiss 2020[98], adults, ileum	150.3 +- 83.93	N/A[m]	N/A[m]
Kiss 2020, adults, jejunum	441.6 +_ 227.5	N/A[m]	N/A[m]
Kiss 2020, paediatrics, ileum	11.73 +- 17.91[k]	N/A[m]	N/A[m]
Kiss 2020, paediatrics, jejunum	18.41 +_ 13.05[k]	N/A[m]	N/A[m]
Harbourt 2012[204], adult microsomes	7.2 ± 3.7	N/A	N/A
Sato 2014, adult microsomes	39.6 ± 21.4	36.6 ± 32.7	15.7 ± 9.81

Using [a]: DGAFYTLK, [b]: TYPVPFQR, [c]: FSVGYTVEK, [d]: SVINDPIYK, [e]: IEIYPTSLTK, [f]: TILDELIQR as probe to infer protein abundance. [g]: using commercial microsomes, [h]: using in-house prepared microsomes, [i]: individual A (measured in triplicate), [j]: individual B (measured in triplicate). [k]: villin-corrected abundance levels in the 0-2 year age group, [m]: only raw data reported. mo: months old, yo: years old. BLQ: below limit of quantification, N/A: no data available.

2.5.2 Method development, strengths and limitations

To assess MS-response linearity, 14 calibrators were prepared ranging from 0.1 fmol/µL to 2000 fmol/µL. All calibration curves had a R^2>0.97, in line with literature[80, 115]. HeLa-cell homogenate was used as matrix for human biopsies, due to the lack of a blank matrix that represents human intestinal homogenates. It was deemed that this human cell-homogenate would serve as a better matrix than digested human serum albumin (HSA) as previously used in intestinal proteomics[196], as the former is a more complex heterogeneous matrix[196] and thus is more representative for assessment of ionisation suppression and enhancement in the MS[115]. This is also corrected for by using stable-isotope-labelled version of the peptide targets and desalting before LC-MS/MS analysis[395].

However, the current study should be viewed as preliminary, as there are limitations. For example, the most significant changes in DMET ontogeny are expected in children younger than 2[145, 178, 180], yet this cohort was underrepresented. Additionally, it should be recognised that it is increase is unlikely a linear process, but a rapid increase in the younger age groups (<2 years old) is expected. However, only a single biopsy from a participant younger than 2 year was collected, so more investigation into the development with age in this youngest cohort is essential (section 1.1.1)[5]. Additional factors in this heterogeneous population, such as diversity in reason for biopsy collection, ethnicity or feeding patterns should also be considered in future studies that should aim to include larger sample sizes for all age bands and include adult participants for direct comparison to available data. A sample size of 20 participants per age band was proposed, but not met. An even larger sample size than this could ensure that there is a representative portion of normal participants, as intestinal comorbidities have been shown to impact DMET levels[124].

A second limitation is the minimal material available. In a validated proteomic assay (complying to strict regulations as e.g. for the FDA), all methods should be standardised and include assays that determine e.g. peptide stability, limit of detection/quantification), extraction efficiency among others, and proteins could be quantified using several concordant peptide probes, each with several transitions (such as **Figure 2.7**). That the measured peptides approach the limit of detection is obvious in **Figure 2.8**, where peptides discordance is observed as the light-to-heavy ratio of the peptides is low. The peptide observed in **Figure 2.4** was also observed in one assay, but not in a repeat run of the same sample. The peptide was qualitatively observed in the first run (four co-eluting transitions; *y6, y8, y7* and *y1*) but not observed in a repeat injection. This could be due to drift in retention time, detector voltages, increased suppression at the ionisation stage in the first quadrupole, any issues in the solvent flow and peptide degradation in the automatic sampler[322, 323, 401]. However, standardisation of these processes was not feasible due to the rareness of obtaining paediatric intestinal tissue, and the lack of standardised approaches to study intestinal DMET proteins. Additionally, there were some issues with the instrumentation too despite the method being correct. However, even being able to quantify some proteins on the limited starting material should already be considered as a major breakthrough for paediatric intestinal DMET quantification, and further work should establish gold standards to strive to a standardised approach with method validation strategies.

The current work here is also limited by the lack of repeat injections of paediatric samples, but this was not possible due to the minimal biopsy sizes (17.85 ± 6.41 mg). In contrast, it is a strong point of this study to be the first to successfully quantify three different DMET-

protein families using such small biopsies, as most studies start with larger surgical waste tissue or diseased donors[98, 135, 270] (the smallest biopsy size reported was 100 mg), isolated intestinal mucosa sections[80] or only looked at one family (e.g. cell membrane isolation[115, 135, 196] or microsomal preparations[79, 204, 205, 247, 273]) where the followed protocol would not have been suitable to study both membrane and microsomal proteins. In a recent review (2020) on transporter proteomics, the authors suggested that a minimum of 100 mg of tissue is required for to obtain sufficient protein for LC-MS/MS analysis[271]. This study clearly demonstrates that smaller intestinal pinch biopsies provide a suitable starting amount as well. Thus, quantification studies on DMET protein quantification via LC-MS/MS can use intestinal pinch biopsies which are easier to collect, rather than acquiring samples as surgical waste or brain-dead donors.

As second strength, this is the first report to use a QconCAT standard that enables quantification for both transporters and metabolising enzymes in one protein. As mentioned in section 1.4.3.12, using a QconCAT as heavy standards reduces cost and time when analysing 10-50 protein targets in 20-100 samples[165, 339]. QconCATs have been used previously to quantify DMET-proteins in adult small intestine (TransCAT[115] and MetCAT[80, 162]). The reported success in quantification of adult intestinal DMET-levels adds to the benefits of its sustainability and transferability between different research groups[80, 115, 402]. However, there was no QconCAT developed before that contains peptide sequences for the three DMET-protein families (transporters, CYP and UGT-enzymes)[340]. Developing a single QconCAT allows for a superior method to compare and interrogate protein correlations between the different families as the standard peptides are generated in a 1:1 ratio, compared to multiple spiking event with separate peptides. The limitation of using a QconCAT is the loss of flexibility when target proteins are expressed in very different levels.

As DMET-abundance in literature are reported in the range of 0.1-100 pmol/mg protein[80, 115], a similar spike level was chosen in this study.

The samples were normalised to the enterocytic marker villin-1[241], as there is a lack of ontogeny reported for this protein[5, 98]. This is commonly done to correct for differences in sampling procedures and the heterogeneity of the intestinal tissue[5, 35, 142, 201, 219]. However, no signal for villin-1 was observed in one sample of a 3-year-old. Not a single heavy peptide was observed in this sample either, indicating this is a technical failure. However, the amount of protein derived from this sample is normal (initial protein concentration of 4.5 mg protein per mL homogenate), and no other samples within the same batch failed, suggesting a complication during the MS-run. A rescue injection (injecting the remaining 10 µL of the same sample) did not improve signal, but this could then also be due to the very low amount of sample on the column. Villin-1 was detected in all other samples. The light-to-heavy ratio for the proteotypic peptide of villin-1 ranged from 0.13 to 1.5 and most peptides could be quantified relatively to QconCAT, indicating an adequate spike-level was chosen prior to LC-MS/MS.

Thirdly, this study scaled established protocols (cryogrinding, normal centrifugation steps, FASP digestion and quantification with a QconCAT[80, 115]) from a nanoflow rate (300 nL/min) to a microflow rate (0.5 mL/min) . Previous proteomic studies where a microflow before (0.3 mL/min) was used before, only targeted n<16 peptides[98, 125, 273]. More commonly, a nanoflow is used in proteomic research[247]. Increasing a nanoflow to a microflow flow can improve peptide retention[403] and separation, diminish ion suppression and allow for thinner chromatographic peaks[401].

Overall, this study provides a simplified method for studying intestinal proteins, using pinch biopsies, a microflow chromatographic system and a unique heavy standard which can be

added to the samples in a single spiking event. The data from this study also suggests that, since the results from this study are comparable to data observed in adults, it is safe to extrapolate DMET-abundancy values from adults and strengthens the input values currently used in PBPK modelling. The clinical impact of the newfound intestinal abundancy data on the PK profile of the CYP3A4-substrate midazolam will be investigated in the next chapter.

2.6 Conclusion

This is the first study to report the ontogeny of intestinal DMET-levels using paediatric pinch biopsies obtained from the duodenum of a paediatric population. Intact samples were cryopulverised, proteins digested using a FASP-protocol. A microflow LC-MS/MS method was developed to quantify 21 DMET-proteins in paediatric duodenal biopsies. As heavy standard, a QconCAT (PaedCAT) containing sequences for three different classes of DMET proteins was developed for the first time. Elution profiles were representative of literature[80, 115, 273].

Five CYP enzymes (CYP2C9, 2C19, 2D6, 3A4, 3A5), 4 drug transporter proteins (ABCB1, ABCC2, ABCG2 and SLC22A1), 3 UGT enzymes (UGT1A1, 2B7 and 2B17) and CES2 were quantified in the duodenal biopsies. In agreement with observed trends in adults, intestinal CYP3A4 was the most abundant CYP-enzyme and UGT2B17 the most abundant UGT. Significant trends with age were detected for CYP3A4 and CES2, corroborating earlier results based on western blotting.

This work shows that pinch biopsies and a microflow LC method are suitable for DMET-protein quantification. Further work includes collecting more paediatric samples, with emphasis on recruiting neonatal participants. The data presented in this work will enhance drug development for the vulnerable paediatric population, via informing predictive tools such as PBPK modelling.

3 CHAPTER THREE

PBPK MODELLING TO SIMULATE THE IMPACT OF THE ONTOGENY OF INTESTINAL CYP3A4 ABUNDANCE ON THE ABSORPTION OF ORAL MIDAZOLAM IN PAEDIATRICS

3.1 Introduction

3.1.1 Oral paediatric midazolam formulations

Midazolam is a short-acting benzodiazepine, frequently used in neonatal and paediatric intensive care units for sedation of critically ill patients, or as premedication for stressful procedures[209, 385, 386]. Available paediatric formulations for the water-soluble midazolam include intravenous (IV), buccal and oral tablets and rectal gels[404], although other formulations (such as nasal sprays[405, 406]) are being developed. The oral route is the preferred route for sedation procedures when possible[407], as the liquid formulations are easier to administer as premedication than parenteral injections, where needles could increase the distress and pain experienced by the child[408]. Oral midazolam paediatric dosing recommendations are 0.25 to 0.5 mg/kg body weight, with a maximum of 20 mg in total[404]. The lower dose (0.3 mg/kg body weight (BW)) is effective in decreasing fear and distress in oncological paediatric patients (1-18 year old) undergoing needle procedures[409].

Midazolam is extensively metabolised (BDDCS Class I[410], section 1.1.2) by intestinal and hepatic CYP3A4 (among other enzymes, see section 3.1.2)[411, 412], forming the hydroxylated form 1-OH-midazolam and others. This 1-OH metabolite contributes to the overall sedation effect[413], reflected in a higher sedation effect observed after oral dosing compared to IV administration (with equal midazolam plasma levels) due to the first-pass effect (see section 1.1.2)[414].

3.1.2 Midazolam as probe for CYP3A4 activity

A paediatric framework to scale other CYP3A4-substrates relative to the clearance of midazolam (comparing albumin binding and extraction ratio) was recently proposed, which

could aid in drug development where paediatric PK profiles are lacking[415]. As oral midazolam is a widely studied drug, a further understanding of its absorption can elucidate the different factors involved, such as intestinal CYP3A4 ontogeny (see also section 1.3). Predicting systemic exposure of midazolam in paediatric populations is important, so that reliable tools can be established and translated to estimate exposure of other CYP3A4-substrates.

Midazolam is a good marker substrate to assess CYP3A4 activity[416, 417]. The compound has a good solubility and permeability[418], indicating it can easily be absorbed along the GIT. As it is a BCS and BDDCS Class I compound (see section 1.1.2), transporter effect is minimal on midazolam disposition. It is mainly metabolised by CYP3A4 (fraction metabolised (f_m) 0.9[419, 420]), with minor metabolism by CYP3A5[406] and various glucuronidation by UGT enzymes[421] or excretion into the urine unchanged. It is widely clinically used so a lot of observed data is available. Additionally, it is an established victim drug to study CYP3A4 drug-drug interactions (DDI), adding to the information of midazolam metabolism[419]. Midazolam (sub-)therapeutic dose-linearity is confirmed in adults (over a 30,000-fold dose range)[422-424] and also across the paediatric range (6 months to 16 year old, 0.25 – 1 mg/kg and for birth – 2 year old, therapeutic doses (detailed doses not shared))[425, 426]. Other non-invasive methods to investigate CYP3A4 activity *in vivo* include for example the erythromycin breath test[427, 428], but this is a suboptimal method as erythromycin is a transporter substrate and, more importantly, a mechanism-based inhibitor for CYP3A4[429]. Other *in vivo* tests use endogenic compounds (such as oxidation of testosterone[5]) and thus are less suitable for activity assessment. As such, midazolam is the best probe for CYP3A4 activity assessment.

3.1.3 Paediatric studies for oral midazolam

A considerable amount of paediatric PK data for midazolam is available, including IV data across the entire paediatric range (2 days to 17 years old adolescents[209, 390, 392]), oral (preterm infants 26-31 weeks gestation)[391], and other administration routes such as rectal and intramuscular in 3-10 year olds[393]. Paediatric CYP3A4 midazolam clearance and bioavailability (F, see section 3.1.5) are dependent on many factors, such as severity of inflammation[430, 431] and age[391, 393, 426, 432]. An obvious disease effect on midazolam clearance has been observed in children[433, 434], but the pathophysiological mechanism behind this has not yet been resolved. Multiple popPK models indicate bodyweight as a major covariate for midazolam clearance[94, 387, 412, 432, 435]. However, body weight was not found to influence midazolam clearance in popPK studies on overweight and obese adolescents[436, 437]. The bioavailability of oral midazolam solutions is widely variable in different age cohorts, with reports of 0.49 (range 0.12-1.00) in preterm neonates[391], 0.66 (range 0.25-0.85) in children of 0-6 years of age[412] and around 0.30 in adults[422, 438, 439].

A selection of studies investigating oral midazolam disposition in paediatrics are described. In Payne *et al*.[393], 56 children (3-10 year old) received intravenous, intramuscular, rectal and oral midazolam (as liquid formulations) in various doses, with the aim to characterise midazolam disposition and difference in bioavailability. Reed *et al*. investigated the formation of 1-OH-midazolam, the bioavailability and the dose linearity of midazolam via oral and IV administration in 87 children (6 months – 16 year)[426]. Johnson *et al.* investigated the PK of a 0.5 mg/kg midazolam in 45 children (9 months – 12 year) and the formation of 1-OH-midazolam, to investigate the sedative effect of both compounds in a PK-PD model[440]. De Wildt *et al*. also investigated the PK and metabolism of oral midazolam in 15 preterm infants (0.1 mg/kg, aged 3-13 days)[391].

3.1.4 P-PBPK models with midazolam

The observed paediatric PK data described before have been fed into different PBPK models, either as basis for modelling or to verify model simulations[441]. For example, the clinical data by De Wildt, Reed, Payne and Johnson was used to compare the clearance and model outcomes of the first paediatric PBPK simulations in Simcyp[10]. The observed data by De Wildt *et al*. was also used to compare the results of allometric scaling and PBPK simulations generated in PK-Sim, where it was deemed the latter were superior in predicting neonatal IV midazolam clearance (n=10, 34-41 weeks gestation)[442]. Other existing models are used to bridge formulations (e.g. rectal gels in adults[443]), or to predict DDIs with midazolam as the victim compound of CYP3A4 inhibition/induction[444]. Intestinal CYP3A4 ontogeny is modelled using the values reported by Johnson *et al*.[5] PBPK models with CYP3A4-inhibitors, for example, risdiplam have been built for adults and extrapolated to the paediatric population[109]. Here, the predicted DDI between risdiplam and midazolam was due to intestinal CYP3A4-inhibition, rather than hepatic. Similarly, co-formulation of oral midazolam with grapefruit juice (to mask the bitterness of midazolam) is contra-indicated[445], as components of the juice inhibit intestinal CYP3A4[445, 446].

3.1.5 Hepatic CYP3A4 for midazolam bioavailability

The bioavailability for the different cohorts are calculated from the product of the fraction absorbed (F_a), gut bioavailability (F_g) and hepatic bioavailability (F_h) (**Equation 3.1**) (see also section 1.1.2).

$$F = F_a * F_g * F_h$$

Equation 3.1. *The oral bioavailability (F) is calculated from the product of the fraction absorbed (F_a), gut bioavailability (F_g) and hepatic bioavailability (F_h).*

Hepatic CYP3A4 is also involved in midazolam clearance. Two hepatic ontogeny functions are available in the Simcyp simulator, based on reviews by Salem[447] (2014) or Upreti-Wahlstrom[448] (2016). These functions dissimilarly predict CYP3A4 in children younger than 2 years particularly[109]. Based on a model that compared both functions, the Upreti function is more suited for predicting paediatric hepatic CYP3A4 activity across the paediatric age range.

3.1.6 Simulating an observed paediatric PK study

Reed *et al*., 2001, investigated the PK profile of midazolam and 1-OH midazolam and midazolam bioavailability in paediatrics using a cross-over design. Paediatric participants were classified in cohorts ranging 6 months to 2 years, 2-12 years and 12-16 years[426]. Here, IV (0.15 mg/kg) and different oral formulations (0.25, 0.5 and 1 mg/kg body weight, with a maximum of 40 mg/kg) were investigated. Differences in PK parameters were observed after oral formulation between the different age groups. As these were not seen after IV administration, it was hypothesised that differences in oral bioavailability leads to the alterations in PK parameters. However, no statistically significant relationship was observed between age and the bioavailability of midazolam due to the high variability (average 0.36, range 0.09-0.71).

Potentially, midazolam clearance is linked to ontogeny of intestinal CYP3A4 expression.

As the study design and common PK parameters (Maximum plasma concentration (C_{max}), AUC and F) are reported in detail in Reed *et al*., it is possible to simulate this trial *in silico*. Furthermore, this study used a wide age range, with discreet age bands and reported its results in a clear and comprehensive manner. By comparing to clinically observed PK data from this study, the accuracy of a P-PBPK model for midazolam using the default intestinal

CYP3A4 ontogeny can be verified. Additionally, it can be determined if adaptation of the default input values to observed physiological data (see also chapter 2) would improve the PBPK prediction of oral midazolam in a paediatric cohort and thus might be used as ontogeny profile for other simulations.

3.2 Aims and objectives

The aim of this chapter is to simulate the influence of intestinal CYP3A4 ontogeny on the PK profile of oral midazolam in a paediatric cohort *via* PBPK modelling.

The objectives of this chapter are:

- To build a P-PBPK model that captures clinically observed PK data of midazolam across different paediatric cohorts, with oral formulations in varying dose strengths, using the default intestinal CYP3A4 ontogeny function within SimCYP.
- To determine if the P-PBPK model predictions are influenced by the abundance of intestinal CYP3A4 using a local sensitivity assay (LSA).
- To determine to what extent integrating the intestinal CYP3A4 abundance (see Chapter 2) influences the predictions of the P-PBPK model, and how this correlates to the predictions of the P-PBPK model using the default simulator ontogeny profile.

3.3 Methods

3.3.1 Simulating the observations of a clinical trial

The clinical trial, reported in Reed *et al.*[426], was mimicked using the Simcyp PBPK-simulator (version 21.0.233.0). Following parameters were selected in the simulator:

3.3.1.1 Drug file

Midazolam is a curated compound in the simulator (i.e. the software developers maintain this drug file in their portfolio, based on extensive literature scouring). A first-order absorption model (no ADAM-component) was used for absorption of an oral midazolam solution. The drug file to model the metabolite 1-OH-midazolam was provided.

3.3.1.2 Population-file

The default paediatric population was used, with following characteristics:

- As hepatic CYP3A4 ontogeny function, the Upreti-Wahlstrom function rather than Salem was used, based on its reported superiority for paediatric modelling[109] and personal communication with modelling experts.
- The default intestinal CYP3A4 ontogeny function in the paediatric population reflected a fraction of adult abundance. The default function was modelled based on the data observed in Johnson *et al.*[5]. The function is given in **Equation 3.2**, with an age-cap (age at which the abundance is the same as adult values) set to 18 years. This is the only curated ontogeny profile available in the simulator for intestinal CYP3A4[10, 109]. This ontogeny input value was not specific for any section in the small intestine, all sections were modelled with this function.

$$Fraction = F_{birth} + \frac{(F_{max} - F_{birth}) * Age^n}{Age_{50}^n + Age^n}$$

Equation 3.2. *Ontogeny of intestinal CYP3A4, derived from Johnson et al[5]. CYP3A4 is expressed as a fraction of the adult abundance, with F_{max} = 1.059; F_{birth} = 0.42; Age_{50} = 2.357; n = 1 and the age-cap set to 18.*

- Protein content of the small intestine was 2978 mg protein per total small intestine (using scraping of the intestinal mucosal layer)[96].
- Adult intestinal CYP3A4 expression was set at 66.2 nmol per small intestine (CV 60%)[449], or 22.23 pmol CYP3A4 per mg small intestinal protein (**Equation 3.3**).

$$CYP3A4\ \left(\frac{nmol}{SI}\right) = CYP3A4\ \left(\frac{pmol}{mg\ SI\ protein}\right) * \frac{2978\ mg\ SI\ protein}{SI} * 10^{-3}$$

Equation 3.3. *Conversion of CYP3A4 expressed per nmol per small intestine (SI) to pmol enzyme per mg SI protein.*

3.3.1.3 Trial-design

The following single oral doses were tested: 0.25 mg/kg, 0.5 mg/kg and 1 mg/kg. There were 67 subjects in 20 trials, reflecting the number included in the original report[426]. Three populations were compared: 6 months to 2 years, 2 years to 12 years and 12 years to 16 years. The number and proportion of females were adjusted to reflect the proportion in the original cohorts: 3 (1:2 male:female), 54 (33:21) and 10 (6:4) participants respectively.

3.3.1.4 Simulation evaluation

The simulation was compared to the observed clinical data using the reported C_{max} and AUC. For this, the mean result of all 67 patients is compared (as the AUC and C_{max} per paediatric cohort are not reported in the original publication). The bioavailability was calculated by the formula given in **Equation 1.1**. The percentage prediction error (PPE) is calculated using **Equation 3.4**[450].

$$PPE = \frac{|predicted\ value - observed\ value\ |}{observed\ value} * 100$$

Equation 3.4. *The prediction error is calculated as the absolute value of the difference between observed and predicted value relative to the observed value.*

The simulations were deemed acceptable if the predicted values were within two-fold of the observed data (AUC ratios (predicted:observed) 0.5 – 2; PPE ≤100%)[451, 452].

3.3.2 Local sensitivity analysis of CYP3A4 abundance

For an automated LSA of the intestinal CYP3A4 abundance on the model outputs, the built-in LSA feature of Simcyp was used. The trials in the automated LSAs were designed as described in section 3.3.1.3. The automated LSA was run with a log-distributed 11-step size in intestinal CYP3A4 abundance from 6.62 nmol/SI (lower limit) to 662 nmol/SI (upper limit) (series being: 6.62, 10.49, 16.63, 26.35, 41.77, 66.20, 104.92, 166.29, 263.55, 417.69, 662.00). The hepatic CYP3A4 abundance and hepatic CYP3A4 ontogeny function were not changed. Parameters under scrutiny to indicate sensitivity were common PK parameters: the plasma concentration time profile (C_p), the area under the curve (AUC), the oral clearance (CL_{PO}) and the intestinal and hepatic bioavailability (F_g and F_h, respectively).

3.3.3 Incorporation of novel intestinal CYP3A4 abundancy data

The CYP3A4 of the oldest participants (14-15 year old) were used as adult input, as an internal control of the dataset (see Chapter 2). For this, the mean abundance of seven participants (23.64 ± 6.33 pmol/mg small intestinal protein) was converted to nmol/small intestine using **Equation 3.3**. The final input parameters were: 70.4 nmol/SI (CV: 28.78).

The individual CYP3A4 abundancy data was converted to fraction of the adult input. A simple linear regression of the relative abundancy data with age was performed. The equation of the simple linear regression of the relative abundancy data (**Equation 3.5**) was entered in the user-defined ontogeny pattern for intestinal CYP3A4 panel in the simulator.

$$Fraction = 0.0235 * age + 0.5287$$

Equation 3.5. *Linear regression of intestinal CYP3A4 (based on n=32 paediatric datapoints) relative to the mean abundance of 14-15 year olds, n=7.*

After incorporation of the adapted ontogeny function, the simulations for the different dosage strengths were performed as previously described.

3.3.4 Statistical analysis

GraphPad Prism version 9.3.1 was used for statistical analysis. Paired t-tests were used to compare the AUC and C_{max} between two sets of simulations, e.g. default and adapted simulations. One-way ANOVA's were used to compare the AUC and C_{max} between three sets of simulations. A statistical test was deemed significant if the p-value was smaller than 0.05 (p<0.05).

3.4 Results

3.4.1 Simulating the observations of a clinical trial

A P-PBPK-simulation was carried out in a similar fashion as a clinical trial to capture the PK of midazolam[426], using the default intestinal CYP3A4 ontogeny function[5]. The results of the simulations (for 67 participants, 6 months – 16 year old, 20 trials), together with the observed clinical values, are given in **Table 3.1** and **Figure 3.1**. The PK profiles of the simulations for the different doses are given in **Figure 3.2**.

Table 3.1. *Observed and predicted C_{max} and AUC of midazolam and 1-OH-midazolam after an oral single-dose administration in three different strengths. Values are presented as mean ± SD.*

Moiety	Dose (mg)	Observed C_{max} (ng/mL)	Predicted C_{max} (ng/mL)	Observed AUC (ng/mL.h)	Predicted AUC (ng/mL.h)
Midazolam	0.25	55.6 ± 30.2	64.2 ± 40.0	137 ± 86	171 ± 118
	0.50	123.2 ± 76.1	134.3 ± 84.3	356 ± 320	357 ± 247
	1.00	185.7 ± 98.6	287.6 ± 181.5	684 ± 581	759 ± 538
1-OH midazolam	0.25	35.6 ± 19.7	34.8 ± 12.7	83 ± 31	94 ± 38
	0.50	70.3 ± 43.2	68.4 ± 25.0	181 ± 80	188 ± 76
	1.00	136.6 ± 64.7	133.5 ± 49.0	393 ± 220	375 ± 152

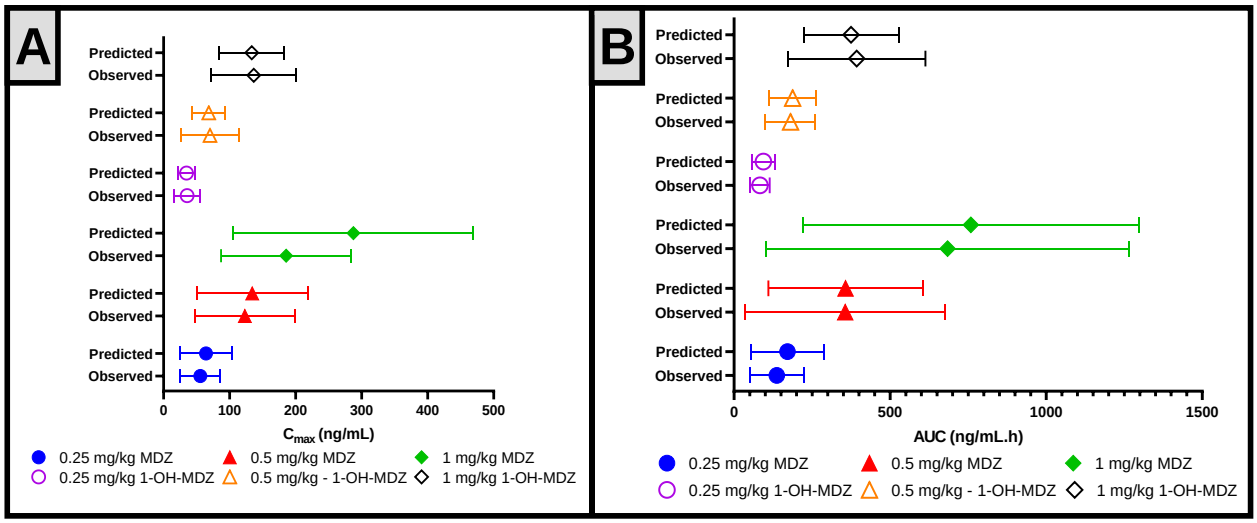

Figure 3.1. *Comparison of predicted and observed (A) C_{max} and (B) AUC of midazolam (closed figures) and 1-OH-midazolam (open figures) with different doses: 0.25 mg/kg (circle), 0.5 mg/kg (triangle), 1 mg/kg (diamond). Symbols depict the mean, error bars denote the SD.*

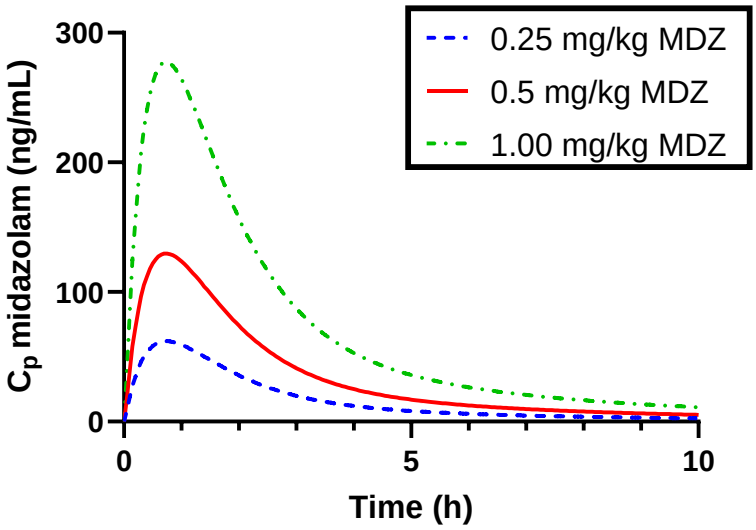

Figure 3.2. *Simulated mean PK profiles of a single-dose oral midazolam (MDZ) in three dosage strengths to a paediatric population (6 months – 16 years old) using the default built-in intestinal CYP3A4 ontogeny function.*

The C_{max} or AUC values were not statistically significant different between the simulations and observed data (p=0.31 and 0.22, respectively). The ratios of predicted to observed data and the PPE are given in **Table 3.2**. All ratios and PPE were within the acceptability criteria previously defined.

Table 3.2. *Ratios (predicted:observed) and PPE of C_{max} and AUC of midazolam and 1-OH-midazolam after an oral single-dose administration in three different strengths.*

	Dose (mg)	Ratio C_{max}	PPE (%) C_{max}	Ratio AUC	PPE (%) AUC
Midazolam	0.25	1.15	15.47	1.25	24.82
	0.50	1.09	9.01	1.00	0.28
	1.00	1.55	54.87	1.11	10.96
1-OH midazolam	0.25	0.98	2.25	1.13	13.25
	0.50	0.97	2.70	1.04	3.87
	1.00	0.97	2.27	0.95	4.58

The oral bioavailability (F) for the different populations is given in **Table 3.3**. The dosage strength did not influence F.

Table 3.3. *Predicted and observed oral bioavailability of midazolam in paediatric cohorts.*

Population	6 months – 2 year old	2 – 12 year old	12 – 16 year old	Population average
Mean ± SD	0.29 ± 0.13	0.32 ± 0.13	0.34 ± 0.12	0.32 ± 0.13
Range (min-max)	0.04 – 0.56	0.03 – 0.65	0.09 – 0.65	0.03 – 0.65
Observed F (mean ± SD)	0.37 ± 0.21	0.35 ± 0.32	N/A*	0.36 ± 0.25

*N/A: not reported in the publication by Reed.

3.4.2 Local sensitivity analysis CYP3A4 abundance

As ontogeny is modelled as a fraction of the adult value, the influence of the intestinal CYP3A4 abundance on the PK profile of midazolam and 1-OH-midazolam was investigated using an automated LSA. The C_p-profile and AUC are reduced with increasing intestinal CYP3A4 abundance (**Figure 3.3A** and **B**). The reduction in exposure is due to an increased clearance (**Figure 3.3C**), as a consequence of increased gut clearance (and lower intestinal bioavailability) (**Figure 3.3D**). As evidenced by the steady F_h, the hepatic CYP3A4 clearance did not influence the observed profile.

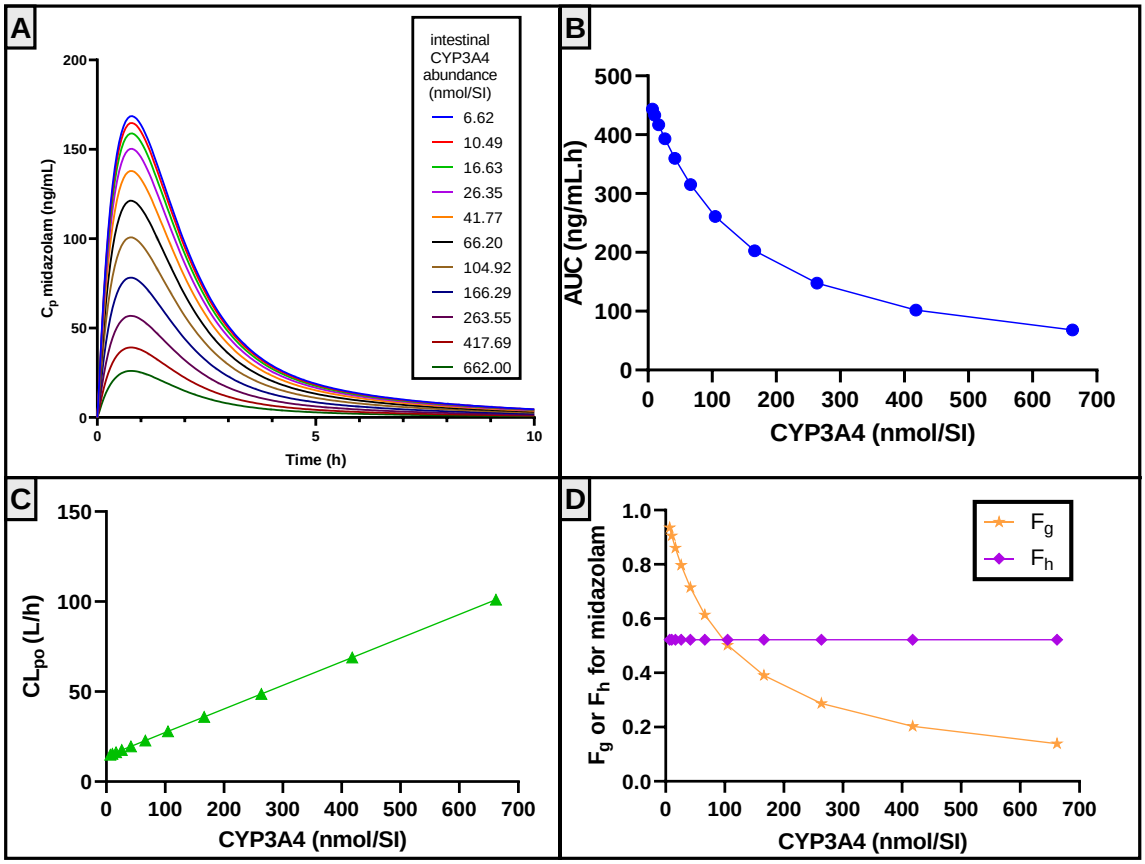

Figure 3.3. *Local sensitivity analysis of the influence of intestinal CYP3A4 abundance on the (A) C_p, (B) AUC, (C) CL_{PO} and (D) F_h and F_g of oral midazolam (0.5 mg/kg).*

3.4.3 Incorporation of novel intestinal CYP3A4 abundancy data

The individual CYP3A4 abundancy data was expressed relative to the mean abundancy value of seven 14-15 year olds. A simple linear regression of the converted abundancy data with age was performed and given in **Equation 3.5**. The trend before and after expression relative to the small intestinal input value are given in **Figure 3.4**.

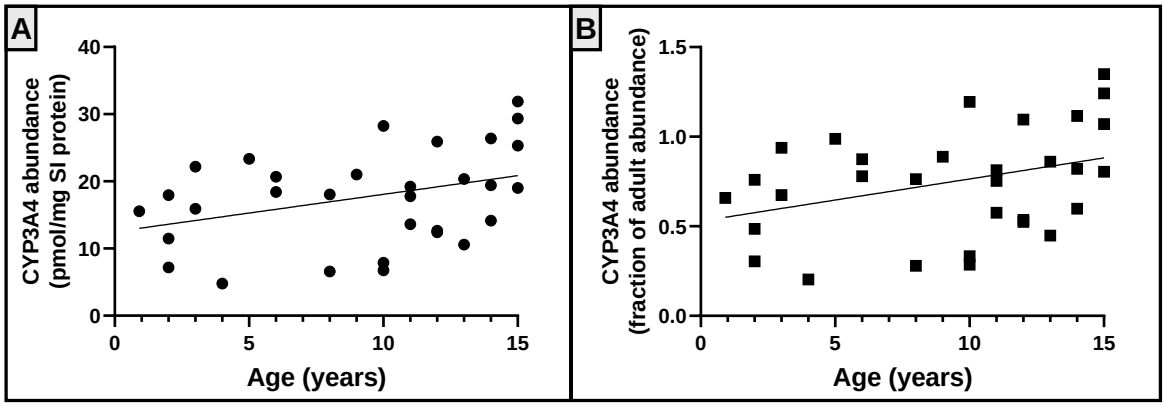

Figure 3.4. *Intestinal CYP3A4 abundance data, given in (A) pmol/mg small intestinal (SI) protein and (B) relative to the mean abundance of 14-15 year olds, n=7. The black line denotes a simple linear regression, for (A): y=0.556*x + 12.50, R^2 = 0.13, for (B): y=0.0235*x+0.5287, R^2 0.13).*

The initial simulations were repeated after incorporation of the adapted intestinal CYP3A4 abundance ontogeny function and adult reference intestinal CYP3A4 abundance. The PK parameters of the adapted simulations, together with the observed data and previously predicted simulations with the default ontogeny are given in **Table 3.4**.

Table 3.4. *Observed and predicted (default and with adapted ontogeny function) Cmax and AUC of midazolam and 1-OH-midazolam after an oral single-dose administration in three different strengths. Values are presented as mean ± SD.*

Moiety		Observed	Predicted default	Predicted adapted	Observed	Predicted default	Predicted adapted
	Dose (mg)	C_{max} (ng/mL)	C_{max} (ng/mL)	C_{max} (ng/mL)	AUC (ng/mL.h)	AUC (ng/mL.h)	AUC (ng/mL.h)
Midazolam	0.25	55.6 ± 30.2	64.2 ± 40.0	65.7 ± 39.2	137 ± 86	171 ± 118	175 ± 115
	0.50	123.2 ± 76.1	134.3 ± 84.3	137.5 ± 83.3	356 ± 320	357 ± 247	365 ± 243
	1.00	185.7 ± 98.6	287.6 ± 181.5	294.8 ± 180.9	684 ± 581	759 ± 538	777 ± 522
1-OH-midazolam	0.25	35.6 ± 19.7	34.8 ± 12.7	34.6 ± 12.5	83 ± 31	94 ± 38	94 ± 38
	0.50	70.3 ± 43.2	68.5 ± 25.0	68.0 ± 24.7	181 ± 80	188 ± 76	188 ± 76
	1.00	136.6 ± 64.7	133.5 ± 49.0	132.7 ± 48.6	393 ± 220	375 ± 152	376 ± 152

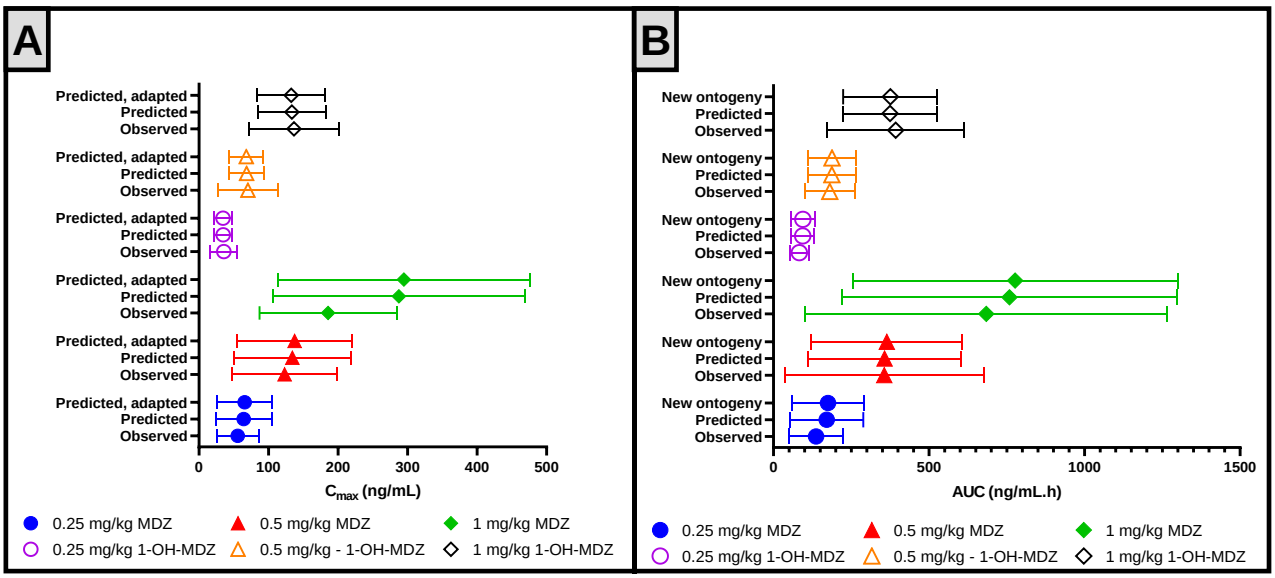

Figure 3.5. *Comparison of observed, predicted with default ontogeny and predicted with adapted ontogeny (A) C_{max} and (B) AUC of midazolam (closed figures) and 1-OH-midazolam (open figures) with different doses: 0.25 mg/kg (circle), 0.5 mg/kg (triangle), 1 mg/kg (diamond). Symbols depict the mean, error bars denote the SD*

An ANOVA-test comparing the differences in C_{max} or AUC between the different simulation dataset was not significant (p=0.30 and 0.20, respectively). The C_p-profiles of the adapted simulations (overlaid with the previous simulations) are given in **Figure 3.6**.

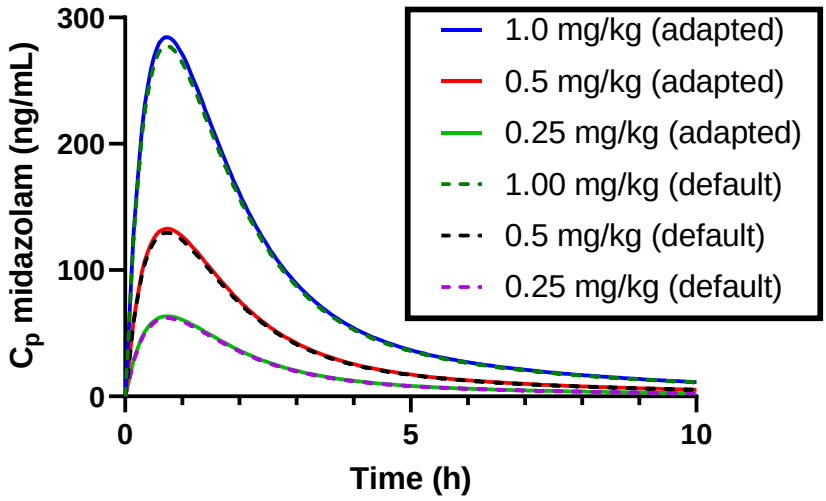

Figure 3.6. *Simulated mean PK profiles of a single-dose oral midazolam in three dosage strengths to a paediatric population (6 months – 16 years old) using an adapted intestinal CYP3A4 ontogeny function ("adapted").The simulations with the default ontogeny ("default") are shown in a striped pattern.*

The ratios of the C_{max} and AUC of the ontogeny-adapted simulations to the observed data and previously predicted simulations with default ontogeny are given in **Table 3.5**. All ratios and PPE were within the predetermined acceptability criteria.

Table 3.5. *Ratios predicted (adapted ontogeny profile:observed and adapted ontogeny:default ontogeny) and PPE of C_{max} and AUC of midazolam and 1-OH-midazolam after an oral single-dose administration in three different strengths.*

		Ratio C_{max}		PPE (%) C_{max}	Ratio AUC		PPE (%) AUC
	Dose (mg)	Adapted to observed	Adapted to default	Adapted to observed	Adapted to observed	Adapted to default	Adapted to observed
Midazolam	0.25	1.18	1.02	18.17	1.28	1.02	27.74
	0.50	1.12	1.02	11.61	1.03	1.02	2.53
	1.00	1.59	1.03	58.75	1.14	1.02	13.60
1-OH midazolam	0.25	0.97	0.99	2.81	1.13	1.00	13.25
	0.50	0.97	0.99	3.27	1.04	1.00	3.87
	1.00	0.97	0.99	2.86	0.96	1.00	4.33

The oral bioavailability (F) for the different populations using the adapted ontogeny function is given in **Table 3.6**. The dosage strength did not influence F.

Table 3.6. *Predicted and observed oral bioavailability of midazolam in paediatric cohorts using an adapted ontogeny function.*

Population	6 months – 2 year old	2 – 12 year old	12 – 16 year old	Population average
Mean ± SD	0.29 ± 0.11	0.33 ± 0.12	0.33 ± 0.11	0.33 ± 0.12
Range (min-max)	0.05 – 0.50	0.03 – 0.63	0.10 – 0.57	0.03 – 0.63
Observed F (mean ± SD)	0.37 ± 0.21	0.35 ± 0.32	N/A*	0.36 ± 0.25

*N/A: not reported in the publication by Reed.

3.5 Discussion

In this work, the influence of intestinal CYP3A4 ontogeny was explored using previous generated abundancy data (see chapter 2). As a reference for clinical data, a publication by Reed *et al*., 2001, was selected as they explored the pharmacokinetic profile of an oral midazolam formulation in three dosage strengths (0.25, 0.5 or 1 mg/kg, with a maximum dose of 40 mg/kg) in a paediatric population[426].

The PK parameters in the simulations using the default ontogeny pattern (based on Johnson *et al*., 2001[5]) followed the clinically observed values (**Table 3.1**, **Figure 3.1**). Especially the exposure (AUC) and C_{max} for the metabolite 1-OH-midazolam were in good agreement (**Table 3.2**), indicating that its formation, and thus metabolism of midazolam (via CYP3A4), is well-represented in the PBPK model. Similarly, the calculated bioavailability for the different paediatric cohorts (**Table 3.3**) closely predicts the observed values in literature. The differences observed in e.g. C_{max} of the parent compound after the 1 mg/kg could be described to an overestimation of absorption. Ontogeny of the gut dimensions (length/diameter) could also contribute to the differences observed[168, 453, 454]. Another possibility is saturation of drug uptake that is not reflected in the model, as hypothesised by Payne *et al.*[393]. They compared different oral doses (0.15, 0.45 and 1 mg/kg body weight) with an IV, intramuscular (IM) or rectal administration of midazolam (all at 0.15 mg/kg dose) in a paediatric cohort (3-10 years, n=56). Here, a 45% reduction of oral bioavailability was observed when the dose was doubled or higher (F=0.27, 0.16 and 0.15 at 0.15, 0.45 and 1.0 mg/kg oral dose respectively). In this study, no effect of dosage on the bioavailability was observed (using 0.25, 0.50 and 1.0 mg/kg, **Table 3.3**, and **Table 3.6**). Reed *et al*. did not report the oral bioavailability from the different tested paediatric doses. However,

midazolam absorption saturation has not been reported elsewhere, and is unlikely to occur as it is well permeable and transporter effects are negligible[418]. A verification of the ontogeny, based on the PK-parameters observed in the different paediatric cohorts (6 months-2 years, 2-12 years and 12-16 years) could not be established, as these data were not reported.

An LSA investigating the influence of intestinal CYP3A4 abundance on the PK of midazolam was performed using 0.5 mg/kg as dose. A clear influence was observed, where the oral midazolam clearance (CL_{PO}) increased due to more intestinal, but not hepatic metabolism (**Figure 3.3**) as the latter was unaltered in the set-up. No correlations between the intestinal and hepatic CYP3A4 content in paediatrics has been reported. In adults, correlations between hepatic and intestinal DMET proteins were investigated via mRNA[455], immunologic[277, 455] or proteomic[231] assays on paired tissues (hepatic and intestinal tissue derived from the same donor). However, no correlations have been found, so it remains unclear whether hepatic and intestinal CYP3A4 content are linked. In this work, the objective was to (solemnly) investigate the influence of intestinal CYP3A4 expression on the bioavailability of oral midazolam. As such, it is deemed acceptable to ignore any hepatic CYP3A4 ontogeny, evidenced by the fixed F_h. In this model, the gut bioavailability ranged from 0.94 to 0.61 for intestinal CYP3A4 abundances ranging from 6.62 to 66.2 nmol per small intestine and a constant hepatic bioavailability of 0.52 (**Figure 3.3D**). Very variable bioavailability and clearance values have been reported in paediatrics[389, 412], where the intestinal metabolism has been observed as little as 0.29% of the total midazolam clearance[94]. Further work on characterising intestinal bioavailability and metabolism of midazolam, especially in younger children is needed.

The intestinal CYP3A4 ontogeny function and the adult reference value were adapted. As an internal control, the mean abundance of intestinal CYP3A4 quantified in duodenal biopsies of 14-15 year old reported previously (Chapter 2) was used as adult reference value. After conversion, the CYP3A4 content was 70.4 nmol for the whole small intestine. This value closely resembles the default value in Simcyp (66.2 nmol/small intestine[449]) and other reports (e.g. 70.5 nmol/small intestine[456]). The ontogeny of intestinal CYP3A4 abundancy based on observed data from biopsies (see **Figure 2.13**) is given by a linear regression with age, where the goodness-of-fit (R^2) is low due to the variability in this population[2] (**Figure 3.4**). The associated variability of CYP3A4 abundance in the model resembles the CV observed on the physiological data. However, a significant strong correlation was detected between CYP3A4 abundance and age previously (**Figure 2.13**). Including more datapoints, with emphasis on quantifying CYP in neonates and infants (as it is expected that the major changes occur at the youngest age [387]) could improve the fitting of the datapoints and improve predictive tools for drug development.

Indeed, the lack of intestinal CYP3A4 abundancy data for the younger children (<2 year) is the main limitation in this study. It is in the neonatal cohort where the largest changes of midazolam clearance compared to adults have been reported[385, 457]. Observed PK data of IV and oral midazolam and the metabolite 1-OH midazolam have been reported in preterm neonates (n=15, 3-13 days postnatal age and 26-31 weeks gestation) [391]. However, simulating the neonatal trial with a P-PBPK model that included the generated physiological data was not possible, as the youngest datapoint generated was from an 11 months old and extrapolation past this terminal value might not represent the actual ontogeny[5].

Additionally, the lack of datapoints for younger participants resulted in a linear fit across the entire paediatric range, rather than a sigmoidal function as based on existing western blot data. Other fits were tried, such as an exponential, logarithmic and power functions, yet these resulted in a lesser fit (data not shown). The currently default sigmoidal function also predicts the largest CYP3A4 changes with age to occur within the neonatal age range. A visual comparison between the default and adapted ontogeny function (**Figure 3.7**) show that the sigmoidal function correlates well to the data reported previously (Chapter 2), with the default function fitting very closely to the youngest datapoints.

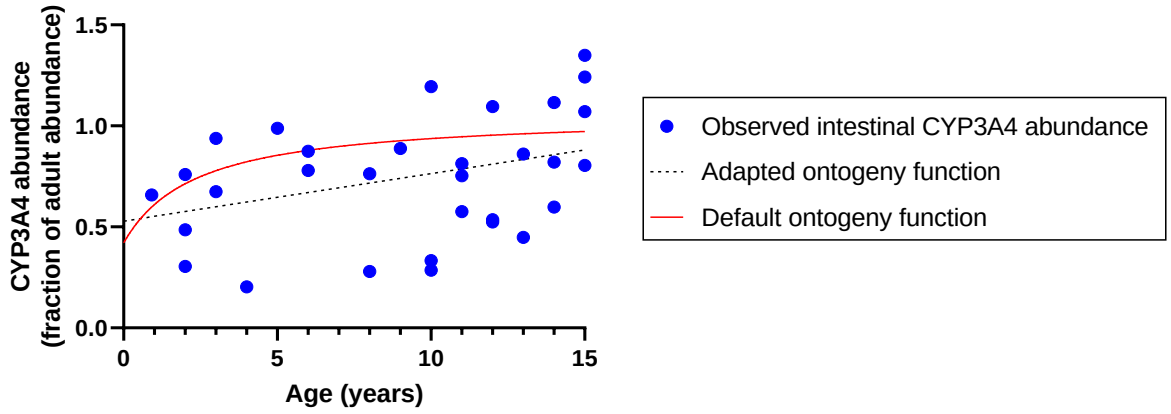

Figure 3.7. *Comparison of default (red, smooth) and adapted (black, dotted) functions for intestinal CYP3A4 ontogeny to observed abundance.*

Additionally, the default ontogeny is based on a larger sample size (n= 74 vs n=34), hence this function might be more appropriate than using a linear fit from a smaller dataset. However, these limitations in the data did not result in clinically different PK profiles for either ontogeny function. Although the influence of intestinal CYP3A4 on midazolam PK was clearly proven, amendments made on the ontogeny profile had minimal impact on the predictions (**Figure 3.5**, **Figure 3.6**, **Table 3.5** and **Table 3.6**). The ratio of default to adapted ontogeny for all doses and moieties are within 0.99-1.03 fold. This further shows that the adapted ontogeny data, based on newfound proteomic data, supports the default ontogeny

pattern in Simcyp[5], and thus underpins current paediatric PBPK modelling and supports their use in predicting paediatric DDI studies. Modelling the PK profile of other compounds with the adapted intestinal CYP3A4 ontogeny function would be futile, as there is not much difference between the two function and thus the clinical impact would be minimal.

DDI studies are currently the most used application in PBPK modelling in adults, with Simcyp as the most frequently used simulator[58]. Because Simcyp is also the most frequently used simulator in paediatric predictions[40], and the use of P-PBPK modelling increased 33-fold in the last two decades[40], its use in paediatric DDI prediction is likely to increase as well[458]. Especially in the younger cohorts (<2 years), PBPK approaches could become more suited for PK predictions compared to allometric scaling due to ontogeny of different factors[62]. Therefore, accurate ontogeny information of metabolising enzymes is required before an effect of an inducer/inhibitor can be reliably predicted. These P-PBPK studies can then be used to waive clinical studies and inform dose labelling decisions, as recently done for guanfacine when co-administered with CYP3A4 inhibitors or inducers in 6-17 year old children[107]. They can also be used as a virtual representation of individual patients ("virtual twin" as a tool for personalised medicine[459]. As no clinical differences were observed after adaptation to generated physiological data, there is reassurance the current default ontogeny profile for intestinal CYP3A4 is well-suited to inform such decisions.

As such, this study does not suggests to abandon the current default intestinal CYP3A4 model, but promotes its use in support of clinical trial design[106] or as replacement for clinical studies[107].

3.6 Conclusion

In PBPK simulations, intestinal CYP3A4 abundance in paediatric populations is given by an ontogeny function based on western blotting. Now that novel intestinal CYP3A4 abundancy data were generated using LC-MS/MS, the suitability of the default and novel ontogeny functions in P-PBPK predicting the clearance of a CYP3A4 was tested. For this, midazolam was chosen as a probe for CYP3A4 activity. Midazolam is a frequently used sedative agent in paediatric medicine as oral solution, with a reported decrease in oral bioavailability upon maturation. It is a widely studied substrate for CYP3A4 metabolism, where the metabolite 1-OH-midazolam is formed among others. As such, midazolam is a well-suited compound to investigate gut wall clearance due to intestinal CYP3A4 ontogeny, which could be used to predict exposure of other CYP3A4-substrated in paediatrics. Using PBPK-models, the PK profile of three different doses of oral midazolam (0.25, 0.50 and 1 mg/kg) were simulated in a paediatric cohort and compared to observed clinical data. The model predicted the observed PK profile of midazolam well, especially its metabolisation to 1-OH-midazolam as evidenced by the similar AUC and C_{max}-ratios for 1-OH-midazolam (0.95-1.13) and low PPE (<15%). Using a local sensitivity analysis, the influence of intestinal CYP3A4 on the prediction of oral midazolam clearance and gut bioavailability was verified. The intestinal CYP3A4 ontogeny profile was then adapted based on generated proteomic data. The resulting simulations were in close correlation to the simulations with the default ontogeny (0.99-1.03) and observed clinical data (0.96-1.59, PPE <60%). No clinical differences between either ontogeny function were observed. The results from this study support the default intestinal CYP3A4 ontogeny profile currently used in the PBPK simulator, and further approves of its use as a tool to replace or refine clinical trials in the paediatric population.

4 CHAPTER FOUR

QUANTIFICATION OF FLUID VOLUMES IN THE PAEDIATRIC COLON USING MAGNETIC RESONANCE IMAGING

A published manuscript was based on the body of this chapter:

Goelen, J.; Alexander, B.; Wijesinghe, H.E.; Evans, E.; Pawar, G.; Horniblow, R.D.; Batchelor, H.K. Quantification of Fluid Volume and Distribution in the Paediatric Colon via Magnetic Resonance Imaging. Pharmaceutics 2021, 13, 1729.

https://doi.org/10.3390/pharmaceutics13101729

4.1 Introduction

Physiological characterisation of the paediatric GIT is necessary for P-PBPK modelling. The amount of free fluid within the colon is important for accurately developing predictive tools, such as P-PBPK modelling or *in vitro* simulations. Currently, adult values[26] are used for simulations (**Table 1.10**) which may not be representative of paediatric physiology, and thus questions how appropriate these predictions are for determining the drug product performance of extended release (XR) formulations. Magnetic Resonance Imaging (MRI) has been used to visualise and quantify fluids within the small and large intestine of adults, and within the small intestine of children. Using MRI scans of the abdomen of a paediatric cohort, free fluid within the large intestine can be quantified and used to improve representability of predictive tools.

4.2 Aim and objectives

The aim of this study was to use MRI to locate and quantify the fluid volumes and number of fluid pockets in the colon of a paediatric population. This data could then be utilised to inform *in vitro* and *in silico* drug development tools and ultimately improve paediatric XR product performance predictions.

More specifically, the objectives of this study include:

- to quantify free fluid volumes and the fluid distribution in pockets within the paediatric colon using MRI;
- to investigate robustness of the followed protocol;
- to explore trends in the dataset *via* investigation the influence of various parameters on fluid volumes such as location within the colon, age, feed status and sex via statistical analysis and comparison to literature.

4.3 Methods

4.3.1 Study design and participants

This work builds on a previous report by Papadatou-Soulou *et al.*[24], which quantified the volume and distribution of free fluid in the stomach and small intestine of paediatric patients using an MRI databank of the abdomen from 49 paediatric participants. The same MRI dataset was used for this observational, retrospective study to quantify the volume of free fluid in the colon. Ethical approval for this study was obtained (REC reference: 18/EM/0251 (IRAS 237159 MRI: Fluid volumes and localisation in paediatric GI tract, **Appendix 9**). The children included in this study required a MRI of the abdomen for clinical purposes (for any organ in the abdomen: disorders with GI, kidney, liver etc.) and permission was obtained to use their anonymised MRI scans for this research. The following exclusion criteria were applied to ensure the cohort was as healthy as possible: patients with an acute abdomen (appendicitis or perforated viscus), malignant bowel disease, surgery (bowel resection, excluding appendicectomy), bowel wall thickening/stricture/fistula/abscess.

The datasets originated from two clinical sites: Birmingham Children's Hospital (BCH) and University Hospitals Coventry and Warwickshire NHS Trust (UHCW). All participants were fasted overnight and in addition, the UHCW site required the children to ingest 500 mL of Oral Klean Prep (a macrogol-based osmotic laxative) 60 min before MRI acquisition took place. This enabled the study to include a fasted and a fluid-fed population.

The MRI acquisition parameters are listed in **Table 4.1**.

Table 4.1. *MRI scanner and acquisition parameters*

Site	UHCW	UHCW	BCH	BCH
Participants	Fluid-fed	Fluid-fed	Fasted	Fasted
1.5 T MR Imaging Unit: series and manufacturer	Optima MR450w, GE Healthcare, Chicago, USA	Aera, Siemens Healthcare, Erlingen, Germany	Siemens MAGNETOM Avanto 1.5 T MRI System, USA	Aera, Siemens Healthcare, Erlingen, Germany
MRI coil	48-channel body coil	Body coil	16-element parallel imaging receiver coil	16-element parallel imaging receiver coil
MRI protocol	Coronal balanced steady-state gradient echo sequence (fast-imaging employing steady-state acquisition, FIESTA)	Coronal balanced steady-state gradient echo sequence (true FISP)	Coronal T2 SPACE sequence	Coronal T2 SPACE sequence
Median slice thickness (range)	4.0 mm (2.998 mm – 6 mm)	6.0 mm (2.998 mm – 6 mm)	0.9 mm (0.09 mm – 0.55 mm)	0.9 mm (0.09 mm – 0.55 mm)
Median intersection gap	5.0 mm	3.0 mm	None	None
Matrix	0.35 x 0.35 mm	1.0 x 1.0 mm	0.8 X 0.8 mm	0.8 X 0.8 mm
Field of view	420 cm^2	420 cm^2	250 cm^2	400 cm^2
TR/ TE	5.7/1.9 ms	652.8/2.1 ms	1700/98 ms	2000/241 ms

4.3.2 Data processing using Horos, ImageJ, Excel and SPSS

Overall, six software packages were used for the software-based determination of colonic fluid and data analysis:

1 Horos (version 3.3.6) to mark the fluid areas per MRI slice in a red shade;

2 ImageJ[460] (version 1.52a) to extract the areas of the marked fluid areas on the MRI slices;

3 Excel (version 1808) for data recording of the extracted information on fluid area;

4 SPSS[461] (version 27, 2020) to perform statistical analysis;

5 GraphPad Prism (version 9.4.1) to perform statistical analysis.

6 Blender (version 2.9) to process the *3D*-rendered models of the paediatric colon.

Horos is a free and open source code software (FOSS) program that is distributed free of charge under the LGPL license at Horosproject.org and sponsored by Nimble Co LLC d/b/a Purview in Annapolis, MD USA[462].

ImageJ is also a FOSS program, developed at the National Institutes of Health from the USA.

Blender is a free and open-source *3D*-creation suite, released under the GNU General Public License.

Only datasets with good resolution (i.e. visible anatomical features with a well-defined outline) and correct T2-weighted MRI sequence were included in the study; this was a total of 46 MRI acquisitions. A *2D*- and *3D*-based processing pipeline were used to quantify the fluid within the MRI datasets, see also **Figure 4.1**.

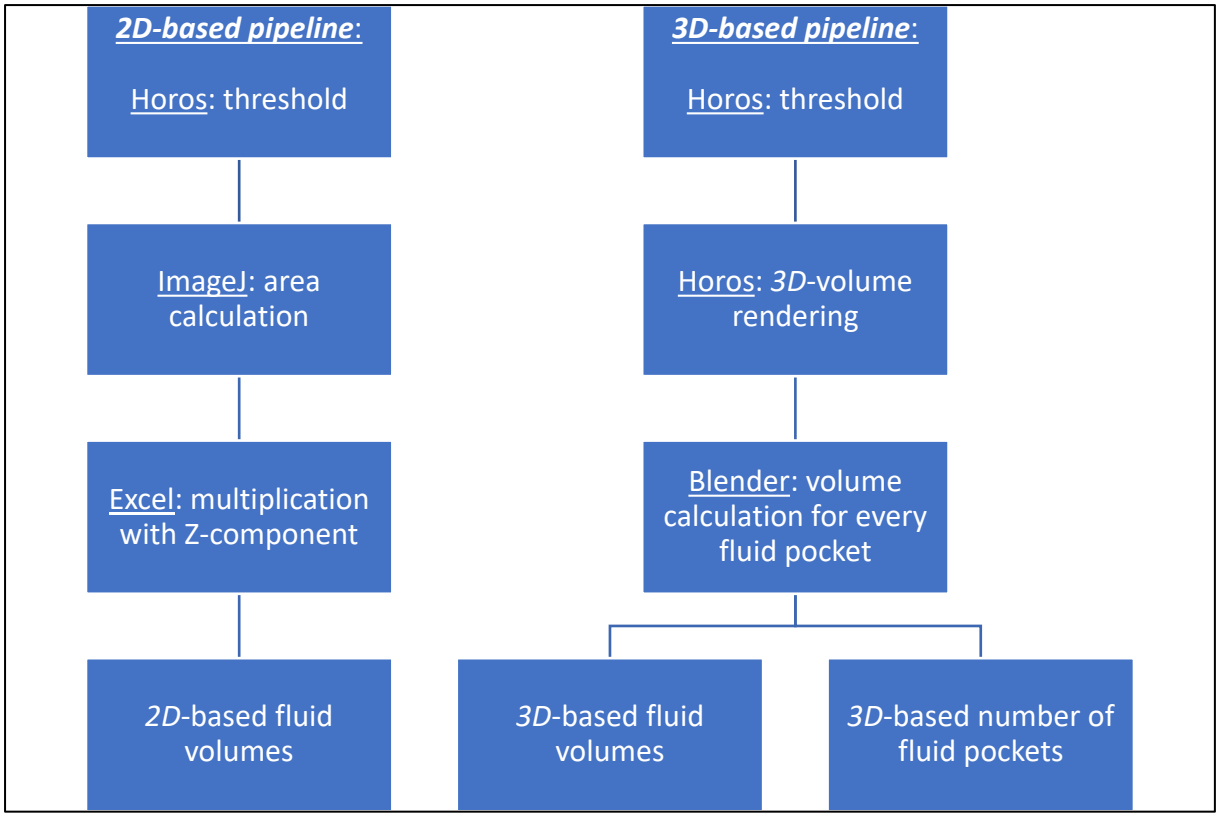

Figure 4.1. *Flowchart depicting the different pipelines used to acquire colonic fluid data from paediatric MRI scans.*

Fluid identification within the MRI slices was based on the intensity of cerebrospinal fluid (CSF) which is routine in interpretation of these images[24, 26, 345, 378, 463]. The average voxel intensity within the CSF was used as threshold value for free fluid.

4.3.2.1 2D-protocol

Two software packages were used for *2D*-fluid volume determination, Horos and ImageJ.

Figure 4.2 shows a schematic overview of the *2D*-based data extraction process.

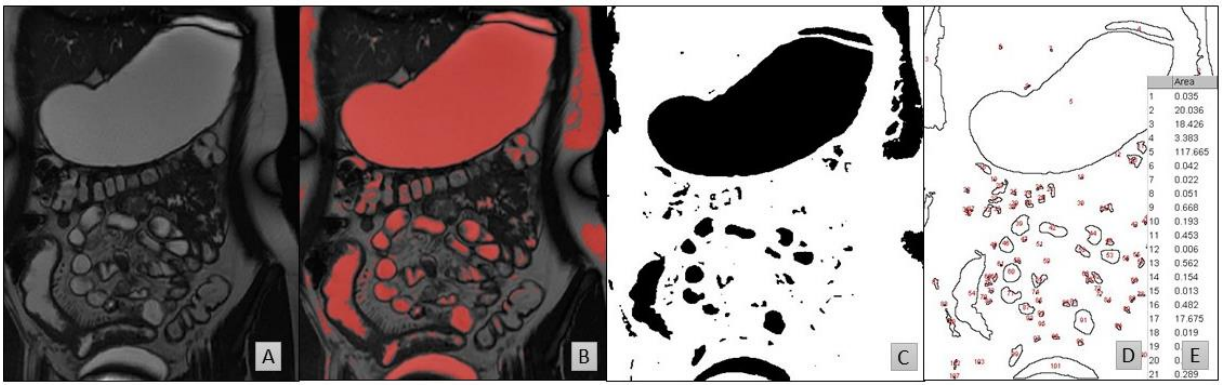

Figure 4.2. *MRI slices taken from a 16 year old fed female. (A) the original MRI slice with (B) fluid highlighted in red after thresholding in Horos based on the CSF. (C) Filtering the red voxels on a Black-on-White print in ImageJ allows for particle analysis, where the results (D and E) show the outlines of the regions of interest and their respective areas calculated.*

Horos was used to open and manipulate the digital imaging and communications in medicine (DICOM)-files and to identify and threshold the free fluid per individual dataset as follows:

1 The image slice most clearly depicting the cerebrospinal fluid (CSF) in the spinal canal was selected to generate a threshold value[24, 463]. This value was generated by drawing a rectangle entirely within the CSF, and then Horos calculated the average voxel intensity of the selected area automatically.

2 The limit for free fluid using this threshold value was set on the whole dataset *via* the plug-in *Global Thresholding Tool*[464]. This highlighted all zones in the entire MRI dataset with a voxel intensity equal to or higher than the threshold value (thus representing free fluid) in a red shade.

Representative images are shown in **Figure 4.3** (thresholding in Horos) and **Figure 4.4** (identifying fluid areas). The images were cropped to only show the specific regions of interest (ROI)[345] in Horos.

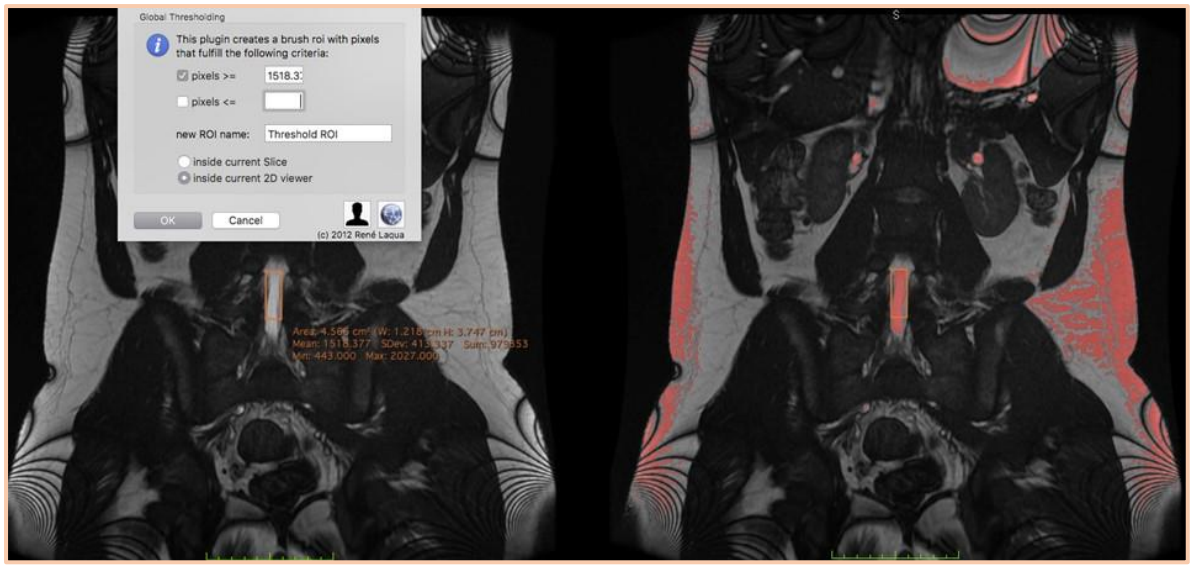

Figure 4.3. *Representative demonstration of the global thresholding tool in Horos, on an image of a 16 year old fluid fed male. Left: the threshold value based on the average voxel intensity of the orange square drawn within the CSF is entered in the global thresholding tool. Right: the same slide after thresholding.*

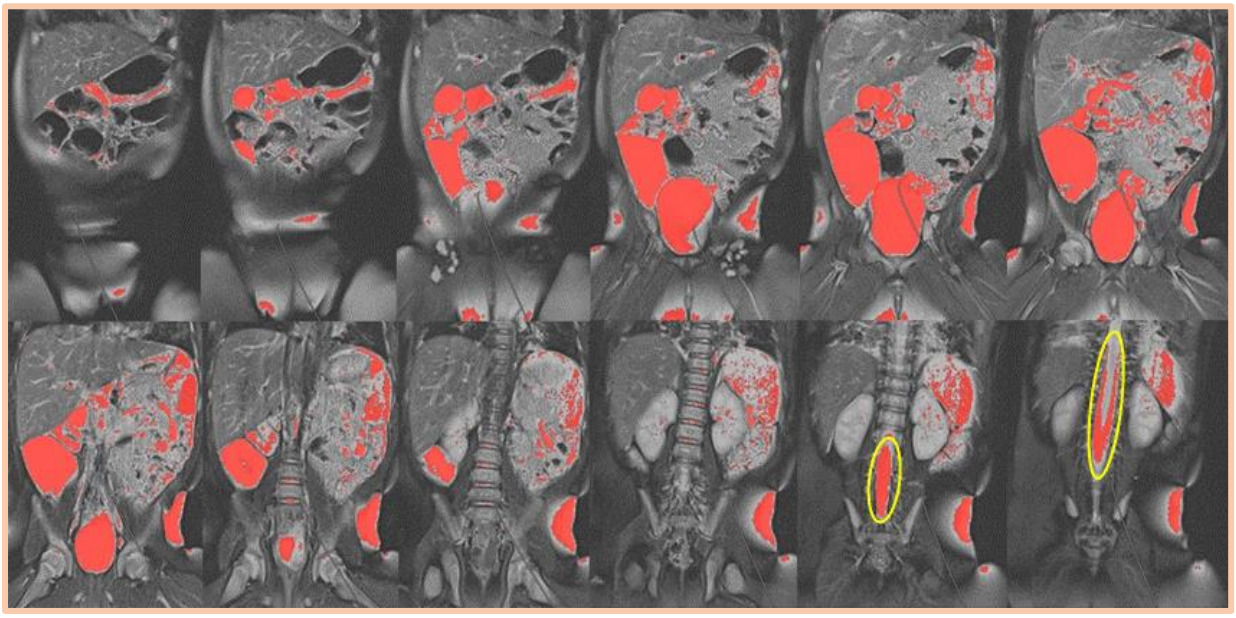

Figure 4.4. *Example MRI dataset after manipulation using Horos on an image set of a 5 month old fasted female. The images (top: left to right, continued bottom: left to right) show a sequence of slices in the coronal plane moving from a ventral to dorsal direction of the subject. The red areas indicate free fluid after thresholding to the CSF of the subject. The CSF is highlighted in yellow ovals; the CSF signal used for thresholding is the red zone in the spinal canal on the image second from the right, bottom row.*

3 The coloured images were transferred to ImageJ[460], where colour thresholding using the Red Blue Green (RBG) channels were converted into a black-white imprint of the free-fluid per image slice. Subsequently, the two-dimensional area of outlined fluid

particles were calculated *via* ImageJ and exported to Excel. Representative images are shown in **Figure 4.5**.

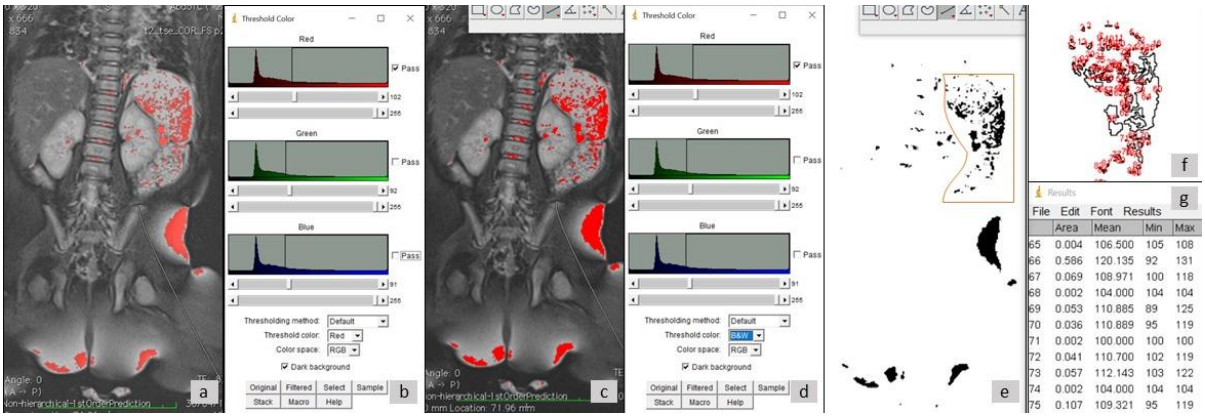

Figure 4.5. *Representative demonstration of thresholding in ImageJ, on an image obtained of a 5 month old fasted female. (a) The image exported from Horos. This was uploaded in ImageJ, followed by (b and c) thresholding on the red channel and adapting the lower limit so the ImageJ-highlights resemble the Horos-image closely. (d) Changing the threshold colour to "Black and White" (B&W) creates (e) a black and white imprint of the red areas. After analysis of the particles in ImageJ, (f) the outline of the particles are annotated and (g) a table containing the area of the black particles from image e is built.*

4 Using Excel and ImageJ, the black particles localised within the colon were manually identified (per segment) or excluded, based on comparison to the original Horos-image and anatomical interpretation[465]. To ensure an accurate classification, two paediatric radiologists assisted in defining the location of colonic fluid pockets. The first image slice, when advancing dorsal to ventral, showing the hepatic flexure (i.e. a shift in the central axis of the colon lumen from a craniocaudal to sagittal orientation) is where the transverse colon was determined to start (on both the ascending-transversal and transversal-descending junctions). This also helped the exclusion of areas that were motion artefacts[466].

5 The volume of each pocket was calculated in Excel, *via* multiplying the Z-component with the two-dimensional particle area. The Z-component is the sum of the slice thickness and the interstitial slice gap. The fluid volume and location (ascending, transverse or descending) of the fluid areas was recorded for every participant. *3D-*

rendering in the *3D*-protocol was employed for joining up and quantifying individual fluid pockets, rather than manual linkage of two-dimensional areas.

A sub-set of 20% of the datasets were analysed by a second operator to investigate operator-bias and robustness of the *2D*-protocol.

4.3.2.2 3D-protocol

Horos and Blender were used to calculate the number of fluid pockets, in addition to quantifying the free fluid volume using a *3D*-model. **Figure 4.6** shows a schematic overview of the *3D*-based data extraction process.

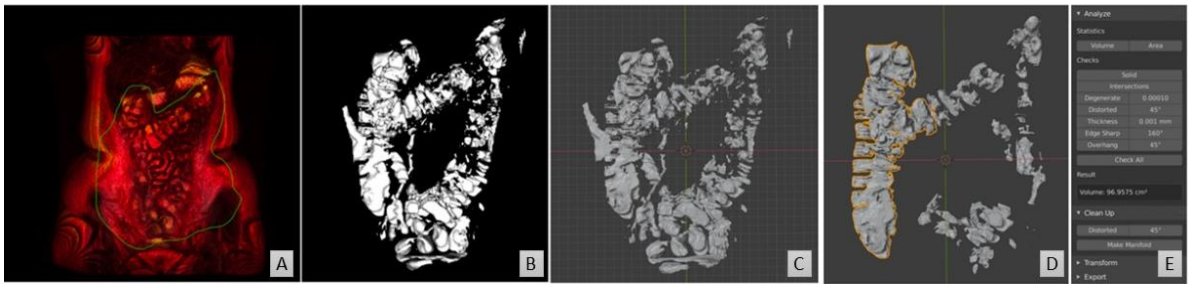

Figure 4.6. *Representative images from the 3D protocol, MRI dataset taken from a 15 year old fluid fed female. (A) 3D rendering in Horos builds a 3D model of the entire dataset. (B) The colon was excised from the 3D model in Horos. (C) The model converted into a stereolithography (STL) file and opened in Blender. (D) Non-colon artefacts are removed. (E) The volume of the individual pockets is calculated in Blender.*

The protocol was as follows:

1 The MRI dataset was converted into a *3D*-model, after the CSF-based thresholding (see *2D*-protocol), *via* the *3D*-volume rendering feature within Horos (**Figure 4.6**A). This method takes the slice thickness and interstitial slice gaps into account when building the *3D*-model.

2 The highlighted free fluid areas within the colon were approximately excised using the scissor tool, resulting in a *3D*-model showing only the fluid pockets (**Figure 4.6**B). This model was then exported as a stereolithography (STL) file (**Figure 4.6**C).

3 The software programme Blender was used to clean up the *3D*-model; the excision of the colon was refined and any non-colon remaining artefacts within the model were removed, consistent with the colon anatomy in the *2D*-model.

4 Blender calculated the volume of each individual pocket. After adjusting the scale within Blender to the scale of the MRI image, the fluid pockets volumes were measured by using the plug-in *Mesh – 3D print toolbox* (**Figure 4.6**D).

The volume was measured for each individual fluid pocket via the volume feature. The sum of all individual fluid pockets gave the number of pockets for the entire dataset, as well as a second (alternative) measurement of the total colonic fluid volume within the paediatric dataset.

4.3.3 Statistical analysis

SPSS and GraphPad Prism were used for statistical analysis on the datasets. The datapoints were subject to statistical analysis in their entirety or grouped in different categories such as age, sex, fed state. A statistical test was deemed significant if the p-value (*p*) was smaller than 0.05.

The following data manipulation steps and examinations were undertaken:

- Identification of outliers via the descriptive statistics functionality.
- To investigate correlations, Pearson's correlation tests were used.
- To compare volumes and number of pockets between two groups (such as investigating fed state), independent sample t-tests were used.
- Where multiple groups were compared, a one-way ANOVA with Bonferroni correction was used. Where multiple measurements on the same participants were

investigated (such as a difference in volume in the three colon segments), an ANOVA of repeated measures with a Greenhouse-Geisser correction and post-hoc Bonferroni correction was used.

4.4 Results

4.4.1 Participant demographics and MRI dataset characteristics

4.4.1.1 Participant demographics

The MR images of 49 participants were available for this study. Three participant datasets were excluded, due to either low resolution or images obtained with an inappropriate acquisition sequence for the employed analysis pipeline (see also **Appendix 10**).

The demographics and MRI acquisition parameters of the remaining 46 participants whose datasets were included in this study are shown in **Appendix 11**. The participants were stratified into age groups according to the ICH E11 classifications[467, 468] (**Table 4.2**). For ease of discussion, the cohort younger than 2 years of age that includes infants and neonates was named as infants collectively, as these represented the biggest portion of this age band. Detailed metadata (specific age, weight and sex) for 6 participants were missing, although their age group was known. Subsequently, these datapoints were excluded for analyses that required sex or specific age.

Furthermore, 4 more datasets were excluded from the *3D*-based determination of fluid volume and number of pockets, as there was too much interfering background, or the colonic fluid was indistinguishable from the small intestinal fluid, which rendered these datasets incompatible with the Blender protocol. The datasets in question are from two infants (5 and 18 months old), a preschool child (3 years old) and a school-age child (6 years old).

Table 4.2. *Demographics of the participants included in this study*

	Number of datasets available	
Age range	**Fasted children**	**Fluid-fed children**
<2 years (neonate/infant/toddler)	9	0
2 – 5 years (pre-school children)	12	0
6 – 11 years (school-age children)	6	2
12 – 16 years (adolescents)	1	16

4.4.1.2 MRI dataset characteristics

Individual MRI datasets varied in number of slices per dataset (ranging from 22 to 192 slices), slice thickness used (ranging from 0.09 mm to 6 mm, with or without a varying interstitial slice gap) and clarity of the CSF fluid. The differences in e.g. slice thickness between the datasets did not interfere with the *2D*-processing pipeline protocol, as this was accounted for *via* thresholding and multiplication using a Z-component.

4.4.2 Colonic fluid volume and number of pockets

The paediatric colon contained an average of 22.5 mL (standard deviation, SD, ± 41.3 mL) of fluid in 15.5 ± 17.5 discreet fluid pockets; the data were not normally distributed and the median volume was 0.8 mL with a median number of 12 pockets (**Table 4.3**).

Table 4.3. *Fluid volumes and number of pockets for the total, ascending, transverse and descending colon*

Colon segment	Total	Ascending	Transverse	Descending
Mean fluid volume ± SD (mL)	22.48 ± 41.30	16.44 ± 27.62	3.78 ± 11.49	2.27 ± 7.09
Median fluid volume (mL)	0.8	0.63	0.004	0.003
Interquartile range of fluid volume (mL)	19.69	18.52	0.65	0.12
Range of fluid volume (min-max) (mL)	0 – 167.47	0 – 102.30	0 – 56.87	0 – 37.94
Mean number of fluid pockets ± SD	15.5 ± 17.5	14.5 ± 16.4	1.0 ± 2.5	0.05 ± 0.2
Median number of fluid pockets	12	10	0	0

The majority of the fluid pockets were smaller than 1 mL; 90.4% of the pockets (557/616) were smaller than 1 mL, which accounted for 5.5% of the total fluid volume (51.5 mL/933.2

mL) in the database. The other 9.6% of the pockets (59/616) were larger than 1 mL and contributed 94.5% to the total fluid volume (881.7 mL/933.2 mL) in the database (**Figure 4.7**). The paediatric colon contained on average 3.6 ± 2.9 pockets larger than 1 mL (**Table 4.4**). The distribution of the different pocket sizes is given in **Figure 4.8**.

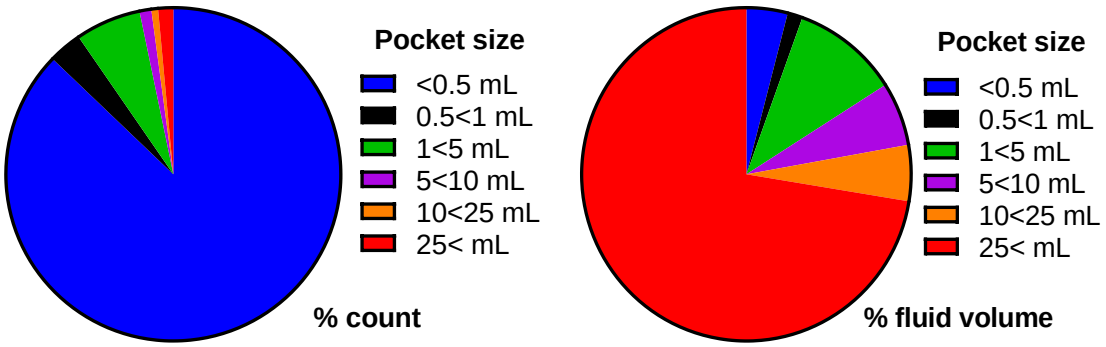

Figure 4.7. *Pie-chart showing the distribution of (left) the relative count of the pocket size and (right) the relative contribution to the fluid observed in the paediatric colon.*

Table 4.4. *Mean and median number and volumes of pockets per participant*

	All pockets		Pockets bigger than 1 mL	
	Number per participant	**Volume (mL)**	**Number per participant**	**Volume (mL)**
Mean ± SD	15.5 ± 17.5	1.52 ± 12.09	3.6 ± 2.9	14.60 ± 36.29
Median	12	0.04	3	3.31

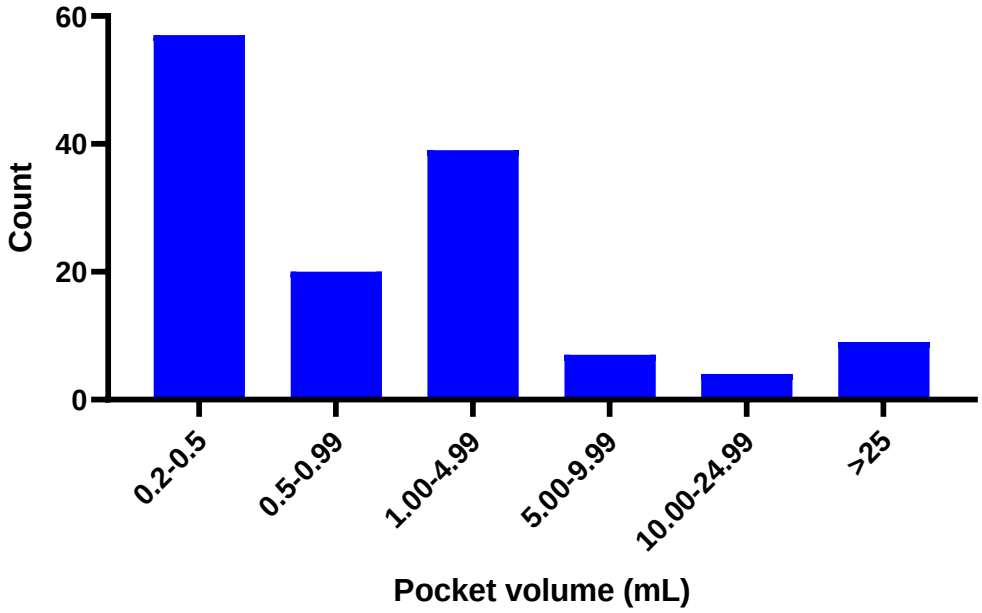

Figure 4.8. *Distribution of fluid pockets based on size.*

There was a large variation observed in the datasets, both in fluid volume and number and size of pockets. No colonic fluid was found in 9 participants, some but less than 1 mL of fluid in 15 participants, whereas 8 datapoints with a total fluid volume higher than 60 mL were classified as statistical outliers, however these were not excluded from the subsequent analysis (shown as open symbols in **Figure 4.9**).

The 9 participants with no visible fluid had no common demographic factor (age group, sex, fed state); neither did the 8 participants with a colon fluid volume higher than 60 mL.

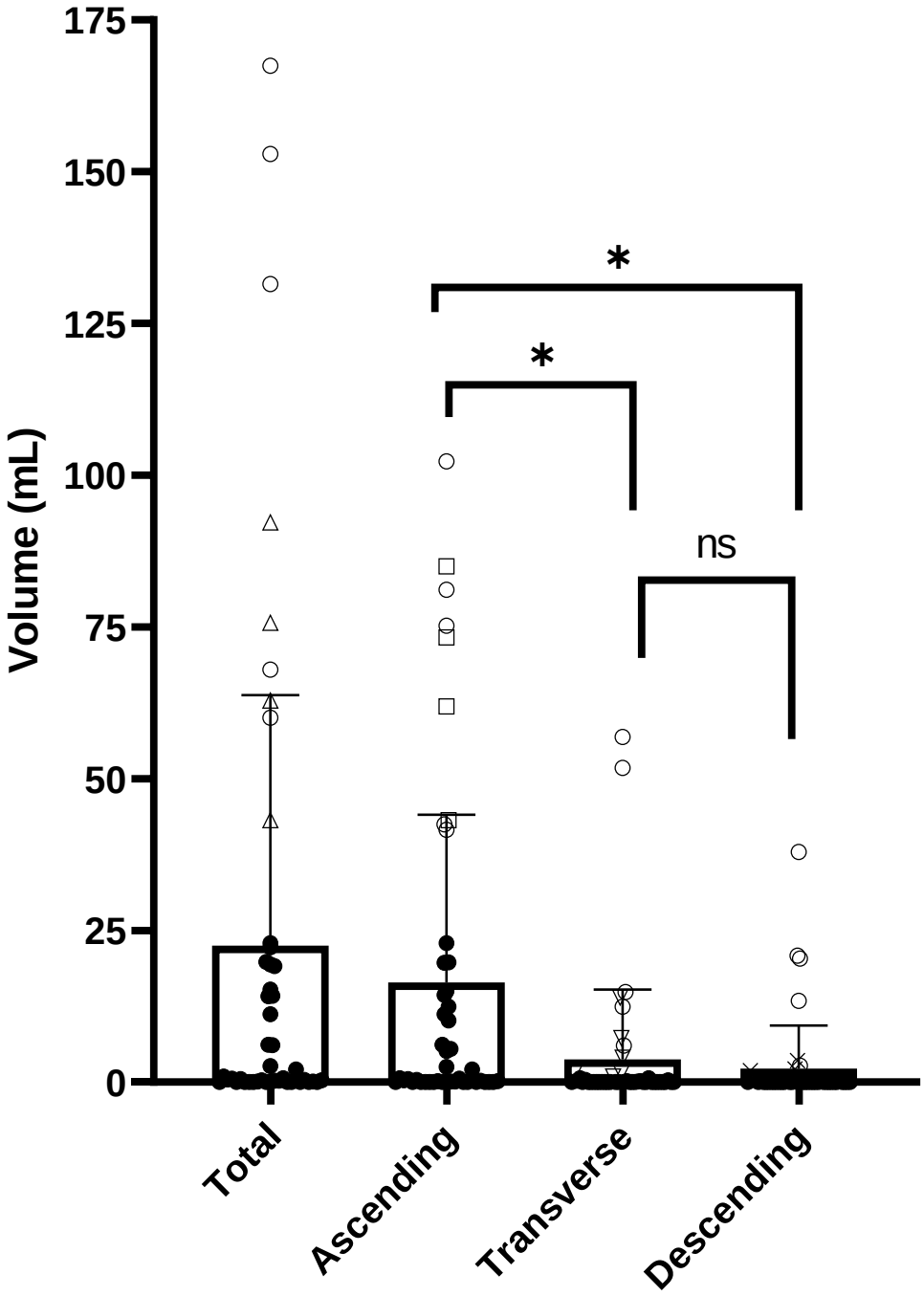

Figure 4.9. *The fluid volume in the total colon and the ascending, transverse and descending segments. The bar chart shows mean values, with standard deviation as the error bar. The * represents a significant difference ($p < 0.05$); ns = not significant. The open symbols indicate the individual datapoints that are statistical outliers: circles are outliers in every section, the other symbols indicate outliers only in that particular segment (triangles in the total colon, squares for the ascending colon, triangles for the transverse colon and crosses for the descending colon).*

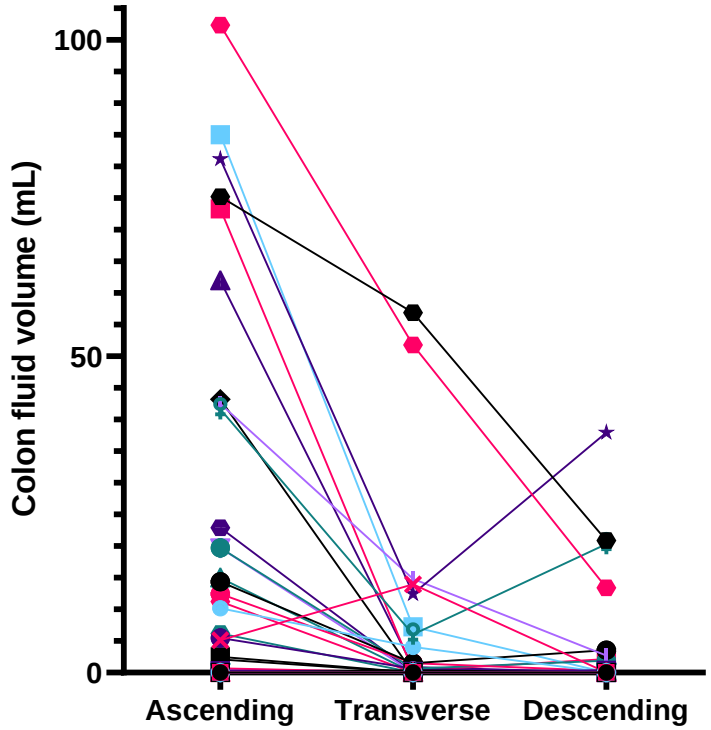

Figure 4.10. *Colon fluid volume in each segment of the colon, linked per participant.*

Data on threshold values, fluid volumes via both protocols and number of pockets in the total and segments of the colon per participant are available in **Appendix 12**.

4.4.2.1 Fluid volume in colon segments

The fluid volumes in the three colon segments were compared, where a wider range of fluid was found in the ascending colon (0 to 102.3 mL) compared to the fluid volumes in the transverse or descending colon (0 to 56.8 mL and to 37.9 mL, respectively). There was a trend for decreased fluid volume in the segments towards the distal colon (**Figure 4.10**). The fluid volumes of the colonic ascending, transverse and descending segments were positively correlated to each other (Pearson's coefficient >0.58, $p < 0.001$ in all cases). ANOVA of repeated measures with a Greenhouse-Geisser correction and post-hoc Bonferroni correction showed that the ascending colon contained the most fluid ($p < 0.001$). No

statistically significant difference was detected between the fluid volumes in the two other segments (Bonferroni post-hoc test p 0.836, >0.05). However, in 4 MRI datasets (with the total volume ranging from 0.004 mL to 0.4 mL) either the transverse or descending colon contained all the fluid (and thus none was present in the ascending colon).

The ascending colon also contained the most fluid pockets compared to the other two segments ($p < 0.001$); no statistically significant difference was found in the number of fluid pockets between the transverse and descending colon. Only the ascending colon contained fluid pockets larger than 1 mL, with the exception of one dataset where a pocket of 249.6 mL was observed that spanned the entire colon. A graphical representation of the distribution of the individual pockets with a volume of up to 25 mL is shown in **Figure 4.11** was created by and reproduced with permission from Benoni Alexander.)

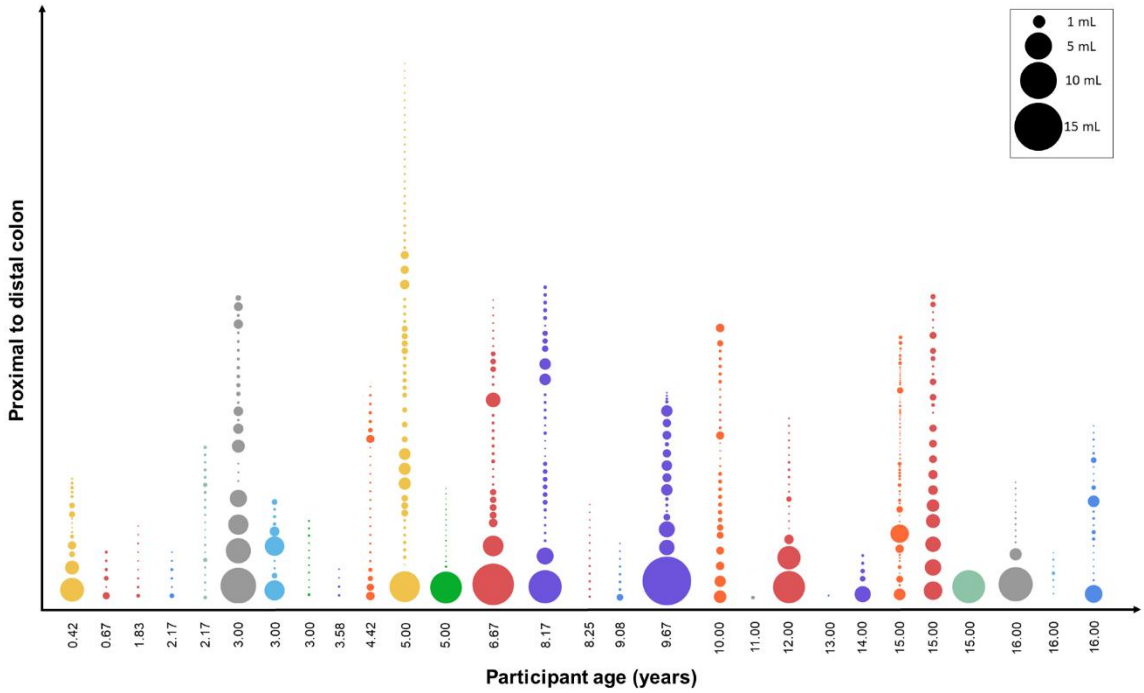

Figure 4.11. *Representation of fluid pockets in the paediatric colon for each participant, arranged in order of increasing age. Each bubble depicts an individual fluid pocket, the size illustrates the relative volume. The nine pockets larger than 25 mL, found in nine individual datasets, are not shown, as these distort the scale.*

4.4.2.2 Effect of covariates on fluid volumes

No correlation was detected in the entire cohort between age and the fluid volumes or number of pockets in the total colon or segments ($p > 0.17$ in all cases, **Table 4.5**, **Figure 4.12**A).

Table 4.5. *Pearson correlation coefficients between fluid volumes and age.*

Age correlation with volume in colon:	Total	Ascending	Transverse	Descending
Pearson correlation coefficient	0.148	0.145	0.205	-0.033
Significance (p-value)	0.326	0.336	0.173	0.830

However, in the preschool population (2-5 years old, $n = 11$), age was positively correlated (Pearson's coefficient >0.65) to total and ascending colonic fluid volume (for both $p < 0.03$, **Figure 4.12**B), but no correlation was found between age and the number of fluid pockets.

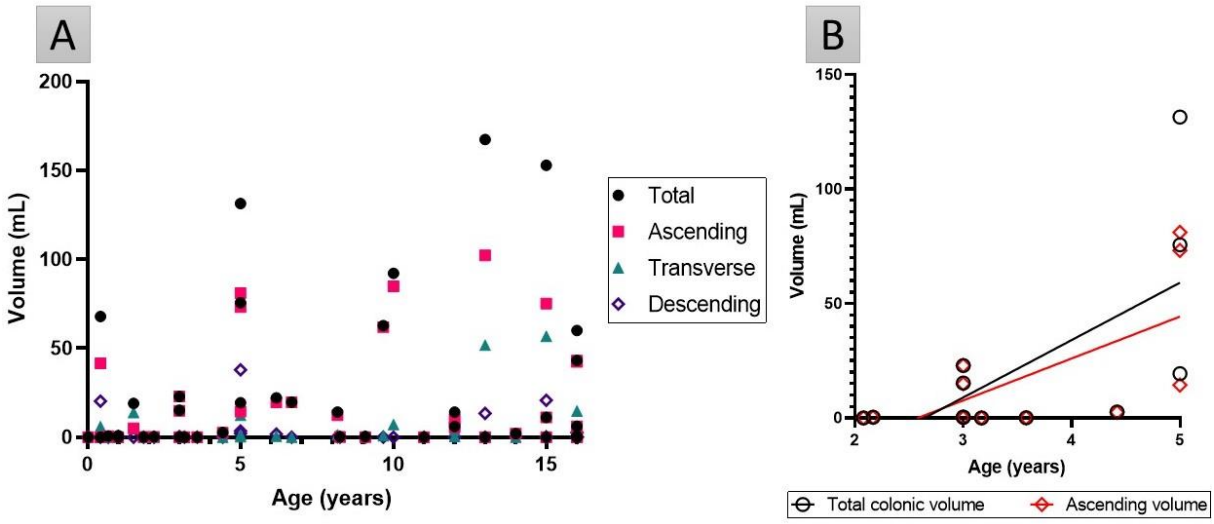

Figure 4.12. *(A) Fluid volume in the total and segments of the colon for every participant as a function of age. No correlations were found, ($p > 0.17$ in all cases). (B) Fluid volume in the total and ascending colon in the preschool population are significantly correlated to age (Pearson's coefficient > 0.65, $p < 0.03$).*

4.4.2.3 Trends with metadata

No significant differences in fluid volumes or the number of pockets were detected (**Table 4.6**) based on fed state (**Figure 4.13**), sex or age group (**Figure 4.14**).

Table 4.6. *Mean volumes (± SD) per fed state, sex and age group for the total and segmented colon, and significance level of the statistical test employed.*

Descriptor		Total (mL)	Ascending (mL)	Transverse (mL)	Descending (mL)
Fed state	Fasted	17.0 (±31.1)	13.3 (±23.2)	1.4 (±3.5)	2.4 (±8.0)
	Fed	30.9 (±53.5)	21.4 (± 33.5)	7.5 (±17.5)	2.1 (± 5.7)
	T-test p-value	0.27	0.339	0.076	0.878
Sex	Male	24.7 (± 56.0)	15.7 (± 34.2)	5.1 (±14.4)	4.0 (±10.9)
	Female	21.4 (±36.8)	15.8 (±25.1)	3.9 (±11.3)	1.7 (±5.5)
	T-test p-value	0.827	0.988	0.786	0.386
Age band	neonate	9.88 (± 22.67)	5.33 (± 13.70)	2.24 (± 4.83)	2.31 (± 6.76)
	preschool	22.38 (± 40.62)	17.48 (± 28.98)	1.22 (± 3.55)	3.67 (±10.85)
	school age	26.52 (± 33.63)	24.86 (±31.71)	1.36 (± 2.43)	0.30 (± 0.64)
	adolescent	27.33 (±52.81)	17.61 (± 30.43)	7.54 (± 18.00)	2.18 (± 5.82)

	One-way ANOVA p-value	0.777	0.536	0.413	0.791

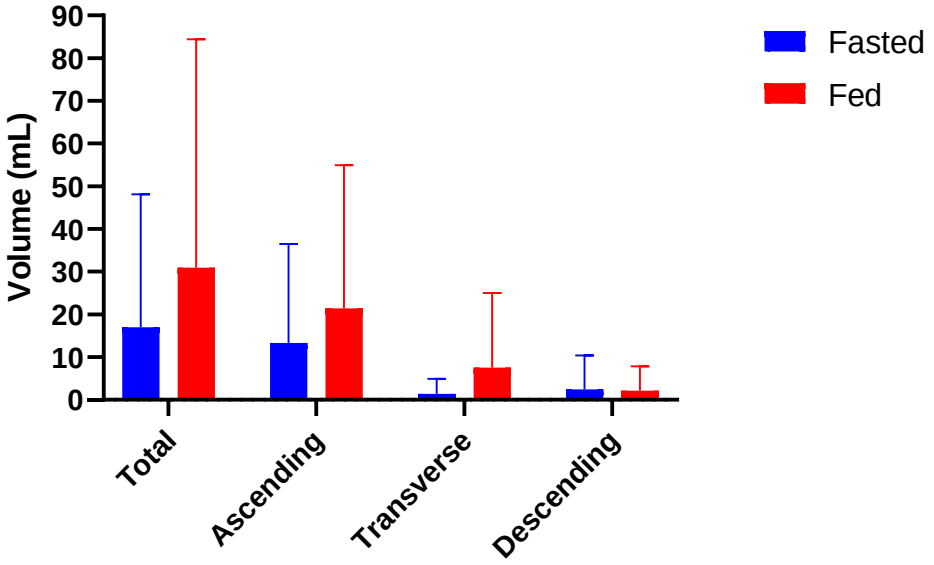

Figure 4.13. *Mean fluid volumes for the total and segmented colon, grouped by fed state. Error bars show SD.*

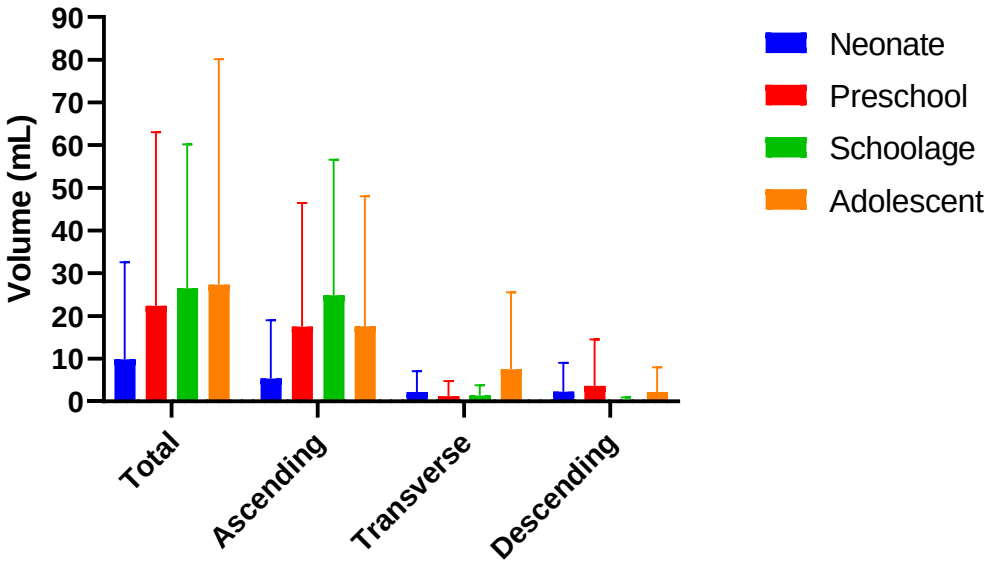

Figure 4.14. *Mean fluid volumes for the total and segmented colon, grouped by age class. Error bars show SD.*

Additionally, no significant difference was observed when comparing between the influence of fed state, or sex, on age-matched subclasses in the school-age cohorts and adolescent (t-

tests: all not significant at the 0.05 level). There were no fluid-fed neonatal or pre-school-age participants.

4.4.3 Robustness of protocol

A second operator processed 20% (*n* = 10) of the MRI datasets via the *2D*-protocol. There was good similarity in total fluid volumes and threshold values between the two operators (Pearson's correlation >0.97 and $p < 0.001$ in both comparisons; **Figure 4.15** and **Figure 4.16**), demonstrating the absence of operator-bias in the *2D*-protocol.

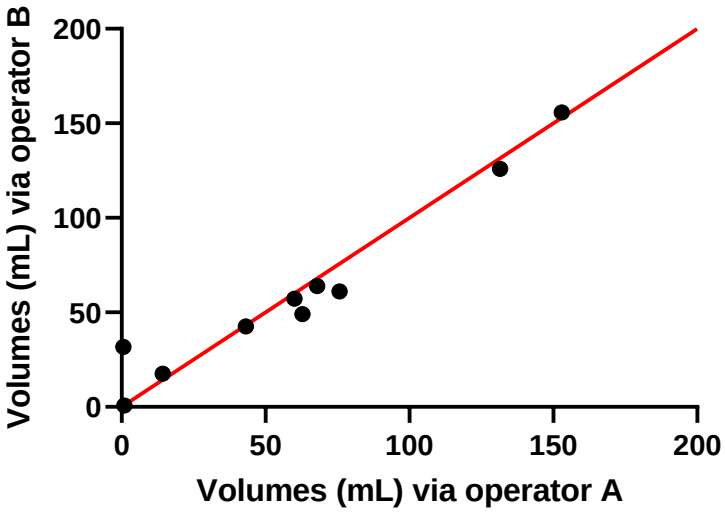

Figure 4.15. *Correlation of fluid volume in the total colon on the same datasets via the 2D-protocol between operators A and B (Pearson's correlation coefficient 0.970, p <0.05, n = 10). The line of identity is given in red.*

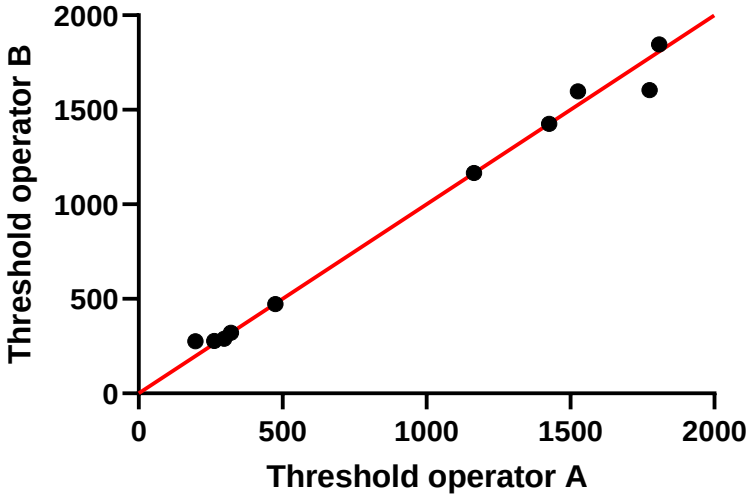

Figure 4.16. *Correlation between the CSF-threshold set on the same datasets between operators A and B (Pearson's correlation coefficient 0.995, $p < 0.05$, $n = 10$). The line of identity is given in red.*

Furthermore, the fluid volumes obtained via the *2D*-based protocol were in good correlation to the *3D*-based protocol (Pearson's correlation 0.939, $p < 0.001$; **Figure 4.17**).

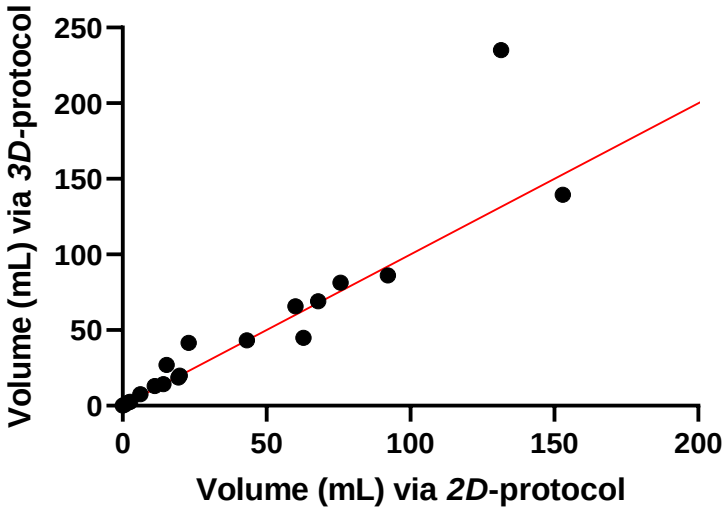

Figure 4.17. *Correlation of the fluid volumes in the total colon on the same datasets between the 2D- and 3D-protocol (Pearson's correlation coefficient 0.939,* p *< 0.05,* n *= 40). The line of identity is given in red.*

Threshold values (used to identify free fluid within the image) based on the CSF voxel intensity varied from 142.8 to 2136.1. Additionally, there were no correlations between the used threshold value and any of the fluid volumes or the number of pockets, demonstrating robustness of the followed protocols (**Table 4.7**).

Table 4.7. *correlation of threshold with volumes and number of pockets*

Correlation of threshold with:	Pearson's correlation coefficient	P	N
Fluid volume in the total colon	0.085	0.573	46
Fluid volume in the ascending colon	0.015	0.924	46
Fluid volume in the transverse colon	0.253	0.090	46
Fluid volume in the descending colon	0.030	0.846	46
Number of pockets	-0.169	0.297	40

There was a significant correlation between of threshold value with age and with weight (Pearson's correlation coefficient 0.77 and 0.75; p <0.05 in both cases). Similarly, there was a significant correlation between slice thickness and age or weight (Pearson's correlation coefficient 0.73 and 0.67, respectively, in both cases p <0.05).

4.5 Discussion

4.5.1 Comparison of fluid volume with literature

This study was the first to report fluid volumes in the paediatric colon using MRI quantification. The median fluid volume found in the total colon was 0.80 mL, the mean 22.48 mL ± 41.30 mL, with a range of 0 mL to 167.5 mL (**Table 4.3**). It was observed that in adults the fluid in the ascending colon is roughly 6 times larger in fasted and 4.2 times larger in the fed state than the ileal fluid volume[345, 469, 470]. A similar comparison in the paediatric population is not possible, as Papadatou-Soulou *et al*.[24] did not report fluid volumes for distinct segments of the small intestine. However, it can be noted that a similar distribution of fluid volume with age (a wider range of values observed with older patients) was seen in the small intestine of the same participants.

Comparison to a very recent report[471] (2022) on paediatric fluid volumes in the gastro-intestinal tract (n=140, aged 0-16 year old) show similar trends in the colon. Here, most of the fluid was observed in the ascending colon with diminishing amounts when progressing distally, and a trend with age was also absent. Similarly, the medians were very comparable (0.80 mL here vs 0.49 mL in the recent publication). Additionally, a broad variability in colonic fluid volume was also observed, including some participants having no fluid within the colon or up to 35 mL. Differences in the employed thresholding method (an automatic approach using an average CSF voxel intensity as done here, or a manually chosen value at 30-40% of the CSF voxel intensity as done by Van der Veken) or in ethnicity and diet (UK versus Belgium) are possible reasons for the discrepancies observed. Additionally, Van der Veken strictly excluded participants that were non-fasted, whereas here the data of fasted and fluid-fed participants were pooled as no difference in fluid volumes due to fed state was observed (**Table 4.6**).

The paediatric results found in this study could also be compared to the adult colon. Despite the reported physical differences between the paediatric and adult colon, a comparison in the amount in fluid is still fundamentally relevant, as adult values are currently used as fluid volume inputs for paediatric colonic absorption modelling[66]. The median paediatric colonic fluid value (0.80 mL) is lower than observed adult medians (2 mL[374] and 8 mL[26]), indicating the colonic fluid volumes are dissimilar between adults and children. However, the mean results from this paediatric study are comparable to values reported for the adult colon (**Table 1.10**, **Figure 4.18**) which was surprising as the physiology of the colon changes with age.

Table 4.8. *Reported fluid volumes in the colon of healthy adults when measured using MRI. N/A means that the data were not reported*

Study	Fed state (intake of food/fluid)	Time of Ingestion before MRI acquisition	Number of participants	Median (min-max) (mL)	Mean (± SD) (mL)
Schiller 2005[26]	Fasted	-	12	8 (1-44)	13 ± 12
	Fed (standardised meal)	1 h		18(2-97)	11 ± 26
Pritchard 2017[374]	Fasted	-	11	2 (0-7)	-
	Fed (500 mL Moviprep)	1 h		140 (104 -347)	-
Murray 2017[345]	Fasted	-	12	N/A (0-11)	2 ± 1
	Fed (240 mL water)	30 min		N/A (0-49)	7 ± 4

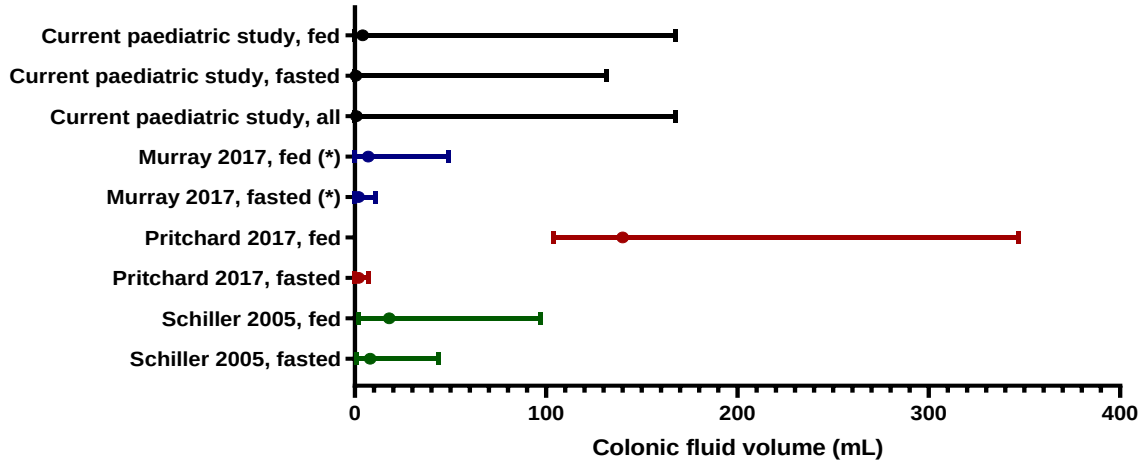

Figure 4.18. *Comparison of the median (closed dot) with associated range reported for colon volumes in adult studies with healthy volunteers. (*): Note that for Murray et al, 2017, the mean instead of median is reported.*

The median total colonic volume (TCV) of healthy children aged 14-18 years is reported to be 227 mL (interquartile range 180 mL – 263 mL)[472], whereas the mean healthy adult TCV is 760 mL (with a 95% confidence interval of 662 mL - 858 mL)[371, 473]. Similarly, the length of the colon increases with age; from 52 cm length in children younger than 2 years of age to 150 cm in adults[453]. Therefore, a smaller colonic free fluid volume in the paediatric colon compared to an adult cohort is expected. However, not all colonic parameters change with maturation, e.g. the pH of the paediatric colon children aged 8-14 years is reported to be comparable to adult values[474, 475]. Similarly, no significant difference was detected in the fluid volumes between the four different age groups (consistent with the existing data on small intestinal and colonic fluid volumes) in children[24, 471].

Although these differences were not significant, performing *in vitro* and *in silico* predictions with the new values for paediatric colonic fluid volume will inherently improve their relevance to children and better support paediatric drug product development[168].

It is hypothesised that the larger paediatric variability and absence of difference between age groups may be related to the relatively small sample size available in every age group. In addition, the participants have potential underlying morbidities as there was a clinical need

for MRI assessment, resulting in a large variability which may have introduced bias into the data. Although such a large variability in fluid volumes is also observed in studies on healthy adult colonic fluid volumes *via* MRI quantification (with values ranging 1 – 347 mL)[374, 378, 476, 477], these studies were performed on a less diverse population compared to the participants in this study.

As the influence of age was investigated by comparing four age groups, the sample size per age group was similar to sample sizes used in the studies on healthy adult volunteers. However, the demographics of the participants in the adult studies were closely controlled; for example, those in Murray *et al.*[345] (*n* = 12) were all 20-22 years old and healthy, to minimise variability in the dataset. Similarly, the studies by Schiller *et al.*[26] and Murray *et al.*[345] were performed in a tightly controlled environment. The variability in studies undertaken using a small group of healthy volunteers in a clinical setting are less likely to capture the real-world variability, compared to studies in a heterogenic paediatric population with potential comorbidities[2, 478]. Hence, outliers were not excluded from statistical analysis. Additionally, it was expected that the extracted data would be subject to inherent variability due to the major physiological changes that comes with maturation of the GIT[168] and (2) the datapoints would not be normally distributed, due to the variation in participant age.

Another source for the larger variability in this study could be the stratification according to the ICH-classifications. It is recognised that there still can be a significant physiological difference between two children in the same age group. For example, gastric emptying in neonates is different based on the type of food (mother milk/type of formula)[479, 480], and there are discrepancies in the reported GIT pH in the first 2 to 5 years[4].

As the generic ICH-classification is based on days/months/years after birth, stratification on a parameter that considers the physicochemical properties of GIT anatomy and contents might have been more appropriate, such as height, BSA or BMI as these are typically used for dose adjustments. However, such data were not collected from the participants. Additionally, such measurements were found to be inadequate covariates for paediatric gastric and small intestinal fluid volumes[471]. A limitation in this study is that data were only available from 49 patients, extracted from two tertiary centres with differing MRI acquisition protocols. The proposed number of participants was as many patients as possible, with at least 10 in each age band according to the ICH classification. This proposed sample size was not met for neonates (0-30 days, n=2), infants (1 month – 2 years, n=7) and school-age children (6-11 years, n=8). Paediatric MRI small bowel is a scarce resource offered mainly in tertiary centres (UHCW and BCH). It is a specialist modality only performed on selected cases, following discussion at a small bowel multidisciplinary meeting and requires interpretation by specialists. Therefore, the number of paediatric participants available for scientific study is small when compared with their adult counterparts. Together, these factors led to a small sample size and even smaller sub-sample size, when comparisons were made based on fed state, sex or age. In addition, the excess variability potentially influences the statistical analysis and interpretation from these groups. Although the sample size is statistically small, it is sizeable considering population type and complexity of the modality; as such, these data should be viewed as preliminary where a larger, well-defined cohort is warranted to provide robust data that will lead to more conclusive claims.

The ascending colon typically contained the highest portion of fluid (**Figure 4.9**). Correlations demonstrated that when fluid is present in the ascending colon, this can act as a predictor for the total colonic volume. The same trend was observed in adults[345, 371] and children[471]. Consequently, as chyme from the small intestine enters the colon, the desiccating function of the colon to transform chyme to drier stools explains this trend[347], where less water is identified in more distal regions. This also explains why mean value of the number of pockets within the descending colon, the most distal segment investigated, is smaller than 1 (median 0).

4.5.2 Comparison of number of fluid pockets with literature

There were on average 3.6 ± 2.9 fluid pockets larger than 1 mL, mainly in the ascending colon. Similarly to adults, the majority of the fluid pockets were very small[345] (**Figure 4.19**, **Figure 4.7** and **Figure 4.11**). In this study, it was found that only 9.6% of the fluid pockets were larger than 1 mL, yet they contributed for 94.5% to the overall volume quantified. The software protocols used in this study did not use any limits on the size of fluid pockets to be quantified, therefore even fluid pockets of 0.01 mL were included in the data. As 90.4% of the fluid pockets were smaller than 1 mL and contributed to only 5.5% of the fluid observed in the study (55.5 mL), their physiological relevance in colonic absorption might be questioned.

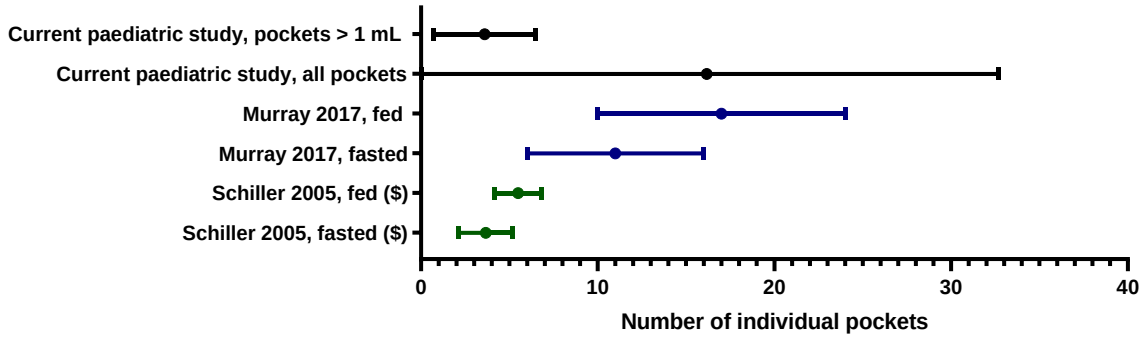

Figure 4.19. *Comparison of the mean and SD reported for the number of fluid pockets in the colon in adult studies with healthy volunteers. ($): Note that for Schiller et al., 2005, the 25% and 75% percentiles are reported instead of the SD.*

However, in the paediatric small intestine, smaller pockets contribute to a larger portion of the overall fluid volume as 66% to 76.3% of the pockets (for fluid-fed and fasted children, respectively) were larger than 1 mL, contributing to 21% - 27% of the observed intestinal fluid volume[24].

4.5.3 Effect of covariates

No correlation was observed between colonic fluid volumes or the number of pockets, and age or weight. This implies that age or weight does not correlate to colonic fluid volumes, which is in contrast with other GIT parameters like gastric pH[4] or the need for fluid intake[467] where the most significant changes are observed in neonates and infants (<2 years)[481].

Current dosage guidelines use allometric scaling based on age, weight or BSA to extrapolate paediatric doses from adult data[23, 168, 467, 482-484]. Further investigation is required to investigate the appropriateness of allometric scaling for colon-specific drug delivery systems (CDDS)[168], especially for poorly soluble drugs that act within the colon. Only in the preschool category (children aged 2 - 5 years, *n* = 12), was age significantly positively correlated to fluid in the total and the ascending colon (**Figure 4.12**B). This implicates that children in this category will have more fluid in their ascending (and thus total) colon as they are closer to 5

years of age; this finding could be due to the small sample size and the large variability seen within these 12 participants.

Similarly, a proposed biorelevant classification system considers the variability with ontogeny, e.g. body weight would be more suitable scalar for younger children, whereas BSA would be more appropriate for older children[4].

Additionally, no fluid was observed in any participant that was 3 years old. Indeed, upon removing the most extreme datapoint (belonging to a 5 year old, with a total and ascending colonic fluid volume of 131 mL.5 and 81.1 mL), both trends are no longer statistically significant (Pearson's correlations for age with total and ascending colon 0.595 and 0.561, $p > 0.05$ in both cases). Although the most significant change in colon length is reported in this age range (4-6 years old) with an increase to 72.3 cm from 52.3 cm in a neonate group (0-2 years of age), further research is needed. No ontogeny in the amount of fluid in the GIT has been reported[24, 467].

A recent survey (2022) across regulatory agencies and pharmaceutical companies indicated only 15.38% of the responders use less than 100 mL for paediatric intestinal biorelevant dissolution testing, yet the median and mean paediatric colonic fluid volume observed here remain far below this value[1]. This is particularly important with respect to findings here as much lower volumes were observed in this study.

Fed state had no impact on fluid volumes (**Figure 4.13**), which could be a result of several factors. Firstly, it was unlikely that Oral Kelan Prep had an impact on the colon volumes in the timeframe of this study, although an effect could not be excluded *a priori*, as literature is conflicting about when an ingested solution reaches the colon since this is subjected to

inter- and intra-variability[371]. In addition, Oral Klean Prep is an osmotic laxative, which draws water into the GIT – therefore, it is not fully representative to a fluid-fed child. Placidi *et al*.[485] reported a significant increase in ascending colon fluid volumes 45 min post-ingestion[485] of 5% mannitol (another osmotic laxative) in 350 mL of water, so a possible effect could not be predicted before analysis. The healthy paediatric population is believed to have a gastric emptying rate[32] and small intestinal transit time (SITT) comparable to adults (SITT 3.49 h ± 1.02 h (mean ± SD)) based on meta-analysis[2, 23, 486], although data suggest children younger than 2 years of age have a slower (longer) SITT[2, 467]. In addition, this meta-SITT was not affected by fed state[486]. The meta-gastric emptying rate and meta-SITT values support the absence of an impact of Oral Klean Prep on the colon volumes as observed in this study. The increase of the free fluid in the colon of fasted adults Pritchard *et al.*[374] observed 60 min post-ingestion of 500 mL Moviprep or Murray *et al*.[345] noticed 30 min post-ingestion of a 240 mL glass water is likely to be due to the gastro-colonic reflex, as hypothesised by Lemmens *et al.*[469]. Secondly, there was no verification of fed state prior to analysis as this study had a real-world setting. The consumption of the full 500 mL Oral Klean Prep was not monitored. In addition, it was not strictly monitored whether the children in the fasted population indeed fasted overnight, although this was part of their clinical instructions. Tighter monitoring on the clinical protocols prior to MRI with specific reference to fasting and ingestion of the solution would improve the interpretation of this MRI data.

4.5.4 Robustness of protocol

As demonstrated by the close correlation between protocols and operators, the software pipelines utilised are robust and reproducible. Therefore, the data extracted from the MRI

datasets are reliable. The software protocols also had similar sensitivity compared to previously reported adult MRI studies, as an identical reference (CSF fluid) to identify the free fluid was used.

Overall, although the median paediatric colonic fluid volume is considerably smaller than the median volume observed in adults, there is substantial variation in the paediatric dataset due to different factors which distorts the distribution and potentially hides the true population-average in healthy children. Further research is needed, ideally on a healthy paediatric cohort where participant demographics can be controlled, to verify the conclusions of this study.

There is substantial variation in the choice of software used to interrogate MRI datasets in order to calculate fluid volumes and pockets[24, 26, 345, 374, 378, 463, 476]. Previous studies have already expressed the need for standardisation of methods[371], as the CSF-based threshold for free fluid is dataset dependent. However, no influence of CSF-threshold values to the obtained data in this study was detected, consistent with literature[24, 26, 345, 378]. In addition, cross-analysis of the extracted values between the *2D*- and *3D*-based protocol and between multiple operators shows that both protocols produce similar results regardless of operator or used modelling approach (**Figure 4.15**, **Figure 4.16** and **Figure 4.17**). Therefore, the use of CSF-based thresholds on the MRI datasets are robust and provide consistent results for colonic fluid analysis.

The observed correlation between thresholding and age or weight is more likely due to differences in MRI-set up (as the MRI datasets of older participants came from the UHCW site, where thicker slices were used). Similarly, there was a significant correlation between slice thickness and age or weight , further indicating that the MRI scanner settings influence

the threshold rather than age. Identical MRI acquisition parameters between different sites might eliminate this bias in prospective similar studies.

4.5.5 Study limitations

The limitations in this study need to be addressed to improve similar future studies. Firstly, MRI quantification of fluid in the GIT does not include water bound in the unstirred boundary layer (UBL)[371, 378, 465]. Although the UBL is believed to play a role in drug absorption[371], its extent is unknown[347]. It should be noted that only the free-flowing water is being quantified in this protocol, based on the fluidity of the CSF[378].

Furthermore, quantification of free fluid has only been validated directly for the adult SI[463], not for the adult or paediatric colon[345]. Underestimation (or overestimation) of the free colonic fluid cannot be excluded[345].

In this paediatric study, MR images originated from patients undergoing investigations due to a medical need and thus the impact of potential underlying diseases could impact colonic physiology and hence perturb the results [466]. Exclusion criteria were pre-defined with the aim to collect datasets from a healthy cohort[24]. The subsequent diagnosis was unknown and therefore these datasets could belong to healthy participants or patients with illness. MRI studies on paediatric populations children already concluded that constipated children have a larger colonic volume[472] and a longer whole gut transit time[487] compared to healthy participants. To highlight this in this study, the dataset originating from a fasted 5 year old male participant of 12.8 kg with the most fluid (which was present in a single pocket volume of 249.6 mL that spanned the entire colon) did not align with the other datapoints (within the same category). The paediatric radiologists assisting in the analysis hypothesised this patient had diarrhoea based on the MR images. However, such high volumes should not be

used for colonic dissolution testing as they could overpredict drug dissolution[469]. A meta-analysis found that 20% of paediatric subjects with abdominal complaints had increased extra-intestinal free fluid, so increased water retention in the colon cannot be excluded[488]. The fluid volumes in this study on the paediatric colon demonstrated a higher inter-individual variability than the adult population, where diet and fed state were controlled[26, 345, 374].

Additionally, collection of the MR images and thus the data regarding luminal fluid in the paediatric colon were a snapshot recording, recorded during routine clinical care. As with many factors in the GIT, luminal fluids in the colon are not stationary values but dynamic[489], with factors such as ileo-caecal transit times, colon secretions, presence of stimulators etc. Although studies exist that *via* MRI quantified changes in the intestinal tract (mobility, luminal fluid, tract volume)[489, 490], the current study did not record MR images on multiple time points. Even though the MRI acquisition took place via two dissimilar protocols, no effect of fed state was observed in the data. To fully exclude potential bias in protocol discrepancies, exact matching protocols at multiple sites should be employed. To even further increase the robustness of data, this preliminary study should be repeated on a larger, well-defined cohort in a more strictly environment.

4.5.6 Study strengths

This pioneering study quantified the free fluid in the paediatric colon, which is of great interest to the pharmaceutical industry[371] for paediatric drug development as clinical studies in the paediatric population often face ethical restrictions[66, 347]. Although most data currently available for *in silico* models are derived from healthy Caucasian adults, accurate physiological data derived from the intended patient population are more appropriate for

biorelevant modelling[60, 491], e.g. to account for an altered GIT physiology due to disease or age[2]. For the first time, *in vitro* and *in silico* models can be developed tailored to the paediatric cohort[2, 347] that are informed by real-world data on the volume of fluid (mean, median, extreme values and variability) within the paediatric colon.

As such, existing assays that estimate drug performance in the paediatric colon could be updated with these novel data on CFV, where the extent of alterations in the results can demonstrate the importance of accurate physiological parameters (see also Chapter 5). With these new CFV data, predictive tools for paediatric drug development can increase their relevance and predictive power to the *in vivo* fate of drug formulations.

4.6 Conclusions

This study successfully quantified the fluid volumes within the paediatric colon. Two methods were employed to quantify fluid in MRI datasets and their robustness was demonstrated via cross-analysis between operators and methods.

The small overall sample size and even smaller sub-population sizes meant that these data are preliminary, and a larger cohort study is required to verify the findings presented here. The median fluid volume for the total paediatric colon (0.8 mL) is comparable to literature data for the adult colon, although the mean paediatric volume (22.48 ± 41.30 mL) is nearly double than the adult value standardly used, i. e., 13 mL. The high variability was also observed in adults. No overall correlation was detected between colonic fluid volumes and age, similar to results in the paediatric SI. Fed state, sex or age across the whole population did not influence the colon fluid volumes. The fact that a significant correlation was observed in the 2–5 years group (who were all fasted) between age and fluid volumes in the entire and ascending colon warrants further investigation. No such correlation was observed for other age groups. Furthermore, the ascending colon contained the most fluid compared with the transverse and descending colon. This study demonstrates the feasibility of obtaining real-world data from MRI to inform physiologically based models.

The novel output from this study will improve the physiological understanding of the paediatric colon, aid biopredictive *in silico* simulations (Chapter 5) and establishing novel, more accurate *in vitro* assays and thus support paediatric drug development that targets the colon, resulting in more age-appropriate medicines for the paediatric population[492, 493].

5 CHAPTER FIVE

PBPK MODELLING TO SIMULATE THE IMPACT OF COLONIC FLUID VOLUME ON ABSORPTION OF AN XR FORMULATION OF QUETIAPINE IN PAEDIATRICS

5.1 Introduction

5.1.1 Quetiapine and schizophrenia

5.1.1.1 Quetiapine as treatment of schizophrenia

Quetiapine is an atypical antipsychotic drug, classified as a BCS class II compound (indicating a low solubility but good permeability). It is a dopamine D2-antagonist[494]. Quetiapine is not licensed for use in children in Europe (by the EMA), whereas it is licensed for use to treat schizophrenia and bipolar disorder for ages 13-17 year by the US FDA[494]. However, it is used under expert supervision for the treatment for schizophrenia and bipolar disorder in ages 12-17 in the United Kingdom (UK)[404].

The drug is commercially available as an IR and XR formulation, in varying dose strengths. PK studies using the IR formulation in paediatric patients (10-17 years old) show this cohort exhibits a similar PK profile compared to adults, so there are no dose adjustment recommendations for the IR formulation in this age range[494, 495]. However, studies using IR quetiapine to assess the efficacy and tolerability in treatment of bipolar disorder used a dosage scheme based on body weight for very young patients (4-6 year old)[496].
The XR quetiapine formulation is developed as a sustained release formulation that releases its drug gradually over time, rather than specifically targeting the colon[359]. The XR formulation is only used for the treatment of schizophrenia, with an initial dose of 50 mg OD and dose titration in steps of 50 mg until the desired effect is obtained[404]. Available XR dosage strengths in the United Kingdom are: 50 mg, 150 mg, 200 mg, 300 mg, 400 mg and 600 mg[404]. A usual paediatric XR dose is 400-800 mg once daily, with a maximum of 800 mg per day. Schizophrenic paediatric patients suffer from an increased weight[497, 498], but there are no recommendations for dose adjustment based on weight. Suitability of the dose

strength is monitored *via* e.g. occurrence of schizophrenic episodes and the Positive and Negative Syndrome Scale (PANNS) score versus tolerability of the dose[494]. Data on the use of quetiapine in a paediatric population is scarce, with no publicly available clinically observed data regarding the PK profile of the XR formulation. Literature advocates establishing a therapeutic plasma concentration reference range of quetiapine for paediatric use[499].

5.1.1.2 Physiological changes due to schizophrenia and antipsychotics

Although physiological changes in adolescent patients suffering from schizophrenia have been described (increased body weight, reduced high density lipoprotein (HDL) cholesterol level and raised triglyceride levels[497]), there is no evidence in literature to suggest the disorder is associated with increased intestinal luminal fluid.

Common side effects of atypical antipsychotics include constipation (due to their anticholinergic effect)[500, 501], reduced GIT motility, nausea and diarrhoea[502]. However, these side-effects are mainly described to clozapine and olanzapine, and less to quetiapine [503]

Recent literature suggests data on adverse events for quetiapine is currently sparse and systematic evaluation should be conducted[494].

An open-label study using quetiapine in preschool (4-6 years) and school-age children (6-15 years) found that body weight, pulse and blood pressure were raised significantly after 8 weeks of treatment with IR quetiapine[496], which was also observed in a second study observing 9-16 year olds[498]. High density lipoprotein (HDL) cholesterol and triglyceride levels were not monitored in the preschool cohort; no effect was observed in the school-age group. Moderate GI disturbance was a prevalent adverse effect in both groups.

5.1.2 Paediatric PBPK model of XR quetiapine

As part of a bridging study in a regulatory submission to the FDA, a quetiapine P-PBPK workspace was developed and published by Johnson *et al*., 2015[66]. The aim of the model was to simulate the exposure of an XR quetiapine formulation in children (10-17 years old) to aid with dosing design, without performing a clinical trial in this population. More specifically, this model investigated the gut bioavailability as quetiapine is predominantly metabolised by CYP3A4. This enzyme is highly expressed in the enterocytes lining the small intestinal tract, with minimal expression in the colon[125]. Therefore, for an XR formulation (compared to an IR formulation) the fraction escaping gut metabolism is greater, with an increased bioavailability as consequence.

The quetiapine PBPK model was built *via* a middle-out[67] "learn-and-confirm" approach[64], where a first set of simulations are used to verify model inputs or comparison, such as recovery of observed clinical PK plasma concentration time profiles, and a second set of simulations to predict the PK profile of XR formulations in the paediatric population.
The different input information is listed below (the purpose of inclusion of the respective component into the model is indicated in italics):

- *In vitro* quetiapine data (including pH-dependent solubility)[504, 505] – *to establish the drug compound*;
- Clinical data on the IR formulation in healthy adults and patients (including enzyme inhibition and drug-drug interaction studies)[506] – *to validate the quetiapine drug file*;
- Clinical data on three different (a slow, normal and fast) XR formulations in healthy adults and patients[507, 508] – *to reflect the adaptations to the formulation design compared to IR formulation*;

- Clinical data on the IR formulation in paediatric patients ages 10-17 year[506] – *to validate the drug file in the paediatric cohort.*

There was no clinical data available to which the observed simulations for the XR formulation in the paediatric population could be compared to. Integrating these data resulted into a PBPK model that allowed for qualitative prediction of the PK profile of an XR quetiapine formulation in a paediatric population. Nearly half of the 300 mg XR dose (49%) was absorbed beyond the small intestinal transit time (i.e. 3.3 h). This PBPK model was approved by the FDA. The drug-specific quetiapine input parameters from the original publication are listed in **Table 5.1**.

Table 5.1. *Quetiapine drug parameters values for PBPK simulations.*

Drug parameter	Value
Molecular weight (g/mol)	382.530
Log P	2.900
Compound type	Diprotic base
pKa 1	3.46
pKa 2	6.93
Blood to plasma ratio (B:P)	1.2682
Haematocrit value	45.000%
Fraction unbound in plasma (f_u)	0.170
Absorption model	ADAM[68]
Regional Permeability ($P_{eff,man}$) (10^{-4} cm/s)	Small intestine (duodenum → ileum IV): 5.1523 Colon: 2[a]
Distribution model	Full PBPK model
Distribution volume (V_{ss}) (L/kg)	4.1802
Elimination	Enzyme kinetics, retrograde model
CL_{po} (L/h)	65 - 138
***CLu_{int}*[b] CYP3A4** (µL/min/pmol isoform)	1.34
Fraction metabolised by CYP3A4 (f_m)	95%
***CLu_{int}* CYP2C9** (µL/min/pmol isoform)	0.106
Fraction metabolised by CYP2C9 (f_m) (%)	4%
***CLu_{int}* CYP2D6** (µL/min/pmol isoform)	0.242
Fraction metabolised by CYP2D6 (f_m) (%)	1%
CL_R (L/h)	0.13
Intrinsic Solubility (mg/mL)	0.43

[a]: optimisation of the colonic permeability input was discussed extensively in the original publication by Johnson et al.[66]; [b]: CLuint: hepatic intrinsic clearance.

The drug compound was set up using a full PBPK model (i.e. a detailed description of drug distribution throughout mathematical compartments representing various organs and tissues). The pharmaceutical phase and absorption phase were described using the ADAM-model[68] (see also section 1.2.3.2), to allow for incorporation of release from the XR formulation within the model.

The release from the IR and XR formulation for quetiapine were integrated into the simulator as follows:

- Immediate release: the IR formulation of quetiapine was set up *via* the diffusion layer model (DLM), incorporating drug particle size, concentration and solubility parameters to model diffusion *via* Fick's law[509, 510] (**Table 5.2**).

Table 5.2. *Input parameters for the IR formulation in the PBPK model.*

Formulation type	Solid formulation
Release model for the IR formulation:	Diffusion Layer Model
Intrinsic Solubility (S_0) (mg/mL)	0.43
User-defined solubility pH profile	Figure 5.1

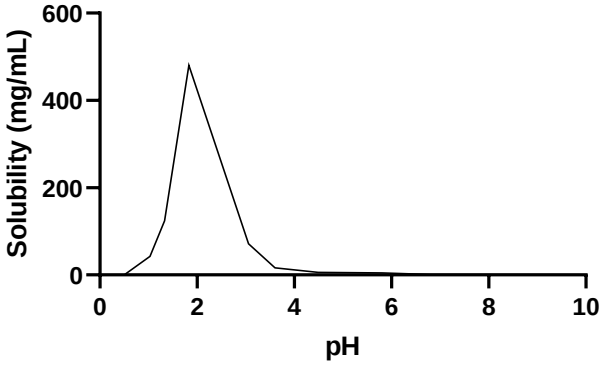

Figure 5.1. *User-defined pH-dependent solubility profile for quetiapine in the PBPK model.*

- Extended release: the XR formulation of quetiapine was set up as a monolithic system, with the release profile derived from discreet *in vitro* dissolution timepoints[508] (**Figure 5.2**). Only drug that is released from the formulation is available for dissolution and absorption within the model, *via* the DLM.

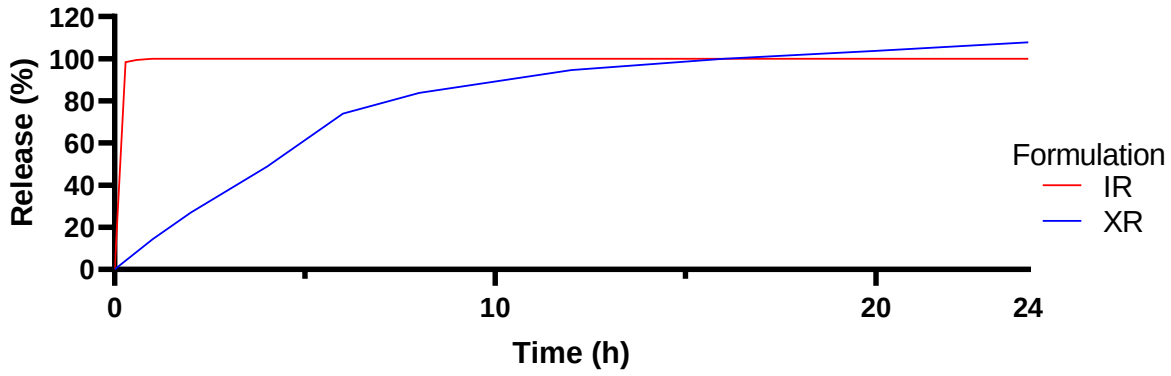

Figure 5.2. *Monolithic system release profile for the XR formulation of quetiapine in the PBPK model.*

The Simcyp default North European-Caucasian adult and standard paediatric population were used as study populations. The trial design, describing the dosing regimen and number of participants, was different between the twice daily IR-formulation and the once-daily XR formulation. The IR model was set up as a twice-daily (τ = 12 h) 400 mg IR dose, for 5 consecutive days (10 doses in total), co-administered with 100 mL water in the fasted state. The trial was run for 7 days, so the terminal phase of elimination was captured within the model as well. The XR original model set up as a once-daily 300 mg XR dose, for 5 consecutive days (5 doses in total) , co-administered with 100 mL water in fasted state. The trial was run for 7 days, so the terminal phase of elimination was captured within the model as well. Both the IR and XR model used 1 trial of 13 participants (1x13).

Similar to the IR formulation, the P-PBPK model suggests a similar exposure in paediatrics and adults after a once daily XR dose[66, 494]. However, the virtual colon in this simulation is not necessarily representative of the paediatric large intestine. The original PBPK model by Johnson *et al*.[66] used a default value of 13 mL for CFVs (CV 4.4%) in both the adult and paediatric population. This volume was based on reported adult values[26]. However, as

detailed in Chapter 4, the reported CFV in an adult cohort are not representative for a paediatric population[26] (**Table 5.3**).

Table 5.3. *Colonic fluid volumes (CFV) in an adult and paediatric cohort based on Magnetic Resonance Imaging fluid analysis.*

Population	Mean (SD) (mL)	Median (min-max) (mL)	Reference
Adults (fasted)	13 (12)	8 (1-44)	Schiller 2005[26]
Children (mix of fed and fasted)	28.48 (41.30)	0.8 (0-167.47)	Goelen 2021[25]

Therefore, the PK profile of an XR formulation in a paediatric patient might be different than currently assumed. This could be especially true for the BCS class II drug quetiapine, as its low solubility means the available amount of water could greatly impact the drug dissolution thus bioavailability. It is already proven that for BCS class II drugs celecoxib[375], sulindac[376] and dexloxiglumide[511], the amount and distribution of fluid in the colon impact the dissolution and absorption of XR products in the colon[469].

With the novel data on paediatric colonic fluid volumes (reported in Chapter 4), its influence on the absorption of an XR quetiapine formulation in this cohort can be investigated *via* PBPK modelling. Subsequently, this would make the current P-PBPK model for XR quetiapine more paediatrically relevant

5.2 Aim and objectives

The overarching aim of this project is to simulate the influence of CFVs on the PK profile of quetiapine in a paediatric cohort (10 – 17 year old) *via* PBPK modelling.

The objectives of this study are:

- To determine if the existing adult PBPK models[66] for the IR and XR formulations of quetiapine (as both these models are built on clinical data) are influenced by CFVs using an automated local sensitivity assay (LSA).
- To determine if the paediatric PBPK model for the XR formulation of quetiapine is influenced by CFVs, using an automated LSA.
- To determine to what extent the PK profile of quetiapine changes when entering subject-specific true data (age, sex, height, weight, CFV) and what the implications of any alterations are on drug exposure.

5.3 Methods

5.3.1 Existing model

The existing PBPK model predicting ADME processes for quetiapine as reported by Johnson *et al*. was used[66]. The original quetiapine model was built in Simcyp version 15, then upgraded and checked for compatibility with Simcyp version 21 (i.e. verifying all inputs match between both versions), which was used for this work.

In order to investigate the influence of colonic fluid volumes absorption profile of an XR formulation rather than studying the clinical efficacy or steady-state concentration levels of quetiapine, following adaptations were made to the original model in this study. Firstly, the trial design was altered to a single OD administration of the XR formulation (with 100 mL water in fasted state), with a total trial run for 36 h. Shortening the trial time and only looking at one dosing event reduces the complexity in the resulting simulations.
In addition, the number of trials and participants was changed to 100x1 (trials x participants) to minimise biological variability, as most parameters in Simcyp come with an associated variability (Gaussian distribution). Increasing the number of participants thus decreases individual variability and increases the chance of simulating with the population averages.

Secondly, the interpolation between the timepoints for the drug release of the XR formulation was changed from linear to a piecewise cubic polynomial fit, to have a more gradual release and smoother interpolation (**Figure 5.3**). Only the normal (not slow/fast) XR formulation was considered for this work (**Figure 5.2**). The IR formulation was used as previously described (**Table 5.2**). The drug-specific quetiapine input parameters are

unchanged from the original publication and are listed in **Table 5.1**. For the automated LSAs, the default adult and paediatric populations were used.

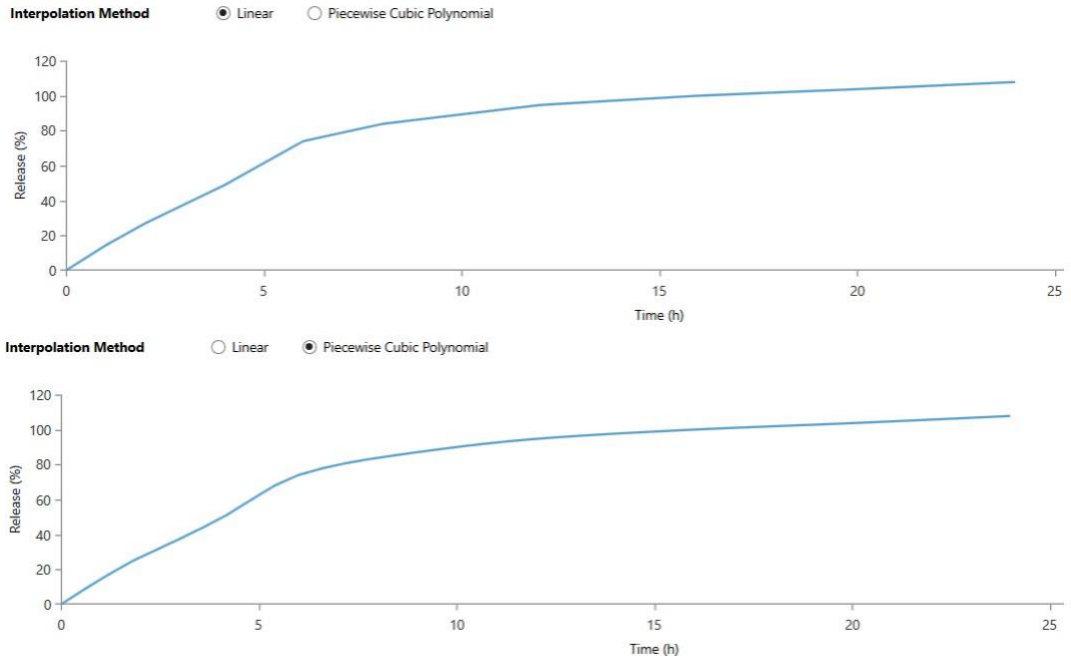

Figure 5.3. *Quetiapine release from the XR formulation was adapted from a linear interpolation to a smoother piecewise cubic polynomial interpolation.*

After implementing these adaptations, simulations with the IR and XR models were performed with a CFV of 13 mL, to identify how much quetiapine is absorbed in each regional fractions of the gut.

5.3.2 Automated Local Sensitivity Analyses

To investigate the influence of the CFV on the IR adult, XR adult and XR paediatric model outputs, automated LSAs were used. For this, the built-in LSA module of Simcyp was used. Parameters under scrutiny to indicate sensitivity were common PK parameters: the plasma concentration time profile (C_p), the AUC, the highest concentration observed in the plasma concentration time profile and the time point for this maximum concentration (C_{max} and T_{max}) and the fraction absorbed (F_a).

The trials in the automated LSAs ran for 6 days, with 5 days dosing events taking place: either 400 mg IR quetiapine was administered (τ = 12 h, a total of 10 doses), or 300 mg XR quetiapine OD (τ = 24 h, a total of 5 doses). The PBPK model predicted the C_p profile for an additional 24 h, to capture the elimination phase (144 h in total). The automated LSAs were ran with a linearly spaced uniform 10-step size in CFV from 1.00 mL (lower limit) to 130.00 mL (upper limit) (series being: 1.00, 15.33, 29.67, 44.00, 58.33, 72.67, 87.00, 101.33, 115.67 and 130.00).

5.3.3 Personalised trials with real CFV data

5.3.3.1 Participant selection and data

To determine how the PK profile of quetiapine changes when entering subject-specific physiological parameters (age, sex, height, weight, CFV), observed data was integrated into the simulator. The CFV data was derived from paediatric patients who underwent MRI of the abdomen for clinical reasons, as mentioned in Chapter 4. Informed Consent was obtained for all participants. These MRI datasets were then analysed *via* different *2D*- and *3D*-based software protocols to extract data on the free flowing fluid within the paediatric colon.

Subjects were eligible for inclusion in this modelling study if:

- subjects were between 10-17 years of age (as this is the age range for which there is clinical IR data in the paediatric cohort, so the model is validated within this age group);

- subjects had a CFV of at least 0.5 mL (as 1.00 mL is the lowest value the simulator accepts for colonic fluid volume).

Based on the age restriction and minimal CFV inclusion criteria, 12 paediatric participants from the MRI CFV study (Chapter 4) were eligible for inclusion in this modelling study. The age restriction was fulfilled by 19 subjects; 12 of these had a CFV ≥0.5 mL (**Figure 5.4**). These 12 patients all belonged to the fluid-fed cohort in the MRI study.

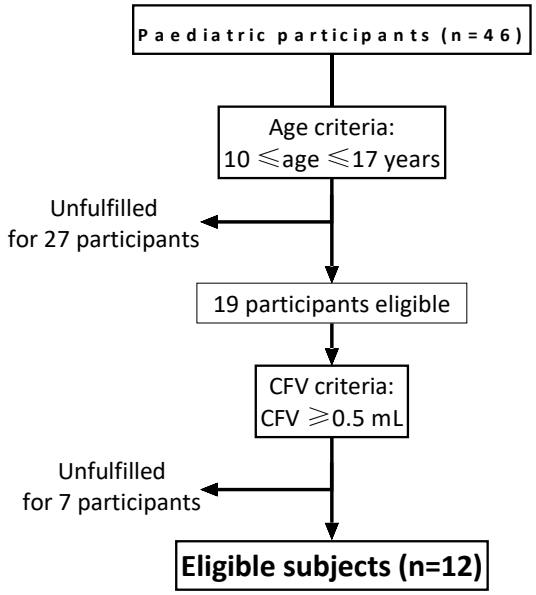

Figure 5.4. *Twelve subjects passed both eligibility criteria.*

The participant data from the MRI CFV study (listed in **Table 5.4**) were loaded into the PBPK model individually per simulation. The model was run in a 100 trial x 1 subject set-up for each of the 12 individuals.

Table 5.4. *Participant metadata and CFVs loaded into the PBPK model individually per simulation*

ID	Age (years)	Sex[a]	Weight (kg)	Height (cm)[b]	Colonic Fluid Volume (mL)
1	10	F	32.6	138	92.21
2	12	F	33.5	150	6.12
3	12	F	33.5	150	14.24
4	13	M	52.7	154.5	167.47
5	14	F	54	159.5	2.07
6	15	F	65	162	11.22
7	15	F	55	162	152.94
8	16	M	54.4	173	0.53
9	16	M	102	173	0.58
10	16	M	56	173	6.16
11	16	F	65	163	43.20
12	16	F	59	163	60.01

[a]: F denotes female, M denotes male; [b]: height taken from national UK growth charts.

The subject-specific CFVs with associated demographic data were entered into the simulator for every single participant as follows:

- Age and sex were fixed in the trial design, where criteria for selection of virtual subjects from the study population are set out.
- Height and weight were fixed within the population description, using the Lua-coding available in the simulator. However, there was no height data available for the subjects included in the MRI study. This was addressed by using the average predicted height (50th percentile) for a specific age and sex reported on the UK national growth charts by the Royal College of Paediatrics and Child Health (RCPCH)[512].
- The CFV was entered in the GI-section of the population characteristics. For eligible patients with a CFV smaller than 1 mL, the value was rounded up to 1 mL.

5.3.3.2 Manual local sensitivity analysis of CFV influence on PK profile in a single participant

To investigate the influence of various CFV on the PK profile of one single participant, a manual LSA was used. For this, the CFV entry in the GI-section of the population file was manually varied between 0-130 mL. PK parameters under scrutiny to signal sensitivity of the model towards CFV include C_p, AUC, C_{max} and T_{max} and F_a.

Modelling of a 0 mL CFV was done by using 1 mL as CFV input (the minimal value), changing the colon regional permeability ($P_{eff,man}$) from 2 x 10^{-4} cm/s to 0.0001 x 10^{-4} cm/s (the minimal value) and changing the absorption rate scalar for the colon from 1 (default) to 0.001 (the minimal value).

5.3.3.3 Comparison of simulated PK from the default CFV vs a measured CFV in paediatric subjects

Simulations for every individual between the default CFV versus the measured data were compared. The model where the metadata is filled in for a specific participant, but the default CFV is still used (13 mL, CV 4.4%), is labelled “default model”. The model where the metadata and the CFV are adapted to a specific participant is labelled “personalised trial”.

5.3.4 Statistical analysis

GraphPad Prism version 9.3.1 was used for statistical analysis. Unpaired t-tests were used to compare the F_a and F_g outputs from the automated LSA adults and paediatrics. Paired t-tests were used to compare the AUC and C_{max} between the default and personalised simulations. Pearson’s correlation tests were used to investigate correlation between the CFV and AUC or C_{max} in the personalised simulations.

5.4 Results

5.4.1 Existing model

A few adaptations were implemented on the published model. Then, simulations on adult were performed for both the IR and XR model, using a CFV of 13 mL, to verify the input of the formulation parameters. How the absorption of quetiapine is spread along the GIT using both formulations is given in **Figure 5.5**.

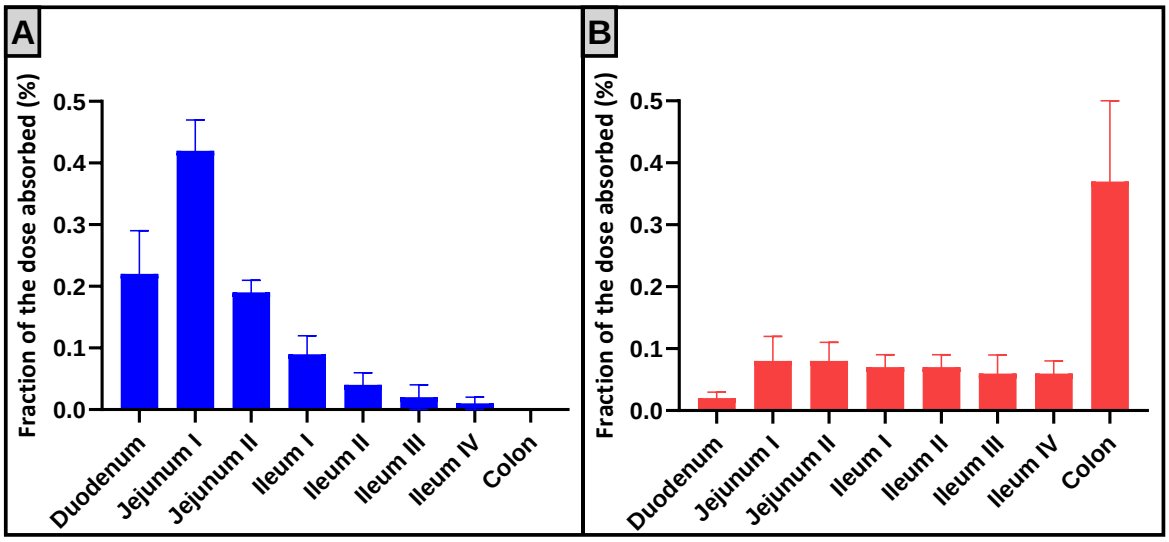

Figure 5.5. *Fraction of the dose absorbed in the different segments of the GIT for (A) the IR and (B) the XR quetiapine formulation.*

5.4.2 Automated Local Sensitivity Analyses

5.4.2.1 Sensitivity to CFV in adult PBPK model

An automated LSA was performed in the adult PBPK model for both the IR and XR formulation, to determine if the PK profile of quetiapine is influenced by the CFV. In the adult IR model, no influence of the PK profile towards CFV was detected (**Figure 5.6**), as shown by the absence of influence on the C_p profile, C_{max}, T_{max} or the AUC. The F_a remained constant over the range of volumes at 0.993, with a constant F_g of 0.758.

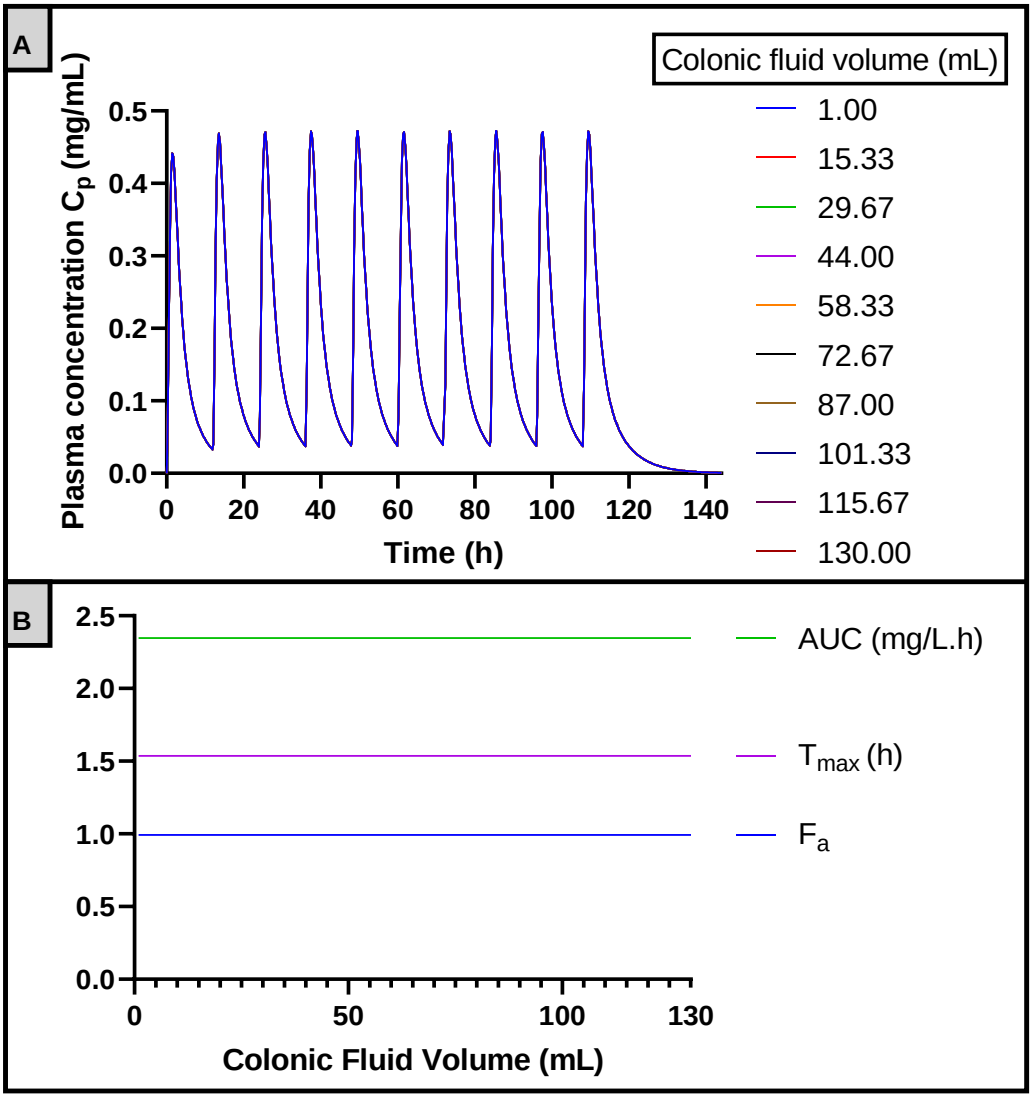

Figure 5.6. *Automated Local Sensitivity Analysis of common PK parameters (A) C_p and (B) F_a, T_{max}, AUC to the colonic fluid volume in the IR quetiapine adult PBPK model.*

In the adult XR model, sensitivity of the PK profile towards CFV was detected in all PK parameters under investigation (C_p, AUC, C_{max} and T_{max} and F_a) (**Figure 5.7**).

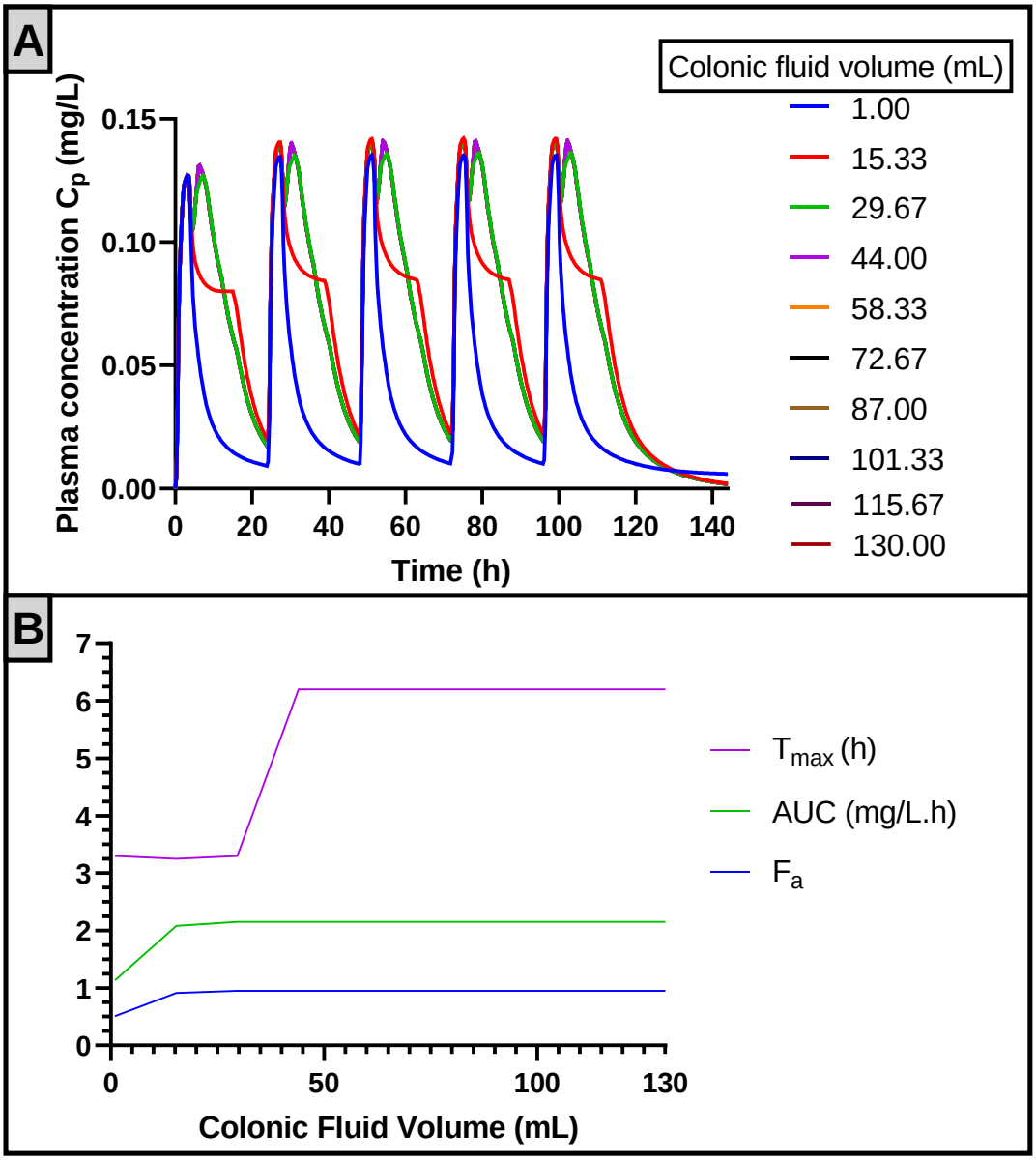

Figure 5.7. *Automated Local Sensitivity Analysis of common PK parameters (A) C_p and (B) F_a, T_{max}, AUC to the colonic fluid volume in the XR quetiapine adult PBPK model.*

Examination of the plasma concentration-time profile reveals two peaks in plasma concentration:

- The first peak is representative of the small intestinal absorption phase. This absorption window is not influenced by the CFV.
- The second peak is representative of the colonic absorption phase.

The C_{max} for the small intestinal absorption phase does not change, the C_{max} for the colonic absorption window (2nd peak) increases up to 0.141 mg/L for a CFV of 29.67 mL. The T_{max} is either 3.3 h (if the small intestinal C_{max} is greater) or 6.2 h (if the colonic C_{max} is greater). The model shows a clear sensitivity in PK profiles with increasing CFV, up to a CFV ≤29.67 mL, after which no considerable effect of increasing CFV can be observed anymore. The F_a increased from 0.508 to 0.950 as the CFV increased (**Table 5.5**).

Table 5.5. *The fraction absorbed (F_a) and gut bioavailability (F_g) from the automated LSA in the adult XR quetiapine PBPK model.*

Colonic Fluid Volume (mL)	F_a (%)	F_g (%)
1.00	50.82	83.23
15.33	91.07	89.75
29.67	94.92	90.09
44.00	95.02	90.09
58.33	95.02	90.09
72.67	95.02	90.09
87.00	95.02	90.09
101.33	95.02	90.09
115.67	95.02	90.09
130.00	95.02	90.09

5.4.2.2 Sensitivity to CFV in paediatric model

The influence of CFV on the PK profile of quetiapine was investigated in the paediatric PBPK model for the XR formulation *via* automated LSA. No LSA was performed in the paediatric IR model, as no influence on the C_p profile is expected here, which is demonstrated by the absence of an effect in the adult IR model. In the paediatric XR model, sensitivity of the PK profile towards CFV was detected in all PK parameters under investigation (C_p, AUC, C_{max} and T_{max} and F_a) (**Figure 5.8**). Similar to the adult XR model, a clear influence of the CFV on the colonic absorption phase was observed (AUC, C_{max}), up to a CFV value ≤29.67 mL. The C_p profile did not change above this threshold. The F_a increased from 0.585 to 0.926 (**Table 5.6**).

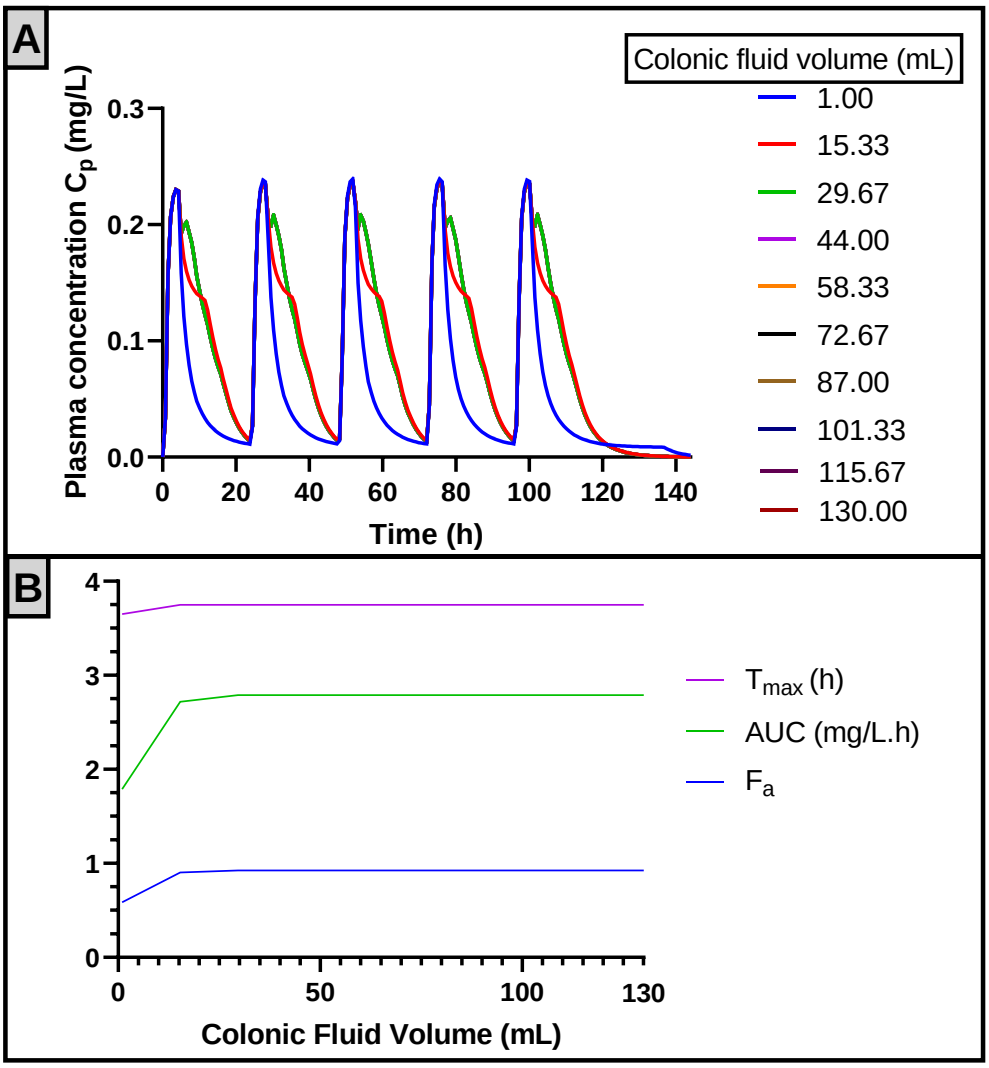

Figure 5.8. *Automated LSA shows the change of common PK parameters (A) C_p and (B) F_a, T_{max}, AUC in the PK profile of an XR formulation of quetiapine in a paediatric cohort with changing CFV.*

Table 5.6. *The fraction absorbed (F_a) and gut bioavailability (F_g) from the automated LSA in the paediatric XR quetiapine PBPK model.*

Colonic Fluid Volume (mL)	F_a (%)	F_g (%)
1.00	58.51	85.27
15.33	90.28	89.98
29.67	92.62	90.20
44.00	92.62	90.20
58.33	92.62	90.20
72.67	92.62	90.20
87.00	92.62	90.20
101.33	92.62	90.20
115.67	92.62	90.20
130.00	92.62	90.20

Although the plasma time concentration responses to increasing CFV look similar between the adult and paediatric cohort, some differences can be observed (**Figure 5.9**).

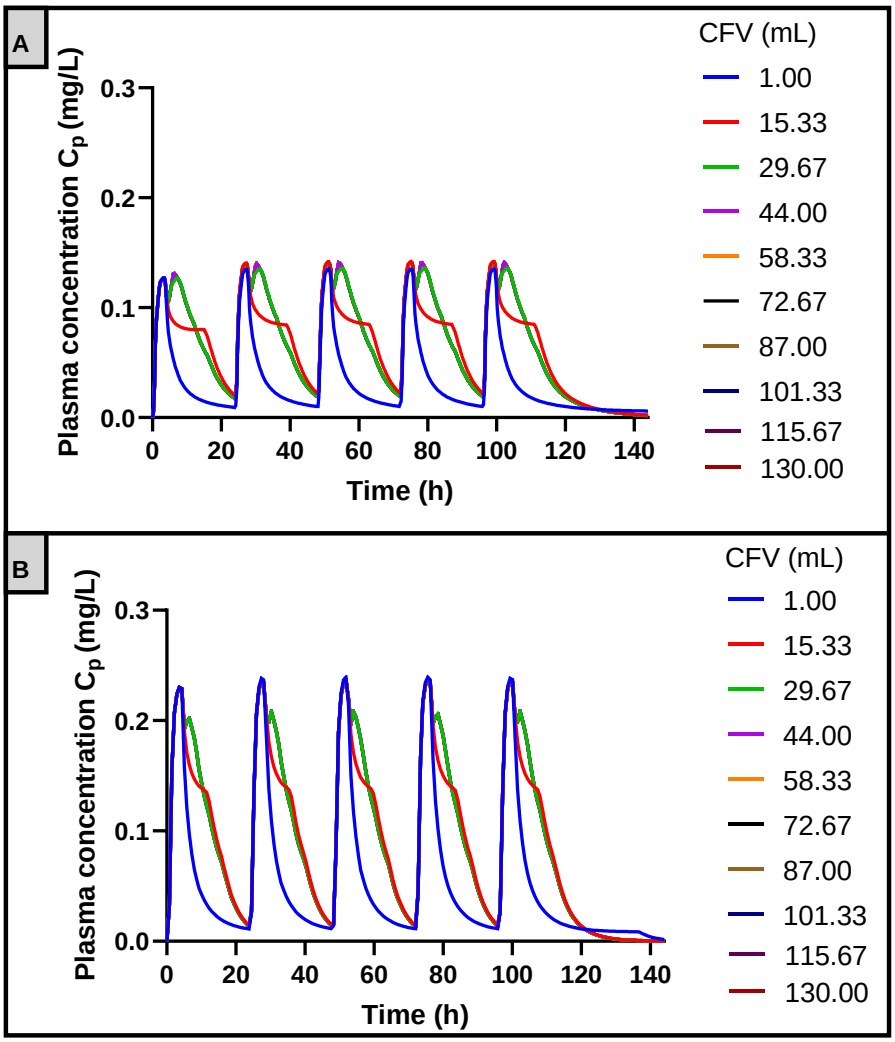

Figure 5.9. *Automated LSA shows the change in the PK profile of an XR formulation of quetiapine in an (A) adult and (B) paediatric cohort with changing CFV.*

Firstly, the peak attributed to the colonic absorption phase is smaller than the small intestinal absorption phase in the paediatric cohort, where these are of similar magnitude in the adult cohort. Secondly, the C_{max} and AUC are around 50% higher in the paediatric cohort (0.237 mg/L and 2.789 mg/L.h, respectively) compared to the adult cohort (0.135 mg/L and 2.152 mg/L.h). The F_a and F_g in the adult and paediatric XR models are not statistically significantly different (t-test, $p>0.05$ in both cases).

5.4.3 Personalised trials with physiological CFV data

5.4.3.1 Manual local sensitivity analysis of CFV influence on PK profile in a single participant

The influence of CFV on the PK profile of an XR formulation of quetiapine was investigated in an individual participant (participant 12 (**Table 5.4**): 16 year old girl, 59 kg, 163 cm) where the colonic fluid volume was varied from 0 mL to 100 mL (**Figure 5.10**) whilst all other PBPK inputs were kept the same.

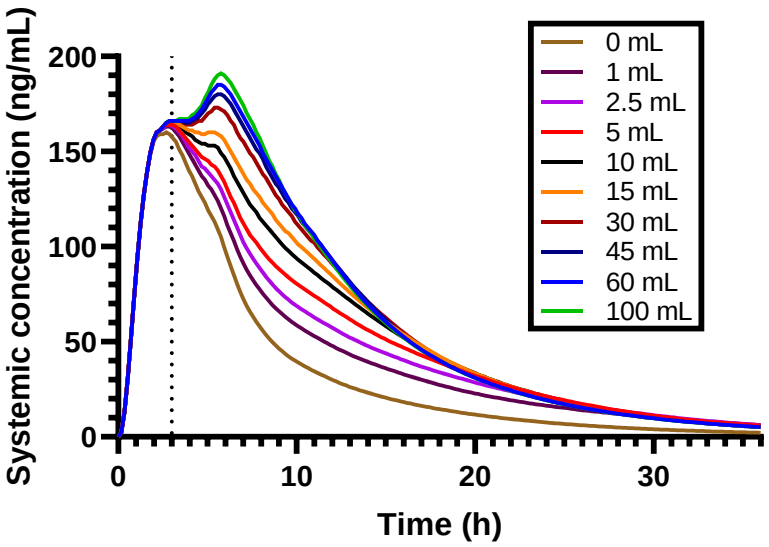

Figure 5.10. *Manual LSA of the plasma profile on of an XR formulation of quetiapine to the colonic fluid volumes in a single paediatric participant (16 year old female, 59 kg, 163 cm). The dashed line shows the onset of the colonic absorption phase.*

Consistent with the previous sensitivity analyses, no difference in the small intestinal absorption phase was detected with changing CFV. The small intestinal absorption contributed 1260 ng/mL.h to the AUC (30% less compared to the AUC absorbed in the SI during the LSA analysis), as evidenced by the model of 0 mL CFV (**Figure 5.11**).

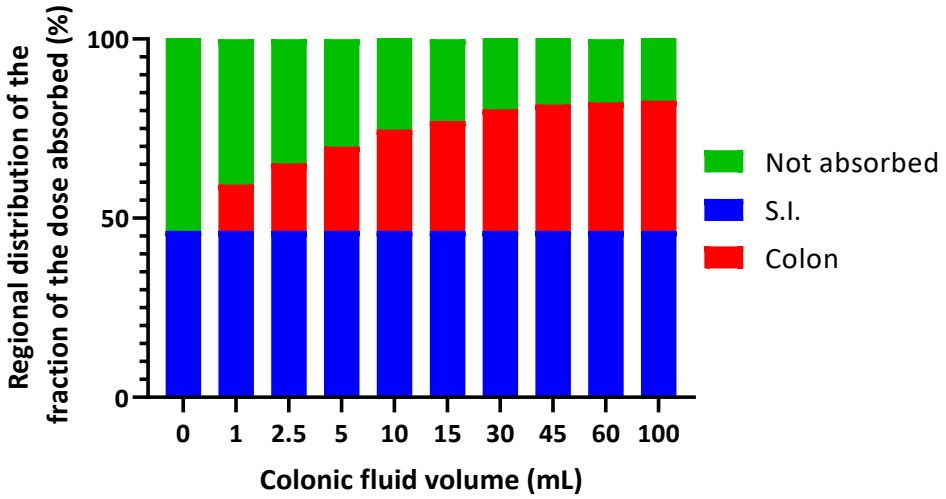

Figure 5.11. *Distribution of the dose absorbed for the small intestine (S.I, blue), colon (red) or not absorbed (green).*

There is a non-linear correlation between the CFV in the model and the amount of drug absorbed in the colonic absorption phase, as observed in both the exposure (AUC) and F_a in the colon (**Figure 5.12**). These correlations have a logarithmic course, indicating that a small change in CFV in the lower range has a higher impact on the AUC and F_a, whereas this effect is less pronounced on the higher CFV range.

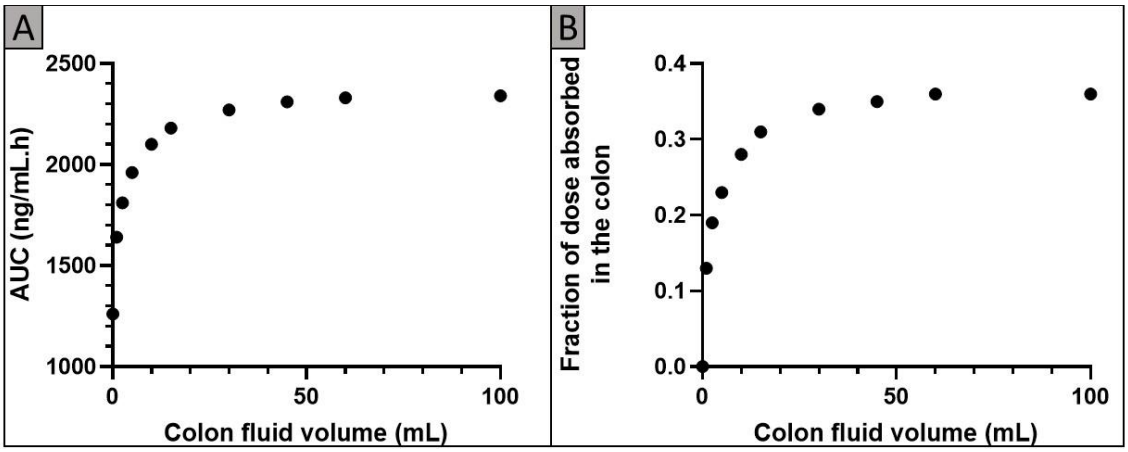

Figure 5.12. *Correlation between the colonic fluid volume and (A) the AUC of the plasma profile, (B) fraction of the dose absorbed in the colon, after administration of an extended release formulation of quetiapine to a single participant (16 year old female, 59 kg, 163 cm).*

5.4.3.2 Comparison of simulated PK from the default CFV vs a measured CFV in paediatric subjects

The results of modelling the default vs the personalised CFV values are shown in **Table 5.7** and **Figure 5.13** below.

Table 5.7. *Personalised to default (PER/DEF) ratios for volume, C_{max} and the AUC of the XR formulation of quetiapine for 12 paediatric participants.*

ID	Age	Personalised CFV (mL)	Volume ratio PER/DEF	C_{max} ratio PER/DEF	AUC ratio PER/DEF
1	10	92.21	7.09	1.13	1.07
2	12	6.12	0.47	0.97	0.94
3	12	14.24	1.10	0.99	1.01
4	14	167.47	12.88	1.16	1.07
5	14	2.08	0.16	0.98	0.84
6	15	11.22	0.86	0.99	0.99
7	15	152.94	11.76	1.15	1.08
8	16	0.53	0.04	0.96	0.77
9	16	0.57	0.04	0.98	0.76
10	16	6.16	0.47	0.97	0.94
11	16	43.20	3.32	1.05	1.08
12	16	60.01	4.62	1.09	1.08

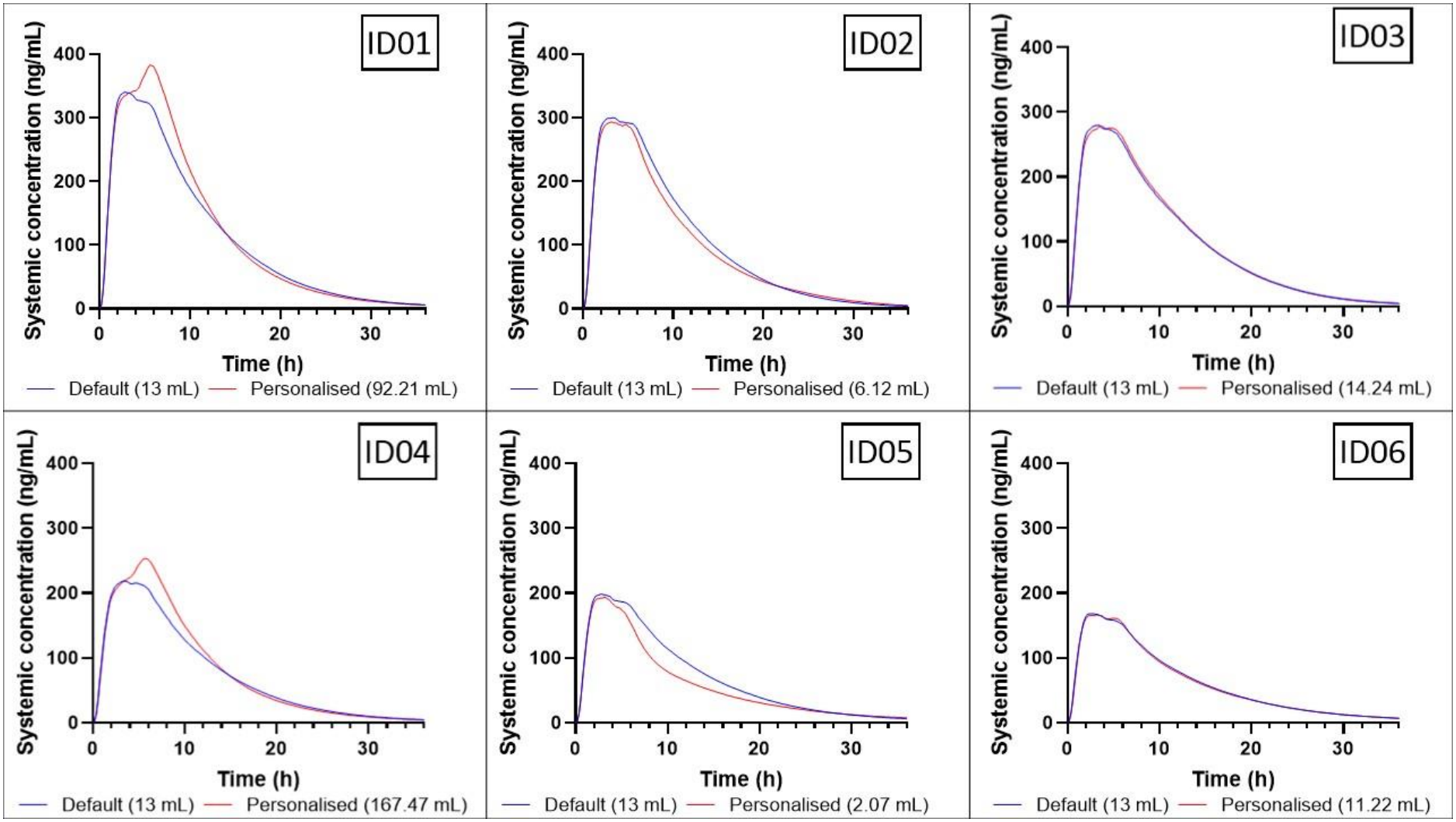

Figure 5.13. *Simulations of the PK profile for XR quetiapine in the default and personalised model for 12 individuals. Metadata on age, weight, sex and height can be found in* ***Table 5.4****.*

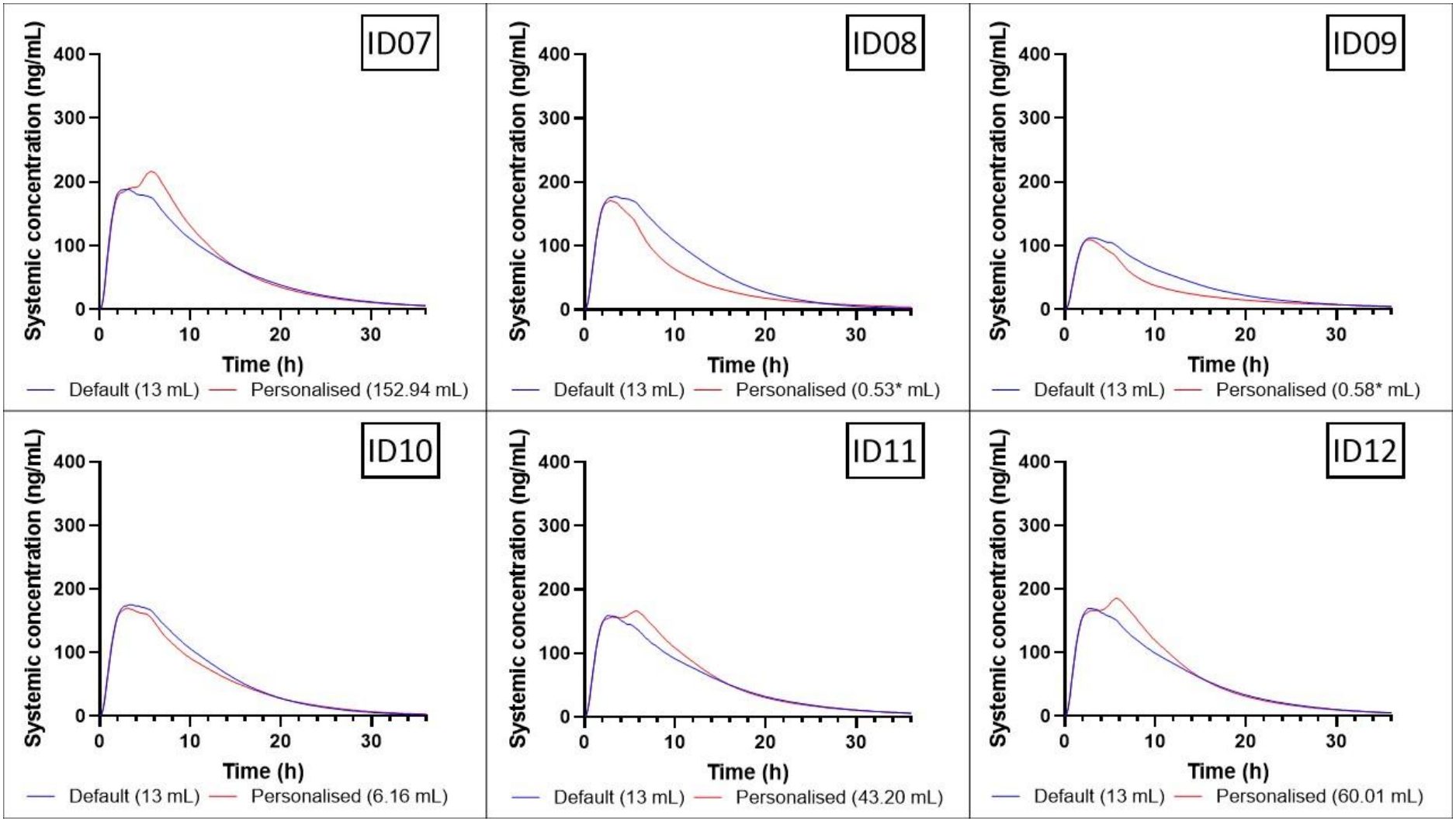

Figure 5.13. *Simulations of the PK profile for XR quetiapine in the default and personalised model for 12 individuals (continued). *: a CFV of 1 mL was used in the Simcyp simulator.*

As observed from the model outputs, the exposure changed relative to the deviation of the personalised CFV from the default value, rather than being influenced by age or height/weight. The volume ratio (personalised/default) is significantly correlated with the predicted C_{max} ratio (Pearson's correlation coefficients 0.96, $p< 0.05$). Similarly, the change in exposure (AUC ratio, personalised/default) is significantly correlated with the volume ratio (personalised/default) (Pearson's correlation coefficients 0.68, $p< 0.05$) with a semi-logarithmic relationship (**Figure 5.14**).

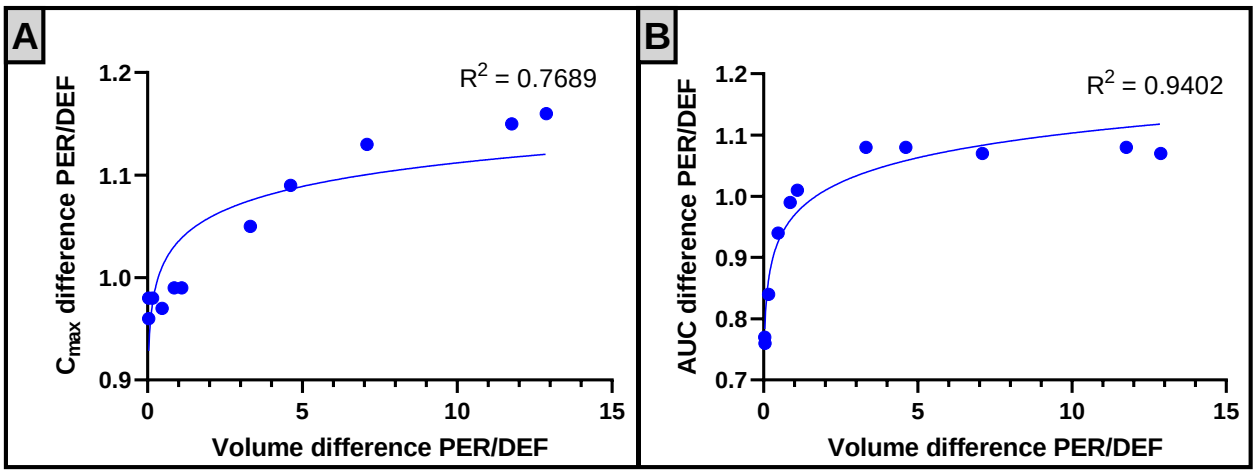

Figure 5.14. *Correlation graph for the volume ratio with the (A) C_{max} and (B)AUC ratio (personalised to default) for 12 paediatric simulations.*

The models for IDs 1, 4, 7, 11 and 12 used a CFV that is at least triple the default value. Similarly, the AUC ratio for the personalised/default model was 1.07-1.08 times higher in the personalised trials, indicating a greater exposure in the personalised trials than with the default values.

Likewise, the models for IDs 5, 8 and 9 showed a lower exposure in the personalised model compared to the default model. The personalised CFV values in these simulations were lower than 2.07 mL with an AUC ratio decreased to 0.76-0.84, indicating up to 24% less exposure in the personalised trial.

A paired t-test demonstrated that the AUC and C_{max} were not significantly different between the default and personalised simulations ($p>0.05$ for both). The difference would also not be considered clinically significant as the AUC ratios are within bioequivalence limits (0.8-1.25)[492].

5.5 Discussion

5.5.1 Automated Local Sensitivity Analyses: suitability of the PBPK model

LSAs were employed to investigate the influence of the CFV on the PK profile of quetiapine in adults. An initial verification step was the absence of any influence by the CFV on the PK profile of quetiapine in the LSA of the adult IR model. As evidenced by the high F_a (0.993) observed in the IR model, nearly the entire IR dose was absorbed during small intestinal transit. This is expected, as an alteration of CFV should not impact proximal absorption profiles.

This was further verified as the PK profile of quetiapine during the LSA on the CFV showed two peaks in the adult XR model. The first peak described the absorption phase in the small intestinal tract, which did not change with altering CFV. The F_a in the small intestine was constant. This absence of influence was expected, as there is no evidence in literature to support the idea that the volume of luminal fluid in the colon affects absorption in the small intestine. The second absorption peak describes the uptake in the colon. A larger colonic absorption peak was observed with an increasing amount of the CFV, up to a value of 29.60 mL, after which the PK profile did not change anymore. Indeed, the adult small intestine absorbed 50.8% of the 300 mg dose, thus 147.6 mg quetiapine is presented to the colon. As quetiapine has a solubility of 4.15 mg/mL around the pH 6.5 (colon) (**Figure 5.1**), the drug should be fully dissolved in this volume of fluid.

LSAs showed that the PK profile in the adult quetiapine XR PBPK model is sensitive to CFV, whereas the IR model did not show any sensitivity (which corroborates the idea an IR formulation is not influenced by the colon). Thus, modelling with paediatric fluid volumes in the paediatric XR model would be logical and relevant.

A similar scenario as the adult model were obtained in the LSA of the CFV on the XR formulation PK profile in the paediatric model. However, it was also observed that the resulting PK profiles for colonic absorption are dissimilar in the LSA for both paediatric and adult cohorts (**Figure 5.9**), which evidences how the LSA takes the dissimilarity between both cohorts into account and justified verification of the sensitivity in the adult model firstly. This discrepancy in drug disposition arises mainly from the difference in body sizes, but also differences in GI residence and transit times. Additionally, the variability in the adult population (where the LSA was carried out in a population representative with age 36 year old) will be smaller than compared to the variability in the paediatric population (where the age population representative was 13.5 year old). Setting the population parameters to cover the age range of interest (10-17 year old) did not change the results from the automated LSA (results not shown). F_a and F_g were not significantly different between the adult and paediatric populations.

5.5.2 Personalised trials with real CFV data

5.5.2.1 Manual sensitivity analysis in a single participant

A manual LSA of the CFV on the PK profile of quetiapine in an XR formulation was carried out on a single participant. As expected, there was no influence of the CFV on small intestinal absorption phase, as evidenced by the overlaying profiles for the first 3 hours after administration representing the small intestinal transit. There was a clear correlation of the amount of drug absorbed in the colon with the luminal colon fluid volume, which unlike the LSA did not result in a complete overlap but rather a plateau being reached.

This could be attributed to the luminal fluid dynamics function within the simulator when using user-defined gut luminal baseline fluid volumes as done in the manual LSA. In contrast with the automated LSA[513], the fluid volumes are treated dynamically here, with an amount of luminal fluid arriving from the foregut being reabsorbed over the gut membrane[513] over time and then passed along to the next section. Hence, the luminal fluid volumes and thus the capability of the drug to dissolve are not static parameters here but dynamic, resulting in the profile as observed in **Figure 5.10**. This correlation between the CFV and the colonic absorption (reflected in the AUC and F_a) was logarithmic, indicating there is a risk of insufficient absorption in the colon when there is limited to no luminal fluid. This could be clinically significant, as the AUC ratio for a colon with CFV = 0 mL compared to CFV = 100 mL is 0.53, which would be outside bioequivalence limits (i.e. 0.8-1.25)[492].

5.5.2.2 Comparison of simulated PK from the default CFV vs a measured CFV in paediatric subjects

Simulations for twelve subjects were performed using subject-specific CFV data and metadata (age, sex, height and weight) (**Figure 5.13**). All personalised simulations were dissimilar from the simulations with the default colonic fluid volume in Simcyp, as evidenced by the change in AUC ratio (personalised/default) and C_{max} ratio (personalised/default) (**Table 5.7**).

The simulations for five subjects (ID 01, 04, 07, 11 and 12) gave an AUC ratio (personalised/default) of at least 1.07 (**Table 5.7**), meaning these subjects absorbed more quetiapine than what simulations predicted using the default CFV value. The input CFV ranged from 43.20 mL to 167.47 mL, so at least three times the default input. However, the

AUC ratio are within bioequivalence acceptance criteria (i.e. 0.80 – 1.25)[492], meaning this would be likely to not be clinically significant regarding the benefit:risk ratio. Similarly, the AUC and C_{max} were not significantly different between the default and personalised simulations ($p>0.05$ for both).

As such, these results suggest caution should be taken when the subject has diarrhoea, as this increases the luminal fluid in the colon and thus results in a higher fraction of the dose being absorbed. However, this extra amount absorbed effect is unlikely to be clinically significant as demonstrated by the AUC ratio and thus there is minimal risk of overdosing. Quetiapine overdosing is marked by hypotension, QT-prolongation, tachycardia and somnolence[514] but is not necessarily fatal. With the right symptomatic treatment, most (but not all) patients with an overdose of quetiapine are recorded to have recovered[515], even a patient with an overdose of 20,000 mg[514].

In contrast, a lower exposure was observed in the personalised trials for three subjects (ID 05, 08 and 09; **Figure 5.13**) when there is little amount of luminal fluid in the colon. For these three subjects, the CFV were 2.08 mL, 0.53 mL and 0.57 mL with an AUC ratio (personalised/default) of 0.84, 0.77 and 0.76 respectively, the latter two being out the bioequivalence acceptance criteria. Although this lower AUC ratio was only observed for three of the twelve participants, they actually represent the majority of the paediatric subjects, as 26 subjects in the MRI study (Chapter 4) had a CFV of <3 mL. In addition, the median CFV in the paediatric colon was 0.80 mL, hence these results suggest the majority of paediatric subjects are at risk for underexposure to the antipsychotic drug and having ineffective therapy.

Quetiapine is gradually titrated up to a working dose[494]. In the XR formulation, a fraction of the dose is already absorbed in the small intestine, which might already be sufficient for treatment. As the dosage strength is increased, a greater amount of the drug is presented to the colon, where variability in the CFV may dissolve a different amount of the drug. Increasing the dose strength of the XR drug may not be linear with absorption and pharmacodynamics, thus caution should be exercised. In the case the CFV is consistently low, a twice-daily IR dosage might be more opportune to prevent underdosing and a schizophrenic episode.

5.5.3 Performance of the PBPK model

This is the first study to investigate the CFV influence on an XR formulation in a P-PBPK model. Performance of XR formulations is dependent of the local environment. Previous literature describes the challenges in predicting colonic absorption of low soluble compounds in adults[372], acknowledging a disconnection of *in vitro* and *in silico* models. As colonic fluid is now characterised in paediatrics, it is possible to integrate this into the simulator and progress PBPK prediction of colonic absorption.

Although the robustness of this accurate model has been demonstrated, the personalised simulations are hypothetical as there was no publicly accessible clinical data against which these models can be validated. Additionally, the cohort where the CFV data originated from is not selectively schizophrenic but rather a general paediatric population was used where the CFV was varied, which is a limitation to this study. Covariates like body weight, HDL-levels or triglyceride levels were not adapted to make the virtual population resemble paediatric schizophrenic patients better. Adapting a PBPK model as such, with personalised

covariates in a manner that individual patients are fully described *in silico* (virtual twin) allows for personalised prediction of the fate of a drug and precision dosing, and thus might improve therapy[459].

Antipsychotic therapy in adolescents is also associated with concomitant drug use[516], but these simulations did not include any co-medication. However, the original simulations by Johnson et al, using virtual "healthy" paediatric subjects (i.e. default inputs), predicted the PK profile for observed clinical data better in schizophrenic paediatric patients than it did for adult simulations (where some inputs such as clearance were adapted so the virtual subjects resembled schizophrenic patients better).

Additionally, paediatric PBPK models standardly use healthy children as subject population, such as done for a paediatric PBPK model of IR lamotrigine in Simcyp[105] or Gastroplus[153]. There is a lack of population descriptors for niche cohorts in the already understudied paediatric population, although there is recent effort in characterising these cohorts, such as done for paediatric patients with spinal muscular atrophy[109]. Further emphasis on characterising the target population for which certain drugs are intended will increase the representability and accuracy of the model predictions.

Furthermore, the 12 paediatric participants for who the PK profile was simulated, had their abdomen examined for clinical reasons. Thus, potential underlying comorbidities can hence not be excluded (no diagnosis was shared with the research team).

As mentioned in Chapter 4, the MRI recording was only a snapshot recording and thus does not consider the fluctuations in GIT fluid volumes[24, 26].

The standard dose given to all 12 subjects (300 mg) might not be the actual dose given to these subjects clinically. The plasma profile for both simulations (default and personalised)

of subject ID 09 (a 16 year old male, 173 cm, 102 kg) falls out the therapeutic plasma concentration range (based on therapeutic drug monitoring (TDM)) for quetiapine in adults (100 – 500 ng/mL)[499]. There is no established range for the paediatric or adolescent cohort. However, due to the similar response described between adults and paediatrics, there are no indications for dose adjustment of quetiapine[517]. So, the simulations represented here could be indicative for real schizophrenic paediatric patients, meaning this subject would likely get a bigger dose based on the too low plasma concentration.

Treatment of GI disturbances should also be considered when treating a schizophrenic patient[501]. The gut function is disturbed by schizophrenia (such as increased gut inflammation (gastritis, enteritis, colitis)[518], increased prevalence of coeliac disease[519, 520], disturbed gut microbiota[521] or association of epithelial permeability in the gut and the blood-brain-barrier[501]), so medical care should focus on improving or restoring the gut function as this is shown to influence the performance of the XR formulation[168].

Quetiapine is cleared *via* mainly CYP3A4 and 2D6 metabolism. The values used to model the clearance are similar in other quetiapine PBPK models[522]. The simulations here do not include the ontogeny patterns discussed in Chapter 2/3, as these data were not available at the time and there is no evidence in literature for ontogeny of these enzymes in the age cohort studied[98]. Additionally, the original predictions of the model by Johnson *et al*. were in very close agreement of the observed data. Similarly, this model of quetiapine (and a quetiapine PBPK model by Zheng *et al*.[522]) do not include any effects on/off the drug transporter P-gp (ABCB1). Firstly, quetiapine is both a substrate and inhibitor for P-gp, implicating it increases its own exposure[66, 523, 524]. At therapeutic levels, P-gp is inhibited so there is no influence on the PK profile of quetiapine. Secondly, as quetiapine is a BCS class II

compound (meaning a good permeability), gut efflux transporters are less involved in drug disposition. Thirdly, the purpose of this work was to investigate any chances in performance of an XR formulation in children by altering the CFV, with quetiapine being a model compound, rather than looking at the clinical indications of the drug. Hence, simulations were performed for a single dose with emphasis on a change in plasma concentrations and ran for 36 h, rather than a week-long trial with multiple doses with emphasis on the steady-state plasma concentration (C_{ss}).

5.6 Conclusion

This is the first study to investigate the influence of the colonic fluid volume on an XR formulation in a P-PBPK model. Performance of XR formulations is dependent on the local gut environment. A previously published PBPK model for an XR formulation of quetiapine to simulate exposure in children has been modified to simulate the influence of the CFV on the PK profile in a paediatric cohort.

Firstly, the LSA showed that the PK profile of an XR quetiapine formulation in adults is influenced by CFV, where the volume cut-off was 29.67 mL after which the drug was entirely dissolved. The same result was observed for a XR quetiapine formulation in a paediatric population with a similar cut-off value. However, modelling with a dynamic fluid volume model saw no cut-off value; exposure (AUC) kept increasing with increasing CFV.

Secondly, although the AUC and C_{max} of all simulations with default CFV input (13 mL) were dissimilar from simulations with real data, most cases were within bio-equivalence limits and no significant difference between the two sets of simulations was observed.

Thirdly, a very low CFV (<2.08 mL) gave AUC and C_{max} values that were below the 80% bioequivalence threshold. Therefore, there is a risk of sub-optimal therapy in paediatric individuals with a low CFV. Furthermore, our data suggested that 54% of paediatric patients have a CFV<2.08 mL, therefore ineffective therapy may be prevalent for the XR quetiapine formulation in the paediatric cohort.

6 THESIS CONCLUSION

Predictive tools are a cornerstone for paediatric drug development. These tools are data-hungry, and appropriate predictions rely on physiologically relevant input parameters that accurately describe the paediatric population. However, many of these important data underpinning predictive tools are lacking. To predict oral drug absorption, more data characterising the intestinal tract and its ontogeny are required.

One of these parameters is the abundance of key DMET proteins in the small intestine – as these can majorly effect drug disposition (BDDCS) and give rise to clinically important food- and drug-drug interactions. Current data are obtained via less sensitive methods, such as mRNA or immunoblotting, whereas recent advances in LC-MS/MS-based protein quantification allows for surrogate quantification of selected target proteins via proteotypic peptides.

Using LC-MS/MS, the abundance of key proteins (**Table 1.4**) were quantified in 34 paediatric duodenal pinch biopsies. For this, a microflow method and a QconCAT allowing for the simultaneous quantification of transporters, CYP- and UGT-enzymes were developed. The PaedCAT standard is the first single standard that allows for simultaneous quantification of both drug transporters and drug metabolising enzyme families. As demonstrated by the similar quality of elution profiles compared to literature, a microflow method is suitable for these assays. As these systems are more common than their nanoflow counterpart, this would allow other laboratories to employ the followed method to generate more (high-quality) proteomic DMET ontogeny data. Five CYP enzymes (CYP2C9, 2C19, 2D6, 3A4, 3A5),

4 drug transporter proteins (ABCB1, ABCC2, ABCG2 and SLC22A1), 3 UGT enzymes (UGT1A1, 2B7 and 2B17) and CES2 were quantified in the paediatric duodenum (**Table 2.7**).The obtained abundancy data and ontogeny trends are in agreement with literature, with similar trends of ontogeny proven or absent. For example, CYP3A4 is one of the major enzymes involved in the drug disposition of a plethora of drugs, and thus extensively studied already. The data in this work shows a clear positive correlation with age (**Figure 2.13**), which corroborates both available data on protein level, but also on the ontogeny in bioavailability of CYP3A4-substrates. The main limitations of these dataset include: the small sample size, particularly for the youngest age cohort (<2 years); the lack of adult biopsies studied (as this would allow for direct comparison to available data); potential underlying comorbidities (as samples were collected as additional sample during clinical care) and the unknown effect of potential underlying comorbidities. Further efforts should also aim to further established the used method, with emphasis on establishing limit of detection/quantification, stability measurements and quantifying a protein using multiple peptide probes and repeatability of quantification.

The newly generated CYP3A4 data was then used as an exemplar to investigate how current PBPK models would respond to the new abundancy data, and whether this would improve predictive capabilities of those models. For this, midazolam was selected as substrate, as it is extensively metabolised by both hepatic and intestinal CYP3A4, it is extensively studied in paediatrics, and it is still commonly used in this cohort as sedative agent. Observed PK profiles were first simulated via PBPK-modelling using default data in Simcyp, showing a good predictive performance (**Figure 3.1**). Then, the default intestinal CYP3A4 ontogeny was substituted to the newfound trend, and the adult values (the ontogeny function is expressed

as fraction of the adult value) are changed to the observed CYP3A4 values of the eldest cohort as internal control. Performing the same trial design in the new set-up did not change the outcomes significantly (**Figure 3.5**, **Figure 3.6**), which is likely due to the fact the default and new ontogeny profile are very similar (**Figure 3.7**). This demonstrates the appropriateness of the current data and models available, and expands the pool of available DMET data for PBPK models.

A second parameter that requires characterisation is the amount of fluid within the colon and its ontogeny, as this fluid is important in drug disintegration and solubilisation in the large intestine. For this, paediatric MRI datasets of the abdomen were available with limited metadata (no final diagnosis was shared). Two different protocols were employed (a more traditional 2D-protocol which is commonly used for these assays, and a novel 3D-rendering protocol). This was the first study to report paediatric colonic fluid data (**Table 4.3**), which is now supported by emerging data from literature[471]. MRI took place based on clinical needs, so underlying comorbidities that might influence the fluid data could not be anticipated/excluded. An additional potential source of bias was the protocol differences between both sites involved in the study (such as MRI set up, age cohorts per site or fed state). However, no influence of these factors was observed on the fluid data. Further work should aim to include more participants of all age cohorts, with clear diagnosis so the impact of disease on the fluid volumes can be assessed. Ideally, an adult cohort would be included to allow comparison to available data. MRI acquisition from different sites should have identical set-ups, and ideally measure participants at regular time points rather than a snap-shot recording, where feasible.

The novel fluid data was then incorporated into an existing PBPK model for XR quetiapine. It was investigated how adapting the default CFV inputs affects the bioavailability and PK profile of IR and XR quetiapine in adults and children (5.4.2). Then, PBPK models were adapted to resemble 12 individual paediatric participants from the MRI study (in terms of age/sex/height) and CFV. The results from these studies generally fell into three scenarios: one where the personalised CFV was similar to the default value (based on adult data), with overlapping PK profiles; one where the personalised CFV was at least three times larger than the default value, but PK parameters were still within bioequivalence limits; and a final scenario where the personalised CFV was considerably lower than the default value, with AUC outside bioequivalence limits. However, although only the minority of the performed simulations had non-bioequivalence, they resemble the majority of the paediatric population, as the median CFV on a cohort level fell within this scenario. As such, insufficient exposure and suboptimal therapy of XR quetiapine in the paediatric population might be prevalent and more investigation on the bioavailability and clinical effectiveness is required.

Future work should investigating the effect of DMET ontogeny on quetiapine bioavailability , with emphasis on the metabolising enzymes. As midazolam and quetiapine are both BDDCS Class I substrates[410], the effect of transporters (and ontogeny) would be negligible, yet the ontogeny of CYP3A4 might influence the bioavailability of these compounds. Due to the lower expression of CYP3A4 in the colon compared to the small intestine integrating the CYP3A4 ontogeny in an XR quetiapine model would be less beneficial, but investigating the combination of novel CFV data and DMET ontogeny on e.g. the absorption and bioavailability of XR amoxicillin (BDDCS Class III) might be of clinical value.

In conclusion, novel intestinal paediatric data was generated – these data should be seen as preliminary where trials with a larger sample size, inclusion of adults, final diagnosis sharing and data collection in a more controlled environment would allow to provide robust data that will lead to more conclusive claims. The novel generated data was integrated into PBPK models to showcase their effect on the bioavailability of oral drugs given to children. Generating these novel data and (integration into PBPK modelling) will improve the representability of paediatric participants in predictive tools, and progress development of age-appropriate formulations.

7 APPENDICES

Appendix 1. *Examples of P-PBPK models from literature*

- **Dose finding**

As a first example, an oral P-PBPK model was developed for voxelotor tablets. Voxelotor is used to treat sickle cell disease and approved by the US FDA for use in children of 12 years and older. By incorporating the changes in blood binding (blood to plasma ratio, B:P) and haematocrit level in adult patients, an adult PBPK model predicted voxelotor exposure that relied closely to observation in clinical trials on adult patients. After this, age-related changes in pathophysiological markers (ontogeny of albumin and haematocrit) were implemented, after which simulations were validated. Based on this P-PBPK model, dosing recommendations for voxelotor tablets were given for children of 9 months to 12 year old, further research is ongoing[61].

A second example is the P-PBPK model for everolimus, which was recently approved as adjunctive therapy for tuberous sclerosis complex-associated drug-resistant partial-onset seizures in children 2 years and older. This disease is a genetic disorder giving rise to benign tumours in different organs, including the brain. Most patients suffer from epilepsy that does not respond to treatment with anti-epileptic drugs. However, the anti-cancer drug everolimus acts on the underlying pathophysiology and is orally taken. Everolimus is a CYP3A4 and P-gp substrate (see sections 1.3.2 and 1.1.1). However, younger patients also suffer from partial seizures due to this genetic disorder. PopPK-PD and PBPK were used to extrapolate to this younger cohort as follows: firstly, a PBPK model was built using clinical data from adults and older children (2-18 year old). Then predictions were made for 2000

patients in the age range of 6-12 months, using the “redefine over time” function in the model (which ensures that, as patients are virtually getting older, the rapid changes in ontogeny are included). Finally, the PK model was linked to a popPD model to predict how effective the drug is in decreasing seizure frequency. Based on these predictions, oral dosing recommendations were given[103].

- **Formulation bridging**

As a first example, it was found that a once-daily extended release (XR) dose can replace two daily immediate release (IR) doses of the antipsychotic quetiapine. Halving the number of required tablets aimed to improve adherence in a teenage cohort. Simcyp PBPK modelling was use to simulate and compare the exposure between a twice daily IR dose and a once daily XR dose of quetiapine. CYP3A4 induction and inhibitions was incorporated in the model. As a result of these simulations, a clinical trial of the quetiapine XR formulation in the paediatric population was avoided[66].

A second example aims to predict exposure of hydrocortisone in an IR and XR formulation in adults and paediatrics for hormone replacement therapy for adrenal insufficiency. The PBPK model was built and verified and is being used to act as a tool to determine dosing regimens in clinical trials[104].

As a third example, a PBPK model for the anti-epileptic drug lamotrigine was adapted to predict single and multiple IR dosing in paediatrics. The adult model was built to verify DDI potential and was based on clinical data for both an IR and XR formulation. The model was adapted to predict lamotrigine exposure following a single or multiple IR dose in children ages 4-17 years old. The results from this study were in close agreement with clinical observed data[105].

- **Assisting drug development for new drugs for children or children-specific pathologies**

A P-PBPK model of oral deflazacort (available as tablets and liquid formulations) for the treatment of Duchenne Muscular Dystrophy accepted as evidence for dosing recommendations and DDI assessment for children older than 5 years old[61, 65].

A P-PBPK model for oral radiprodil for ages 2-14 months for the treatment of the life-threatening Infantile Spasm Syndrome was used to inform an ongoing clinical trial. A paediatric oral dose was needed that was effective (as this disease is life-threatening) but did not give rise to unwanted side-effects. Therefore, a P-PBPK model was developed that captured the ADME and ontogeny processes and could predict receptor occupancy. This model was then coupled to a PD-model to predict efficacy. No ontogeny in radiprodil elimination was observed. A low receptor occupancy and a low dose escalation approach were followed as initial dosing guidance in an ongoing, open trial, and the model also provided guidance on dose escalation for three paediatric patients. Predictions were in close agreement to the observations from the trial[106].

- **Drug-drug interaction studies in children**

Guanfacine is available as XR formulation for treatment of ADHD in children and adolescents. The drug is a CYP3A4 substrate. A PBPK model was built on existing clinical data in healthy adults using mono therapy, and was verified against clinical PK data with the presence of inducers and inhibitors. Dosing recommendations for co-medication with strong

CYP3A4 inducers/inhibitors were provided and approved by the US FDA without extra clinical studies in children[107, 108].

Risdiplam is used for treatment of Spinal Muscular Atrophy, a deteriorating disease that typically starts in infancy or childhood. In 2020, oral formulations of risdiplam was approved for treatment of this disease in patients of 2 months and older. However, as the drug is a CYP3A4 inhibitor, DDI potential needed to be assessed but this is not possible in the paediatric population. Therefore a PBPK model predicting DDI in healthy adults was built and extrapolated to paediatric patients as part of regulatory submission. The results show there is a negligible DDI risk in children[61, 109].

- **<u>Optimising combination therapy for the paediatric population</u>**

P-PBPK models can also be used to identify the best combination of drug moieties for optimal exposure and clinical response of a specific disease. Cystic fibrosis is a deteriorating disease affecting children 12 year and older. Currently, dual therapies are available, but a recent study suggested triple combination of oral elexacaftor, tezacaftor, and ivacaftor was superior to dual therapies[110]. Therefore, patients will need to transition to the combination of three drugs. However, there were no clinical trials to guide on how to transition. Three PBPK models were built, one for every drug and then combined to look at exposure. Initial models show that immediate transfer of patients 12 year and older are having a better PD response[111, 112], clinical trials on children younger than 12 are ongoing[61].

Appendix 2. *Ethical approval letter for PaedGIFT*

Ymchwil Iechyd a Gofal Cymru
Health and Care Research Wales

NHS
Health Research Authority

Dr Hannah Batchelor
Senior Lecturer in pharmaceutics, formulation and drug delivery.
University of Birmingham
Robert Aitken Building
Edgbaston
Birmingham
B15 2TT

Email: hra.approval@nhs.net
Research-permissions@wales.nhs.uk

04 February 2019

Dear Dr Batchelor

HRA and Health and Care Research Wales (HCRW) Approval Letter

Study title:	**Characterisation of fluids and mucosal tissues from paediatric stomach and small intestinal tract to enable development of biorelevant models to predict drug absorption**
IRAS project ID:	**251909**
Protocol number:	**RG_18-233**
REC reference:	**18/WM/0390**
Sponsor	**University of Birmingham**

I am pleased to confirm that HRA and Health and Care Research Wales (HCRW) Approval has been given for the above referenced study, on the basis described in the application form, protocol, supporting documentation and any clarifications received. You should not expect to receive anything further relating to this application.

How should I continue to work with participating NHS organisations in England and Wales?
You should now provide a copy of this letter to all participating NHS organisations in England and Wales, as well as any documentation that has been updated as a result of the assessment.

Following the arranging of capacity and capability, participating NHS organisations should **formally confirm** their capacity and capability to undertake the study. How this will be confirmed is detailed in the "*summary of assessment*" section towards the end of this letter.

You should provide, if you have not already done so, detailed instructions to each organisation as to how you will notify them that research activities may commence at site following their confirmation of capacity and capability (e.g. provision by you of a 'green light' email, formal notification following a site

IRAS project ID	251909

initiation visit, activities may commence immediately following confirmation by participating organisation, etc.).

It is important that you involve both the research management function (e.g. R&D office) supporting each organisation and the local research team (where there is one) in setting up your study. Contact details of the research management function for each organisation can be accessed here.

How should I work with participating NHS/HSC organisations in Northern Ireland and Scotland?
HRA and HCRW Approval does not apply to NHS/HSC organisations within the devolved administrations of Northern Ireland and Scotland.

If you indicated in your IRAS form that you do have participating organisations in either of these devolved administrations, the final document set and the study wide governance report (including this letter) has been sent to the coordinating centre of each participating nation. You should work with the relevant national coordinating functions to ensure any nation specific checks are complete, and with each site so that they are able to give management permission for the study to begin.

Please see IRAS Help for information on working with NHS/HSC organisations in Northern Ireland and Scotland.

How should I work with participating non-NHS organisations?
HRA and HCRW Approval does not apply to non-NHS organisations. You should work with your non-NHS organisations to obtain local agreement in accordance with their procedures.

What are my notification responsibilities during the study?
The document "*After Ethical Review – guidance for sponsors and investigators*", issued with your REC favourable opinion, gives detailed guidance on reporting expectations for studies, including:

- Registration of research
- Notifying amendments
- Notifying the end of the study

The HRA website also provides guidance on these topics, and is updated in the light of changes in reporting expectations or procedures.

I am a participating NHS organisation in England or Wales. What should I do once I receive this letter?
You should work with the applicant and sponsor to complete any outstanding arrangements so you are able to confirm capacity and capability in line with the information provided in this letter.

The sponsor contact for this application is as follows:

Name: David Law
Tel: 01214147618
Email: researchgovernance@contacts.bham.ac.uk

Who should I contact for further information?
Please do not hesitate to contact me for assistance with this application. My contact details are below.

IRAS project ID	251909

Your IRAS project ID is **251909**. Please quote this on all correspondence.

Yours sincerely

Andrea Bell
Assessor

Email: hra.approval@nhs.net

Copy to: *David Law – Sponsor contact*
Kelly Hard, Birmingham Children's Hospital NHS Trust – Lead NHS R&D contact

Appendix 3: *Methodology optimisation of protein extraction using animal small intestinal and adult human colonic tissue.*

To optimise the methodology of cell lysis and target protein extraction, different protocols (centrifugation/ultracentrifugation, shotgun-proteomics) using mock animal small intestinal and human adult colonic tissue were performed. The final methodology was largely based on the work by Couto *et al*.[80], but other routes reflecting the strategy by Harwood *et al.*[115] were also explored.

Rat tissue was obtained as leftover material from the Biomedical Services Unit (BMSU). Five rat "pinch" biopsies (average 5.8 mg, range 2.4 mg – 11.4 mg) were homogenised individually using a glass Dounce homogeniser in 500 µL RIPA lysing buffer (same composition as in section 2.3.2). The samples were homogenised using a minimal of 100 strokes on ice. Visual observations about lysing progress were recorded. After 100 strokes, the contents of the Dounce homogeniser were very foamy, as a result of the repeatedly agitation of the buffer containing detergent. The homogenates were sonicated for 3 s and centrifuged in a precooled centrifuge at 14 000 *g*, 4°C for 5 min. Visually, a pellet was formed in all samples after centrifugation. The supernatants of two samples were further ultracentrifugated at 100 000 *g*, 4 °C for 1 h. However, no pellet was observed visible with the naked eye after ultracentrifugation. After resuspending the pellets in an appropriate amount of lysing buffer, the protein concentration for all fractions was determined using Pierce's BCA kit. Western blotting was used as a tool to simultaneously compare the suitability of the lysing method and fractionation of the biopsy lysate to enrich the target proteins. Protein samples (20 µg, with a 6:1 (v/v) ratio sample:dye (Promega) containing 2-mercaptoethanol (1% (v/v)) and bromophenol blue (0.001% (w/v))). were loaded on a resolving gel containing 8% total acrylamide (**Appendix 3** - Table 7.1).

Appendix 3 *- Table 7.1 overview of ratios used for a 10% resolving/stacking gel in SDS-PAGE, for two gels*

Chemical	**Resolving gel for 8 % acrylamide content**	**Resolving gel for 10% acrylamide content**	**Resolving gel for 12% acrylamide content**	**Stacking gel**
Ammonium persulphate	0.03 g	0.03 g	0.03 g	0.03 g
Deionised H2O	4.8 mL	3.5 mL	1.9 mL	3.7 mL
Tris buffer (pH 8.8, sodium dodecyl sulphate 0.2% (w/v))	10 mL	10 mL	10 mL	-
Tris buffer (pH 6.8, sodium dodecyl sulphate 0.2% (w/v))	-	-	-	5 mL
Acrylamide/bisacrylamide (30%/8%)	5.2mL	6.5 mL	8.1 mL	1.3 mL
Tetramethylethylenediamine (TEMED)	60 µl	60 µl	60 µl	60 µl

Gels were prepared by mixing the resolving gel contents rapidly and pouring into a glass cast, covering with a layer of 2-propanol. After setting and removal of the isopropanol, the stacking gel was poured on top and left to set. After an initial run of the sample through the stacking gel for 15 min at 90 V, the voltage was increased to 180 V. The gels were ran in an electrophoresis buffer containing Tris (25 mM, pH 8.3), glycine (0.192M) and sodium dodecyl sulphate (0.01 % (w/v)). The electrophoresis was stopped when the protein front reached the end of the gel. Then, the protein resolved gels were transferred onto Hybond PVDF membranes, which were activated by soaking in methanol for 1 min and subsequently washed in transfer buffer (Tris (48 mM), glycine (39 mM), sodium dodecyl sulphate (0.0375 % (w/v)) and methanol (20 % (v/v)). Transfer of the proteins from gel to membrane was performed in a cooled transfer tank containing transfer buffer, for 90 min at 90 V.

After transfer, the membranes were blocked for one hour under gentle agitation (45 osc/min, room temperature (RT)) in blocking solution: Tris-buffered saline tween (TBST) (Tris (150 mM, pH 8.0), sodium chloride (150 mM), Tween-20 (0.05% (v/v)) supplemented with dried milk powder (5 % (w/v)). Then, the membranes were incubated in the primary

antibody solutions [P-gp (1:10 000 in 5% (w/v) skimmed milk in TBST, Abcam (AB170904), CYP3A4 (1:10 000 in 5% (w/v) skimmed milk in TBST), Abcam (AB3572), and beta-actin (1:4 000 in 5% (w/v) skimmed milk in TBST), as a positive control] overnight at 4 °C with constant agitation (16 osc/min). Next, the membranes were washed three times with TBST (6 mL) under severe agitation (60 osc/min, RT, 10 min each). After washing, the membranes were incubated with secondary peroxidase conjugated antibody (anti-rabbit, 1:10 000 dilution, Jackson Immunoresearch UK (111-035-003)) in TBST supplemented with dried milk powder (5 % (w/v)) for 1 h under gentle agitation (30 osc/min, RT). Then, the membranes were washed again for three times with TBST as above before being exposed to an ECL detection reagent (5 mL, Amersham ECL Western Blotting Detection Reagents, GE Healthcare) for five minutes, gently rubbing the reagent over the sealed membranes prior to development in a dark room. Numerous repeats of these western blots suggested that the proteins of interest (P-gp and CYP3A4) are mainly found in the supernatant after a normal centrifuge, but were inconclusive. Multiple optimisation steps at the stage of the tissue lysis (Dounce homogenisation using different buffers/variation of strokes, other lysis methods such as rough-walled microcentrifuge tubes, pestle and mortar), centrifugation (different speeds and timings) or western blotting (varying antibody concentration, voltages, strengths of the gel, timings) could improve signal collection and confidence, but this was out the objectives of this thesis. It was also hypothesised rat tissue might not be a suitable alternative for human enterocytes. As such, the experiment was repeated with Caco-2 cells.

A Caco-2 pellet of cells (0.175 g after washing with PBS) was resuspended in 1.75 mL RIPA-PI buffer, which then underwent two freeze-thaw cycles with liquid nitrogen for cell lysis. The cell lysate was centrifuged (14 000 g, 5 min, 4 °C) and separated into three fractions (1: resuspension before centrifugation, 2: supernatant and 3: pellet, resuspended in 130 µL

RIPA-PI buffer). Both a gel having a total acrylamide of 10% and 12% were used. Again, the western blot was carried out correctly, as evidenced by the beta-actin signal (results not shown). However, compared to the observation on the rat intestine, multiple CYP3A4 bands are observed on the blot. The high amount of individual bands for the CYP-enzymes is potentially due to the relative high concentration of CYP-antibody used and the strong homology in the cytochrome P450 3A subfamily, as this is not observed in similar work on rat intestine[170]. This blot clearly shows that the transporter proteins concentrate in the supernatant compared to the pellet. However, the resuspended pellet contains a small fraction of CYP-enzymes, potentially due to incomplete homogenisation and thus incomplete liberation from the endoplasmic reticulum. It was further hypothesised that the Caco-2 cells are not an appropriate surrogate for the paediatric biopsies, so we obtained adult colonic samples from the Biorepository at the University of Birmingham.

Similarly, western blots were carried out to qualitatively assess where and if the target proteins are isolated using colonic tissue from two adults (no metadata shared). Again, although correct execution (as evidenced by the signal of the positive control of beta-actin), the results of these blots did not allow for a conclusion whether the target proteins isolate in one of the fractions, after centrifugation of 9000 *g* or 14000 *g*. However, previous western blots show that there is no signal for P-gp in the pellet with a signal in the supernatant, indicating that lysis method is adequate for cell membrane-bound transporter proteins. A spin of cell homogenate at 9000 *g* is common for isolating microsomal fractions (CYP/UGT proteins).

The impact of the centrifugation speed on protein recovery was also explored via proteomic analysis on adult colonic tryptic protein digests. The samples described above were processed according to following initial FASP protocol:

1. Add 70 µg of a 1 µg/µL protein in the extraction buffer in an 0.5 mL microcentrifuge tube.
2. Reduction: add 200 µL of 100 mM 1,4-dithiotreitol (DTT) and incubate at 56 °C for 40 min.
3. FASP-filters (Vivaspin 500, MWCO 30 kDa): briefly wash using ultrapure water at 14 000 *g*, at room temperature (RT).
4. Add the reduced samples to the washed FASP filters and spin at 14 000 *g* for 20 min, RT. Discard filtrate.
5. Alkylation: add 200 µL of a 50 mM iodoacetamide (IAA) and leave to incubate in the dark, 30 min, RT.
6. Spin the alkylated samples at 14 000 *g* for 20 min, RT. Discard filtrate.
7. Wash of alkylating agent: Wash the samples with 200 µL of a 25 mM ammonium bicarbonate buffer (pH 8.5) and centrifuge at 14 000 *g*, 20 min.
8. Digestion: Add 10 µL of a 0.2 mg/mL trypsin-Lys-C mixture (Promega, Trypsin/Lys-C Mix, Mass Spec Grade) and 30 µL of 25 mM ammonium bicarbonate buffer to every sample and incubate at 37°C overnight (105 rpm).
9. Recovery of peptides: add 100 µL of a 100 mM ammonium bicarbonate (pH 8.5) to the filters, and subsequently spin at 14000 *g* for 20 min. Collect the filtrates in an 0.5 mL microcentrifuge tube for every sample.
10. Recovery of peptides bis: second elution by adding 100 µL 0.5 M NaCl to the filters and centrifuge for 14 000 *g*, for 20 min). Add the filtrates to the previously collected filtrates for every sample.
11. Dry the peptides in a vacuum concentrator at RT for 2h.

One set of duplicates was analysed on an in-house Bruker Impact qTOF instrument, running data dependent acquisition over a 90 minute gradient of 0-40% acetonitrile in 0.1% formic acid (15 cm x 100 µm C18 column). No difference was detected between either centrifugation speed (9 000 *g* or 14 000 *g*). Target proteins from both families were not detected, but the markers villin-1 and Na/K-ATPase were, which gave confidence in the digestion protocol. This is an older, less sensitive LC-MS/MS so it may not detect low-abundant proteins. However, some PEG polymer contamination was detected.

The other set of duplicates was sent to PolyQuant, the German producer of PaedCAT. The adult samples were sent for shotgun LC-MS/MS experiments, to identify appropriate proteotypic peptide sequence useful for quantification. Most of the target proteins were detected here (detected: ABCB1, ABCG2, ATP1A1, CES2, CYP2D6, CYP3A4, CYP3A5, UGT1A1, UGT2B17, UGT2B7, VIL1, ATP1A2, ATP1A3, UGT1A3, UGT1A4, UGT1A9. Not detected: ABCC3, ABCC4, CYP2C9, CYP2C19, CYP2J2). This gave confidence in both the extraction procedure and digestion protocol.

The PEG contamination was also detected here. The PEG contamination is thought to originate from the detergent in the RIPA-buffer IGEPAL CA-630, which is PEG based. However, this buffer was already used in processing all paediatric biopsies. It was demonstrated that using 8 M urea in 0.1 M Tris/HCl pH 8.5 as solution medium for every chemical in the FASP digestion and implementation of more washes after alkylation gets rid of most PEG contamination (**Appendix 3** - Figure 7.1).

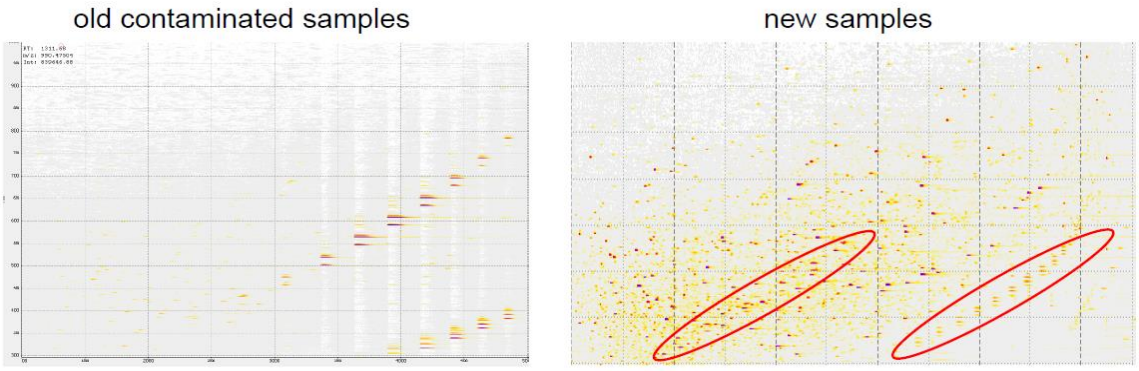

Appendix 3 *- Figure 7.1: Comparison of the m/z-values in function of retention time before and after including more wash steps and switching to 8 M urea in 0.1 M Tris/HCl pH 8.5 buffer in FASP.*

This optimised protocol (which was the final protocol as shown in section 2.3.3) also resulted in 2 to 5 times more peptide and protein identification. No influence of centrifugation speed was detected here either.

As such, the protein extraction method was selected using pestle and mortar and only normal centrifugation at 9000 g for 5 min, 4°C as this is frequently used before and neither Western blot nor LC-MS/MS detected a difference with centrifugation at 14 000 *g*.

Appendix 4. *List of chemicals used in the LC-MS/MS analysis*

Item	Manufacturer	Reference Code
Pestle and mortar	SigmaAldrich	Z409057-1EA, Deep form, Outer diameter 65 mm, Agate
Cryovial	Greiner Bio-one GMBH	Cryo.S TM – 123279
IGEPAL CA-630	SigmaAldrich	I3021-100mL
Sodium deoxycholate	SigmaAldrich	D6750-25g
Sodium dodecyl sulphate (SDS)	Sigma	L3771-500g
cOmplete protease inhibitor cocktail	Roche Diagnostics	11697498001
BCA assay	Pierce BCA Protein Assay	Ref 23225
Bovine Serum Albumin (BSA) standard	Thermo Scientific	Ref 23209
Urea, Reagentplus, >99.5%	Sigma-Aldrich	U1250-1KG
Trizma hydrochloride	Sigma-Aldrich	93363
Amicon Ultra 0.5 mL Centrifugal Filter	Merck Millipore Ltd, Ireland	UFC500396
PaedCAT	Polyquant GmbH, Germany	PaedCAT
1,4-Dithiotreitol (DTT)	Roche Diagnostics GmbH, Germany	Ref 10197777001
Iodoacetamide	Sigma-Aldrich	I6125
Ammonium bicarbonate, BioUltra, >99.5%	Sigma-Aldrich	09830-1KG
Acetonitrile	Thermo Scientific	89871C
Trifluoroacetic acid, Reagentplus, 99%	Sigma-Aldrich	T62200
Trypsin/Lys-C Mix, Mass Spec Grade	Promega corporation, USA	V5073
Pierce C18 tips 100 µL	Thermo Scientific	Ref 87784
Protein Low Bind Tubes 1.5mL PCR clean	VWR	Ref 525-0133
Water, Optima LC/MS	Fisher Chemical	W6-4
Acetonitrile, Optima LC/MS Grade	Fisher Chemical	A955-212
Formic Acid, Optima LC/MS	Fisher Chemical	A117-10X1AMP

Appendix 5. *PaedCAT sequence and characteristics.*

POLYQUANT

Quality Assurance Documentation

Certificate of Analysis

10/02/2022

Order number: 100324

Protein: QconCAT "PaedCAT" Expression in *E.coli*

Label :	^{13}C ^{15}N – Arg/Lys
Purification :	Ni-Sepharose
Buffer :	50 mM sodium phosphate, pH 7.4 6 M GdnHCl 500 mM Imidazole
Storage :	- 70°C
Target Protein concentration :	0.28 mg/ml (2.8 nmol/ml)
Labelling efficiency :	99.3 % for peptides ending on R 98.9 % for peptides ending on K
Purity :	79% (229 host contaminant proteins were identified)
Aliquots :	5 x 500 µl
Quantity of target protein :	700 µg
Note: concentration, labelling and purity of target protein were determined by LC-MS/MS	

Sequence:

M-expression enhacer sequence (168AA, 18.35kDa)-
MGTKGAIETEPAVKQEIGWFDVHDVGELNTRAGAVAEEVLAAIRFYDPLAGKVIQELGLDKTIIFSIHQPRLFDSLTLL
ASGRIFNSTDYPASQRQLLNNILRYLGGDDLDTSAIRIDGLNVADIGLHDLRSQLTIIPQDPILFSGTLRAEGEISDPFRL
TVTLFFPSAIERVFVAVTLYGAVRITILVTHQLQYLKIVEIPFNSTNKYQLSIHKNIAFFSTNCVEGTARNICFFSTNCVEG
TARNITFFSTNCVEGTARFAPPEPPESWSGVRLGVLGFFSTGDKSFFGGNYIKIYGPVFTLYFGLERGHFPLAERGIFPL
AERLPPGPTPLPVIGNILQIGIKAFLTQLDELLTEHRDIEVQGFRSSYVGDEASSKVIGQGQQPSTAARFEYQDSWFQ
QLLKEVTNFLRLSLGGLLQPEKPVVLKSAISIAEDEEWKRLRSLLSPTFTSGKDTINFLSKSAISLAEDEEWKRIRSLLSPT
FTSGKHTLLVWAPNHYQVVKENTIYLKVQQCGIHSKLSPSFADLFRGHEIVVLAPDASLYIRDGAFYTLKTYPVPFQR
YLSIPTVFFLREVSVVDILSHASVWLFRGLQVPLPRYLSIPAVFFWRTYSTSYTLEDLDRAFAHAQWKSVINDPIYKFSV
GYTVEKTILDELIQRIEIYPTSLTKGSLNITTPGLQIWRLFQVQGTGANNTKDPETPIIVVKIVPEPQPKLAAALEHHHH
HH

891 aa 100.15 kDa (labelled, monoisotopic) pI: 5.90

83.6 % of the sequence was identified in LC-MS/MS:

Protein coverage

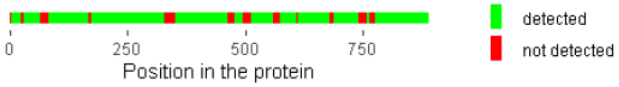

Electrophoresis:

visualization of crude: SDS PAGE, 12.5%, Coomassie staining, samples M and 1 from the same gel, lanes between M and 1 are not shown

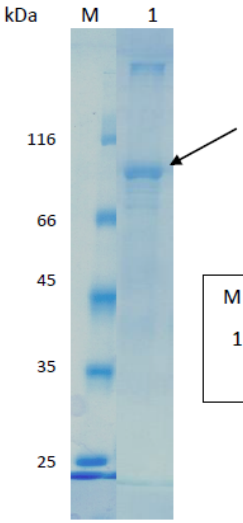

M	Unstained Protein Molecular Weight Marker(Fermentas,#SM0431)
1	PaedCAT (purified, 13C 15N – Arg/Lys labelled)

Appendix 6. *overview of target peptides and scheduled transitions for native and standard peptides used for quantification on PaedCAT. PaedCAT yields stable-isotope-labelled peptides with a terminal lysine ($^{13}C_6{}^{15}N_2$) and arginine ($^{13}C_6{}^{15}N_4$).*

Peptide target	Native / standard	Precursor (*m/z*)	Ret. Time	Q3.1 (*m/z*)	Q3.2 (*m/z*)	Q3.3 (*m/z*)	Q3.4 (*m/z*)	Q3.5 (*m/z*)	Q3.6 (*m/z*)	Start Time (min.)	End Time (min.)
AGAVAEEVLAAIR	native	635.4	18.3	971.6	900.5	642.4	430.3			14.7	16.3
AGAVAEEVLAAIR	standard	640.4	18.3	981.6	910.5	652.4	440.3			14.7	16.3
FYDPLAGK	native	455.7	14.89	485.3	388.3	275.2	204.1			11.3	12.9
FYDPLAGK	standard	459.7	14.89	493.3	396.3	283.2	212.1			11.3	12.9
VIQELGLDK	native	507.8	12.85	545.3	432.2	262.1	147.1			9.5	11.1
VIQELGLDK	standard	511.8	12.85	553.3	440.3	270.2	155.1			9.5	11.1
LFDSLTLLASGR	native	646.9	18.77	717.4	503.3	390.2	319.2			15.2	16.8
LFDSLTLLASGR	standard	651.9	18.77	727.4	513.3	400.2	329.2			15.2	16.8
YLGGDDLDTSAIR	native	698.3	14.01	662.3	547.3	175.1	180.1			10.5	12.1
YLGGDDLDTSAIR	standard	703.3	14.01	672.4	557.3	185.1	185.1			10.5	12.1
QLLNNILR	native	492.3	15.69	742.5	515.3	288.2	175.1			12.2	13.8
QLLNNILR	standard	497.3	15.69	752.5	525.3	298.2	185.1			12.2	13.8
AEGEISDPFR	native	560.8	13.78	419.2	322.2	175.1	311.2			10.3	11.9
AEGEISDPFR	standard	565.8	13.78	429.2	332.2	185.1	316.2			10.3	11.9
IDGLNVADIGLHDLR	native	541.0	17.51	1009.5	288.2	175.1	412.2			13.9	15.5
IDGLNVADIGLHDLR	standard	544.3	17.51	1019.6	298.2	185.1	417.2			13.9	15.5
ITILVTHQLQYLK	native	785.5	31.34	260.2	276.2	212.1	130.6			26	33
ITILVTHQLQYLK	standard	789.5	31.34	268.2	280.2	216.1	134.6			26	33
IVEIPFNSTNK	native	631.3	14.64	1049.5	807.4	404.2	225.1	181.6		11.1	12.7
IVEIPFNSTNK	standard	635.4	14.64	1057.5	815.4	408.2	229.1	185.6		11.1	12.7
NITFFSTNC[+114.042928] VEGTAR	native	887.4	37.8	347.2	175.1	174.1	123.6			30	38
NITFFSTNC[+114.042928] VEGTAR	standard	892.4	37.8	357.2	185.1	179.1	128.6			30	38
LGVLGFFSTGDK	native	620.8	19.29	654.3	507.2	319.2	262.1			15.7	17.3
LGVLGFFSTGDK	standard	624.8	19.29	662.3	515.3	327.2	270.2			15.7	17.3
SFFGGNYIK	native	516.8	15.43	651.3	594.3	260.2	147.1			11.9	13.5

SFFGGNYIK	standard	520.8	15.43	659.4	602.3	268.2	155.1			11.9	13.5
GHFPLAER	native	463.7	10.93	585.3	304.2	175.1	195.1			7.8	9.4
GHFPLAER	standard	468.7	10.93	595.3	314.2	185.1	195.1			7.8	9.4
GIFPLAER	native	451.8	15.79	585.3	488.3	175.1	293.2			12.2	13.8
GIFPLAER	standard	456.8	15.79	595.3	498.3	185.1	298.2			12.2	13.8
AFLTQLDELLTEHR	native	562.6	20.4	655.4	441.2	312.2	175.1			16.8	18.4
AFLTQLDELLTEHR	standard	566.0	20.4	665.4	451.2	322.2	185.1			16.8	18.4
DIEVQGFR	native	482.2	13.35	735.4	606.3	507.3	379.2			9.9	11.5
DIEVQGFR	standard	487.3	13.35	745.4	616.3	517.3	389.2			9.9	11.5
FEYQDSWFQQLLK	native	866.4	20.95	1164.6	260.2	147.1	277.1			17.4	19
FEYQDSWFQQLLK	standard	870.4	20.95	1172.6	268.2	155.1	277.1			17.4	19
VIGQGQQPSTAAR	native	656.9	8.6	915.5	602.3	175.1	607.3			5.6	7.2
VIGQGQQPSTAAR	standard	661.9	8.6	925.5	612.3	185.1	612.3			5.6	7.2
EVTNFLR	native	439.7	13.27	650.4	435.3	288.2	175.1			9.9	11.5
EVTNFLR	standard	444.7	13.27	660.4	445.3	298.2	185.1			9.9	11.5
DTINFLSK	native	469.3	14.59	608.3	494.3	234.1	147.1			11.1	12.7
DTINFLSK	standard	473.3	14.59	616.4	502.3	242.2	155.1			11.1	12.7
VQQC[+114.042928]GIHSK	native	557.3	14.34	371.2	234.1	147.1	271.2	242.6	228.1	10.9	12.5
VQQC[+114.042928]GIHSK	standard	561.3	14.34	379.2	242.2	155.1	275.2	246.7	228.1	10.9	12.5
LSPSFADLFR	native	576.8	19.07	855.4	768.4	435.3	175.1			15.4	17
LSPSFADLFR	standard	581.8	19.07	865.4	778.4	445.3	185.1			15.4	17
ENTIYLK	native	440.7	11.29	423.3	260.2	147.1	212.1			8.1	9.7
ENTIYLK	standard	444.7	11.29	431.3	268.2	155.1	216.1			8.1	9.7
DGAFYTLK	native	457.7	13.79	671.4	260.2	400.2				10.4	12
DGAFYTLK	standard	461.7	13.79	679.4	268.2	404.2				10.4	12
TYPVPFQR	native	504.3	13.69	743.4	646.4	547.3				10.2	11.8
TYPVPFQR	standard	509.3	13.69	753.4	656.4	557.3				10.2	11.8
YLSIPTVFFLR	native	452.6	9.79	288.2	175.1	341.2				6.7	8.3

YLSIPTVFFLR	standard	455.9	9.79	298.2	185.1	346.2				6.7	8.3
EVSVVDILSHASVWLFR	native	653.0	31.19	218.1	88.1	207.8	145.8			28.1	29.7
EVSVVDILSHASVWLFR	standard	656.4	31.19	223.1	93.1	211.1	149.1			28.1	29.7
GLQVPLPR	native	440.3	14.46	581.4	482.3	272.2	175.1			11	12.6
GLQVPLPR	standard	445.3	14.46	591.4	492.3	282.2	185.1			11	12.6
YLSIPAVFFWR	native	699.9	11.86	508.3	175.1	461.8	413.2			8.6	10.2
YLSIPAVFFWR	standard	704.9	11.86	518.3	185.1	466.8	418.2			8.6	10.2
TYSTSYTLEDLDR	native	782.4	15.02	1299.6	1024.5	861.4	647.3	518.3	175.1	11.5	13.1
TYSTSYTLEDLDR	standard	787.4	15.02	1309.6	1034.5	871.4	657.3	528.3	185.1	11.5	13.1
AFAHAQWK	native	479.7	10.37	532.3	333.2	147.1	335.2			7.2	8.8
AFAHAQWK	standard	483.8	10.37	540.3	341.2	155.1	339.2			7.2	8.8
FSVGYTVEK	native	515.3	12.99	476.3	375.2	276.2	147.1			9.6	11.2
FSVGYTVEK	standard	519.3	12.99	484.3	383.2	284.2	155.1			9.6	11.2
SVINDPIYK	native	524.8	13.07	862.5	749.4	310.2	147.1			9.6	11.2
SVINDPIYK	standard	528.8	13.07	870.5	757.4	318.2	155.1			9.6	11.2
TILDELIQR	native	550.8	17.95	886.5	658.4	529.3	175.1			14.4	16
TILDELIQR	standard	555.8	17.95	896.5	668.4	539.4	185.1			14.4	16
IEIYPTSLTK	native	582.8	14.8	646.4	448.3	248.2	147.1			11.3	12.9
IEIYPTSLTK	standard	586.8	14.8	654.4	456.3	256.2	155.1			11.3	12.9
LFQVQGTGANNTK	native	689.4	11.64	604.3	476.2	248.2	147.1	274.1	389.2	8.4	10
LFQVQGTGANNTK	standard	693.4	11.64	612.3	484.3	256.2	155.1	278.2	389.2	8.4	10
DPETPIIVVK	native	555.8	14.33	668.5	345.2	246.2	147.1			10.8	12.4
DPETPIIVVK	standard	559.8	14.33	676.5	353.3	254.2	155.1			10.8	12.4

Appendix 7. *Individual abundancy data per protein for individual samples. Abundancy values are given in pmol/mg protein and normalised to villin-1. .*

ID	Age[£]	ABCB1[a]	ABCB1[b]	ABCC2	ABCG2[c]	ABCG2[d]	ATP1A1	CES2	CYP2C19	CYP2C9	CYP2D6	CYP3A4	CYP3A5	SLC2A1	UGT1A1[e]	UGT1A1[f]	UGT2B17[g]	UGT2B17[h]	UGT2B7[i]	UGT2B7[j]	VIL1
UK001	13	1.51	1.32	1.48	1.79	3.80	68.33	100.79	3.17	3.08	1.45	20.36	5.84	8.58	20.08	24.35	53.66	76.81	9.05	4.56	100.00
UK002	10	1.12	2.97	2.90	N/A	N/A	72.52	89.38	3.70	2.61	7.79	28.24	10.43	3.63	28.24	11.32	31.41	26.36	6.43	3.17	100.00
UK003	13	3.00	2.72	3.25	1.19	3.79	55.19	83.17	3.33	2.06	3.54	N/A	6.71	10.25	N/A	4.24	33.46	48.19	N/A	1.52	100.00
UK004	2	0.65	0.65	1.06	0.89	2.71	40.07	51.64	1.95	1.55	1.44	11.48	5.08	3.91	N/A	2.95	34.73	57.20	2.99	1.50	100.00
UK005	11	N/A	N/A	1.49	N/A	N/A	25.29	41.02	0.90	1.33	1.82	19.21	2.13	4.61	12.10	7.40	17.18	16.57	4.18	2.70	100.00
UK006	8	0.98	1.45	1.11	1.34	2.98	44.51	69.40	1.95	2.18	0.71	18.04	4.46	4.72	N/A	10.16	26.19	23.85	4.90	3.08	100.00
UK007	6	1.35	1.40	2.01	N/A	5.52	47.94	70.87	1.63	2.86	1.88	20.67	4.34	5.33	12.86	10.66	38.10	62.64	5.58	3.30	100.00
UK008	2	1.00	1.05	1.01	0.84	2.69	33.76	67.19	1.12	1.81	1.81	17.97	2.55	2.39	16.29	11.44	22.69	27.16	3.32	2.78	100.00
UK011	14	0.57	0.73	N/A	0.71	N/A	36.54	70.61	N/A	1.78	N/A	26.37	2.54	N/A	14.41	11.33	35.35	44.52	3.86	1.85	100.00
UK012	15	N/A	1.51	4.52	N/A	3.29	108.59	132.34	3.02	3.47	1.74	31.89	6.30	8.91	21.97	19.92	28.92	106.30	11.56	N/A	100.00
UK013	11	0.72	1.13	1.66	1.17	N/A	34.69	51.02	0.94	1.89	2.47	13.62	2.42	5.42	14.24	8.92	N/A	1.43	4.01	1.98	100.00
UK014	14	2.41	2.27	2.00	N/A	7.15	62.67	71.65	3.32	3.52	3.01	19.41	8.60	7.76	18.09	13.04	41.97	54.64	N/A	3.08	100.00
UK017	14	0.91	1.01	0.76	N/A	3.72	26.04	68.68	1.22	1.45	0.72	14.14	3.39	2.32	10.00	9.69	28.81	48.98	1.99	3.27	100.00
UK018	12	0.46	0.57	0.56	0.49	N/A	21.44	47.96	1.56	1.84	1.31	12.41	1.36	N/A	9.61	5.14	8.70	14.16	2.54	1.24	100.00
UK024	11	1.07	1.06	0.82	0.62	N/A	42.36	98.77	1.70	1.87	1.02	17.79	2.78	3.44	12.02	9.61	18.01	35.37	4.01	2.93	100.00
UK026	13	1.86	1.78	1.89	1.89	4.79	41.39	63.67	2.96	2.51	3.76	10.59	6.30	N/A	13.17	6.51	6.89	4.08	N/A	1.98	100.00
UK028	12	0.92	1.76	N/A	0.97	N/A	38.08	112.65	4.53	2.55	2.99	25.91	6.66	N/A	20.09	6.21	61.32	104.80	N/A	2.94	100.00
UK029	15	1.75	1.33	N/A	1.21	N/A	35.80	126.63	2.03	2.77	1.84	29.35	8.31	N/A	19.12	9.02	27.50	31.98	4.88	2.79	100.00

UK031	9	1.32	0.97	1.72	0.49	2.99	35.37	76.85	2.80	2.14	1.29	21.00	2.85	2.82	16.27	11.83	30.62	40.27	4.70	2.72	100.00
UK033	15	1.43	1.40	1.05	0.94	2.40	33.30	120.14	1.26	1.55	1.00	19.02	2.85	3.38	11.90	12.46	4.19	1.73	4.08	3.55	100.00
UK034	15	1.84	1.74	1.38	N/A	6.11	50.69	100.43	3.52	3.42	2.40	25.31	N/A	N/A	17.46	6.90	30.57	36.32	N/A	6.28	100.00
UK036	5	0.58	0.64	0.94	N/A	1.32	25.24	43.25	0.58	1.39	0.51	23.36	1.93	1.59	6.62	5.55	27.22	43.02	3.55	3.23	100.00
UK041	12	0.64	1.29	0.86	N/A	2.83	27.36	77.30	1.60	2.28	1.60	12.67	1.75	4.19	14.50	14.67	23.32	26.01	5.14	2.16	100.00
UK042	3	1.73	1.29	1.31	1.71	3.15	29.44	96.51	2.01	2.61	1.59	15.93	3.07	2.97	9.74	9.90	27.25	37.10	3.58	2.51	100.00
UK044	8	2.13	3.40	2.21	1.88	10.12	47.23	70.91	1.19	2.83	N/A	6.60	6.19	N/A	13.85	N/A	N/A	22.57	6.35	2.46	100.00
UK046	3	1.24	1.13	1.26	0.80	3.86	38.57	67.62	3.06	1.90	1.01	22.18	2.43	2.23	13.50	9.22	31.42	49.60	2.26	2.28	100.00
UK047	7	0.96	N/A	1.38	N/A	N/A	32.06	33.36	1.67	1.83	N/A	N/A	3.55	N/A	N/A	98.83	N/A	23.94	7.34	1.14	100.00
UK048	6	1.34	1.32	1.26	N/A	5.18	36.34	86.59	1.87	2.41	1.30	18.42	3.41	N/A	6.60	4.27	37.17	41.20	2.91	2.33	100.00
UK049	0.9166666	1.32	1.41	1.12	1.30	1.55	53.16	68.11	2.01	1.94	1.06	15.56	2.96	3.05	16.72	5.57	20.42	31.40	4.26	2.76	100.00
UK050	10	0.63	1.64	1.40	N/A	4.37	29.06	65.98	1.80	1.49	5.25	7.88	4.77	N/A	15.40	1.85	20.10	25.84	N/A	1.53	100.00
UK051	10	6.28	4.22	5.73	N/A	7.80	90.29	100.32	5.41	6.60	4.14	6.76	N/A	17.50	30.79	N/A	N/A	54.73	8.51	3.10	100.00
UK052	6	1.66	1.00	0.80	0.85	2.40	33.41	74.44	1.00	1.48	0.85	18.27	3.70	4.10	13.87	8.08	N/A	4.18	2.38	1.27	100.00
UK054	2	1.62	1.68	2.90	N/A	4.25	69.43	73.83	1.02	2.81	3.02	7.19	N/A	6.50	21.83	5.87	20.84	20.93	9.22	1.95	100.00
UK055	4	2.83	2.51	2.41	N/A	N/A	49.18	68.59	2.00	2.32	3.19	4.80	4.15	N/A	14.39	2.03	N/A	11.72	5.15	1.48	100.00

[£]: age given in years. Using [a]: AGAVAEEVLAAIR, [b]: FYDPLAGK, [c]: LFDSLTLLASGR, [d]: VIQELGLD, [e]: DGAFYTLK, [f]: TYPVPFQR; [g]: FSVGYTVEK; [h]: SVINDPIY; [i]: IEIYPTSLTK or [j]: TILDELIQR as probe to infer protein concentration.

***Appendix 8**. Protein abundancy numbers stratified by age-group*

	Preschool children (2-5 year old)					School age children (6-11 year old)					Adolescents (12-16 year old)				
Protein	N	Min.	Max.	Mean	SD	N	Min.	Max.	Mean	SD	N	Min.	Max.	Mean	SD
CES2	7	43.25	96.51	66.95	16.93	13	33.36	100.32	71.45	20.41	13	47.96	132.34	90.46	26.79
CYP2C19	7	0.58	3.06	1.68	0.83	13	0.9	5.41	2.04	1.28	12	1.22	4.53	2.63	1.06
CYP2C9	7	1.39	2.81	2.06	0.54	13	1.33	6.6	2.42	1.35	13	1.45	3.52	2.48	0.73
CYP2D6	7	0.51	3.19	1.80	0.99	11	0.71	7.79	2.59	2.24	12	0.72	3.76	2.11	1.01
CYP3A4	7	4.8	23.36	14.70	7.16	12	6.6	28.24	16.38	6.53	12	10.59	31.89	20.62	7.16
CYP3A5	6	1.93	5.08	3.20	1.19	12	2.13	10.43	4.25	2.25	12	1.36	8.6	5.05	2.54
UGT1A1[a]	6	6.62	21.83	13.73	5.27	11	6.6	30.79	16.02	7.15	12	9.61	21.97	15.87	4.17
UGT1A1[b]	7	2.03	11.44	6.71	3.58	11	1.85	98.83	16.63	27.43	13	4.24	24.35	11.04	5.94
UGT2B17[c]	6	20.84	34.73	27.36	5.20	8	17.18	38.1	27.35	8.31	13	4.19	61.32	29.59	16.91
UGT2B17[d]	7	11.72	57.2	35.25	16.21	13	1.43	62.64	29.15	17.68	13	1.73	106.3	46.04	33.61
UGT2B7[e]	7	2.26	9.22	4.30	2.34	12	2.38	8.51	5.11	1.80	8	1.99	11.56	5.39	3.28
UGT2B7[f]	7	1.48	3.23	2.25	0.65	13	1.14	3.3	2.44	0.74	12	1.24	6.28	2.94	1.41
ABCB1[g]	7	0.58	2.83	1.37	0.78	12	0.63	6.28	1.63	1.52	12	0.46	3	1.44	0.78
ABCB1[h]	7	0.64	2.51	1.28	0.65	11	0.97	4.22	1.87	1.12	13	0.57	2.72	1.49	0.58
ABCC2	7	0.94	2.9	1.56	0.78	13	0.8	5.73	1.88	1.29	10	0.56	4.52	1.78	1.24
ABCG2[i]	4	0.8	1.71	1.06	0.43	6	0.49	1.88	1.06	0.51	8	0.49	1.89	1.15	0.49
ABCG2[j]	6	1.32	4.25	3.00	1.03	8	2.4	10.12	5.17	2.66	9	2.4	7.15	4.21	1.55
SLC22A1	6	1.59	6.5	3.27	1.77	9	2.82	17.5	5.73	4.50	7	2.32	10.25	6.48	26.79

Using [a]: DGAFYTLK, [b]: TYPVPFQR, [c]: FSVGYTVEK, [d]: SVINDPIYK, [e]: IEIYPTSLTK, [f]: TILDELIQR, [g]: AGAVAEEVLAAIR, [h]: FYDPLAGK, [i]: LFDSLTLLASGR, [j]: VIQELGLDK as probe to infer protein abundance for these five proteins with two proteotypic peptides.

Min: minimum. Max: maximum. *: abundancy values of participants for which no diagnosis were available are only included in the "total" column

Appendix 9. *Ethical Approval for MRI: Fluid volumes and localisation in paediatric GI tract*

Ymchwil Iechyd a Gofal Cymru
Health and Care Research Wales

NHS
Health Research Authority

Dr Hannah Katharine Batchelor
Senior Lecturer in pharmaceutics, formulation and drug delivery
University of Birmingham
School of Pharmacy
Robert Aitken Building
Birmingham
B15 2TT

Email: hra.approval@nhs.net
Research-permissions@wales.nhs.uk

22 August 2018

Dear Dr Batchelor

HRA and Health and Care Research Wales (HCRW) Approval Letter

Study title:	**Measurement of fluid volumes and localisation within the gastrointestinal tract of paediatric populations using MRI data**
IRAS project ID:	**237159**
Protocol number:	**RG_17-057**
REC reference:	**18/EM/0251**
Sponsor	**University of Birmingham**

I am pleased to confirm that HRA and Health and Care Research Wales (HCRW) Approval has been given for the above referenced study, on the basis described in the application form, protocol, supporting documentation and any clarifications received. You should not expect to receive anything further relating to this application.

How should I continue to work with participating NHS organisations in England and Wales?
You should now provide a copy of this letter to all participating NHS organisations in England and Wales, as well as any documentation that has been updated as a result of the assessment.

Following the arranging of capacity and capability, participating NHS organisations should **formally confirm** their capacity and capability to undertake the study. How this will be confirmed is detailed in the "*summary of assessment*" section towards the end of this letter.

You should provide, if you have not already done so, detailed instructions to each organisation as to how you will notify them that research activities may commence at site following their confirmation of capacity and capability (e.g. provision by you of a 'green light' email, formal notification following a site initiation visit, activities may commence immediately following confirmation by participating organisation, etc.).

IRAS project ID	237159

It is important that you involve both the research management function (e.g. R&D office) supporting each organisation and the local research team (where there is one) in setting up your study. Contact details of the research management function for each organisation can be accessed here.

How should I work with participating NHS/HSC organisations in Northern Ireland and Scotland?
HRA and HCRW Approval does not apply to NHS/HSC organisations within the devolved administrations of Northern Ireland and Scotland.

If you indicated in your IRAS form that you do have participating organisations in either of these devolved administrations, the final document set and the study wide governance report (including this letter) has been sent to the coordinating centre of each participating nation. You should work with the relevant national coordinating functions to ensure any nation specific checks are complete, and with each site so that they are able to give management permission for the study to begin.

Please see IRAS Help for information on working with NHS/HSC organisations in Northern Ireland and Scotland.

How should I work with participating non-NHS organisations?
HRA and HCRW Approval does not apply to non-NHS organisations. You should work with your non-NHS organisations to obtain local agreement in accordance with their procedures.

What are my notification responsibilities during the study?
The document "*After Ethical Review – guidance for sponsors and investigators*", issued with your REC favourable opinion, gives detailed guidance on reporting expectations for studies, including:

- Registration of research
- Notifying amendments
- Notifying the end of the study

The HRA website also provides guidance on these topics, and is updated in the light of changes in reporting expectations or procedures.

I am a participating NHS organisation in England or Wales. What should I do once I receive this letter?
You should work with the applicant and sponsor to complete any outstanding arrangements so you are able to confirm capacity and capability in line with the information provided in this letter.

The sponsor contact for this application is as follows:

Name: Dr Sean Jennings

Email: researchgovernance@contacts.bham.ac.uk.

Who should I contact for further information?
Please do not hesitate to contact me for assistance with this application. My contact details are below.

Your IRAS project ID is **237159**. Please quote this on all correspondence.

IRAS project ID	237159

Yours sincerely

Thomas Fairman
HRA Assessor

Email: hra.approval@nhs.net

Copy to: *Dr Sean Jennings, University of Birmingham, (Sponsor Contact)*
Ms Ceri Jones, University Hospitals Coventry & Warwickshire NHS Trust, (Lead NHS R&D Contact)

Appendix 10. *Overview of excluded MRI datasets.*

Age (age band)	Fed state	Reason for exclusion
1-month old (neonate)	Fasted	A low resolution (and subsequent insufficient quality of the MRI scans) and an abundant amount of gas within the colon.
3 year-9 months old (pre-school child)	Fasted	A low resolution thus insufficient quality of the MRI scans.
6 year old (school-age child)	Fasted	The wrong MRI sequence was used (a T2 HASTE sequence), resulting in a dataset that was not suitable for data extraction *via* Horos and ImageJ as slices were overlapping, which would invalidate the fluid volume calculations.

Appendix 11. *Data on participants demographics and MRI set-up.*

ID	Age	Age (years)	Age group	Weight (kg)	Sex (Male (M) or Female (F))	Fed state	Hospital	Echo Time TE (ms)	Repetition time TR (ms)	Z-axis (cm)
2	2 w	0.04	newborn	N/A	F	fasted	BCH	241	2660.65	0.09
3	5 m	0.42	newborn	6.8	F	fasted	BCH	87	3200	0.55
4	5 m	0.42	newborn	7.1	F	fasted	BCH	241	4008.18	0.09
5	8 m	0.67	newborn	8.8	F	fasted	BCH	117	1400	0.16
6	12 m	1.00	newborn	9.7	F	fasted	BCH	241	3012.22	0.09
7	1 w	0.02	newborn	2.88	F	fasted	BCH	241	3012.22	0.09
8	1 y 10 m	1.83	newborn	11	M	fasted	BCH	221	2943.23	0.09
9	18 m	1.50	newborn	11	F	fasted	BCH	241	2844.65	0.09
10	12 m	1.00	newborn	7.2	M	fasted	BCH	704	4356.24	0.09
12	2 y 2 m	2.17	pre-school	10	F	fasted	BCH	240	2960.74	0.09
13	3 y 2 m	3.17	pre-school	16.3	F	fasted	BCH	241	3021.27	0.09
14	2 y 1 m	2.08	pre-school	12.2	F	fasted	BCH	241	3010.72	0.09
15	3 y 7 m	3.58	pre-school	12	M	fasted	BCH	241	2907.49	0.09
16	6 y 8 m	6.67	school-age	22.1	F	fasted	BCH	241	3161.32	0.09

18	5 y	5.00	pre-school	12.8	M	fasted	BCH	87	2200	0.55
19	4 y 5 m	4.42	pre-school	16.9	F	fasted	BCH	241	3011.71	0.09
20	6 y 2 m	6.17	school-age	N/A	F	fasted	BCH	241	2747.37	0.09
21	8 y 3 m	8.25	school-age	15.9	M	fasted	BCH	241	2900.01	0.09
22	9 y 1 m	9.08	school-age	39.1	F	fasted	BCH	87	3200	0.55
23	8 y 2 m	8.17	school-age	35.3	M	fasted	BCH	241	3022.19	0.09
24	9 y 8 m	9.67	school-age	28.7	F	fasted	BCH	241	3466.53	0.09
25	15 y	15.00	adolescents	N/A	M	fasted	BCH	242	3987.78	0.09
30	12	12.00	adolescents	33.5	F	fed	UHCW	1.8	4.822	0.6995
31	13	13.00	adolescents	52.7	M	fed	UHCW	1.896	5.695	0.498
32	12	12.00	adolescents	33.5	F	fed	UHCW	1.8	4.822	0.6995
34	15	15.00	adolescents	55	F	fed	UHCW	1.896	5.661	0.4997
35	16	16.00	adolescents	59	F	fed	UHCW	1.896	5.844	0.498
36	15	15.00	adolescents	65	F	fed	UHCW	1.896	5.604	0.5
37	15	15.00	adolescents	94	F	fed	UHCW	1.896	5.604	0.5
38	10	10.00	school-age	32.6	F	fed	UHCW	2.1	652.77	0.2998
39	11	11.00	school-age	28	M	fed	UHCW	2.1	652.77	0.3
40	13	13.00	adolescents	65	F	fed	UHCW	2.13	623.86	0.5
41	14	14.00	adolescents	54	F	fed	UHCW	1.72	4.253	0.7
42	15	15.00	adolescents	58	F	fed	UHCW	1.896	5.604	0.5
43	16	16.00	adolescents	54.4	M	fed	UHCW	1.9	5.716	0.4994
44	16	16.00	adolescents	65	F	fed	UHCW	1.9	5.764	0.4982
45	16	16.00	adolescents	60	F	fed	UHCW	1.896	5.604	0.5
46	16	16.00	adolescents	57	M	fed	UHCW	2.02	4.598	0.5988
47	16	16.00	adolescents	56	M	fed	UHCW	1.724	4.635	0.628
48	16	16.00	adolescents	102	M	fed	UHCW	1.888	5.519	0.4983
49	3	3.00	pre-school	N/A	N/A	fasted	BCH	241	3012.72	0.09
50	3	3.00	pre-school	N/A	N/A	fasted	BCH	241	2903	0.09
51	3	3.00	pre-school	N/A	N/A	fasted	BCH	221	3011.76	0.09

52	3	3.00	pre-school	N/A	N/A	fasted	BCH	241	3012.22	0.09
53	5	5.00	pre-school	N/A	N/A	fasted	BCH	241	4016.56	0.09
54	5	5.00	pre-school	N/A	N/A	fasted	BCH	241	3168.3	0.09

Appendix 12. *Data on used threshold values, fluid volumes via both protocols and number of pockets in the total and segments of the colon per participant.*

ID	Total colonic fluid volume via *2D* protocol (mL)	Total colonic fluid volume via *3D* protocol (mL)	Total Number of fluid pockets	Number of fluid pockets in ascending colon	Number of fluid pockets in transverse colon	Number of fluid pockets in descending colon	Threshold value	Fluid volume in ascending colon via *2D* protocol (mL)	Fluid volume in transverse colon via *2D* protocol (mL)	Fluid volume in descending colon via *2D* protocol (mL)
2	0	0	0	0	0	0	292.94	0	0	0
3	67.998	69.0434	16	16	0	0	474.7	41.603	6.055	20.34
4	0.0046	N/A	N/A	N/A	N/A	N/A	334	0.0046	0	0
5	0.6755	0.817	19	19	0	0	450.91	0.6755	0	0
6	0.9164	1.0537	21	17	4	0	320.56	0.3458	0.1744	0.3962
7	0	0	0	0	0	0	248.97	0	0	0
8	0.2306	0.2962	19	19	0	0	316.78	0.2306	0	0
9	19.092	N/A	N/A	N/A	N/A	N/A	259.36	5.1182	13.964	0.0093
10	0	0	0	0	0	0	336.07	0	0	0
12	0.3219	0.3474	11	10	1	0	339.9	0.2905	0.0058	0.0257
13	0	0	0	0	0	0	302.92	0	0	0
14	0	0	0	0	0	0	396.7	0	0	0
15	0.0929	0.1196	5	5	0	0	253.81	0.0923	0.0005	0
16	19.835	19.8487	47	46	0	1	217.96	19.719	0	0.1161
18	131.49	249.602	1	1	1	1	262.35	81.123	12.423	37.943
19	2.6663	2.5484	35	31	4	0	186.71	2.5183	0.0281	0.12
20	22.226	N/A	N/A	N/A	N/A	N/A	167.42	19.704	0.6523	1.8694

21	0.3236	0.3515	32	32	0	0	355.95	0.1415	0.1822	0
22	0.4065	0.498	8	8	0	0	416.81	0	0.3966	0.0099
23	14.164	14.1689	34	34	0	0	142.79	12.436	1.4667	0.2614
24	62.872	44.942	19	13	6	0	296.71	61.925	0.9086	0.0392
25	0.0037	0.004	1	1	0	0	335.03	0	0.0037	0
30	14.238	14.2883	23	20	3	0	1526	10.153	4.0535	0.0322
31	167.47	N/A	N/A	N/A	N/A	N/A	1092.5	102.3	51.767	13.399
32	6.1234	N/A	N/A	N/A	N/A	N/A	1717.3	5.5002	0.6233	0
34	152.94	139.55	19	19	0	0	1808	75.205	56.867	20.868
35	60.011	65.7035	65	53	12	0	1425.6	42.458	14.839	2.7141
36	11.22	13.0425	26	26	0	0	1672.1	11.22	0	0
37	0	0	0	0	0	0	1526.7	0	0	0
38	92.208	86.2179	35	32	3	0	336.85	84.962	7.2465	0
39	0.0873	0.0842	2	2	0	0	227.13	0	0	0.0873
40	0.026	0.0257	8	8	0	0	229.6	0	0	0.026
41	2.0748	2.211	5	5	0	0	1462.8	2.0748	0	0
42	0	0	0	0	0	0	1592	0	0	0
43	0.5303	0	0	0	0	0	1793.1	0.5303	0	0
44	43.198	43.2104	13	13	0	0	1165.4	43.185	0.0055	0.007
45	0	0	0	0	0	0	2136.1	0	0	0
46	0	0	0	0	0	0	939.84	0	0	0
47	6.1601	7.6259	1	1	0	0	1360.7	6.1601	0	0
48	0.5775	0.1449	7	7	0	0	1775	0.5775	0	0
49	15.239	26.8771	24	24	0	0	223.91	14.977	0.0049	0.2563
50	22.917	41.5957	13	13	0	0	217.63	22.917	0	0
51	0.2453	0.2919	24	24	0	0	271.35	0.082	0.1346	0.0287
52	0.4325	N/A	N/A	N/A	N/A	N/A	216.05	0.1685	0.2582	0.0058
53	75.708	81.3068	17	10	7	0	197	73.249	0.3104	2.1482
54	19.414	18.5813	71	71	0	0	168.84	14.384	1.4831	3.5474

8 REFERENCES

1. Van der Veken, M., et al., *Practical and operational considerations related to paediatric oral drug formulation: An industry survey.* International Journal of Pharmaceutics, 2022. **618**: p. 121670.
2. Vinarov, Z., et al., *Impact of gastrointestinal tract variability on oral drug absorption and pharmacokinetics: an UNGAP review.* European Journal of Pharmaceutical Sciences, 2021: p. 105812.
3. Van Den Abeele, J., et al., *Gastric fluid composition in a paediatric population: Age-dependent changes relevant for gastrointestinal drug disposition.* Eur J Pharm Sci, 2018. **123**: p. 301-311.
4. Batchelor, H.K., N. Fotaki, and S. Klein, *Paediatric oral biopharmaceutics: key considerations and current challenges.* Adv Drug Deliv Rev, 2014. **73**: p. 102-26.
5. Johnson, T.N., et al., *Enterocytic CYP3A4 in a paediatric population: developmental changes and the effect of coeliac disease and cystic fibrosis.* Br J Clin Pharmacol, 2001. **51**(5): p. 451-60.
6. Mooij, M.G., et al., *Ontogeny of oral drug absorption processes in children.* Expert Opin Drug Metab Toxicol, 2012. **8**(10): p. 1293-303.
7. Bowles, A., et al., *Specific aspects of gastro-intestinal transit in children for drug delivery design.* International Journal of Pharmaceutics, 2010. **395**(1): p. 37-43.
8. Weaver, L.T., M.F. Laker, and R. Nelson, *Intestinal permeability in the newborn.* Arch Dis Child, 1984. **59**(3): p. 236-41.
9. *Report of the task group on reference man ICRP Publication 23 (1975).* Annals of the ICRP, 1980. **4**(3-4): p. III-III.
10. Johnson, T.N., A. Rostami-Hodjegan, and G.T. Tucker, *Prediction of the clearance of eleven drugs and associated variability in neonates, infants and children.* Clin Pharmacokinet, 2006. **45**(9): p. 931-56.
11. EMA, *Clinical Investigation of Medicinal Products in the Paediatric Population*, I.T. E11, Editor. 2001.
12. *WHO: recommended definitions, terminology and format for statistical tables related to the perinatal period and use of a new certificate for cause of perinatal deaths. Modifications recommended by FIGO as amended October 14, 1976.* Acta Obstet Gynecol Scand, 1977. **56**(3): p. 247-53.
13. Batchelor, H.K. and J.F. Marriott, *Paediatric pharmacokinetics: key considerations.* Br J Clin Pharmacol, 2013. **79**(3): p. 395-404.
14. EMA, *GUIDELINE ON THE ROLE OF PHARMACOKINETICS IN THE DEVELOPMENT OF MEDICINAL PRODUCTS IN THE PAEDIATRIC POPULATION*, C.F.M.P.F.H.U. (CHMP), Editor. 2006: London.
15. Rostami-Hodjegan, A., *Physiologically based pharmacokinetics joined with in vitro-in vivo extrapolation of ADME: a marriage under the arch of systems pharmacology.* Clin Pharmacol Ther, 2012. **92**(1): p. 50-61.
16. Varma, M.V., et al., *Physicochemical space for optimum oral bioavailability: contribution of human intestinal absorption and first-pass elimination.* J Med Chem, 2010. **53**(3): p. 1098-108.

17. Dahlgren, D. and H. Lennernäs, *Intestinal Permeability and Drug Absorption: Predictive Experimental, Computational and In Vivo Approaches.* Pharmaceutics, 2019. **11**(8).
18. Amidon, G.L., et al., *A theoretical basis for a biopharmaceutic drug classification: the correlation of in vitro drug product dissolution and in vivo bioavailability.* Pharm Res, 1995. **12**(3): p. 413-20.
19. Wu, C.Y. and L.Z. Benet, *Predicting drug disposition via application of BCS: transport/absorption/ elimination interplay and development of a biopharmaceutics drug disposition classification system.* Pharm Res, 2005. **22**(1): p. 11-23.
20. Charalabidis, A., et al., *The Biopharmaceutics Classification System (BCS) and the Biopharmaceutics Drug Disposition Classification System (BDDCS): Beyond guidelines.* Int J Pharm, 2019. **566**: p. 264-281.
21. Chen, M.L., et al., *The BCS, BDDCS, and regulatory guidances.* Pharm Res, 2011. **28**(7): p. 1774-8.
22. Abdel-Rahman, S.M., et al., *Summary of the National Institute of Child Health and Human Development-best pharmaceuticals for Children Act Pediatric Formulation Initiatives Workshop-Pediatric Biopharmaceutics Classification System Working Group.* Clin Ther, 2012. **34**(11): p. S11-24.
23. Maharaj, A.R. and A.N. Edginton, *Examining Small Intestinal Transit Time as a Function of Age: Is There Evidence to Support Age-Dependent Differences among Children?* Drug Metab Dispos, 2016. **44**(7): p. 1080-9.
24. Papadatou-Soulou, E., et al., *Magnetic Resonance Imaging Quantification of Gastrointestinal Liquid Volumes and Distribution in the Gastrointestinal Tract of Children.* Mol Pharm, 2019. **16**(9): p. 3896-3903.
25. Goelen, J., et al., *Quantification of Fluid Volume and Distribution in the Paediatric Colon via Magnetic Resonance Imaging.* Pharmaceutics, 2021. **13**(10): p. 1729.
26. Schiller, C., et al., *Intestinal fluid volumes and transit of dosage forms as assessed by magnetic resonance imaging.* Aliment Pharmacol Ther, 2005. **22**(10): p. 971-9.
27. Zughaid, H., et al., *Bile salt composition is secondary to bile salt concentration in determining hydrocortisone and progesterone solubility in intestinal mimetic fluids.* Int J Pharm, 2012. **422**(1-2): p. 295-301.
28. Lange, D., et al., *Effect of a cola beverage on the bioavailability of itraconazole in the presence of H2 blockers.* J Clin Pharmacol, 1997. **37**(6): p. 535-40.
29. Huang, N.N. and R.H. High, *Comparison of serum levels following the administration of oral and parenteral preparations of penicillin to infants and children of various age groups.* J Pediatr, 1953. **42**(6): p. 657-8.
30. Pedersen, S. and G. Steffensen, *Absorption characteristics of once-a-day slow-release theophylline preparation in children with asthma.* J Pediatr, 1987. **110**(6): p. 953-9.
31. Heimann, G., *Enteral absorption and bioavailability in children in relation to age.* European Journal of Clinical Pharmacology, 1980. **18**(1): p. 43-50.
32. Bonner, J.J., et al., *Does age affect gastric emptying time? A model-based meta-analysis of data from premature neonates through to adults.* Biopharm Drug Dispos, 2015. **36**(4): p. 245-257.
33. Brouwer, K.L., et al., *Human Ontogeny of Drug Transporters: Review and Recommendations of the Pediatric Transporter Working Group.* Clin Pharmacol Ther, 2015. **98**(3): p. 266-87.

34. Estudante, M., et al., *Intestinal drug transporters: an overview.* Adv Drug Deliv Rev, 2013. **65**(10): p. 1340-56.
35. Watkins, P.B., *The barrier function of CYP3A4 and P-glycoprotein in the small bowel.* Adv Drug Deliv Rev, 1997. **27**(2): p. 161-170.
36. Feltrin, C. and C.M. Oliveira Simoes, *Reviewing the mechanisms of natural product-drug interactions involving efflux transporters and metabolic enzymes.* Chem Biol Interact, 2019. **314**: p. 108825.
37. Johnson, T.N. and M. Thomson, *Intestinal Metabolism and Transport of Drugs in Children: The Effects of Age and Disease.* Journal of Pediatric Gastroenterology and Nutrition, 2008. **47**(1): p. 3-10.
38. Oda, S., et al., *A comprehensive review of UDP-glucuronosyltransferase and esterases for drug development.* Drug Metab Pharmacokinet, 2015. **30**(1): p. 30-51.
39. Achour, B., J. Barber, and A. Rostami-Hodjegan, *Expression of hepatic drug-metabolizing cytochrome p450 enzymes and their intercorrelations: a meta-analysis.* Drug Metab Dispos, 2014. **42**(8): p. 1349-56.
40. Johnson, T.N., B.G. Small, and K. Rowland Yeo, *Increasing application of pediatric physiologically based pharmacokinetic models across academic and industry organizations.* CPT Pharmacometrics Syst Pharmacol, 2022. **11**(3): p. 373-383.
41. Rodriguez, W., et al., *Improving Pediatric Dosing Through Pediatric Initiatives: What We Have Learned.* Pediatrics, 2008. **121**(3): p. 530-539.
42. Bartelink, I.H., et al., *Guidelines on paediatric dosing on the basis of developmental physiology and pharmacokinetic considerations.* Clin Pharmacokinet, 2006. **45**(11): p. 1077-97.
43. Björkman, S., *Prediction of drug disposition in infants and children by means of physiologically based pharmacokinetic (PBPK) modelling: theophylline and midazolam as model drugs.* Br J Clin Pharmacol, 2005. **59**(6): p. 691-704.
44. Johnson, T.N., *The problems in scaling adult drug doses to children.* Arch Dis Child, 2008. **93**(3): p. 207-11.
45. Munzenberger, P.J. and P. McKercher, *Pediatric dosing--the pharmacist's dilemma.* Contemp Pharm Pract, 1980. **3**(1): p. 11-4.
46. Yellepeddi, V., et al., *State-of-the-Art Review on Physiologically Based Pharmacokinetic Modeling in Pediatric Drug Development.* Clin Pharmacokinet, 2019. **58**(1): p. 1-13.
47. Calvier, E.A., et al., *Allometric Scaling of Clearance in Paediatric Patients: When Does the Magic of 0.75 Fade?* Clin Pharmacokinet, 2017. **56**(3): p. 273-285.
48. Dumont, C., et al., *Optimal sampling times for a drug and its metabolite using SIMCYP(®) simulations as prior information.* Clin Pharmacokinet, 2013. **52**(1): p. 43-57.
49. Khalil, F. and S. Läer, *Physiologically based pharmacokinetic modeling: methodology, applications, and limitations with a focus on its role in pediatric drug development.* J Biomed Biotechnol, 2011. **2011**: p. 907461.
50. Van Den Driessche, M., et al., *Lactose-[13C]ureide breath test: a new, noninvasive technique to determine orocecal transit time in children.* J Pediatr Gastroenterol Nutr, 2000. **31**(4): p. 433-8.
51. Ferro, A., *Paediatric prescribing: why children are not small adults.* Br J Clin Pharmacol, 2015. **79**(3): p. 351-3.

52. Joseph, P.D., J.C. Craig, and P.H. Caldwell, *Clinical trials in children.* Br J Clin Pharmacol, 2015. **79**(3): p. 357-69.
53. EMA, *GUIDELINE ON THE INVESTIGATION OF MEDICINAL PRODUCTS IN THE TERM AND PRETERM NEONATE*, C.f.M.P.f.H. Use, Editor. 2007: London.
54. Momper, J.D., Y. Mulugeta, and G.J. Burckart, *Failed Pediatric Drug Development Trials.* Clin Pharmacol Ther, 2015. **98**(3): p. 245-51.
55. Guidi, M., C. Csajka, and T. Buclin, *Parametric Approaches in Population Pharmacokinetics.* J Clin Pharmacol, 2022. **62**(2): p. 125-141.
56. De Cock, R.F., et al., *The role of population PK-PD modelling in paediatric clinical research.* Eur J Clin Pharmacol, 2011. **67 Suppl 1**(Suppl 1): p. 5-16.
57. Cella, M., et al., *Paediatric drug development: are population models predictive of pharmacokinetics across paediatric populations?* Br J Clin Pharmacol, 2011. **72**(3): p. 454-64.
58. El-Khateeb, E., et al., *Physiological-based pharmacokinetic modeling trends in pharmaceutical drug development over the last 20-years; in-depth analysis of applications, organizations, and platforms.* Biopharm Drug Dispos, 2021. **42**(4): p. 107-117.
59. Aarons, L., *Physiologically based pharmacokinetic modelling: a sound mechanistic basis is needed.* Br J Clin Pharmacol, 2005. **60**(6): p. 581-583.
60. Maharaj, A.R. and A.N. Edginton, *Physiologically based pharmacokinetic modeling and simulation in pediatric drug development.* CPT Pharmacometrics Syst Pharmacol, 2014. **3**(11): p. e150.
61. Rowland Yeo, K. and T.N. Johnson, *Advancing Pediatric Drug Development and Regulatory Acceptance Using Simcyp PBPK: from Birth to Young Adult*, Certara, Editor. 2022.
62. Grimstein, M., et al., *Physiologically Based Pharmacokinetic Modeling in Regulatory Science: An Update From the U.S. Food and Drug Administration's Office of Clinical Pharmacology.* J Pharm Sci, 2019. **108**(1): p. 21-25.
63. Krekels, E.H., et al., *Systematic evaluation of the descriptive and predictive performance of paediatric morphine population models.* Pharm Res, 2011. **28**(4): p. 797-811.
64. Johnson, T.N., et al., *A best practice framework for applying physiologically-based pharmacokinetic modeling to pediatric drug development.* CPT Pharmacometrics Syst Pharmacol, 2021. **10**(9): p. 967-972.
65. Shebley, M., et al., *Physiologically Based Pharmacokinetic Model Qualification and Reporting Procedures for Regulatory Submissions: A Consortium Perspective.* Clin Pharmacol Ther, 2018. **104**(1): p. 88-110.
66. Johnson, T.N., D. Zhou, and K.H. Bui, *Development of physiologically based pharmacokinetic model to evaluate the relative systemic exposure to quetiapine after administration of IR and XR formulations to adults, children and adolescents.* Biopharm Drug Dispos, 2014. **35**(6): p. 341-352.
67. Tsamandouras, N., A. Rostami-Hodjegan, and L. Aarons, *Combining the 'bottom up' and 'top down' approaches in pharmacokinetic modelling: fitting PBPK models to observed clinical data.* Br J Clin Pharmacol, 2015. **79**(1): p. 48-55.
68. Jamei, M., et al., *Population-based mechanistic prediction of oral drug absorption.* Aaps j, 2009. **11**(2): p. 225-37.

69. Gobeau, N., et al., *Evaluation of the GastroPlus™ Advanced Compartmental and Transit (ACAT) Model in Early Discovery.* Pharmaceutical Research, 2016. **33**(9): p. 2126-2139.
70. Sjögren, E., H. Thörn, and C. Tannergren, *In Silico Modeling of Gastrointestinal Drug Absorption: Predictive Performance of Three Physiologically Based Absorption Models.* Mol Pharm, 2016. **13**(6): p. 1763-78.
71. Bolger, M.B., V. Lukacova, and W.S. Woltosz, *Simulations of the nonlinear dose dependence for substrates of influx and efflux transporters in the human intestine.* Aaps j, 2009. **11**(2): p. 353-63.
72. Wu, F., et al., *Computational Approaches in Preclinical Studies on Drug Discovery and Development.* Front Chem, 2020. **8**: p. 726.
73. Prieto Garcia, L., et al., *Does the choice of applied physiologically-based pharmacokinetics platform matter? A case study on simvastatin disposition and drug–drug interaction.* CPT: Pharmacometrics & Systems Pharmacology, 2022. **11**(9): p. 1194-1209.
74. Kuepfer, L., et al., *Applied Concepts in PBPK Modeling: How to Build a PBPK/PD Model.* CPT Pharmacometrics Syst Pharmacol, 2016. **5**(10): p. 516-531.
75. Jamei, M., et al., *The Simcyp population-based ADME simulator.* Expert Opin Drug Metab Toxicol, 2009. **5**(2): p. 211-23.
76. Kostewicz, E.S., et al., *PBPK models for the prediction of in vivo performance of oral dosage forms.* Eur J Pharm Sci, 2014. **57**: p. 300-21.
77. Jamei, M., et al., *The simcyp population based simulator: architecture, implementation, and quality assurance.* In Silico Pharmacol, 2013. **1**: p. 9.
78. Abuqayyas, L. and J.P. Balthasar, *Application of PBPK modeling to predict monoclonal antibody disposition in plasma and tissues in mouse models of human colorectal cancer.* J Pharmacokinet Pharmacodyn, 2012. **39**(6): p. 683-710.
79. Hatley, O.J., et al., *Quantifying gut wall metabolism: methodology matters.* Biopharm Drug Dispos, 2017. **38**(2): p. 155-160.
80. Couto, N., et al., *Quantitative Proteomics of Clinically Relevant Drug-Metabolizing Enzymes and Drug Transporters and Their Intercorrelations in the Human Small Intestine.* Drug Metab Dispos, 2020. **48**(4): p. 245-254.
81. Hellriegel, E.T., T.D. Bjornsson, and W.W. Hauck, *Interpatient variability in bioavailability is related to the extent of absorption: implications for bioavailability and bioequivalence studies.* Clin Pharmacol Ther, 1996. **60**(6): p. 601-7.
82. Strolin Benedetti, M. and E.L. Baltes, *Drug metabolism and disposition in children.* Fundam Clin Pharmacol, 2003. **17**(3): p. 281-99.
83. Berseth, C.L., *Neonatal small intestinal motility: Motor responses to feeding in term and preterm infants.* The Journal of Pediatrics, 1990. **117**(5): p. 777-782.
84. Ke, A., et al., *Towards a Best Practice Approach in PBPK Modeling: Case Example of Developing a Unified Efavirenz Model Accounting for Induction of CYPs 3A4 and 2B6.* CPT: Pharmacometrics & Systems Pharmacology, 2016. **5**(7): p. 367-376.
85. International Programme on Chemical, S. and C. Inter-Organization Programme for the Sound Management of, *Characterization and application of physiologically based phamacokinetic models in risk assessment*. 2010, World Health Organization: Geneva.

86. Nestorov, I.A., L.J. Aarons, and M. Rowland, *Physiologically based pharmacokinetic modeling of a homologous series of barbiturates in the rat: a sensitivity analysis.* J Pharmacokinet Biopharm, 1997. **25**(4): p. 413-47.
87. Gueorguieva, I., I.A. Nestorov, and M. Rowland, *Reducing whole body physiologically based pharmacokinetic models using global sensitivity analysis: diazepam case study.* J Pharmacokinet Pharmacodyn, 2006. **33**(1): p. 1-27.
88. Maharaj, A.R., J.S. Barrett, and A.N. Edginton, *A workflow example of PBPK modeling to support pediatric research and development: case study with lorazepam.* Aaps j, 2013. **15**(2): p. 455-64.
89. Haycock, G.B., G.J. Schwartz, and D.H. Wisotsky, *Geometric method for measuring body surface area: a height-weight formula validated in infants, children, and adults.* J Pediatr, 1978. **93**(1): p. 62-6.
90. DuBois, D. and E. DuBois, *A formula to estimate the approximate surface area if heigt and weight are known.* Arch Intern Med, 1916. **17**: p. 863-71.
91. Johnson, T.N., et al., *Changes in liver volume from birth to adulthood: a meta-analysis.* Liver Transpl, 2005. **11**(12): p. 1481-93.
92. Guyton, A.C., T.Q. Richardson, and J.B. Langston, *Regulation of cardiac output and venous return.* Clin Anesth, 1964. **3**: p. 1-34.
93. Rubin, M.I., E. Bruck, and M. Rapoport, *Maturation of renal function in childhood; clearance studies.* J Clin Invest, 1949. **28**(5 Pt 2): p. 1144-62.
94. Brussee, J.M., et al., *First-Pass CYP3A-Mediated Metabolism of Midazolam in the Gut Wall and Liver in Preterm Neonates.* CPT Pharmacometrics Syst Pharmacol, 2018. **7**(6): p. 374-383.
95. *Basic anatomical and physiological data for use in radiological protection: reference values. A report of age- and gender-related differences in the anatomical and physiological characteristics of reference individuals. ICRP Publication 89.* Ann ICRP, 2002. **32**(3-4): p. 5-265.
96. Paine, M.F., et al., *Characterization of interintestinal and intraintestinal variations in human CYP3A-dependent metabolism.* J Pharmacol Exp Ther, 1997. **283**(3): p. 1552-62.
97. Yang, J., G.T. Tucker, and A. Rostami-Hodjegan, *Cytochrome P450 3A expression and activity in the human small intestine.* Clin Pharmacol Ther, 2004. **76**(4): p. 391.
98. Kiss, M., et al., *Ontogeny of Small Intestinal Drug Transporters and Metabolizing Enzymes Based on Targeted Quantitative Proteomics.* Drug Metabolism and Disposition, 2021: p. DMD-AR-2021-000559.
99. Bermejo, M., et al., *A Mechanistic Physiologically-Based Biopharmaceutics Modeling (PBBM) Approach to Assess the In Vivo Performance of an Orally Administered Drug Product: From IVIVC to IVIVP.* Pharmaceutics, 2020. **12**(1).
100. Salerno, S.N., et al., *Pediatric Drug-Drug Interaction Studies: Barriers and Opportunities.* Clin Pharmacol Ther, 2019. **105**(5): p. 1067-1070.
101. Gonzalez, D. and J. Sinha, *Pediatric Drug-Drug Interaction Evaluation: Drug, Patient Population, and Methodological Considerations.* J Clin Pharmacol, 2021. **61 Suppl 1**(Suppl 1): p. S175-s187.
102. Cristea, S., et al., *The Influence of Drug Properties and Ontogeny of Transporters on Pediatric Renal Clearance through Glomerular Filtration and Active Secretion: a Simulation-Based Study.* Aaps j, 2020. **22**(4): p. 87.

103. Combes, F.P., et al., *Model-Informed Drug Development for Everolimus Dosing Selection in Pediatric Infant Patients.* CPT Pharmacometrics Syst Pharmacol, 2020. **9**(4): p. 230-237.
104. Bonner, J.J., et al., *Development and verification of an endogenous PBPK model to inform hydrocortisone replacement dosing in children and adults with cortisol deficiency.* Eur J Pharm Sci, 2021. **165**: p. 105913.
105. Conner, T.M., R.C. Reed, and T. Zhang, *A Physiologically Based Pharmacokinetic Model for Optimally Profiling Lamotrigine Disposition and Drug-Drug Interactions.* Eur J Drug Metab Pharmacokinet, 2019. **44**(3): p. 389-408.
106. Johnson, T.N., et al., *Use of a physiologically based pharmacokinetic-pharmacodynamic model for initial dose prediction and escalation during a paediatric clinical trial.* Br J Clin Pharmacol, 2021. **87**(3): p. 1378-1389.
107. Li, A., et al., *Development of Guanfacine Extended-Release Dosing Strategies in Children and Adolescents with ADHD Using a Physiologically Based Pharmacokinetic Model to Predict Drug-Drug Interactions with Moderate CYP3A4 Inhibitors or Inducers.* Paediatr Drugs, 2018. **20**(2): p. 181-194.
108. Li, A., et al., *Correction to: Development of Guanfacine Extended-Release Dosing Strategies in Children and Adolescents with ADHD Using a Physiologically Based Pharmacokinetic Model to Predict Drug-Drug Interactions with Moderate CYP3A4 Inhibitors or Inducers.* Paediatr Drugs, 2018. **20**(2): p. 205.
109. Cleary, Y., et al., *Model-Based Drug-Drug Interaction Extrapolation Strategy From Adults to Children: Risdiplam in Pediatric Patients With Spinal Muscular Atrophy.* Clin Pharmacol Ther, 2021. **110**(6): p. 1547-1557.
110. Heijerman, H.G.M., et al., *Efficacy and safety of the elexacaftor plus tezacaftor plus ivacaftor combination regimen in people with cystic fibrosis homozygous for the F508del mutation: a double-blind, randomised, phase 3 trial.* Lancet, 2019. **394**(10212): p. 1940-1948.
111. Tsai, A., et al., *Physiologically Based Pharmacokinetic Modeling of CFTR Modulation in People with Cystic Fibrosis Transitioning from Mono or Dual Regimens to Triple-Combination Elexacaftor/Tezacaftor/Ivacaftor.* Pulm Ther, 2020. **6**(2): p. 275-286.
112. Tsai, A., et al., *Correction to: Physiologically Based Pharmacokinetic Modeling of CFTR Modulation in People with Cystic Fibrosis Transitioning from Mono or Dual Regimens to Triple-Combination Elexacaftor/Tezacaftor/Ivacaftor.* Pulm Ther, 2020. **6**(2): p. 287.
113. El-Khateeb, E., et al., *Quantitative mass spectrometry-based proteomics in the era of model-informed drug development: Applications in translational pharmacology and recommendations for best practice.* Pharmacology & Therapeutics, 2019. **203**: p. 107397.
114. Harwood, M., *Towards a Fully Mechanistic Prediction of Oral Drug Absorption: Investigating Intestinal Transporter Abundance & Function Relationships*, in *Faculty of Medical and Human Sciences*. 2015, University of Manchester: Manchester. p. 277.
115. Harwood, M.D., et al., *Application of an LC-MS/MS method for the simultaneous quantification of human intestinal transporter proteins absolute abundance using a QconCAT technique.* J Pharm Biomed Anal, 2015. **110**: p. 27-33.
116. Oswald, S., et al., *Intestinal expression of P-glycoprotein (ABCB1), multidrug resistance associated protein 2 (ABCC2), and uridine diphosphate-*

glucuronosyltransferase 1A1 predicts the disposition and modulates the effects of the cholesterol absorption inhibitor ezetimibe in humans. Clin Pharmacol Ther, 2006. **79**(3): p. 206-17.
117. Glaeser, H., et al., *Intestinal drug transporter expression and the impact of grapefruit juice in humans.* Clin Pharmacol Ther, 2007. **81**(3): p. 362-70.
118. Westphal, K., et al., *Induction of P-glycoprotein by rifampin increases intestinal secretion of talinolol in human beings: a new type of drug/drug interaction.* Clin Pharmacol Ther, 2000. **68**(4): p. 345-55.
119. Bailey, D.G., et al., *Interaction of citrus juices with felodipine and nifedipine.* Lancet, 1991. **337**(8736): p. 268-9.
120. Kolars, J.C., et al., *First-pass metabolism of cyclosporin by the gut.* Lancet, 1991. **338**(8781): p. 1488-90.
121. Paine, M.F., et al., *First-pass metabolism of midazolam by the human intestine.* Clin Pharmacol Ther, 1996. **60**(1): p. 14-24.
122. Ducharme, M.P., L.H. Warbasse, and D.J. Edwards, *Disposition of intravenous and oral cyclosporine after administration with grapefruit juice.* Clin Pharmacol Ther, 1995. **57**(5): p. 485-91.
123. Kupferschmidt, H.H., et al., *Interaction between grapefruit juice and midazolam in humans.* Clin Pharmacol Ther, 1995. **58**(1): p. 20-8.
124. de Waal, T., et al., *The impact of inflammation on the expression of drug transporters and metabolic enzymes in colonic tissue from ulcerative colitis patients.* Int J Pharm, 2022. **628**: p. 122282.
125. Drozdzik, M., et al., *Protein abundance of clinically relevant multidrug transporters along the entire length of the human intestine.* Mol Pharm, 2014. **11**(10): p. 3547-55.
126. Cheung, K.W.K., et al., *Incorporating Ontogeny in Physiologically Based Pharmacokinetic Modeling to Improve Pediatric Drug Development: What We Know About Developmental Changes in Membrane Transporters.* J Clin Pharmacol, 2019. **59 Suppl 1**: p. S56-s69.
127. Berggren, S., et al., *Gene and protein expression of P-glycoprotein, MRP1, MRP2, and CYP3A4 in the small and large human intestine.* Mol Pharm, 2007. **4**(2): p. 252-7.
128. Englund, G., et al., *Regional levels of drug transporters along the human intestinal tract: co-expression of ABC and SLC transporters and comparison with Caco-2 cells.* Eur J Pharm Sci, 2006. **29**(3-4): p. 269-77.
129. Hilgendorf, C., et al., *Expression of thirty-six drug transporter genes in human intestine, liver, kidney, and organotypic cell lines.* Drug Metab Dispos, 2007. **35**(8): p. 1333-40.
130. Meier, Y., et al., *Regional Distribution of Solute Carrier mRNA Expression Along the Human Intestinal Tract.* Drug Metabolism and Disposition, 2007. **35**(4): p. 590-594.
131. Seithel, A., et al., *Variability in mRNA expression of ABC- and SLC-transporters in human intestinal cells: comparison between human segments and Caco-2 cells.* Eur J Pharm Sci, 2006. **28**(4): p. 291-9.
132. Zimmermann, C., et al., *MAPPING OF MULTIDRUG RESISTANCE GENE 1 AND MULTIDRUG RESISTANCE-ASSOCIATED PROTEIN ISOFORM 1 TO 5 mRNA EXPRESSION ALONG THE HUMAN INTESTINAL TRACT.* Drug Metabolism and Disposition, 2005. **33**(2): p. 219-224.
133. Mouly, S. and M.F. Paine, *P-Glycoprotein Increases from Proximal to Distal Regions of Human Small Intestine.* Pharmaceutical Research, 2003. **20**(10): p. 1595-1599.

134. Paine, M.F., et al., *The human intestinal cytochrome P450 "pie".* Drug Metab Dispos, 2006. **34**(5): p. 880-6.
135. Drozdzik, M., et al., *Protein Abundance of Clinically Relevant Drug Transporters in the Human Liver and Intestine: A Comparative Analysis in Paired Tissue Specimens.* Clin Pharmacol Ther, 2019. **105**(5): p. 1204-1212.
136. Harwood, M.D., et al., *The Regional-Specific Relative and Absolute Expression of Gut Transporters in Adult Caucasians: A Meta-Analysis.* Drug Metab Dispos, 2019. **47**(8): p. 854-864.
137. Couto, N., et al., *Correction to "Quantitative Proteomics of Clinically Relevant Drug-Metabolizing Enzymes and Drug Transporters and Their Intercorrelations in the Human Small Intestine".* Drug Metab Dispos, 2020. **48**(5): p. 407.
138. Sjögren, E., et al., *In silico predictions of gastrointestinal drug absorption in pharmaceutical product development: application of the mechanistic absorption model GI-Sim.* Eur J Pharm Sci, 2013. **49**(4): p. 679-98.
139. Vertzoni, M., et al., *Impact of regional differences along the gastrointestinal tract of healthy adults on oral drug absorption: An UNGAP review.* Eur J Pharm Sci, 2019. **134**: p. 153-175.
140. Olivares-Morales, A., et al., *Translating Human Effective Jejunal Intestinal Permeability to Surface-Dependent Intrinsic Permeability: a Pragmatic Method for a More Mechanistic Prediction of Regional Oral Drug Absorption.* Aaps j, 2015. **17**(5): p. 1177-92.
141. Kunta, J.R. and P.J. Sinko, *Intestinal drug transporters: in vivo function and clinical importance.* Curr Drug Metab, 2004. **5**(1): p. 109-24.
142. Miyauchi, E., et al., *Quantitative Atlas of Cytochrome P450, UDP-Glucuronosyltransferase, and Transporter Proteins in Jejunum of Morbidly Obese Subjects.* Mol Pharm, 2016. **13**(8): p. 2631-40.
143. van Groen, B.D., et al., *Ontogeny of Hepatic Transporters and Drug-Metabolizing Enzymes in Humans and in Nonclinical Species.* Pharmacol Rev, 2021. **73**(2): p. 597-678.
144. Galetin, A. and J.B. Houston, *Intestinal and hepatic metabolic activity of five cytochrome P450 enzymes: impact on prediction of first-pass metabolism.* J Pharmacol Exp Ther, 2006. **318**(3): p. 1220-9.
145. Streekstra, E.J., et al., *Application of proteomics to understand maturation of drug metabolizing enzymes and transporters for the optimization of pediatric drug therapy.* Drug Discov Today Technol, 2021. **39**: p. 31-48.
146. van Groen, B.D., et al., *Proteomics of human liver membrane transporters: a focus on fetuses and newborn infants.* European Journal of Pharmaceutical Sciences, 2018. **124**: p. 217-227.
147. Prasad, B., et al., *Interindividual Variability in Hepatic Organic Anion-Transporting Polypeptides and P-Glycoprotein (ABCB1) Protein Expression: Quantification by Liquid Chromatography Tandem Mass Spectroscopy and Influence of Genotype, Age, and Sex.* Drug Metabolism and Disposition, 2014. **42**(1): p. 78-88.
148. Prasad, B., et al., *Ontogeny of Hepatic Drug Transporters as Quantified by LC-MS/MS Proteomics.* Clinical Pharmacology & Therapeutics, 2016. **100**(4): p. 362-370.
149. Prasad, B., et al., *Interindividual variability in the hepatic expression of the human breast cancer resistance protein (BCRP/ABCG2): effect of age, sex, and genotype.* J Pharm Sci, 2013. **102**(3): p. 787-93.

150. Bhatt, D.K., et al., *Age- and Genotype-Dependent Variability in the Protein Abundance and Activity of Six Major Uridine Diphosphate-Glucuronosyltransferases in Human Liver.* Clinical Pharmacology & Therapeutics, 2019. **105**(1): p. 131-141.
151. Dubaisi, S., et al., *Developmental Expression of the Cytosolic Sulfotransferases in Human Liver.* Drug Metabolism and Disposition, 2019. **47**(6): p. 592-600.
152. Ladumor, M.K., et al., *Ontogeny of Hepatic Sulfotransferases and Prediction of Age-Dependent Fractional Contribution of Sulfation in Acetaminophen Metabolism.* Drug Metabolism and Disposition, 2019. **47**(8): p. 818-831.
153. Ladumor, M.K., et al., *A repository of protein abundance data of drug metabolizing enzymes and transporters for applications in physiologically based pharmacokinetic (PBPK) modelling and simulation.* Sci Rep, 2019. **9**(1): p. 9709.
154. Bhatt, D.K., et al., *Hepatic Abundance and Activity of Androgen- and Drug-Metabolizing Enzyme UGT2B17 Are Associated with Genotype, Age, and Sex.* Drug Metabolism and Disposition, 2018. **46**(6): p. 888-896.
155. Bhatt, D.K., et al., *Age-dependent Protein Abundance of Cytosolic Alcohol and Aldehyde Dehydrogenases in Human Liver.* Drug Metabolism and Disposition, 2017. **45**(9): p. 1044-1048.
156. Sadler, N.C., et al., *Hepatic Cytochrome P450 Activity, Abundance, and Expression Throughout Human Development.* Drug Metabolism and Disposition, 2016. **44**(7): p. 984-991.
157. Zane, N.R., et al., *Cytochrome P450 and flavin-containing monooxygenase families: age-dependent differences in expression and functional activity.* Pediatric Research, 2018. **83**(2): p. 527-535.
158. Cheung, K.W.K., et al., *A Comprehensive Analysis of Ontogeny of Renal Drug Transporters: mRNA Analyses, Quantitative Proteomics, and Localization.* Clinical Pharmacology & Therapeutics, 2019. **106**(5): p. 1083-1092.
159. Li, C.Y., et al., *Optimized Renal Transporter Quantification by Using Aquaporin 1 and Aquaporin 2 as Anatomical Markers: Application in Characterizing the Ontogeny of Renal Transporters and Its Correlation with Hepatic Transporters in Paired Human Samples.* The AAPS Journal, 2019. **21**(5): p. 88.
160. Achour, B., et al., *Liquid Biopsy Enables Quantification of the Abundance and Interindividual Variability of Hepatic Enzymes and Transporters.* Clinical Pharmacology and Therapeutics, 2021. **109**(1): p. 222-232.
161. Couto, N., et al., *Quantification of Proteins Involved in Drug Metabolism and Disposition in the Human Liver Using Label-Free Global Proteomics.* Mol Pharm, 2019. **16**(2): p. 632-647.
162. Al-Majdoub, Z.M., et al., *Quantification of Proteins Involved in Intestinal Epithelial Handling of Xenobiotics.* Clinical Pharmacology and Therapeutics, 2020.
163. Al-Majdoub, Z.M., et al., *Mass spectrometry-based abundance atlas of ABC transporters in human liver, gut, kidney, brain and skin.* FEBS Letters, 2020. **594**(23): p. 4134-4150.
164. Al Feteisi, H., et al., *Identification and quantification of blood-brain barrier transporters in isolated rat brain microvessels.* J Neurochem, 2018. **146**(6): p. 670-685.
165. Al Feteisi, H., et al., *Choice of LC-MS Methods for the Absolute Quantification of Drug-Metabolizing Enzymes and Transporters in Human Tissue: a Comparative Cost Analysis.* The AAPS Journal, 2015. **17**(2): p. 438-446.

166. Mooij, M.G., et al., *Human Intestinal PEPT1 Transporter Expression and Localization in Preterm and Term Infants.* Drug Metab Dispos, 2016. **44**(7): p. 1014-9.
167. Mooij, M.G., et al., *Ontogeny of human hepatic and intestinal transporter gene expression during childhood: age matters.* Drug Metab Dispos, 2014. **42**(8): p. 1268-74.
168. Stillhart, C., et al., *Impact of gastrointestinal physiology on drug absorption in special populations—An UNGAP review.* European Journal of Pharmaceutical Sciences, 2020. **147**: p. 105280.
169. Johnson, T.N., *The development of drug metabolising enzymes and their influence on the susceptibility to adverse drug reactions in children.* Toxicology, 2003. **192**(1): p. 37-48.
170. Johnson, T.N., M.S. Tanner, and G.T. Tucker, *A comparison of the ontogeny of enterocytic and hepatic cytochromes P450 3A in the rat.* Biochem Pharmacol, 2000. **60**(11): p. 1601-10.
171. Konieczna, A., et al., *Differential expression of ABC transporters (MDR1, MRP1, BCRP) in developing human embryos.* J Mol Histol, 2011. **42**(6): p. 567-74.
172. Vannay, A., et al., *Increased expression of hypoxia-inducible factor 1alpha in coeliac disease.* Pediatr Res, 2010. **68**(2): p. 118-22.
173. Fakhoury, M., et al., *Impact of inflammation on the duodenal mRNA expression of CYP3A and P-glycoprotein in children with Crohn's disease.* Inflamm Bowel Dis, 2006. **12**(8): p. 745-9.
174. Fakhoury, M., et al., *mRNA expression of MDR1 and major metabolising enzymes in human fetal tissues.* Drug Metab Pharmacokinet, 2009. **24**(6): p. 529-36.
175. Fakhoury, M., et al., *LOCALIZATION AND mRNA EXPRESSION OF CYP3A AND P-GLYCOPROTEIN IN HUMAN DUODENUM AS A FUNCTION OF AGE.* Drug Metabolism and Disposition, 2005. **33**(11): p. 1603-1607.
176. Miki, Y., et al., *Steroid and xenobiotic receptor (SXR), cytochrome P450 3A4 and multidrug resistance gene 1 in human adult and fetal tissues.* Mol Cell Endocrinol, 2005. **231**(1-2): p. 75-85.
177. Giacomini, K.M., et al., *Membrane transporters in drug development.* Nat Rev Drug Discov, 2010. **9**(3): p. 215-36.
178. Zamek-Gliszczynski, M.J., et al., *Transporters in Drug Development: 2018 ITC Recommendations for Transporters of Emerging Clinical Importance.* Clin Pharmacol Ther, 2018. **104**(5): p. 890-899.
179. Hillgren, K.M., et al., *Emerging transporters of clinical importance: an update from the International Transporter Consortium.* Clin Pharmacol Ther, 2013. **94**(1): p. 52-63.
180. Xie, F., X. Ding, and Q.Y. Zhang, *An update on the role of intestinal cytochrome P450 enzymes in drug disposition.* Acta Pharm Sin B, 2016. **6**(5): p. 374-383.
181. Zhou, X., et al., *Quantitative Proteomic Analysis of Porcine Intestinal Epithelial Cells Infected with Porcine Deltacoronavirus Using iTRAQ-Coupled LC-MS/MS.* Journal of Proteome Research, 2020. **19**(11): p. 4470-4485.
182. Fritz, A., et al., *Expression of clinically relevant drug-metabolizing enzymes along the human intestine and their correlation to drug transporters and nuclear receptors: An intra-subject analysis.* Basic Clin Pharmacol Toxicol, 2019. **124**(3): p. 245-255.
183. Bruckmueller, H., et al., *Clinically Relevant Multidrug Transporters Are Regulated by microRNAs along the Human Intestine.* Mol Pharm, 2017. **14**(7): p. 2245-2253.

184. Li, C.Y., et al., *Major glucuronide metabolites of testosterone are primarily transported by MRP2 and MRP3 in human liver, intestine and kidney.* J Steroid Biochem Mol Biol, 2019. **191**: p. 105350.
185. Dawson, P.A., *Role of the intestinal bile acid transporters in bile acid and drug disposition.* Handb Exp Pharmacol, 2011(201): p. 169-203.
186. Lloret-Linares, C., et al., *Oral Morphine Pharmacokinetic in Obesity: The Role of P-Glycoprotein, MRP2, MRP3, UGT2B7, and CYP3A4 Jejunal Contents and Obesity-Associated Biomarkers.* Mol Pharm, 2016. **13**(3): p. 766-773.
187. de Waart, D.R., et al., *Oral availability of cefadroxil depends on ABCC3 and ABCC4.* Drug Metab Dispos, 2012. **40**(3): p. 515-21.
188. Brandsch, M., *Drug transport via the intestinal peptide transporter PepT1.* Curr Opin Pharmacol, 2013. **13**(6): p. 881-7.
189. Brandsch, M., I. Knütter, and E. Bosse-Doenecke, *Pharmaceutical and pharmacological importance of peptide transporters.* J Pharm Pharmacol, 2008. **60**(5): p. 543-85.
190. Weitschies, W., et al., *Bioavailability of amoxicillin and clavulanic acid from extended release tablets depends on intragastric tablet deposition and gastric emptying.* Eur J Pharm Biopharm, 2008. **70**(2): p. 641-8.
191. Barr, W.H., et al., *Differential absorption of amoxicillin from the human small and large intestine.* Clin Pharmacol Ther, 1994. **56**(3): p. 279-85.
192. Cortvriendt, W.R., J.S. Verschoor, and W. Hespe, *Bioavailability study of a new amoxicillin tablet designed for several modes of oral administration.* Arzneimittelforschung, 1987. **37**(8): p. 977-9.
193. Ganapathy, M.E., et al., *Valacyclovir: a substrate for the intestinal and renal peptide transporters PEPT1 and PEPT2.* Biochem Biophys Res Commun, 1998. **246**(2): p. 470-5.
194. Han, H., et al., *5'-Amino acid esters of antiviral nucleosides, acyclovir, and AZT are absorbed by the intestinal PEPT1 peptide transporter.* Pharm Res, 1998. **15**(8): p. 1154-9.
195. Yang, B. and D.E. Smith, *Significance of peptide transporter 1 in the intestinal permeability of valacyclovir in wild-type and PepT1 knockout mice.* Drug Metab Dispos, 2013. **41**(3): p. 608-14.
196. Groer, C., et al., *LC-MS/MS-based quantification of clinically relevant intestinal uptake and efflux transporter proteins.* J Pharm Biomed Anal, 2013. **85**: p. 253-61.
197. Tucker, T.G., et al., *Absolute immunoquantification of the expression of ABC transporters P-glycoprotein, breast cancer resistance protein and multidrug resistance-associated protein 2 in human liver and duodenum.* Biochem Pharmacol, 2012. **83**(2): p. 279-85.
198. Oswald, S., et al., *Mass spectrometry-based targeted proteomics as a tool to elucidate the expression and function of intestinal drug transporters.* The AAPS Journal, 2013. **15**(4): p. 1128-1140.
199. Wenzel, C., M. Drozdzik, and S. Oswald, *Organic Cation Transporter 1 an Intestinal Uptake Transporter: Fact or Fiction?* Front Pharmacol, 2021. **12**: p. 648388.
200. Gertz, M., J.B. Houston, and A. Galetin, *Physiologically based pharmacokinetic modeling of intestinal first-pass metabolism of CYP3A substrates with high intestinal extraction.* Drug Metab Dispos, 2011. **39**(9): p. 1633-42.

201. Pinto, A.G., et al., *Diltiazem inhibits human intestinal cytochrome P450 3A (CYP3A) activity in vivo without altering the expression of intestinal mRNA or protein.* Br J Clin Pharmacol, 2005. **59**(4): p. 440-6.
202. Ritter, J.K., *Roles of glucuronidation and UDP-glucuronosyltransferases in xenobiotic bioactivation reactions.* Chem Biol Interact, 2000. **129**(1-2): p. 171-93.
203. Williams, J.A., et al., *DRUG-DRUG INTERACTIONS FOR UDP-GLUCURONOSYLTRANSFERASE SUBSTRATES: A PHARMACOKINETIC EXPLANATION FOR TYPICALLY OBSERVED LOW EXPOSURE (AUC_I/AUC) RATIOS.* Drug Metabolism and Disposition, 2004. **32**(11): p. 1201-1208.
204. Harbourt, D.E., et al., *Quantification of human uridine-diphosphate glucuronosyl transferase 1A isoforms in liver, intestine, and kidney using nanobore liquid chromatography-tandem mass spectrometry.* Anal Chem, 2012. **84**(1): p. 98-105.
205. Sato, Y., et al., *Optimized methods for targeted peptide-based quantification of human uridine 5'-diphosphate-glucuronosyltransferases in biological specimens using liquid chromatography-tandem mass spectrometry.* Drug Metab Dispos, 2014. **42**(5): p. 885-9.
206. Takahara, N., et al., *Uridine diphosphate glucuronosyl transferase 1 family polypeptide A1 gene (UGT1A1) polymorphisms are associated with toxicity and efficacy in irinotecan monotherapy for refractory pancreatic cancer.* Cancer Chemother Pharmacol, 2013. **71**(1): p. 85-92.
207. Lamego, J., et al., *Carboxylesterase 2 production and characterization in human cells: new insights into enzyme oligomerization and activity.* Appl Microbiol Biotechnol, 2013. **97**(3): p. 1161-73.
208. Berggren, S., et al., *Regional transport and metabolism of ropivacaine and its CYP3A4 metabolite PPX in human intestine.* Journal of Pharmacy and Pharmacology, 2003. **55**(7): p. 963-972.
209. Nahara, M.C., et al., *Pharmacokinetics of midazolam in critically ill pediatric patients.* Eur J Drug Metab Pharmacokinet, 2000. **25**(3-4): p. 219-21.
210. Burtin, P., et al., *Population pharmacokinetics of midazolam in neonates.* Clin Pharmacol Ther, 1994. **56**(6 Pt 1): p. 615-25.
211. Mathews, H.M., et al., *A pharmacokinetic study of midazolam in paediatric patients undergoing cardiac surgery.* Br J Anaesth, 1988. **61**(3): p. 302-7.
212. Chen, Y.T., et al., *Ontogenic expression of human carboxylesterase-2 and cytochrome P450 3A4 in liver and duodenum: postnatal surge and organ-dependent regulation.* Toxicology, 2015. **330**: p. 55-61.
213. Hendijani, F., N. Azarpira, and M. Kaviani, *Effect of CYP3A5*1 expression on tacrolimus required dose for transplant pediatrics: A systematic review and meta-analysis.* Pediatr Transplant, 2018: p. e13248.
214. Zong, Y.P., et al., *Effects of CYP3A5 polymorphisms on tacrolimus pharmacokinetics in pediatric kidney transplantation: a systematic review and meta-analysis of observational studies.* World J Pediatr, 2017. **13**(5): p. 421-426.
215. Duan, P., et al., *Assessing CYP2C19 Ontogeny in Neonates and Infants Using Physiologically Based Pharmacokinetic Models: Impact of Enzyme Maturation Versus Inhibition.* CPT: Pharmacometrics & Systems Pharmacology, 2019. **8**(3): p. 158-166.
216. Chidambaran, V., S. Sadhasivam, and M. Mahmoud, *Codeine and opioid metabolism: implications and alternatives for pediatric pain management.* Curr Opin Anaesthesiol, 2017. **30**(3): p. 349-356.

217. Tang, M., et al., *Antiplatelet agents aspirin and clopidogrel are hydrolyzed by distinct carboxylesterases, and clopidogrel is transesterificated in the presence of ethyl alcohol.* J Pharmacol Exp Ther, 2006. **319**(3): p. 1467-76.
218. Smith, N.F., W.D. Figg, and A. Sparreboom, *Pharmacogenetics of irinotecan metabolism and transport: an update.* Toxicol In Vitro, 2006. **20**(2): p. 163-75.
219. Zhang, H., et al., *Regional Proteomic Quantification of Clinically Relevant Non-Cytochrome P450 Enzymes along the Human Small Intestine.* Drug Metab Dispos, 2020. **48**(7): p. 528-536.
220. Gall, W.E., et al., *Differential glucuronidation of bile acids, androgens and estrogens by human UGT1A3 and 2B7.* J Steroid Biochem Mol Biol, 1999. **70**(1-3): p. 101-8.
221. Kuehl, G.E., et al., *Glucuronidation of nonsteroidal anti-inflammatory drugs: identifying the enzymes responsible in human liver microsomes.* Drug Metab Dispos, 2005. **33**(7): p. 1027-35.
222. Prueksaritanont, T., et al., *Mechanistic studies on metabolic interactions between gemfibrozil and statins.* J Pharmacol Exp Ther, 2002. **301**(3): p. 1042-51.
223. Green, M.D. and T.R. Tephly, *Glucuronidation of amines and hydroxylated xenobiotics and endobiotics catalyzed by expressed human UGT1.4 protein.* Drug Metab Dispos, 1996. **24**(3): p. 356-63.
224. Green, M.D., W.P. Bishop, and T.R. Tephly, *Expressed human UGT1.4 protein catalyzes the formation of quaternary ammonium-linked glucuronides.* Drug Metab Dispos, 1995. **23**(3): p. 299-302.
225. Kemp, D.C., P.W. Fan, and J.C. Stevens, *Characterization of raloxifene glucuronidation in vitro: contribution of intestinal metabolism to presystemic clearance.* Drug Metab Dispos, 2002. **30**(6): p. 694-700.
226. Chen, M., et al., *Identification of Human UGT2B7 as the Major Isoform Involved in the O-Glucuronidation of Chloramphenicol.* Drug Metabolism and Disposition, 2010. **38**(3): p. 368-375.
227. Kauffman, R.E., et al., *Pharmacokinetics of chloramphenicol and chloramphenicol succinate in infants and children.* J Pediatr, 1981. **98**(2): p. 315-20.
228. Feder, H.M., Jr., C. Osier, and E.G. Maderazo, *Chloramphenicol: A review of its use in clinical practice.* Rev Infect Dis, 1981. **3**(3): p. 479-91.
229. Weiss, C.F., A.J. Glazko, and J.K. Weston, *Chloramphenicol in the newborn infant. A physiologic explanation of its toxicity when given in excessive doses.* N Engl J Med, 1960. **262**: p. 787-94.
230. Sutherland, J.M., *Fatal cardiovascular collapse of infants receiving large amounts of chloramphenicol.* AMA J Dis Child, 1959. **97**(6): p. 761-7.
231. Drozdzik, M., et al., *Protein Abundance of Clinically Relevant Drug-Metabolizing Enzymes in the Human Liver and Intestine: A Comparative Analysis in Paired Tissue Specimens.* Clin Pharmacol Ther, 2018. **104**(3): p. 515-524.
232. Ohno, S. and S. Nakajin, *Determination of mRNA expression of human UDP-glucuronosyltransferases and application for localization in various human tissues by real-time reverse transcriptase-polymerase chain reaction.* Drug Metab Dispos, 2009. **37**(1): p. 32-40.
233. Lown, K.S., et al., *Interpatient heterogeneity in expression of CYP3A4 and CYP3A5 in small bowel. Lack of prediction by the erythromycin breath test.* Drug Metab Dispos, 1994. **22**(6): p. 947-55.

234. van de Kerkhof, E.G., et al., *Innovative methods to study human intestinal drug metabolism in vitro: precision-cut slices compared with ussing chamber preparations.* Drug Metab Dispos, 2006. **34**(11): p. 1893-902.
235. Kararli, T.T., *Comparison of the gastrointestinal anatomy, physiology, and biochemistry of humans and commonly used laboratory animals.* Biopharm Drug Dispos, 1995. **16**(5): p. 351-80.
236. Cheng, H. and C.P. Leblond, *Origin, differentiation and renewal of the four main epithelial cell types in the mouse small intestine. I. Columnar cell.* Am J Anat, 1974. **141**(4): p. 461-79.
237. van der Flier, L.G. and H. Clevers, *Stem cells, self-renewal, and differentiation in the intestinal epithelium.* Annu Rev Physiol, 2009. **71**: p. 241-60.
238. Athman, R., D. Louvard, and S. Robine, *The epithelial cell cytoskeleton and intracellular trafficking. III. How is villin involved in the actin cytoskeleton dynamics in intestinal cells?* Am J Physiol Gastrointest Liver Physiol, 2002. **283**(3): p. G496-502.
239. Friederich, E., et al., *From the structure to the function of villin, an actin-binding protein of the brush border.* Bioessays, 1990. **12**(9): p. 403-8.
240. Khurana, S., et al., *Ileal microvillar protein villin is tyrosine-phosphorylated and associates with PLC-gamma1. Role of cytoskeletal rearrangement in the carbachol-induced inhibition of ileal NaCl absorption.* J Biol Chem, 1997. **272**(48): p. 30115-21.
241. West, A.B., et al., *Localization of villin, a cytoskeletal protein specific to microvilli, in human ileum and colon and in colonic neoplasms.* Gastroenterology, 1988. **94**(2): p. 343-52.
242. Moll, R., et al., *Villin: a cytoskeletal protein and a differentiation marker expressed in some human adenocarcinomas.* Virchows Arch B Cell Pathol Incl Mol Pathol, 1987. **54**(3): p. 155-69.
243. Hodin, R.A., A. Shei, and S. Meng, *Transcriptional activation of the human villin gene during enterocyte differentiation.* J Gastrointest Surg, 1997. **1**(5): p. 433-8; discussion 438.
244. Kaminsky, L.S. and M.J. Fasco, *Small intestinal cytochromes P450.* Crit Rev Toxicol, 1991. **21**(6): p. 407-22.
245. Mohri, K. and Y. Uesawa, *Enzymatic Activities in the Microsomes Prepared from Rat Small Intestinal Epithelial Cells by Differential Procedures.* Pharmaceutical Research, 2001. **18**(8): p. 1232-1236.
246. Fasco, M.J., et al., *Rat small intestinal cytochromes P450 probed by warfarin metabolism.* Mol Pharmacol, 1993. **43**(2): p. 226-33.
247. Asher, G.N., J.K. Fallon, and P.C. Smith, *UGT concentrations in human rectal tissue after multidose, oral curcumin.* Pharmacol Res Perspect, 2016. **4**(2): p. e00222.
248. Crick, F.H., *On protein synthesis.* Symp Soc Exp Biol, 1958. **12**: p. 138-63.
249. Picotti, P. and R. Aebersold, *Selected reaction monitoring-based proteomics: workflows, potential, pitfalls and future directions.* Nat Methods, 2012. **9**(6): p. 555-66.
250. Jalali, M., J. Zaborowska, and M. Jalali, *Chapter 1 - The Polymerase Chain Reaction: PCR, qPCR, and RT-PCR*, in *Basic Science Methods for Clinical Researchers*, M. Jalali, F.Y.L. Saldanha, and M. Jalali, Editors. 2017, Academic Press: Boston. p. 1-18.
251. Fraga, D., T. Meulia, and S. Fenster, *Real-Time PCR.* Current Protocols Essential Laboratory Techniques, 2008. **00**(1): p. 10.3.1-10.3.34.

252. Pfaffl, M.W., *A new mathematical model for relative quantification in real-time RT–PCR.* Nucleic Acids Research, 2001. **29**(9): p. e45-e45.
253. Farkas, D.H. and C.A. Holland, *Chapter 3 - Overview of Molecular Diagnostic Techniques and Instrumentation*, in *Cell and Tissue Based Molecular Pathology*, R.R. Tubbs and M.H. Stoler, Editors. 2009, Churchill Livingstone: Philadelphia. p. 19-32.
254. Ponchel, F., et al., *Real-time PCR based on SYBR-Green I fluorescence: An alternative to the TaqMan assay for a relative quantification of gene rearrangements, gene amplifications and micro gene deletions.* BMC Biotechnology, 2003. **3**(1): p. 18.
255. Holland, P.M., et al., *Detection of specific polymerase chain reaction product by utilizing the 5'----3' exonuclease activity of Thermus aquaticus DNA polymerase.* Proc Natl Acad Sci U S A, 1991. **88**(16): p. 7276-80.
256. Lanciotti, R.S., *Molecular Amplification Assays for the Detection of Flaviviruses*, in *Advances in Virus Research*, T.J. Chambers and T.P. Monath, Editors. 2003, Academic Press. p. 67-99.
257. Alegria-Schaffer, A., A. Lodge, and K. Vattem, *Performing and optimizing Western blots with an emphasis on chemiluminescent detection.* Methods Enzymol, 2009. **463**: p. 573-99.
258. Burnette, W.N., *"Western blotting": electrophoretic transfer of proteins from sodium dodecyl sulfate--polyacrylamide gels to unmodified nitrocellulose and radiographic detection with antibody and radioiodinated protein A.* Anal Biochem, 1981. **112**(2): p. 195-203.
259. Mahmood, T. and P.C. Yang, *Western blot: technique, theory, and trouble shooting.* N Am J Med Sci, 2012. **4**(9): p. 429-34.
260. Sakamoto, A., et al., *Reliability and robustness of simultaneous absolute quantification of drug transporters, cytochrome P450 enzymes, and Udp-glucuronosyltransferases in human liver tissue by multiplexed MRM/selected reaction monitoring mode tandem mass spectrometry with nano-liquid chromatography.* J Pharm Sci, 2011. **100**(9): p. 4037-43.
261. Manea, M., et al., *Mass spectrometric identification of the trypsin cleavage pathway in lysyl-proline containing oligotuftsin peptides.* J Pept Sci, 2007. **13**(4): p. 227-36.
262. Hedstrom, L., *Trypsin: a case study in the structural determinants of enzyme specificity.* Biol Chem, 1996. **377**(7-8): p. 465-70.
263. Berezin, I.V., et al., *The Mechanism of the α-Chymotrypsin and Trypsin-Catalyzed Hydrolysis of Amides.* European Journal of Biochemistry, 1973. **38**(3): p. 529-536.
264. Kamiie, J., et al., *Quantitative atlas of membrane transporter proteins: development and application of a highly sensitive simultaneous LC/MS/MS method combined with novel in-silico peptide selection criteria.* Pharm Res, 2008. **25**(6): p. 1469-83.
265. Prasad, B., et al., *Toward a Consensus on Applying Quantitative Liquid Chromatography-Tandem Mass Spectrometry Proteomics in Translational Pharmacology Research: A White Paper.* Clin Pharmacol Ther, 2019. **106**(3): p. 525-543.
266. Niessen, J., et al., *Expression of ABC-type transport proteins in human platelets.* Pharmacogenet Genomics, 2010. **20**(6): p. 396-400.
267. Yu, Q., et al., *Sample multiplexing for targeted pathway proteomics in aging mice.* Proceedings of the National Academy of Sciences, 2020. **117**(18): p. 9723-9732.
268. Gerber, S.A., et al., *Absolute quantification of proteins and phosphoproteins from cell lysates by tandem MS.* Proc Natl Acad Sci U S A, 2003. **100**(12): p. 6940-5.

269. Harwood, M.D., et al., *Lost in centrifugation: accounting for transporter protein losses in quantitative targeted absolute proteomics.* Drug Metab Dispos, 2014. **42**(10): p. 1766-72.
270. Grangeon, A., et al., *Determination of CYP450 Expression Levels in the Human Small Intestine by Mass Spectrometry-Based Targeted Proteomics.* International Journal of Molecular Sciences, 2021. **22**(23): p. 12791.
271. Achour, B., et al., *Mass Spectrometry of Human Transporters.* Annu Rev Anal Chem (Palo Alto Calif), 2020. **13**(1): p. 223-247.
272. Bruyère, A., et al., *Development of an optimized procedure for the preparation of rat intestinal microsomes: comparison of hepatic and intestinal microsomal cytochrome P450 enzyme activities in two rat strains.* Xenobiotica, 2009. **39**(1): p. 22-32.
273. Gröer, C., et al., *Absolute protein quantification of clinically relevant cytochrome P450 enzymes and UDP-glucuronosyltransferases by mass spectrometry-based targeted proteomics.* J Pharm Biomed Anal, 2014. **100**: p. 393-401.
274. Quaroni, A. and J. Hochman, *Development of intestinal cell culture models for drug transport and metabolism studies.* Adv Drug Deliv Rev, 1996. **22**(1): p. 3-52.
275. van de Kerkhof, E.G., I.A. de Graaf, and G.M. Groothuis, *In vitro methods to study intestinal drug metabolism.* Curr Drug Metab, 2007. **8**(7): p. 658-75.
276. Akazawa, T., et al., *High Expression of UGT1A1/1A6 in Monkey Small Intestine: Comparison of Protein Expression Levels of Cytochromes P450, UDP-Glucuronosyltransferases, and Transporters in Small Intestine of Cynomolgus Monkey and Human.* Mol Pharm, 2018. **15**(1): p. 127-140.
277. von Richter, O., et al., *Cytochrome P450 3A4 and P-glycoprotein expression in human small intestinal enterocytes and hepatocytes: a comparative analysis in paired tissue specimens.* Clin Pharmacol Ther, 2004. **75**(3): p. 172-83.
278. Burke, M.D. and S. Orrenius, *Isolation and comparison of endoplasmic reticulum membranes and their mixed function oxidase activities from mammalian extrahepatic tissues.* Pharmacol Ther, 1979. **7**(3): p. 549-99.
279. Damre, A., S.R. Mallurwar, and D. Behera, *Preparation and characterization of rodent intestinal microsomes: comparative assessment of two methods.* Indian J Pharm Sci, 2009. **71**(1): p. 75-7.
280. Lin, J.H., M. Chiba, and T.A. Baillie, *Is the role of the small intestine in first-pass metabolism overemphasized?* Pharmacol Rev, 1999. **51**(2): p. 135-58.
281. Burden, D.W. *Guide to the Homogenization of Biological Samples*. 2012.
282. Simpson, R.J., *Disruption of cultured cells by nitrogen cavitation.* Cold Spring Harb Protoc, 2010. **2010**(11): p. pdb.prot5513.
283. Gottlieb, R.A. and S. Adachi, *Nitrogen cavitation for cell disruption to obtain mitochondria from cultured cells.* Methods Enzymol, 2000. **322**: p. 213-21.
284. Zunjarrao, S.C., R. Sriraman, and R.P. Singh, *Effect of processing parameters and clay volume fraction on the mechanical properties of epoxy-clay nanocomposites.* Journal of Materials Science, 2006. **41**(8): p. 2219-2228.
285. Shah, T.R., H. Koten, and H.M. Ali, *Chapter 5 - Performance effecting parameters of hybrid nanofluids*, in *Hybrid Nanofluids for Convection Heat Transfer*, H.M. Ali, Editor. 2020, Academic Press. p. 179-213.
286. Taylor, A.C., *7 - Advances in nanoparticle reinforcement in structural adhesives*, in *Advances in Structural Adhesive Bonding*, D.A. Dillard, Editor. 2010, Woodhead Publishing. p. 151-182.

287. Lindeskog, P., et al., *Isolation of rat intestinal microsomes: partial characterization of mucosal cytochrome P-450.* Arch Biochem Biophys, 1986. **244**(2): p. 492-501.
288. Hoensch, H.P., et al., *Isolation of human hepatic microsomes and their inhibition by cimetidine and ranitidine.* Eur J Clin Pharmacol, 1985. **29**(2): p. 199-206.
289. Ham, B.M., et al., *The Influence of Sample Preparation and Replicate Analyses on HeLa Cell Phosphoproteome Coverage.* Journal of Proteome Research, 2008. **7**(6): p. 2215-2221.
290. Kratz, F., et al., *Cleaning of biomaterial surfaces: protein removal by different solvents.* Colloids Surf B Biointerfaces, 2015. **128**: p. 28-35.
291. Saveliev, S.V., et al., *Mass Spectrometry Compatible Surfactant for Optimized In-Gel Protein Digestion.* Analytical Chemistry, 2013. **85**(2): p. 907-914.
292. Botelho, D., et al., *Top-down and bottom-up proteomics of SDS-containing solutions following mass-based separation.* J Proteome Res, 2010. **9**(6): p. 2863-70.
293. Dapic, I., et al., *Proteome analysis of tissues by mass spectrometry.* Mass Spectrom Rev, 2019. **38**(4-5): p. 403-441.
294. Feng, R., et al., *Calreticulin down-regulation inhibits the cell growth, invasion and cell cycle progression of human hepatocellular carcinoma cells.* Diagnostic Pathology, 2015. **10**(1): p. 149.
295. Padilla-Benavides, T., et al., *The polarized distribution of Na+,K+-ATPase: role of the interaction between {beta} subunits.* Mol Biol Cell, 2010. **21**(13): p. 2217-25.
296. Lowry, O.H., et al., *Protein measurement with the Folin phenol reagent.* J Biol Chem, 1951. **193**(1): p. 265-75.
297. Noble, J.E. and M.J. Bailey, *Quantitation of protein.* Methods Enzymol, 2009. **463**: p. 73-95.
298. Sapan, C.V., R.L. Lundblad, and N.C. Price, *Colorimetric protein assay techniques.* Biotechnol Appl Biochem, 1999. **29**(2): p. 99-108.
299. Bradford, M.M., *A rapid and sensitive method for the quantitation of microgram quantities of protein utilizing the principle of protein-dye binding.* Anal Biochem, 1976. **72**: p. 248-54.
300. Fountoulakis, M., J.F. Juranville, and M. Manneberg, *Comparison of the Coomassie brilliant blue, bicinchoninic acid and Lowry quantitation assays, using non-glycosylated and glycosylated proteins.* J Biochem Biophys Methods, 1992. **24**(3-4): p. 265-74.
301. Simonian, M.H. and J.A. Smith, *Spectrophotometric and colorimetric determination of protein concentration.* Curr Protoc Mol Biol, 2006. **Chapter 10**: p. Unit 10.1A.
302. Smith, P.K., et al., *Measurement of protein using bicinchoninic acid.* Anal Biochem, 1985. **150**(1): p. 76-85.
303. Brenner, A.J. and E.D. Harris, *A quantitative test for copper using bicinchoninic acid.* Anal Biochem, 1995. **226**(1): p. 80-4.
304. Howard, M., et al., *GASP and FASP are Complementary for LC-MS/MS Proteomic Analysis of Drug-Metabolizing Enzymes and Transporters in Pig Liver.* Proteomics, 2018. **18**(24): p. e1800200.
305. Langenfeld, E., et al., *Mass spectrometry-based absolute quantification of microsomal cytochrome P450 2D6 in human liver.* Proteomics, 2009. **9**(9): p. 2313-2323.
306. Manza, L.L., et al., *Sample preparation and digestion for proteomic analyses using spin filters.* Proteomics, 2005. **5**(7): p. 1742-5.

307. Wiśniewski, J.R., et al., *Universal sample preparation method for proteome analysis.* Nature Methods, 2009. **6**(5): p. 359-362.
308. Al-Majdoub, Z.M., et al., *Proteomic Quantification of Human Blood-Brain Barrier SLC and ABC Transporters in Healthy Individuals and Dementia Patients.* Mol Pharm, 2019. **16**(3): p. 1220-1233.
309. Fischer, R. and B.M. Kessler, *Gel-aided sample preparation (GASP)--a simplified method for gel-assisted proteomic sample generation from protein extracts and intact cells.* Proteomics, 2015. **15**(7): p. 1224-9.
310. Fang, P., et al., *Controlling nonspecific trypsin cleavages in LC-MS/MS-based shotgun proteomics using optimized experimental conditions.* Analyst, 2015. **140**(22): p. 7613-21.
311. Zhai, L., et al., *Systematic research on the pretreatment of peptides for quantitative proteomics using a C_{18} microcolumn.* Proteomics, 2013. **13**(15): p. 2229-37.
312. Sahu, P.K., et al., *An overview of experimental designs in HPLC method development and validation.* J Pharm Biomed Anal, 2018. **147**: p. 590-611.
313. Unger, K.K. and A.I. Liapis, *Adsorbents and columns in analytical high-performance liquid chromatography: A perspective with regard to development and understanding.* Journal of Separation Science, 2012. **35**(10-11): p. 1201-1212.
314. González Fernández-Niño, S.M., et al., *Standard flow liquid chromatography for shotgun proteomics in bioenergy research.* Front Bioeng Biotechnol, 2015. **3**: p. 44.
315. Wilm, M. and M. Mann, *Analytical Properties of the Nanoelectrospray Ion Source.* Analytical Chemistry, 1996. **68**(1): p. 1-8.
316. Percy, A.J., et al., *Comparison of standard- and nano-flow liquid chromatography platforms for MRM-based quantitation of putative plasma biomarker proteins.* Anal Bioanal Chem, 2012. **404**(4): p. 1089-101.
317. Vialaret, J., et al., *Nano-flow vs standard-flow: Which is the more suitable LC/MS method for quantifying hepcidin-25 in human serum in routine clinical settings?* J Chromatogr B Analyt Technol Biomed Life Sci, 2018. **1086**: p. 110-117.
318. Uchida, Y., et al., *A study protocol for quantitative targeted absolute proteomics (QTAP) by LC-MS/MS: application for inter-strain differences in protein expression levels of transporters, receptors, claudin-5, and marker proteins at the blood-brain barrier in ddY, FVB, and C57BL/6J mice.* Fluids Barriers CNS, 2013. **10**(1): p. 21.
319. Pozniak, B.P. and R.B. Cole, *Current measurements within the electrospray emitter.* Journal of the American Society for Mass Spectrometry, 2007. **18**(4): p. 737-748.
320. Nadler, W.M., et al., *MALDI versus ESI: The Impact of the Ion Source on Peptide Identification.* Journal of Proteome Research, 2017. **16**(3): p. 1207-1215.
321. Ho, C.S., et al., *Electrospray ionisation mass spectrometry: principles and clinical applications.* Clin Biochem Rev, 2003. **24**(1): p. 3-12.
322. Yost, R.A. and C.G. Enke, *Triple quadrupole mass spectrometry for direct mixture analysis and structure elucidation.* Anal Chem, 1979. **51**(12): p. 1251-64.
323. Yost, R.A. and C.G. Enke, *Selected ion fragmentation with a tandem quadrupole mass spectrometer.* Journal of the American Chemical Society, 1978. **100**(7): p. 2274-2275.
324. Tada, I., et al., *Creating a Reliable Mass Spectral-Retention Time Library for All Ion Fragmentation-Based Metabolomics.* Metabolites, 2019. **9**(11).
325. Colangelo, C.M., et al., *Review of software tools for design and analysis of large scale MRM proteomic datasets.* Methods, 2013. **61**(3): p. 287-98.

326. Escher, C., et al., *Using iRT, a normalized retention time for more targeted measurement of peptides.* Proteomics, 2012. **12**(8): p. 1111-1121.
327. Donato, P., et al., *Mass spectrometry detection in comprehensive liquid chromatography: Basic concepts, instrumental aspects, applications and trends.* Mass Spectrometry Reviews, 2012. **31**(5): p. 523-559.
328. Roepstorff, P. and J. Fohlman, *Proposal for a common nomenclature for sequence ions in mass spectra of peptides.* Biomed Mass Spectrom, 1984. **11**(11): p. 601.
329. Pino, L.K., et al., *The Skyline ecosystem: Informatics for quantitative mass spectrometry proteomics.* Mass Spectrom Rev, 2020. **39**(3): p. 229-244.
330. Henderson, C.M., et al., *Skyline Performs as Well as Vendor Software in the Quantitative Analysis of Serum 25-Hydroxy Vitamin D and Vitamin D Binding Globulin.* Clin Chem, 2018. **64**(2): p. 408-410.
331. Maclean, B., et al., *Effect of collision energy optimization on the measurement of peptides by selected reaction monitoring (SRM) mass spectrometry.* Anal Chem, 2010. **82**(24): p. 10116-24.
332. MacLean, B., et al., *Skyline: an open source document editor for creating and analyzing targeted proteomics experiments.* Bioinformatics, 2010. **26**(7): p. 966-8.
333. Picotti, P., R. Aebersold, and B. Domon, *The implications of proteolytic background for shotgun proteomics.* Mol Cell Proteomics, 2007. **6**(9): p. 1589-98.
334. Keerthikumar, S. and S. Mathivanan, *Proteotypic Peptides and Their Applications.* Methods Mol Biol, 2017. **1549**: p. 101-107.
335. Consortium, T.U., *UniProt: the universal protein knowledgebase in 2021.* Nucleic Acids Research, 2020. **49**(D1): p. D480-D489.
336. Sayers, E.W., et al., *Database resources of the national center for biotechnology information.* Nucleic Acids Res, 2022. **50**(D1): p. D20-d26.
337. Qiu, X., H. Zhang, and Y. Lai, *Quantitative targeted proteomics for membrane transporter proteins: method and application.* Aaps j, 2014. **16**(4): p. 714-26.
338. Mirzaei, H., et al., *Comparative Evaluation of Current Peptide Production Platforms Used in Absolute Quantification in Proteomics.* Molecular & Cellular Proteomics, 2008. **7**(4): p. 813-823.
339. Beynon, R.J., et al., *Multiplexed absolute quantification in proteomics using artificial QCAT proteins of concatenated signature peptides.* Nature Methods, 2005. **2**(8): p. 587-589.
340. Vasilogianni, A.M., et al., *A family of QconCATs (Quantification conCATemers) for the quantification of human pharmacological target proteins.* J Proteomics, 2022. **261**: p. 104572.
341. Lebert, D., et al., *Production and use of stable isotope-labeled proteins for absolute quantitative proteomics.* Methods Mol Biol, 2011. **753**: p. 93-115.
342. Busch, D., et al., *LC-MS/MS method for the simultaneous quantification of intestinal CYP and UGT activity.* J Pharm Biomed Anal, 2018. **155**: p. 194-201.
343. Tsume, Y., et al., *In Vivo Predictive Dissolution and Simulation Workshop Report: Facilitating the Development of Oral Drug Formulation and the Prediction of Oral Bioperformance.* Aaps j, 2018. **20**(6): p. 100.
344. Yu, A., et al., *Measurement of in vivo Gastrointestinal Release and Dissolution of Three Locally Acting Mesalamine Formulations in Regions of the Human Gastrointestinal Tract.* Mol Pharm, 2017. **14**(2): p. 345-358.

345. Murray, K., et al., *Magnetic Resonance Imaging Quantification of Fasted State Colonic Liquid Pockets in Healthy Humans.* Mol Pharm, 2017. **14**(8): p. 2629-2638.
346. Mudie, D.M., G.L. Amidon, and G.E. Amidon, *Physiological parameters for oral delivery and in vitro testing.* Mol Pharm, 2010. **7**(5): p. 1388-405.
347. Vinarov, Z., et al., *Current challenges and future perspectives in oral absorption research: An opinion of the UNGAP network.* Adv Drug Deliv Rev, 2021. **171**: p. 289-331.
348. Zhang, X., et al., *Mechanistic Oral Absorption Modeling and Simulation for Formulation Development and Bioequivalence Evaluation: Report of an FDA Public Workshop.* CPT Pharmacometrics Syst Pharmacol, 2017. **6**(8): p. 492-495.
349. Nicolas, J.M., et al., *Oral drug absorption in pediatrics: the intestinal wall, its developmental changes and current tools for predictions.* Biopharm Drug Dispos, 2017. **38**(3): p. 209-230.
350. Yu, G., Q.-S. Zheng, and G.-F. Li, *Similarities and differences in gastrointestinal physiology between neonates and adults: a physiologically based pharmacokinetic modeling perspective.* The AAPS Journal, 2014. **16**(6): p. 1162-1166.
351. Basit, A.W., *Advances in Colonic Drug Delivery.* Drugs, 2005. **65**(14): p. 1991-2007.
352. Maroni, A., et al., *Oral colon delivery of insulin with the aid of functional adjuvants.* Adv Drug Deliv Rev, 2012. **64**(6): p. 540-556.
353. Dubey, S.K., et al., *Oral peptide delivery: challenges and the way ahead.* Drug Discov Today, 2021.
354. Del Curto, M.D., et al., *Preparation and evaluation of an oral delivery system for time-dependent colon release of insulin and selected protease inhibitor and absorption enhancer compounds.* Journal of Pharmaceutical Sciences, 2009. **98**(12): p. 4661-4669.
355. Chey, W.D., et al., *Randomized Trial of 2 Delayed-Release Formulations of Linaclotide in Patients With Irritable Bowel Syndrome With Constipation.* Am J Gastroenterol, 2021. **116**(2): p. 354-361.
356. Wilson, C.G., *The transit of dosage forms through the colon.* Int J Pharm, 2010. **395**(1-2): p. 17-25.
357. Tubic-Grozdanis, M., et al., *Pharmacokinetics of the CYP 3A Substrate Simvastatin following Administration of Delayed Versus Immediate Release Oral Dosage Forms.* Pharmaceutical Research, 2008. **25**(7): p. 1591-1600.
358. Amidon, S., J.E. Brown, and V.S. Dave, *Colon-targeted oral drug delivery systems: design trends and approaches.* AAPS PharmSciTech, 2015. **16**(4): p. 731-41.
359. Kulinowski, P., et al., *An understanding of modified release matrix tablets behavior during drug dissolution as the key for prediction of pharmaceutical product performance – case study of multimodal characterization of quetiapine fumarate tablets.* International Journal of Pharmaceutics, 2015. **484**(1): p. 235-245.
360. Verrotti, A., et al., *Extended-release formulations in epilepsy.* J Child Neurol, 2007. **22**(4): p. 419-26.
361. Garbacz, G. and S. Klein, *Dissolution testing of oral modified-release dosage forms.* J Pharm Pharmacol, 2012. **64**(7): p. 944-68.
362. Corte, T., et al., *Beclomethasone dipropionate in microscopic colitis: Results of an exploratory open-label multicentre study (COLCO).* United European Gastroenterol J, 2019. **7**(9): p. 1183-1188.

363. Zhang, M. and D. Merlin, *Nanoparticle-Based Oral Drug Delivery Systems Targeting the Colon for Treatment of Ulcerative Colitis.* Inflamm Bowel Dis, 2018. **24**(7): p. 1401-1415.
364. Ye, B. and D.R. van Langenberg, *Mesalazine preparations for the treatment of ulcerative colitis: Are all created equal?* World J Gastrointest Pharmacol Ther, 2015. **6**(4): p. 137-44.
365. Awad, A., et al., *Clinical translation of advanced colonic drug delivery technologies.* Adv Drug Deliv Rev, 2022. **181**: p. 114076.
366. Fotaki, N. and M. Vertzoni, *Biorelevant dissolution methods and their applications in in vitroin vivo correlations for oral formulations.* Open Drug Delivery Journal, 2010. **4**(SPEC. ISSUE 1): p. 2-13.
367. Löbenberg, R., et al., *Dissolution testing as a prognostic tool for oral drug absorption: dissolution behavior of glibenclamide.* Pharm Res, 2000. **17**(4): p. 439-44.
368. Jantratid, E., et al., *Application of biorelevant dissolution tests to the prediction of in vivo performance of diclofenac sodium from an oral modified-release pellet dosage form.* Eur J Pharm Sci, 2009. **37**(3-4): p. 434-41.
369. Fotaki, N., et al., *A comparative study of different release apparatus in generating in vitro-in vivo correlations for extended release formulations.* Eur J Pharm Biopharm, 2009. **73**(1): p. 115-20.
370. Philip, A.K. and B. Philip, *Colon targeted drug delivery systems: a review on primary and novel approaches.* Oman medical journal, 2010. **25**(2): p. 79-87.
371. Sulaiman, S. and L. Marciani, *MRI of the Colon in the Pharmaceutical Field: The Future before us.* Pharmaceutics, 2019. **11**(4).
372. Georgaka, D., et al., *Evaluation of Dissolution in the Lower Intestine and Its Impact on the Absorption Process of High Dose Low Solubility Drugs.* Mol Pharm, 2017. **14**(12): p. 4181-4191.
373. Vertzoni, M., et al., *Biorelevant media to simulate fluids in the ascending colon of humans and their usefulness in predicting intracolonic drug solubility.* Pharm Res, 2010. **27**(10): p. 2187-96.
374. Pritchard, S.E., et al., *Assessment of motion of colonic contents in the human colon using MRI tagging.* Neurogastroenterol Motil, 2017. **29**(9).
375. Lemmens, G., et al., *Insight into the colonic disposition of celecoxib in humans.* Eur J Pharm Sci, 2020. **145**: p. 105242.
376. Lemmens, G., et al., *Insight into the Colonic Disposition of Sulindac in Humans.* J Pharm Sci, 2021. **110**(1): p. 259-267.
377. Stamatopoulos, K., et al., *Dynamic Colon Model (DCM): A Cine-MRI Informed Biorelevant In Vitro Model of the Human Proximal Large Intestine Characterized by Positron Imaging Techniques.* Pharmaceutics, 2020. **12**(7): p. 659.
378. Mudie, D.M., et al., *Quantification of gastrointestinal liquid volumes and distribution following a 240 mL dose of water in the fasted state.* Mol Pharm, 2014. **11**(9): p. 3039-47.
379. Pritchard, S.E., et al., *Fasting and postprandial volumes of the undisturbed colon: normal values and changes in diarrhea-predominant irritable bowel syndrome measured using serial MRI.* Neurogastroenterol Motil, 2014. **26**(1): p. 124-30.
380. Conner, T.M., et al., *Physiologically based pharmacokinetic modeling of disposition and drug-drug interactions for valproic acid and divalproex.* Eur J Pharm Sci, 2018. **111**: p. 465-481.

381. Wu, X., et al., *Physiologically based pharmacokinetic modelling of treprostinil after intravenous injection and extended-release oral tablet administration in healthy volunteers: An extrapolation to other patient populations including patients with hepatic impairment.* Br J Clin Pharmacol, 2022. **88**(2): p. 587-599.
382. Danesh, B.J., et al., *Comparison of weight, depth, and diagnostic adequacy of specimens obtained with 16 different biopsy forceps designed for upper gastrointestinal endoscopy.* Gut, 1985. **26**(3): p. 227-231.
383. Hines, R.N., P.M. Simpson, and D.G. McCarver, *Age-Dependent Human Hepatic Carboxylesterase 1 (CES1) and Carboxylesterase 2 (CES2) Postnatal Ontogeny.* Drug Metab Dispos, 2016. **44**(7): p. 959-66.
384. Laizure, S.C., et al., *The role of human carboxylesterases in drug metabolism: have we overlooked their importance?* Pharmacotherapy, 2013. **33**(2): p. 210-22.
385. Jacqz-Aigrain, E. and P. Burtin, *Clinical pharmacokinetics of sedatives in neonates.* Clin Pharmacokinet, 1996. **31**(6): p. 423-43.
386. Blumer, J.L., *Clinical pharmacology of midazolam in infants and children.* Clin Pharmacokinet, 1998. **35**(1): p. 37-47.
387. Ince, I., et al., *A novel maturation function for clearance of the cytochrome P450 3A substrate midazolam from preterm neonates to adults.* Clin Pharmacokinet, 2013. **52**(7): p. 555-65.
388. de Wildt, S.N., et al., *Ontogeny of midazolam glucuronidation in preterm infants.* Eur J Clin Pharmacol, 2010. **66**(2): p. 165-70.
389. de Wildt, S.N., et al., *Pharmacodynamics of midazolam in pediatric intensive care patients.* Ther Drug Monit, 2005. **27**(1): p. 98-102.
390. de Wildt, S.N., et al., *Population pharmacokinetics and metabolism of midazolam in pediatric intensive care patients.* Crit Care Med, 2003. **31**(7): p. 1952-8.
391. de Wildt, S.N., et al., *Pharmacokinetics and metabolism of oral midazolam in preterm infants.* Br J Clin Pharmacol, 2002. **53**(4): p. 390-2.
392. de Wildt, S.N., et al., *Pharmacokinetics and metabolism of intravenous midazolam in preterm infants.* Clin Pharmacol Ther, 2001. **70**(6): p. 525-31.
393. Payne, K., et al., *The pharmacokinetics of midazolam in paediatric patients.* Eur J Clin Pharmacol, 1989. **37**(3): p. 267-72.
394. Brill, M.J., et al., *Midazolam pharmacokinetics in morbidly obese patients following semi-simultaneous oral and intravenous administration: a comparison with healthy volunteers.* Clin Pharmacokinet, 2014. **53**(10): p. 931-41.
395. Bhatt, D.K. and B. Prasad, *Critical Issues and Optimized Practices in Quantification of Protein Abundance Level to Determine Interindividual Variability in DMET Proteins by LC-MS/MS Proteomics.* Clin Pharmacol Ther, 2018. **103**(4): p. 619-630.
396. Wegler, C., et al., *Variability in Mass Spectrometry-based Quantification of Clinically Relevant Drug Transporters and Drug Metabolizing Enzymes.* Mol Pharm, 2017. **14**(9): p. 3142-3151.
397. Silva, J.C., et al., *Quantitative proteomic analysis by accurate mass retention time pairs.* Anal Chem, 2005. **77**(7): p. 2187-200.
398. Chougule, P., et al., *Isolation and characterization of human primary enterocytes from small intestine using a novel method.* Scand J Gastroenterol, 2012. **47**(11): p. 1334-43.
399. El-Khateeb, E., et al., *Proteomic Quantification of Changes in Abundance of Drug-Metabolizing Enzymes and Drug Transporters in Human Liver Cirrhosis: Different*

Methods, Similar Outcomes. Drug Metabolism and Disposition, 2021. **49**(8): p. 610-618.
400. Vyhlidal, C.A., et al., *Effect of Crohn's Disease on Villous Length and CYP3A4 Expression in the Pediatric Small Intestine.* Clinical and Translational Science, 2020.
401. Lenco, J., et al., *Conventional-Flow Liquid Chromatography-Mass Spectrometry for Exploratory Bottom-Up Proteomic Analyses.* Analytical Chemistry, 2018. **90**(8): p. 5381-5389.
402. Russell, M.R., et al., *Alternative fusion protein strategies to express recalcitrant QconCAT proteins for quantitative proteomics of human drug metabolizing enzymes and transporters.* J Proteome Res, 2013. **12**(12): p. 5934-42.
403. Krokhin, O.V. and V. Spicer, *Generation of accurate peptide retention data for targeted and data independent quantitative LC-MS analysis: Chromatographic lessons in proteomics.* Proteomics, 2016. **16**(23): p. 2931-2936.
404. Paediatric Formulary Committee, *BNF for Children (Online)*. 2022, BMJ Group, Pharmaceutical Press, and RCPCH Publications: London.
405. Detyniecki, K., et al., *Safety and efficacy of midazolam nasal spray in the outpatient treatment of patients with seizure clusters-a randomized, double-blind, placebo-controlled trial.* Epilepsia, 2019. **60**(9): p. 1797-1808.
406. Bouw, M.R., et al., *Clinical pharmacokinetic and pharmacodynamic profile of midazolam nasal spray.* Epilepsy Res, 2021. **171**: p. 106567.
407. Ashley, P., P. Anand, and K. Andersson, *Best clinical practice guidance for conscious sedation of children undergoing dental treatment: an EAPD policy document.* Eur Arch Paediatr Dent, 2021. **22**(6): p. 989-1002.
408. Ljungman, G., et al., *Pain in paediatric oncology: interviews with children, adolescents and their parents.* Acta Paediatr, 1999. **88**(6): p. 623-30.
409. Hedén, L., et al., *Low-dose oral midazolam reduces fear and distress during needle procedures in children with cancer.* Pediatr Blood Cancer, 2009. **53**(7): p. 1200-4.
410. Benet, L.Z., F. Broccatelli, and T.I. Oprea, *BDDCS applied to over 900 drugs.* Aaps j, 2011. **13**(4): p. 519-47.
411. Christopher Gorski, J., et al., *Regioselective biotransformation of midazolam by members of the human cytochrome P450 3A (CYP3A) subfamily.* Biochemical Pharmacology, 1994. **47**(9): p. 1643-1653.
412. van Groen, B.D., et al., *The Oral Bioavailability and Metabolism of Midazolam in Stable Critically Ill Children: A Pharmacokinetic Microtracing Study.* Clin Pharmacol Ther, 2021. **109**(1): p. 140-149.
413. Mandema, J.W., et al., *Pharmacokinetic-pharmacodynamic modeling of the central nervous system effects of midazolam and its main metabolite alpha-hydroxymidazolam in healthy volunteers.* Clin Pharmacol Ther, 1992. **51**(6): p. 715-28.
414. Crevoisier, C., et al., *Relationship between plasma concentration and effect of midazolam after oral and intravenous administration.* Br J Clin Pharmacol, 1983. **16 Suppl 1**(Suppl 1): p. 51s-61s.
415. Brussee, J.M., et al., *A Pediatric Covariate Function for CYP3A-Mediated Midazolam Clearance Can Scale Clearance of Selected CYP3A Substrates in Children.* Aaps j, 2019. **21**(5): p. 81.

416. Smits, A., et al., *A Physiology-Based Pharmacokinetic Framework to Support Drug Development and Dose Precision During Therapeutic Hypothermia in Neonates.* Front Pharmacol, 2020. **11**: p. 587.
417. Thummel, K.E., et al., *Use of midazolam as a human cytochrome P450 3A probe: I. In vitro-in vivo correlations in liver transplant patients.* J Pharmacol Exp Ther, 1994. **271**(1): p. 549-56.
418. Tolle-Sander, S., et al., *Midazolam exhibits characteristics of a highly permeable P-glycoprotein substrate.* Pharm Res, 2003. **20**(5): p. 757-64.
419. Han, B., et al., *Optimization of drug-drug interaction study design: comparison of minimal physiologically based pharmacokinetic models on prediction of CYP3A inhibition by ketoconazole.* Drug Metab Dispos, 2013. **41**(7): p. 1329-38.
420. Higashikawa, F., et al., *In-vivo and in-vitro metabolic clearance of midazolam, a cytochrome P450 3A substrate, by the liver under normal and increased enzyme activity in rats.* J Pharm Pharmacol, 1999. **51**(4): p. 405-10.
421. Hyland, R., et al., *In vitro and in vivo glucuronidation of midazolam in humans.* Br J Clin Pharmacol, 2009. **67**(4): p. 445-54.
422. Lappin, G., et al., *Use of microdosing to predict pharmacokinetics at the therapeutic dose: experience with 5 drugs.* Clin Pharmacol Ther, 2006. **80**(3): p. 203-15.
423. Hohmann, N., et al., *Midazolam microdose to determine systemic and pre-systemic metabolic CYP3A activity in humans.* Br J Clin Pharmacol, 2015. **79**(2): p. 278-85.
424. Halama, B., et al., *A nanogram dose of the CYP3A probe substrate midazolam to evaluate drug interactions.* Clin Pharmacol Ther, 2013. **93**(6): p. 564-71.
425. van Groen, B.D., et al., *Dose-linearity of the pharmacokinetics of an intravenous [(14) C]midazolam microdose in children.* Br J Clin Pharmacol, 2019. **85**(10): p. 2332-2340.
426. Reed, M.D., et al., *The single-dose pharmacokinetics of midazolam and its primary metabolite in pediatric patients after oral and intravenous administration.* J Clin Pharmacol, 2001. **41**(12): p. 1359-69.
427. Watkins, P.B., *Noninvasive tests of CYP3A enzymes.* Pharmacogenetics, 1994. **4**(4): p. 171-84.
428. Watkins, P.B., *Erythromycin breath test.* Clin Pharmacol Ther, 2000. **67**(5): p. 577-8.
429. Paine, M.F., et al., *Cytochrome P450 3A4 and P-glycoprotein mediate the interaction between an oral erythromycin breath test and rifampin.* Clin Pharmacol Ther, 2002. **72**(5): p. 524-35.
430. Vet, N.J., et al., *The effect of critical illness and inflammation on midazolam therapy in children.* Pediatr Crit Care Med, 2012. **13**(1): p. e48-50.
431. Brussee, J.M., et al., *Predicting CYP3A-mediated midazolam metabolism in critically ill neonates, infants, children and adults with inflammation and organ failure.* Br J Clin Pharmacol, 2018. **84**(2): p. 358-368.
432. Kos, M.K., et al., *Maturation of midazolam clearance in critically ill children with severe bronchiolitis: A population pharmacokinetic analysis.* Eur J Pharm Sci, 2020. **141**: p. 105095.
433. Altamimi, M.I., H. Sammons, and I. Choonara, *Inter-individual variation in midazolam clearance in children.* Arch Dis Child, 2015. **100**(1): p. 95-100.
434. Ince, I., et al., *Critical illness is a major determinant of midazolam clearance in children aged 1 month to 17 years.* Ther Drug Monit, 2012. **34**(4): p. 381-9.

435. van Groen, B.D., et al., *Proof of Concept: First Pediatric [(14) C]microtracer Study to Create Metabolite Profiles of Midazolam.* Clin Pharmacol Ther, 2020. **108**(5): p. 1003-1009.
436. van Rongen, A., et al., *Population pharmacokinetics of midazolam and its metabolites in overweight and obese adolescents.* Br J Clin Pharmacol, 2015. **80**(5): p. 1185-96.
437. van Rongen, A., et al., *Higher Midazolam Clearance in Obese Adolescents Compared with Morbidly Obese Adults.* Clin Pharmacokinet, 2018. **57**(5): p. 601-611.
438. Thummel, K.E., et al., *Oral first-pass elimination of midazolam involves both gastrointestinal and hepatic CYP3A-mediated metabolism.* Clin Pharmacol Ther, 1996. **59**(5): p. 491-502.
439. Galetin, A., M. Gertz, and J.B. Houston, *Potential role of intestinal first-pass metabolism in the prediction of drug-drug interactions.* Expert Opin Drug Metab Toxicol, 2008. **4**(7): p. 909-22.
440. Johnson, T.N., et al., *Contribution of midazolam and its 1-hydroxy metabolite to preoperative sedation in children: a pharmacokinetic-pharmacodynamic analysis.* Br J Anaesth, 2002. **89**(3): p. 428-37.
441. Edginton, A.N., et al., *A mechanistic approach for the scaling of clearance in children.* Clin Pharmacokinet, 2006. **45**(7): p. 683-704.
442. Mansoor, N., et al., *Prediction of Clearance and Dose of Midazolam in Preterm and Term Neonates: A Comparative Study Between Allometric Scaling and Physiologically Based Pharmacokinetic Modeling.* Am J Ther, 2019. **26**(1): p. e32-e37.
443. Zhu, J., et al., *Physiologically based pharmacokinetic/pharmacodynamic modeling to evaluate the absorption of midazolam rectal gel.* Eur J Pharm Sci, 2021. **167**: p. 106006.
444. Salerno, S.N., et al., *Leveraging Physiologically Based Pharmacokinetic Modeling and Experimental Data to Guide Dosing Modification of CYP3A-Mediated Drug-Drug Interactions in the Pediatric Population.* Drug Metab Dispos, 2021. **49**(9): p. 844-855.
445. Goho, C., *Oral midazolam-grapefruit juice drug interaction.* Pediatr Dent, 2001. **23**(4): p. 365-6.
446. Lundahl, J., et al., *Effects of grapefruit juice ingestion--pharmacokinetics and haemodynamics of intravenously and orally administered felodipine in healthy men.* Eur J Clin Pharmacol, 1997. **52**(2): p. 139-45.
447. Salem, F., et al., *A re-evaluation and validation of ontogeny functions for cytochrome P450 1A2 and 3A4 based on in vivo data.* Clin Pharmacokinet, 2014. **53**(7): p. 625-36.
448. Upreti, V.V. and J.L. Wahlstrom, *Meta-analysis of hepatic cytochrome P450 ontogeny to underwrite the prediction of pediatric pharmacokinetics using physiologically based pharmacokinetic modeling.* J Clin Pharmacol, 2016. **56**(3): p. 266-83.
449. LTD, S., *Simcyp Version V19*. 2019: Sheffield, UK.
450. Wu, G., M. Baraldo, and M. Furlanut, *Calculating percentage prediction error: a user's note.* Pharmacol Res, 1995. **32**(4): p. 241-8.
451. Zhou, W., et al., *Predictive Performance of Physiologically Based Pharmacokinetic and Population Pharmacokinetic Modeling of Renally Cleared Drugs in Children.* CPT Pharmacometrics Syst Pharmacol, 2016. **5**(9): p. 475-83.
452. Anderson, B.J., K. Allegaert, and N.H.G. Holford, *Population clinical pharmacology of children: general principles.* European Journal of Pediatrics, 2006. **165**(11): p. 741-746.

453. Mirjalili, S.A., G. Tarr, and M.D. Stringer, *The length of the large intestine in children determined by computed tomography scan.* Clin Anat, 2017. **30**(7): p. 887-893.
454. Wilson, J.P., *Surface area of the small intestine in man.* Gut, 1967. **8**(6): p. 618-21.
455. Ulvestad, M., et al., *Impact of OATP1B1, MDR1, and CYP3A4 expression in liver and intestine on interpatient pharmacokinetic variability of atorvastatin in obese subjects.* Clin Pharmacol Ther, 2013. **93**(3): p. 275-82.
456. Frechen, S., et al., *A semiphysiological population pharmacokinetic model for dynamic inhibition of liver and gut wall cytochrome P450 3A by voriconazole.* Clin Pharmacokinet, 2013. **52**(9): p. 763-81.
457. de Wildt, S.N., et al., *Cytochrome P450 3A: ontogeny and drug disposition.* Clin Pharmacokinet, 1999. **37**(6): p. 485-505.
458. Verscheijden, L.F.M., et al., *Physiologically-based pharmacokinetic models for children: Starting to reach maturation?* Pharmacology & Therapeutics, 2020: p. 107541.
459. Polasek, T.M. and A. Rostami-Hodjegan, *Virtual Twins: Understanding the Data Required for Model-Informed Precision Dosing.* Clin Pharmacol Ther, 2020. **107**(4): p. 742-745.
460. Schneider, C.A., W.S. Rasband, and K.W. Eliceiri, *NIH Image to ImageJ: 25 years of image analysis.* Nature Methods, 2012. **9**(7): p. 671-675.
461. *IBM Corp. Released 2020. IBM SPSS Statistics for Windows, Version 27.0. Armonk, NY: IBM Corp.*
462. The Horos Project. *https://horosproject.org/faqs/*. [cited 2020.
463. Hoad, C.L., et al., *Non-invasive quantification of small bowel water content by MRI: a validation study.* Phys Med Biol, 2007. **52**(23): p. 6909-22.
464. Laqua, R. *Global Thresholding v1.0 OsiriX Plugin [Software]*. Zenodo 2016; Available from: https://osirixpluginbasics.wordpress.com/2012/10/30/plugin-global-thresholding/.
465. Grimm, M., et al., *Gastric Emptying and Small Bowel Water Content after Administration of Grapefruit Juice Compared to Water and Isocaloric Solutions of Glucose and Fructose: A Four-Way Crossover MRI Pilot Study in Healthy Subjects.* Mol Pharm, 2018. **15**(2): p. 548-559.
466. Sharif, H., et al., *Imaging Measurement of Whole Gut Transit Time in Paediatric and Adult Functional Gastrointestinal Disorders: A Systematic Review and Narrative Synthesis.* Diagnostics (Basel), 2019. **9**(4).
467. Guimarães, M., et al., *Biopharmaceutical considerations in paediatrics with a view to the evaluation of orally administered drug products – a PEARRL review.* Journal of Pharmacy and Pharmacology, 2019. **71**(4): p. 603-642.
468. Use, C.f.M.P.f.H., *Reflection paper: formulations of choice for the paediatric population.* EMEA, London, 2006.
469. Lemmens, G., et al., *Drug Disposition in the Lower Gastrointestinal Tract: Targeting and Monitoring.* Pharmaceutics, 2021. **13**(2).
470. Diakidou, A., et al., *Characterization of the contents of ascending colon to which drugs are exposed after oral administration to healthy adults.* Pharm Res, 2009. **26**(9): p. 2141-51.
471. Van der Veken, M., et al., *Gastrointestinal Fluid Volumes in Pediatrics: A Retrospective MRI Study.* Pharmaceutics, 2022. **14**(9): p. 1935.

472. Sharif, H., et al., *Colonic Volume Changes in Paediatric Constipation Compared to Normal Values Measured Using MRI.* Diagnostics (Basel), 2021. **11**(6).
473. Nilsson, M., et al., *Quantification and variability in colonic volume with a novel magnetic resonance imaging method.* Neurogastroenterol Motil, 2015. **27**(12): p. 1755-63.
474. Fallingborg, J., et al., *Measurement of Gastrointestinal pH and Regional Transit Times in Normal Children.* Journal of Pediatric Gastroenterology and Nutrition, 1990. **11**(2): p. 211-214.
475. Broesder, A., et al., *pH-dependent ileocolonic drug delivery, part I: in vitro and clinical evaluation of novel systems.* Drug Discovery Today, 2020. **25**(8): p. 1362-1373.
476. Murray, K.A., et al., *Corticotropin-releasing factor increases ascending colon volume after a fructose test meal in healthy humans: a randomized controlled trial.* Am J Clin Nutr, 2016. **103**(5): p. 1318-26.
477. Wilkinson-Smith, V., et al., *The MRI colonic function test: Reproducibility of the Macrogol stimulus challenge.* Neurogastroenterol Motil, 2020. **32**(11): p. e13942.
478. Kim, H.-S., S. Lee, and J.H. Kim, *Real-world Evidence versus Randomized Controlled Trial: Clinical Research Based on Electronic Medical Records.* Journal of Korean medical science, 2018. **33**(34): p. e213-e213.
479. Smits, A., et al., *Physiologically based pharmacokinetic (PBPK) modeling and simulation in neonatal drug development: how clinicians can contribute.* Expert Opin Drug Metab Toxicol, 2019. **15**(1): p. 25-34.
480. Staelens, S., et al., *Gastric emptying in healthy newborns fed an intact protein formula, a partially and an extensively hydrolysed formula.* Clin Nutr, 2008. **27**(2): p. 264-8.
481. Neal-Kluever, A., et al., *Physiology of the Neonatal Gastrointestinal System Relevant to the Disposition of Orally Administered Medications.* Drug Metab Dispos, 2019. **47**(3): p. 296-313.
482. Del Moral Sanchez, J.M., et al., *Biopharmaceutical optimization in neglected diseases for paediatric patients by applying the provisional paediatric biopharmaceutical classification system.* Br J Clin Pharmacol, 2018. **84**(10): p. 2231-2241.
483. delMoral-Sanchez, J.-M., et al., *Classification of WHO Essential Oral Medicines for Children Applying a Provisional Pediatric Biopharmaceutics Classification System.* Pharmaceutics, 2019. **11**(11): p. 567.
484. Gandhi, S.V., et al., *Considerations for a Pediatric Biopharmaceutics Classification System (BCS): application to five drugs.* AAPS PharmSciTech, 2014. **15**(3): p. 601-611.
485. Placidi, E., et al., *The effects of loperamide, or loperamide plus simethicone, on the distribution of gut water as assessed by MRI in a mannitol model of secretory diarrhoea.* Aliment Pharmacol Ther, 2012. **36**(1): p. 64-73.
486. Abuhelwa, A.Y., D.J.R. Foster, and R.N. Upton, *A Quantitative Review and Meta-models of the Variability and Factors Affecting Oral Drug Absorption-Part II: Gastrointestinal Transit Time.* Aaps j, 2016. **18**(5): p. 1322-1333.
487. Sharif, H., et al., *Feasibility Study of a New Magnetic Resonance Imaging Mini-capsule Device to Measure Whole Gut Transit Time in Paediatric Constipation.* J Pediatr Gastroenterol Nutr, 2020. **71**(5): p. 604-611.
488. Chapa-Rodriguez, A., et al., *Poor Agreement Between Imaging and Histologic and Colonoscopy Findings in Pediatric Patients.* Journal of Pediatric Gastroenterology and Nutrition, 2018. **66**(2): p. 263-267.

489. Marciani, L., et al., *Stimulation of colonic motility by oral PEG electrolyte bowel preparation assessed by MRI: comparison of split vs single dose.* Neurogastroenterol Motil, 2014. **26**(10): p. 1426-36.
490. Hoad, C.L., et al., *Colon wall motility: comparison of novel quantitative semi-automatic measurements using cine MRI.* Neurogastroenterol Motil, 2016. **28**(3): p. 327-35.
491. Huang, W., S.L. Lee, and L.X. Yu, *Mechanistic approaches to predicting oral drug absorption.* Aaps j, 2009. **11**(2): p. 217-24.
492. Pawar, G., et al., *Development of a Pediatric Relative Bioavailability/Bioequivalence Database and Identification of Putative Risk Factors Associated With Evaluation of Pediatric Oral Products.* The AAPS Journal, 2021. **23**(3): p. 57.
493. delMoral-Sanchez, J.-M., et al., *Availability of Authorizations from EMA and FDA for Age-Appropriate Medicines Contained in the WHO Essential Medicines List for Children 2019.* Pharmaceutics, 2020. **12**(4): p. 316.
494. Masi, G., et al., *Use of quetiapine in children and adolescents.* Paediatr Drugs, 2015. **17**(2): p. 125-40.
495. Pagsberg, A.K., et al., *Quetiapine versus aripiprazole in children and adolescents with psychosis--protocol for the randomised, blinded clinical Tolerability and Efficacy of Antipsychotics (TEA) trial.* BMC Psychiatry, 2014. **14**: p. 199.
496. Joshi, G., et al., *A prospective open-label trial of quetiapine monotherapy in preschool and school age children with bipolar spectrum disorder.* Journal of Affective Disorders, 2012. **136**(3): p. 1143-1153.
497. Findling, R.L., et al., *Efficacy and safety of quetiapine in adolescents with schizophrenia investigated in a 6-week, double-blind, placebo-controlled trial.* J Child Adolesc Psychopharmacol, 2012. **22**(5): p. 327-42.
498. Scheffer, R.E., et al., *Rapid quetiapine loading in youths with bipolar disorder.* J Child Adolesc Psychopharmacol, 2010. **20**(5): p. 441-5.
499. Hiemke, C., et al., *Consensus Guidelines for Therapeutic Drug Monitoring in Neuropsychopharmacology: Update 2017.* Pharmacopsychiatry, 2018. **51**(1-02): p. 9-62.
500. De Hert, M., et al., *Prevalence and severity of antipsychotic related constipation in patients with schizophrenia: a retrospective descriptive study.* BMC Gastroenterol, 2011. **11**: p. 17.
501. Severance, E.G., et al., *Gastroenterology issues in schizophrenia: why the gut matters.* Current psychiatry reports, 2015. **17**(5): p. 27-27.
502. Palmer, S.E., et al., *Life-threatening clozapine-induced gastrointestinal hypomotility: an analysis of 102 cases.* J Clin Psychiatry, 2008. **69**(5): p. 759-68.
503. Stanniland, C. and D. Taylor, *Tolerability of atypical antipsychotics.* Drug Saf, 2000. **22**(3): p. 195-214.
504. Grimm, S.W., et al., *Effects of cytochrome P450 3A modulators ketoconazole and carbamazepine on quetiapine pharmacokinetics.* Br J Clin Pharmacol, 2006. **61**(1): p. 58-69.
505. Völgyi, G., et al., *Study of pH-dependent solubility of organic bases. Revisit of Henderson-Hasselbalch relationship.* Analytica Chimica Acta, 2010. **673**(1): p. 40-46.
506. Winter, H.R., et al., *Steady-State Pharmacokinetic, Safety, and Tolerability Profiles of Quetiapine, Norquetiapine, and Other Quetiapine Metabolites in Pediatric and Adult*

Patients with Psychotic Disorders. Journal of Child and Adolescent Psychopharmacology, 2008. **18**(1): p. 81-98.
507. Figueroa, C., et al., *Pharmacokinetic profiles of extended release quetiapine fumarate compared with quetiapine immediate release.* Prog Neuropsychopharmacol Biol Psychiatry, 2009. **33**(2): p. 199-204.
508. Bui, K., W. Earley, and S. Nyberg, *Pharmacokinetic profile of the extended-release formulation of quetiapine fumarate (quetiapine XR): clinical implications.* Current Medical Research and Opinion, 2013. **29**(7): p. 813-825.
509. Wang, J. and D.R. Flanagan, *General solution for diffusion-controlled dissolution of spherical particles. 1. Theory.* J Pharm Sci, 1999. **88**(7): p. 731-8.
510. Wang, J. and D.R. Flanagan, *General solution for diffusion-controlled dissolution of spherical particles. 2. Evaluation of experimental data.* J Pharm Sci, 2002. **91**(2): p. 534-42.
511. Tannergren, C., et al., *Toward an increased understanding of the barriers to colonic drug absorption in humans: implications for early controlled release candidate assessment.* Mol Pharm, 2009. **6**(1): p. 60-73.
512. RCPCH, *UK Growth Chart*. 2012: www.growthcharts.RCPCH.ac.uk.
513. Pepin, X.J.H., et al., *Understanding Mechanisms of Food Effect and Developing Reliable PBPK Models Using a Middle-out Approach.* Aaps j, 2021. **23**(1): p. 12.
514. PRAVEEN P. FERNANDES, M.D. , and and WILLIAM A. MARCIL, M.D. , Omaha, Neb., *Death Associated With Quetiapine Overdose.* American Journal of Psychiatry, 2002. **159**(12): p. 2114-2114.
515. Peridy, E., et al., *Quetiapine Poisoning and Factors Influencing Severity.* J Clin Psychopharmacol, 2019. **39**(4): p. 312-317.
516. Holzer, L., et al., *Quetiapine in adolescents with non-affective psychotic disorders: an open-label trial.* Pharmacopsychiatry, 2011. **44**(3): p. 87-95.
517. Whitney, Z., et al., *Therapeutic drug levels of second generation antipsychotics in youth: a systematic review.* J Child Adolesc Psychopharmacol, 2015. **25**(3): p. 234-45.
518. Hemmings, G., *Schizophrenia.* Lancet, 2004. **364**(9442): p. 1312-3.
519. Eaton, W., et al., *Coeliac disease and schizophrenia: population based case control study with linkage of Danish national registers.* BMJ (Clinical research ed.), 2004. **328**(7437): p. 438-9.
520. Cascella, N.G., et al., *Prevalence of celiac disease and gluten sensitivity in the United States clinical antipsychotic trials of intervention effectiveness study population.* Schizophr Bull, 2011. **37**(1): p. 94-100.
521. Braniste, V., et al., *The gut microbiota influences blood-brain barrier permeability in mice.* Sci Transl Med, 2014. **6**(263): p. 263ra158.
522. Zheng, L., et al., *Dose Adjustment of Quetiapine and Aripiprazole for Pregnant Women Using Physiologically Based Pharmacokinetic Modeling and Simulation.* Clin Pharmacokinet, 2021. **60**(5): p. 623-635.
523. El Ela, A.A., et al., *Identification of P-glycoprotein substrates and inhibitors among psychoactive compounds--implications for pharmacokinetics of selected substrates.* J Pharm Pharmacol, 2004. **56**(8): p. 967-75.
524. Boulton, D.W., et al., *In vitro P-glycoprotein affinity for atypical and conventional antipsychotics.* Life Sci, 2002. **71**(2): p. 163-9.